A TASK BASED DESIGN PROCEDURE AND MODELLING APPROACHES FOR INDUSTRIAL CRYSTALLIZATION PROCESSES

Abhilash Radhakrishnan Menon

A TASK BASED DESIGN PROCEDURE AND MODELLING APPROACHES FOR INDUSTRIAL CRYSTALLIZATION PROCESSES

PROEFSCHRIFT

ter verkrijging van de graad van doctor
aan de Technische Universiteit Delft
op gezag van de Rector Magnificus prof. dr. ir. J.T.Fokkema,
voorzitter van het College voor Promoties,
in het openbaar te verdedigen op woensdag 6 december 2006 om 10.00 uur

door

Abhilash Radhakrishnan MENON

Master of Technological Design - Chemical Engineering (University of Twente, the Netherlands)
geboren te Palghat (India)

Dit proefschrift is goedgekurd door de promotoren:

Prof. ir. J. Grievink

Prof. dr. ir. P.J. Jansens

Samenstelling promotiecommissie:

Rector Magnificus	Voorzitter
Prof. ir. J. Grievink	Technische Universiteit Delft, promotor
Prof. dr. ir. P.J. Jansens	Technische Universiteit Delft, promotor
Dr. ir. H.J.M. Kramer	Technische Universiteit Delft, toegevoegd promotor
Prof.dr.ir. P.M.J. Van den Hof	Technische Universiteit Delft
Prof.dr.ir. A.B. de Haan	Technische Universiteit Eindhoven
Dr. M. Rauls	BASF, Ludwigshafen, Germany
Dr. ir. S.K. Bermingham	Process Systems Enterprise Ltd, UK
Prof. dr. G.J. Witkamp	Technische Universiteit Delft (reservelid)

Published by : Abhilash R. Menon, Delft

ISBN-10: 90-9021029-6

ISBN-13: 978-90-9021029-2

Keywords: industrial crystallization, task based design, dynamic modelling, conceptual process design, population balances, multi-dimensional, nucleation, growth rate dispersion, superstructure

Printed by PrintPartners Ipskamp in the Netherlands

to mummy and papa

Summary

A TASK-BASED DESIGN PROCEDURE AND MODELLING APPROACHES FOR INDUSTRIAL CRYSTALLIZATION PROCESSES

Abhilash R. Menon
ISBN-10: 90-9021029-6 / ISBN-13: 978-90-9021029-2
December 2006

The process industry must respond to needs and expectations in society, involving increased sustainability of material cycles, competitive capital productivity, as well as higher customer expectations regarding product functionality and performance. To support this objective, effective and inventive design approaches are needed, taking a product and process life span perspective. Although crystallization is one of the older unit operations in the chemical industry, the design and operation of crystallization processes still pose many problems. Many plants produce crystals, which do not satisfy the defined quality specifications. The current market need is to operate crystallization and downstream processes in an optimal and cost-efficient manner, in strongly fluctuating market conditions. Despite the importance of crystallization, there is a relative lack of systematic design procedures and predictive models to overcome the before-mentioned problems and to design crystallizers for flexible product specifications in multi-purpose plants.

This dissertation aims to address these issues from three perspectives:

1. Formulation of a synthesis-oriented approach towards the conceptual design of (innovative) configurations for crystallization equipment.
2. Validation of existing crystallization rate models, partly developed within Delft University of Technology against fed-batch experimental data.
3. Improvement of the process design models to describe specific phenomena observed in practice in certain continuous crystallization processes.

Crystallization as a unit operation in chemical process industry is first introduced in Chapter 1, with regards to the applicability, advantages and problems encountered in practice. A motivation is given of the selection of design and modelling as research topics to enhance crystallization technology. Then, a short review is presented in the form of a state-of-the-art in the modelling and design of industrial crystallization processes. This essentially builds up the platform for setting the objectives and scope of research for this thesis, which in a nutshell, can be summarized as novel contributions to population balance modelling and a synthesis approach for industrial crystallization processes. The scope of this research is bounded by the nature of the chemical system, crystallization method, operation mode and crystallizer type.

A novel task-based procedure for the conceptual design of a solution crystallization process unit is proposed in Chapter 2. The aim is to reduce cost of resources and capital, and possibly lead to process intensification. The design of solid state processes and in particular crystallization processes have been the subject of past academic research. Rossiter and Douglas (1986) and Ng(2001) discuss systematic procedures for designing an integrated crystallization system considering the interaction between crystallization and downstream processing. Taking the interaction between product and process designs into account, Bermingham(2003) proposed a systematic and hierarchical design procedure for improving the quality of both, the design of crystallization processes and the design process. This multi-level design procedure covers the whole range from product design to the staging in a crystallization unit. At each level, it allows one to systematically and simultaneously deal with the large number of initial design specifications, design and operational variables and the wide variety of domain knowledge involved at any particular stage of the design process.
The task-based design approach proposed in this thesis is embedded within an extended systematic hierarchical design procedure as proposed by Bermingham(2000), aiming to arrive at novel, optimum configuration of crystallizer units. The physical task concept facilitates a more synthesis-focussed approach, as a functional alternative to the traditional way of thinking in geometric structures for equipment in process analysis. The synthesis approach is to represent the crystallization process as a set of basic functions (tasks) each of which transforms the physical state of matter from an initial state to some final desired target state by means of a physical event. These tasks are connected in a network to accomplish the transformation of the feed into the product within quality specifications. The main thrust in this chapter is on the development of an ontology for the task-based approach. In this approach, alternative ways of structuring the tasks are allowed which will lead to the generation of superstructures, from which optimum crystallization process(es) and crystallizer configuration(s) can be identified. Since the process network generated by means of task-based design is based on physical events, it can also be used in a process modelling environment employing compartmental structures for synthesis, analysis and optimization studies. Such studies are the final step in the application of the task-based concept.

Chapter 3 provides an overview on the dominant mechanisms that play a role in solution crystallization processes. An introduction into the thermodynamic aspects of crystallization is also presented. In the second half of this chapter, the process modelling framework developed by Bermingham(1998, 2003a,b) is described briefly. This model framework which comprises of population balance equations in addition to mass and energy balances is built within a dynamic modelling tool gPROMS. This process model can be applied for design and optimization purposes and used to predict the relations between crystallizer geometry and operating conditions on one hand and production capacity and crystal quality on the other.

Fed-batch experiments performed for the evaporative unseeded crystallization of ammonium sulphate from water in a 75L Draft Tube and 1100L Draft Tube Baffle crystallizer are discussed in Chapter 4. The heat input, mixing conditions and fines removal rate were selected as the primary actuators for the process. During the experiments, the process actuators were kept at constant levels or were varied stepwise and their effect on the final product quality of the batch was studied. The study reveals a significant influence of the actuators on the initial start-up and dynamic behavior of the process, especially the effect of the propeller frequency and the fines removal rate. The heat input was found to be less critical in affecting the overall process dynamics in fed-batch processes. Dynamic parameter estimation studies showed that the kinetic parameters for surface integration rate constant (k_r) and the surface-related energy increase (Γ) are strongly correlated. The parameter sets obtained give a reasonable fit with experimental data when used to test the descriptive and predictive quality of the rigorous crystallizer models, for varying process conditions.

A novel approach is introduced in Chapter 5 to improve the description of the dynamic behaviour of industrial crystallizers using a two population balance model to discriminate between primary and secondary nuclei. A heterogeneous primary nucleation model (Kashchiev, 2000) is implemented in a

rigorous crystallizer model framework to capture the sustained oscillatory behavior observed in industrial draft-tube baffle (DTB) crystallizers for the crystallization of well-soluble compounds. The distinction between primary and secondary nuclei in the modelling framework is realized by using two different growth rates within the dispersed phase. The total crystal population is split up into two distinct and interacting populations, one representing the primary (no strain) population of crystals and the other the secondary (strained) population. Such a two-population balance model exhibits the sustained cyclic response for a 1100L DTB crystallizer, for an ammonium-sulphate water system. Including the degree of heterogeneity (ψ) and the two parameters; surface integration rate constant (k_r) and condition for deformation (I_v^*) from the growth model, the primary nucleation model framework has three unknown parameters which are fitted using measured transients from experiments performed on pilot-plant crystallizers. The effect of the heterogeneity factor (ψ) on the dynamics of the process, suggests that the parameter ψ is very sensitive and hence, plays a very critical role in predicting the start-up and dynamics of the process.
The single compartment models show that the value of ψ needed to trigger a primary nucleation event is too low and unrealistic ($\psi < 0.1$). The multi-compartment models improved on the value of ψ (0.135 – 0.14) making it a more realistic value, to trigger primary nucleation for the system ammonium sulphate. Here it is possible to create higher supersaturation levels in certain localized region(s) of the crystallizer, say the boiling zone. Hence, the energy barrier to nucleation in these compartment(s) can be significantly reduced to effect a primary nucleation event.
One of the main observations from the one-compartment and multi-compartment simulations, which was counter-intuitive, was the distribution of the crystals over the primary and secondary populations, wherein the primary class was found to be the more dominant population of the two. This could be an artifact of the simulation or from another perspective, this could as well be a matter of fact that primary nucleation plays a more dominant role in determining the process dynamics.
Validation of the model with experimental data, for the continuous evaporative crystallization of ammonium-sulphate from water, in 1100L DTB and 75L DT crystallizers, show that the inclusion of a primary nucleation event definitely increases the descriptive capability of the model, thus justifying the need for two interacting nucleation mechanisms. The simulation results give a very good description of the start-up phase of the crystallizer operation, the dynamics of the process as well as the final steady-state values.

Two secondary nucleation mechanisms with a dependency on supersaturation, viz. the embryo coagulation secondary nucleation (ECSN) proposed by Qian and Botsaris (Qian, 1997) and the surface nucleation mechanism proposed by Mersmann(1996), have been analyzed in Chapter 6 to explain the sustained cyclic behavior in DTB crystallizers. A two-population balance strategy was adopted to discriminate between competing nucleation mechanisms. The models equipped with the ECSN mechanism were not able to describe the oscillatory behavior as the dependence of ECSN on supersaturation turned out to be too weak. Surface nucleation yielded much better results and compartmental modelling approach using a two-compartmental model has been used to simulate a 1100L DTB crystallizer with a boiling zone that has a locally higher supersaturation. The surface nucleation bursts could exclusively be located into the boiling zone and the simulation results give a very good description of the start-up phase of the crystallizer operation, the dynamics of the process as well as the final steady-state values. This proves that even a small spatial region like the boiling zone can have a large influence on the dynamic behavior of evaporative crystallizers. Extension to a three compartmental model with a fines dissolver gave less severe oscillations.

To explain the phenomenon of growth rate dispersion (GRD), a new mechanism postulating the healing of a plastically deformed crystal due to GRD has been incorporated in a two-dimensional population balance equation model. This is the subject matter of Chapter 7. Besides the size of the crystals, also the strain in the crystal lattice has a pronounced effect on the growth rate of the individual crystals, justifying the need to include strain as an internal particle coordinate when modelling crystallization processes which involve secondary nucleation by attrition. Strain and size can be seen as two independent states of each particle, which change with time due to the release of strain by the

plastically deformed crystal. Healing, a phenomenon which describes the mechanism how a plastically deformed crystal releases it's strain, is assumed to be proportional to the strain and to the rate of change of either the length, the area, or the volume of the crystal. In this thesis, the healing mechanism is assumed to be more closely associated with the crystal surface area and thus, more of a surface related phenomenon, that is to say the lattice strain is not distributed uniformly over the entire volume of the crystal, but rather the strain is localized at the outer layers of the crystal where the deformation in the breakage process are the highest. The main consequence here is that not the entire attrition fragment dissolves at high strain energies but, rather the dissolution is restricted to the deformed crystal surface layer. This process leads to a reduction in the strain levels the crystal experiences, thus providing an opportunity to grow again, which is considered to be physically a more realistic scenario. The application of such a multi-dimensional growth model in a rigorous crystallization modelling tool enables the description of the steep upward curvature resulting from the higher content of fine particles and provides an interesting insight into the observed broadening of the crystal size distribution (CSD) due to GRD. Model validation by means of plant data for an evaporative crystallization process in a 22L DT crystallizer shows that healing of the strained fragments is proportional to the surface area of the crystals, which supports the hypothesis in this thesis.

The main findings of the research are summarized and evaluated with respect to the underlying research questions in Chapter 8.
The design research can proceed in two directions. Firstly, the ontology is a suitable platform to develop a computer-assisted synthesis tool for crystallization units. To this end, a structure model for generating superstructures is needed in combination with a technique for screening and selection of the better options. Secondly, the practical viability of this task-based approach and the results are to be proven by means of experimental programs in which small scale new designs are built and tested.
On the modelling front, some of the current simplifying assumptions can be relaxed and tested for practical significance. This can involve a more fundamental look at the role of strain in the crystals originating from primary and activated nucleation and the outgrowth of the attrited fragments. In addition, the interactions between fluiddynamics and particle kinetics can be refined. It is desirable to find a suitable compromise between the simple lumped compartment description and the extremely detailed CFD models.
Last but not the least, with the progress in molecular modelling, the number of product features to be considered in the modelling and simulation of product formation can be extended to cover lattice structure, morphology, crystal habit in addition to crystal size and lattice strain.

REFERENCES

Bermingham, S.K., Neumann, A.M., Kramer, H.J.M., Verheijen, P.J.T., van Rosmalen, G.M. and Grievink, J. (2000). A design procedure and predictive models for solution crystallization processes. *AIChE Symp. Series 323*, **96**, pp. 250-264

Bermingham, S.K. (2003a). *A Design Procedure And Predictive Models For Solution Crystallization Processes- Development And Application*, Ph.D. Thesis, Delft University of Technology, the Netherlands, ISBN 90-407-2395-8

Bermingham, S.K., Verheijen, P.J.T. and Kramer, H.J.M. (2003b). Optimal design of solution crystallization processes with rigorous models, *Trans. IChemE*, 81, part A, pp.893-903

Bermingham, S.K., Kramer, H.J.M. and Rosmalen van, G.M. (1998). Towards on-scale crystallizer design using compartmental models, *Computers and Chemical Engineering*, 22, pp.S355-S362

Kaschiev, D. (2000). *Nucleation: Basic Theory with Applications*, Butterworth-Heinemann Ltd. Oxford, U.K.

Mersmann, A.,(1996). Supersaturation and nucleation, *Trans. Inst. Chem. Eng.*, 74, pp. 812-820

Qian, R. and Botsaris,G. (1997). A new mechanism for nuclei formation in suspension crystallizers: the role of interparticle forces, *Chemical Engineering Science*, vol. 52, No. 20, pp.3429-3440

Rossiter, A.P. and Douglas, J.M. (1986). Design and optimization of solids processes. I: A hierarchical decision procedure for process synthesis of solids systems. *Chem. Eng. Res. Des.*, 64, pp.175-183

Wibowo, C., Chang, W., Ng, K.M. (2001).Design of Integrated Crystallization Systems, Vol. 47, No.11, *AIChE Journal,* pp.2474-2492

CONTENTS

1

General Introduction

Crystallization as a unit operation in chemical process industry is first introduced with regards to the applicability, advantages and problems encountered in practice. A motivation is given of the selection of design and modelling as research topics to enhance crystallization technology. Then a short review is presented in the form of a state-of-the-art in the modelling and design of industrial crystallization processes. This essentially builds up the platform for setting the objectives and scope of research for this thesis, which can be summarized as novel contributions to population balance modelling and a synthesis approach for industrial crystallization processes. The scope of this research is bounded by the nature of the chemical system, crystallization method, operation mode and crystallizer type.

1.1 INDUSTRIAL CRYSTALLIZATION

Crystallization is a well known and commonly used unit operation in the chemical process industry for a purification, separation, and/or production step. Crystallization can be carried out from a solution, vapor or melt. This thesis deals with applications involving crystallization only from the solution which is the most widely used crystallization method in the chemical industry. Crystallization is the formation of solid crystals from a clear solution, wherein the solubility characteristics of certain materials are exploited to produce particles of a very high purity. In modern chemical engineering parlance, it is a simultaneous heat and mass transfer process with a strong dependence on fluid and particle mechanics. Furthermore, it takes place in multiphase and multi-component systems, and is concerned with time-variant-distributed particulate solids that are rather difficult to characterize uniquely. In recent years, melt crystallization is receiving increased recognition as a purification technique for the production of ultrapure organic chemicals due to it's considerable energy savings and minimum problems regarding solvent recovery and waste disposal problems. In *solution* or *suspension* crystallization, mass transfer is the dominant effect in the process whereas heat transfer plays a dominant role in *melt* crystallization(Ulrich, 1992).

Crystallization is important as an industrial process because of the number of materials that are and can be marketed in the form of crystals with good handling properties. It's wide use is probably due to the highly purified and attractive form of a chemical solid which can be obtained from relatively impure solutions in a single processing step. In terms of energy requirements, crystallization requires much less energy (see Table 1.1) for separation than do distillation and other commonly used methods of purification. In addition, it can be performed at relatively low temperatures and on a scale that varies from a few grams up to thousands of tons per day. The most significant data in Table 1.1 are for water, where common applications of the process include the freeze concentration of fruit juices and desalination of sea-water for the production of potable water (Tavare, 1995).

Table 1.1 Energies required for crystallization and distillation (Tavare, 1995)

	Crystallization		Distillation	
Substance	Melting point (K)	Enthalpy of crystallization (kJ/kg)	Boiling point (K)	Enthalpy of vaporization (kJ/kg)
Water	273	334	373	2260
Benzene	278	126	353	394
o-Cresol	304	115	464	410
m-Cresol	285	117	476	423
p-Cresol	308	110	475	435
o-Xylene	248	128	414	347
m-Xylene	225	109	412	343
p-Xylene	286	161	411	340
o-Nitrotoluene	269	120	495	344
m-Nitrotoluene	289	109	506	364
p-Nitrotoluene	325	113	511	366

The economic potential and importance of crystallization is huge (Kirk-Othmer, 1987). Many specialty chemicals, such as pharmaceuticals, agrochemicals, pigments, dyestuffs, catalysts, zeolites, proteins, and food products, involve crystallization or precipitation as a crucial part of their manufacture, and usually require batch or semi-batch processing because of their low tonnage capacity.

Crystallization is applied in continuous operation on a large scale, for the bulk production of inorganic materials like potassium chloride (a fertilizer), sodium chloride, and ammonium sulphate (a fertilizer), and organic materials like adipic acid (a raw material for nylon), paraxylene (a raw material for polyester), and pentaerythritol (used for coatings).

On a small scale, crystallization is often applied batch wise to obtain high purity fine chemicals or pharmaceuticals, such as aspartame (a sweetener), L-serine (an amino acid), and L-ascorbine (vitamin C).

Another interesting area where crystallization finds useful application is in the field of biotechnology. For instance, crystallization can be used to determine the structure of both native and synthesized

therapeutically important proteins. It can also be used as a final purification step and as a stable form for protein storage.
In most of the above applications, crystallization is an important step in a process sequence, and therefore an increased emphasis on the better integration of this step into the associated upstream and/or downstream processing operations is needed. In addition, from a scientific persepctive, crystallization is a multidisciplinary subject: interactions with bordering disciplines like physical chemistry, chemical reaction engineering, and surface, material, mineral and biological sciences provide an important insight into this subject.

Crystallization has long been considered an art rather than a science, although recent theoretical discoveries and new analytical techniques have produced a change in this historic position. Despite its wide spread use and the long history of experience that exists in the chemical process industry, the design and operation of crystallization processes still pose many problems. In addition, there has been a shift from bulk towards fine chemistry and from base chemicals towards life-science products over the past decade. The majority of the products in these expanding branches of industry are particulate and crystalline. Whereas in the base-chemicals industry, usually low margin products are produced in dedicated large-scale continuously operated plants, in the fine-chemicals sector typically high-value added products are produced as small batches in multi-product plants. Especially, in this era of rapidly changing market demands, the bulk as well as the fine chemical products have to be produced in fast changing quantities and qualities. Summarizing, the current market is seeing a shift from:

- single-product to multi-product plants
- dedicated to simple general equipment with a multi-purpose use of crystallization process equipment
- equipment design to faster process development & product development technologies

for which the current market need is:

- to operate crystallization and downstream processes in an optimal and cost-efficient manner, in strongly fluctuating market conditions, at the same time meeting stringent product quality specifications
- to make use of fundamental physical models as knowledge "carriers" (knowledge management)
- to generate "master" model(s) that can be applied to a wide range of processes
- to focus on (model based) control of product quality

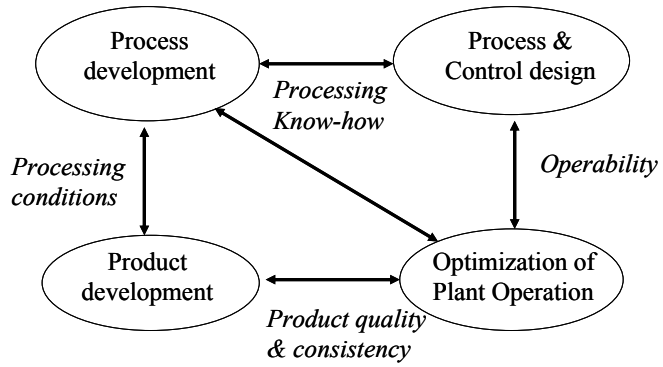

Figure 1.1 Interaction between technology and manufacturing activities in an industrial environment

The structuring of the technology and manufacturing activities as occurring in a business is depicted in Figure 1.1. This figure aims to show the business related activities in a company.
In order to cater to the above-mentioned market needs, it is very important to understand the relationship between process and product performance on the one hand and design and operational variables on the other. This can be realized if there is a sufficiently good process design model and also a systematic design procedure for the process development effort. The following section aims to give an overview on the state-of-the-art in the modelling and design of industrial crystallization processes.

1.2 STATE-OF-THE-ART : DESIGN AND MODELLING OF INDUSTRIAL CRYSTALLIZATION PROCESSES

For process design, scale-up and control purposes, much attention has been paid to modelling crystallization processes. Traditionally, population balance models play a major role in this field of research. These models describe the evolution of a population of crystals as a function of process conditions, compound and solvent properties and crystallizer type and layout. Parameters for these models are determined typically from lab-scale reactors of a few litres volume. A highly desirable feature for population balance models would be to use parameters obtained from laboratory experiments to model processes accurately at an industrial scale. One major issue that raises difficulties in proposing adequate population balance models is that the relation between crystallizer design, scale, operation, compound properties and the resulting product is highly non-linear in nature due to the complex interactions between rate processes determining the states of the crystal(s) and the fluiddynamics. Hence, it is still a challenge to arrive at a more general predictive and descriptive crystallization model and systematic design procedure, that covers a wide range of crystallization processes, operating modes and applicable to a variety of systems. Certain phenomena that are observed in industrial crystallization processes can still not be captured well by the existing models, let alone testing these rigorous models for predictive purposes.

1.2.1 Design

The process industry must respond to needs and expectations in society, involving increased sustainability of material cycles, competitive capital productivity, as well as higher customer expectations regarding product functionality and performance. To support this objective, effective and inventive design methods are needed, taking a product and process life – span perspective. The design of chemical process, including crystallization, is driven by needs for reduced investment costs, lower levels of energy consumption (e.g. reduced CO_2 emissions), ability to maintain consistent product quality and flexibility for multiple product grades. Over the last ten years in the field of chemical engineering for solids processes, systematic design procedures have been developed which mainly focus upon the synthesis and (economic) evaluation tasks of the design process (Rajagopal(1992), Dye and Ng(1995), Berry and Ng(1997)). Rossiter and Douglas (1986) and Ng(2001) discuss a systematic procedure for designing an integrated crystallization system by considering the interaction between crystallization and downstream processing. More recently, Bermingham(2000) proposed a systematic and hierarchical design procedure for improving the quality of both, the design of crystallization processes and the design process. This multi-level design procedure takes the interaction between product and process designs into account and covers the whole range from product design to the staging of compartments in a crystallization unit. At each level, it allows one to systematically and simultaneously deal with the large number of initial design specifications, design and operational variables and the wide variety of domain knowledge involved at any particular stage of the design process. The benefits of a structured approach to design provide:

- a useful platform for the experienced designer and a means of enhancing the expertise of the less experienced designer
- methods to enable the capture, storage and reuse of design process knowledge for complex, dynamic and often iterative processes, and flexibility to accommodate new technologies and design tools
- support for multiple alternative design tasks and guidance on the most appropriate ordering of tasks
- support for the integration of other design tools required for specific design tasks, thus providing an integrated design environment
- a useful, usable design environment which is cost effective to install and use

The strength of the design approach developed by Bermingham(2000,2003a) and extended by Westhoff(2002, 2004) with instrumentation and control design levels, is in the careful structuring of the decision making process and in covering the full range of conceptual design. While the design approach of Bermingham(2000) is a significant step forward in mapping out the entire design space and route, their fill-in of the design route is in a sense traditional by a strong focus on the design analysis steps. There is room for potential improvement at the synthesis level for a crystallization unit. Their synthesis approach is still based on a (traditional way of) thinking in geometric structures for equipment. A geometric compartment was taken as the basic building block for the synthesis of a multi-compartment unit and the resulting physical behavior is computed. The structuring of the compartments is not directly based on a functional approach of what the unit is supposed to do from a physical point of view. Meanwhile, in the chemical engineering design community, the task-based synthesis concept got off the ground - *the shape of the process equipment must follow from space-time demands of the sequence of physical tasks needed to transform the feed(s) into product(s)*, i.e. the equipment must facilitate the physical tasks that are needed for the unit operation, than the other way around. Hence, a more direct functional approach to process synthesis would start from the **physical task concept** and the specified processing duties. When the principle "form follows function" is applied, the required physical tasks and duties are supposed to shape the equipment structure. This task-based concept got a boost up in the late 90's when Eastman Chemical Company (Siirola 1995,1996) made its reactive distillation technology for methyl-acetate.

Such a fundamental approach, which is more synthesis-driven, is needed for process integration. It is the author's hypothesis that a task-based approach for the design of industrial crystallization processes could be helpful in getting more inventions (e.g. for process intensification). It seems that in current practice, when a process flow sheet is directly composed with conventional process equipment, chances for inventive solutions are missed. The task-based approach aims to create a wider solution space and ultimately arrive at innovative crystallization designs/configurations.

1.2.2 Modelling

Modelling of crystallization processes in this thesis, essentially aims at the development of a process modelling framework that can be used for generation, evaluation and optimization of design alternatives. The main focus will be on developing, testing and evaluating the predictive capability of this process model with respect to the influence of crystallizer geometry, scale, operating conditions and process actuators on the process behavior and product quality. The first challenge is to find an adequate de-coupling between fluiddynamics and kinetics while the second challenge which is an inverse problem, is to validate these models by means of experimental data. These challenges stem from a lack of physical understanding of the relevant kinetic processes occurring within the crystallizer. A simulation tool enabling optimization and experimental design for a wide range of crystallization processes will maximize the added value in production by enabling market responsive plant operation. Such a simulation/modelling tool can find application[1] in the following areas:

- Analysis of process design
- Optimization of process design
- Optimization of process operation
- Process performance monitoring
- Analysis of control procedure(s)
- Operator training
- Model reduction for advanced process control (APC) algorithms

Continuous crystallization plays a vital role in the production of many particulate chemicals ranging from table salt to fertilizers. Decreasing margins for bulk chemicals necessitate the design of

[1] Generally, simplified or reduced design models for process synthesis would definitely find a mention in this list. But, in crystallization, that stage has not yet been reached where crystallization processes can be designed from a synthesis perspective. This thesis aims to address process synthesis from a conceptual stand-point which is the subject of Chapter 2.

economically optimized plants. Unfortunately, continuous crystallization processes often exhibit a poorly damped dynamic behavior. Also, for some crystallizers a drift off during operation to an oscillatory state has been reported (Randolph, 1977). These oscillations lead to variations of the crystal size distribution (CSD) and the mean particle size over time. Since mean particle size and CSD are key factors to the product quality, cost intensive reworking of the product is often necessary.
Grosch(2003) considered the stability and the ability to reject disturbances of the process during the design phase. Here, an integrated design and control problem was formulated as an optimization problem that includes an economic objective function and constraints that rigorously guarantee a desired performance of the closed-loop process. Doing so enabled the identification of an economically optimum operating point and the best possible tuning of the controller. Additionally, bottlenecks in terms of the constraints and the controller could be identified.

Previous research studies within Delft (Neumann(2001), Bermingham(2003a) & Westhoff (2002)) approached this problem more from a design perspective, aiming at arriving at a comprehensive process modelling framework that could explain these dynamic behavior in industrial crystallization processes. Their studies concluded that there were areas where significant improvement can be expected by inclusion of certain kinetic mechanisms in the process model, which can boost the predictive and descriptive capabilities of the design model. The primary areas, which need improvement with regards to the descriptive quality of the models were identified as follows :

- Sustained cyclic behavior observed in the case of continuous evaporative crystallization of ammonium-sulphate from water in DTB crystallizers (see Figure 1.2).
- Broadening of the crystal size distribution (CSD) and the steep upward curvature observed at low size classes in the semi-log plot of population number density vs crystal size (see Figure 1.3).

The sustained cyclic behavior is believed to be due to the lack of adequate/proper nucleation mechanisms in the modelling framework. The broadening aspect and the steep upward curvature has been attributed by several authors to improper modelling of *growth rate dispersion* (GRD) or absence of mechanisms(in the modelling framework) which take into account the phenomenon of GRD.

The modelling architecture approaches the problem from a *process design* perspective, with in-depth modelling using population balances along with the mass and energy balance equations. These models can account for a detailed study of the fluiddynamics in three-phase slurries (which can be done using Computational Fluid Dynamics, for example) (Urban(1999), ten Cate(2000), Kougoulos(2005), PSE). But at the same time, the rigorous dynamic process model can be reduced (by model reduction and model linearization techniques) to suit studies for control applications, where an accurate estimate of the kinetics may not be required. Again, simplified models can be used as a start in the task-based design approach that was discussed in the earlier section.

Sustained cyclic behavior
A major problem with many continuous industrial crystallization processes is the occurrence of crystal size distribution (CSD) oscillations (Eek, 1995), inspite of the fact that the system might be at steady-state as regards the energy and material balances. The dynamics in the CSD can be a result of disturbances (feed changes, blockages, utility failures), changes in operating conditions (start-up, shut-down, grade changes), or simply the fact that the process is open loop unstable (Bermingham, 2003).
With a cycling CSD periodically (see Figure 1.2), an excessive number density of fine crystals will be present in the product, which can severely hamper solid-liquid separation processes further downstream (eg. filtration) and can result in equipment fouling, caking, etc. All these problems and bottlenecks can cause significant production losses and lower the yield.
An extensive study has been done by Bermingham(1998, 2003a)on the development of a rigorous model framework for a wide range of crystallization processes and crystallizers.

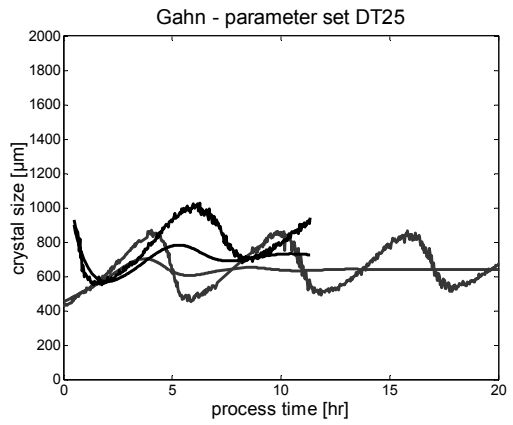

Figure 1.2 Fit between simulated and experimental data for a 1100L DTB continuous crystallization process (Bermingham, 2003)

These predictive crystallizer models give a reasonable prediction of the median crystal size and the overall dynamic trend, but exhibits one significant shortcoming: the inability to predict the very pronounced and in some cases even sustained oscillations of the product CSD (Neumann, 2001) in a 1100L DTB crystallizer, when using kinetic parameters obtained from an experiment performed on a 22L draft-tube (DT) crystallizer. The system studied was the continuous evaporative crystallization of ammonium-sulphate from water. At this stage, it is not clear whether this inability is a result of the uncertainties surrounding the parameter estimates or whether it is intrinsic to the structure of the kinetic model.

As suggested by Farrell (1995), the sustained oscillatory behavior observed in DTB crystallizers could arise due to the locally distributed supersaturation within the crystallizer, which reaches its peak in the boiling zone. The consequence could be a spontaneous primary nucleation event here. Primary nucleation requires relatively high supersaturation levels and regions with poor mixing properties can have a locally higher supersaturation, say for example, the boiling zone of the crystallizer. It has been confirmed that high supersaturation levels are present in foam layers of industrial evaporative crystallizers and as a result excessive crystal scaling is often found at the liquid level on the vessel wall.

Growth Rate Dispersion

GRD is the phenomenon wherein crystals of the same size and material exhibit a variation in crystal growth rates, under identical global conditions of supersaturation, temperature and fluiddynamics. Why such crystals should exhibit a wide distribution in growth rates from zero to some maximum value is not fully understood. What is known is that GRD has a significant influence on the crystal size distribution (CSD) of the crystalline product in industrial crystallizers, especially in the low size range. The consequence of GRD is an increase in the number of small, slow growing crystals (Daudey, 1987) and therefore, a reduction of the mean particle size. This results in a steep upward curvature in the low size class range as shown in Figure 1.3.

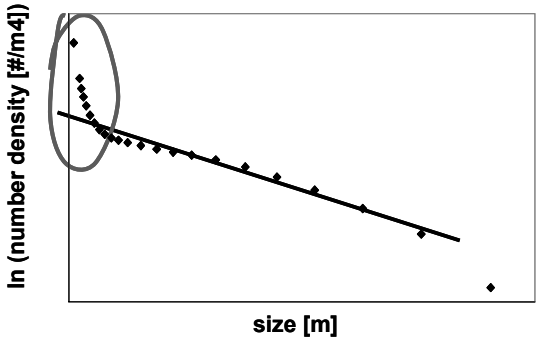

Figure 1.3 Semi-logarithmic plot of population number density vs crystal size

Many theories can be cited in literature which explain this phenomenon of GRD. The prominent amongst them attribute GRD to the dislocation structure of individual crystals and varying degrees of strain in the crystal lattice (Ristic, 1990, Van der Heijden, 1992, Zacher and Mersmann, 1995, Herden (1997)). Variation in the number of dislocations at the surface of secondary nuclei, induced by the formation process was reported to explain the observed differences in the growth rate (Berglund and Larson, 1982), (Bhat, 1987). For the sodium nitrate growth rate distributions, integral strain and dislocations have both been cited (Jones, 2000) as determining factors of crystal growth rates. Gahn and Mersmann (1999a;1999b) presented a size-dependent growth model

(SDG), which correlates the strain in the crystal lattice to the driving force for crystal growth. But this SDG model has it's limitations, such as dissolution of small crystals and unsatisfactory description of the broadening of the CSD in growth experiments (Westhoff, 2002). More recently, Gerstlauer (2001) presented a two-dimensional population balance model, in which the growth is dependent on the crystal length and the internal lattice strain of the individual crystals. Strain and size can be seen as two independent states of each particle, which change with time due to the release of strain by the plastically deformed crystal.

1.3 RESEARCH OBJECTIVES, APPROACH & SCOPE OF THESIS

In view of the above-mentioned problems and challenges that still exist in the design, operation and control of industrial crystallization processes, the following overall objectives have been defined for the multi-disciplinary research project (CrysCODE®, Delft University of Technology (2001-2005)) as a whole:

- *integration of the state-of-the-art knowledge into a full-scale design and control procedure for industrial crystallization processes*
- *development of procedures for the modelling, monitoring, manipulation and optimization of batch crystallization processes*

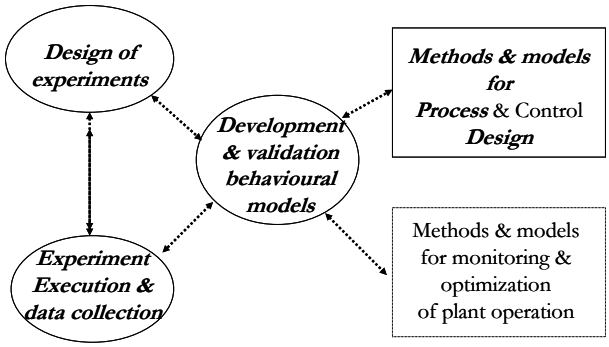

Figure 1.4 Knowledge development activities within a process engineering research environment

Figure 1.4 shows the knowledge development activities as conducted in a process engineering research project (among which CrysCODE® falls). The CrysCODE® project is a co-operation between different research groups at the Delft University of Technology and several industrial partners. This work is aimed at the (further) development of a rigorous modelling framework for design and optimization of industrial crystallization processes, the extension and development of a hierarchical task-based design procedure for the synthesis and optimization of the process, the detailed equipment and the optimal operation conditions. The three participating groups from the Delft University of Technology in this research program are the chairs of Separation Technology, Process Systems Engineering and the Systems & Control group. Cristiana Virone (PhD student on crystallization technology) focuses on the fundamental aspects of crystallization mechanisms and the development of novel technologies to influence the crystallization process. Abhilash Menon (PhD student on design and modelling) focuses on the development of novel design procedures and modelling approaches to build up a rigorous modelling and analysis design tool. Alex Kalbasenka (PhD student on control) looks into the control aspects related to crystallization processes. The industrial partners who financially supported this research program were : Ajinomoto (Japan), Akzo Nobel (the Netherlands), BP (USA), DSM (the Netherlands), Purac Biochem (the Netherlands) and Solvay (Belgium). A more detailed overview on the history of the crystallization research at Delft University of Technology can be found in Appendix A1.1.

In line with the overall research objective for the CrysCODE® project, the objectives and scope of research for this thesis is now summarized as follows:

development of

- *a novel design procedure enabling a task-oriented approach for the synthesis of innovative crystallizer configurations*
- *novel modelling strategies for industrial crystallization processes to predict the product quality and process performance as a function of the crystallization method, operation mode, equipment type and scale of operation, and operating conditions*

These objectives are further split into sub-objectives as follows:

- *development of a novel conceptual task-based design ontology for general industrial crystallization processes, which combines the knowledge available from literature with that gathered within the UNIAK project, to extend the systematic design procedure, particularly with respect to the synthesis phase of the design*

  We will limit ourselves to the hierarchical design platform of Bermingham(2000) (see Figure 1.5) and largely focus on the level at which the crystallization stages and compartment configurations are designed. For this level, the first step of a synthesis technique is developed.

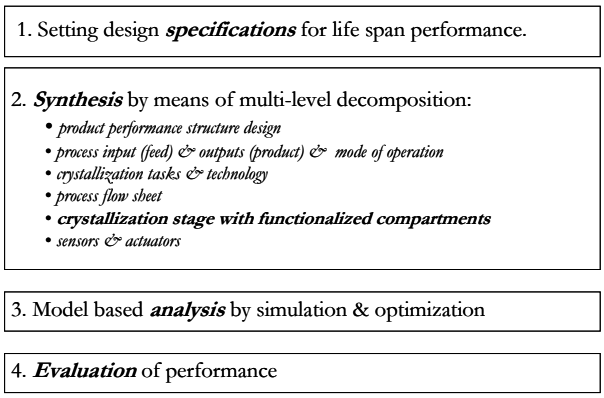

Figure 1.5 Steps in a design platform for a crystallization process

Any synthesis technique comprises of four elements:

i. An ontology, describing the objects and their features as used for synthesis;
ii. A structure model governing how objects can be connected;
iii. A synthesis technique (e.g. by use of heuristic rules and/or by mathematical optimization) to generate alternative structures;
iv. A behavioral model describing the physical behavior of a structure;

Chapter 2 actually delivers the 'ontology' of such a task-based design and the elements for the structural and the behavioral models. The ontology is the meta-model needed for any implementation of the design procedure in a computer-assisted synthesis tool. It must be pointed out that an implementation has not been realized yet; let alone the testing of the effectiveness of the synthesis technique. The development of the ontology is already a significant conceptual challenge. The full development of a synthesis procedure will be the subject of future research in the design of crystallization equipment.

- *experimental study of the effect of different actuators on product quality for batch crystallization processes, on crystallizers of different scale and type and subsequent validation of the rigorous crystallizer models*

  With regards to the availability of plant data for batch crystallization processes, there is lot of experimental data available in open literature, on dedicated studies for different crystallization

mechanisms like growth, nucleation, agglomeration, etc. However, dynamic process data for experiments done using a particular system, under different process conditions and crystallizers of different scale and type, is very scarce. This is even more so the case for plant data on (semi-) industrial scale equipments. For crystallization, the properties of the final product result not only from the chemical and thermodynamic properties of the compound to be crystallized, but also from the fluiddynamics, other possible actuators(eg. fines removal system) and the crystal-hardware interactions, either directly or through the kinetic processes of nucleation, growth, attrition, and agglomeration. In order to investigate all these effects on product quality, batch experiments are performed for the evaporative unseeded crystallization of ammonium sulphate from water in (semi-)industrial scale crystallizers. The 1100L DTB and 75L DT crystallizers are used to study the scale and type effects with the primary actuators being the heat input, mixing conditions and fines removal rate. Dynamic parameter estimation studies are then performed using these experimental data to estimate relevant kinetic parameters.

- *improving the descriptive capability of the rigorous crystallizer models for continuous crystallization processes, mainly focussing on two areas:*

  - **Sustained cyclic behavior observed in DTB crystallizers**
    A novel approach is investigated, to improve the description of the dynamic behaviour of industrial DTB crystallizers, using a two population balance model to discriminate between different nucleation mechanisms and subsequent growth rates. The primary nucleation models from classical nucleation theory (Kashchiev, 2000) and some activated secondary nucleation models from literature (Mersmann (1996) and Qian & Botsaris (1997)) are used as the primary candidates to test this hypothesis, as all these mechanisms have a strong dependency on supersaturation. These mechanisms are in addition to the attrition model for secondary nucleation developed by Gahn & Mersmann (1999a,b).
    The distinction between primary and secondary nuclei in the modelling framework is realized by using two different growth rate expressions within the dispersed phase. The total crystal population is split up into two distinct and interacting populations, one representing the primary (no strain) population of crystals and the other, the secondary (strained) population, with a uni-directional transition from the unstrained population to the strained population.

  - **CSD broadening effects and steep upward curvature due to GRD**
    The product quality cannot be solely defined in terms of chemical and phase composition. A crystalline product is also characterized by its size distribution, morphology, polymorphism and the amount of strain as well as the uptake of solvent or impurities in the crystal lattice. In continuous crystallization processes of well soluble compounds, eg. the evaporative crystallization of ammonium-sulphate from water, it is generally assumed that secondary nucleation and growth rate are the dominant kinetic phenomena (Bermingham(2003), Gahn & Mersmann (1999a,b)). In this model, the secondary nuclei are formed as a result of collisions of the crystals with the impeller (attrition) and are characterized by the presence of a certain amount of lattice strain which severely affect the growth behaviour of these nuclei. This has been regarded as one of the chief causes of growth rate dispersion and hence, it is very important to consider the strain effects on the growth and healing of strained crystals. Modelling-wise, this is made possible by making use of a two-dimensional population balance equation wherein, strain and size are seen as two independent states of each particle, which change with time due to the release of strain by the plastically deformed crystal. For this purpose, dynamic simulation studies on industrial-scale crystallizers for the continuous crystallization of ammonium-sulphate from water are examined.

Scope of thesis

Crystallization as such is a very broad discipline and encompasses a variety of ways in which crystallization can be conceived. This is especially true when one thinks about the method of crystallization, the different equipment configurations possible, the operating modes, etc. Hence, to narrow down the applicability and relevance of this research in the general field of industrial crystallization, the scope has been defined as follows:

- Chemical system: Crystallization of relatively well-soluble substances will be under investigation, eg. $(NH_4)_2SO_4$, KNO_3, etc.
- Crystallization method: This is the method employed to generate supersaturation, which is very system specific. In this research, crystallization by evaporation of solvent will be mainly considered.
- Operating mode: Both, batch and continuous operation will be considered.
- Crystallizer type: Experimental studies will employ the 75L draft-tube and 1100L draft-tube baffle crystallizers which can be operated in batch/continuous mode.
- Product quality aspects: The crystal size distribution (CSD) which is one of the yardsticks for measuring the product quality, will be taken as the means to measure the product quality characteristics.
- Crystallization process unit as key object of design, (ignoring higher levels of aggregation, like integration with down stream processing & plant wide heat integration & control)

1.4 STRUCTURE OF THE THESIS

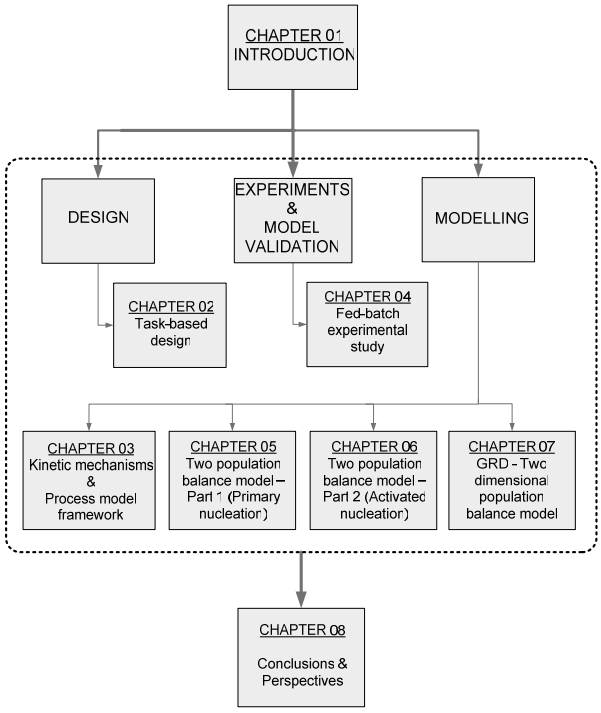

Figure 1.6 Thesis tree-diagram

Figure 1.6 represents a tree-diagram of the structure of this thesis. Chapter 2 largely contributes to the development of a synthesis method for a crystallization unit, with the aim to reduce cost of resources and capital, and possibly leading to process intensification.

Chapter 3 gives a brief summary of the crystallization mechanisms relevant to this thesis and also the process modelling framework used for the dynamic simulation studies.With a view to understanding batch crystallization technology better, fed-batch experiments performed on the (semi-)industrial scale crystallizers, for the crystallization of ammonium-sulphate from water, are discussed in Chapter 4. Chapter 5 and Chapter 6 introduce the concept of the two-population balance model approach, in order to explain the sustained oscillatory response observed in the case of DTB crystallizers. Chapter 5 specifically looks into the use of a primary nucleation rate expression from classical nucleation theory while Chapter

6 discusses the use of activated secondary nucleation mechanisms. Chapter 7 deals with the phenomenon of growth rate dispersion wherein a two-dimensional population balance model is developed which embeds within it, the crystal size and crystal lattice strain as two internal coordinates. Finally, Chapter 8 winds up this thesis and presents the important conclusions from this research and an outlook towards future investigation(s) in the area of industrial crystallization.

Abbreviations

CrysCODE	Crystallizer Control and Design
UNIAK	Universele Instrumentatie en Automatisering van Kristallisatoren (A Dutch acronym which stands for Universal Instrumentation and Automation of Crystallizers)
DTB	Draft Tube Baffle Crystallizer
DT	Draft Tube Crystallizer
CSD	Crystal Size Distribution
GRD	Growth Rate Dispersion

REFERENCES

Berglund, K.A. & Larson, M.A. (1982). Growth of contact nuclei of citric acid monohydrate, *AIChE Symposium series*, 78, 215, 9

Bermingham, S.K., Neumann, A.M., Kramer, H.J.M., Verheijen, P.J.T., van Rosmalen, G.M. and Grievink, J. (2000). A design procedure and predictive models for solution crystallization processes. *AIChE Symp. Series 323*, **96**, pp. 250-264

Bermingham, S.K. (2003a). *A Design Procedure And Predictive Models For Solution Crystallization Processes- Development And Application*, Ph.D. Thesis, Delft University of Technology, the Netherlands, ISBN 90-407-2395-8

Bermingham, S.K., Verheijen, P.J.T. and Kramer, H.J.M. (2003b). Optimal design of solution crystallization processes with rigorous models, *Trans. IChemE*, 81, part A, pp.893-903

Bermingham, S.K., Kramer, H.J.M. and Rosmalen van, G.M. (1998). Towards on-scale crystallizer design using compartmental models, *Computers and Chemical Engineering*, 22, pp.S355-S362

Berry, D.A. and Ng, K.M. (1997). Synthesis of reactive crystallization processes, *AIChE Journal*, 43, pp.1737-1750

Bhat, H.L., Sherwood, J.N., Shripathi, T. (1987). The influence of stress, strain and fracture of crystals on the crystal growth process, *Chemical Engineering Science*, 42, pp.609-618

Daudey, P.J. (1987). *Crystallization of Ammonium Sulphate, secondary nucleation and growth kinetics in suspension*, PhD Thesis, Delft University of Technology, The Netherlands

Dye, S.R. and Ng, K.M. (1995). Fractional crystallization: design alternatives and tradeoffs, *AIChE Journal*, 41, pp.2427-2438

Eek, R.A., Dijkstra, S. and van Rosmalen, G.M. (1995). Dynamic modeling of suspension crystallizers, using experimental data, *AIChE Journal*, 41 (3), pp.571-584

Farrell, R.J., Belokovskiy, A., Bennett, D. (1995). Simulated oscillations and control strategy for an ammonium sulfate DTB crystallizer, *AIChE Annual Meeting*, Miami beach, Florida, Nov.12-17, Paper 12e

Gahn, C. & Mersmann, A. (1999a). Brittle fracture in crystallization processes Part A: Attrition and abrasion of brittle solids, *Chemical Engineering Science*, 54, pp.1273-1282

Gahn, C. & Mersmann, A. (1999b). Brittle fracture in crystallization processes Part B: Growth of fragments and scale-up of suspension crystallizers, *Chemical Engineering Science*, 54, pp.1283-1292

Gerstlauer, A., Mitrovic, A., Motz, S., Gilles, E.D. (2001). A population model for crystallization processes using two independent particle properties, *Chemical Engineering Science*, 56, pp. 2553-2565

Grosch, R.; Mönnigmann, M. & Marquardt, W. (2003). Integrated robust optimal design and control of an MSMPR crystallization process, *AIChE Annual Meeting 2003*, San Francisco, USA, 16-21 Nov

Heijden, A.E.D.M. & Van der Eerden, J.P. (1992). Growth Rate Dispersion: The role of lattice strain, *Journal of Crystal Growth*, 118, pp. 14-26

Herden, A., and Lacmann,R. (1997). The crystallization of potassium nitrate II. Growth rate dispersion, *Journal of Crystal Growth*, 179, pp.592-604

Jones, C.M., Larson, M.A., Ristic, R.I., Sherwood, J.N. (2000). The role of dislocations, integral strain, and supersaturation on the growth rates of sodium nitrate, *Journal of Crystal Growth*, 208, pp. 520 – 524

Kaschiev, D. (2000). *Nucleation: Basic Theory with Applications*, Butterworth-Heinemann Ltd. Oxford, U.K.

Kirk-Othmer, *Encyclopaedia of Chemical Technology*, John Wiley & Sons, New York, 1987

Kougoulos, E., Jones, A.G., Wood-Kaczmar, M.W. (2005). CFD modelling of mixing and heat transfer in batch cooling crystallizers : Aiding the development of a hybrid predictive compartmental model, *Chem. Engg. Res. and Des.*, 83(A1), pp.30-39

Mersmann, A.,(1996). Supersaturation and nucleation, *Trans. Inst. Chem. Eng.*, 74, pp. 812-820

Neumann, A.M.(2001).*Characterizing industrial crystallizers of different scale and type.* PhD Thesis, Delft University of Technology, Delft, the Netherlands, ISBN 90-6464-882-4

PSE, Hybrid Multizonal gPROMS-CFD: High-precision multizonal gPROMS models with automated CFD coupling, http://www.psenterprise.com/gproms/hybrid multizonal.html

Qian, R. and Botsaris,G. (1997). A new mechanism for nuclei formation in suspension crystallizers: the role of interparticle forces, *Chemical Engineering Science*, vol. 52, No. 20, pp.3429-3440

Rajagopal, S., Ng, K.M. and Douglas, J.M. (1992). A hierarchical procedure for the conceptual design of solids processes. *Computers and Chemical Engineering*,, 16, pp.675-689

Randolph,A., Beckmann, J. and Kraljevich, Z. (1977). Crystal size distribution dynamics in a classified crystallizer. *AIChE Journal*, 23, pp.500–509

Ristić,R.I., Sherwood, J.N., Shripathi, T. (1990). Strain variation in the growth sectors of potash alum single crystals and it's relationship to growth rate dispersion, *Journal of Crystal Growth*, 102, pp.245-248

Rossiter, A.P. and Douglas, J.M. (1986). Design and optimisation of solids processes. I: A hierarchical decision procedure for process synthesis of solids systems, *Chem. Eng. Res. Des.*, 64, pp.175-183

Siirola, J. J. (1995). An industrial perspective on process synthesis, 4*th International Conference on Foundations of Computer-Aided Process Design (FOCAPD), AIChE Symp. Series*, 91 (306), pp.222 – 233

Siirola, J. J. (1996). Industrial applications of chemical process synthesis, *Advances in Chemical Engineering,* 23, pp.1 – 92

Tavare, N.S. (1995). *Industrial Crystallization : Process Simulation Analysis and Design*, Plenum Press, New York

Ten Cate, A., Bermingham, S.K., Derksen, J.J., Kramer, H.J.M. (2000). Compartmental modelling of an 1100L DTB crystallizer based on Large Eddy flow simulation, *10th European Conference on Mixing*, Delft, the Netherlands

Ulrich, J. (1992). Melt Crystallization, In A.S.Myerson, editior, *Handbook of Industrial Crystallization*, chapter 7, pp.151-163, Butterworth-Heinemann, Boston

Urban, Z and Liberis, L. (1999). Hybrid gPROMS-CFD modelling of an industrial scale crystallizer with rigorous crystal nucleation and growth kinetics and a full population balance, *Chemputer 99 Conference*, Dusseldorf

Westhoff, G.M.(2002). *Design and analysis of suspension crystallizers: Aspects of crystallization kinetics and product quality*, PhD Thesis, Delft University of Technology, the Netherlands, ISBN 90-6464-138-2

Westhoff, G.M., Kramer, H.J.M., Jansens, P.J. and Grievink, J. (2004). Design of a multi-functional crystallizer for research purposes, *Chemical Engineering Research and Design*, 82(A7), pp.865-880

Wibowo,C., Chang,W., Ng, K.M. (2001). Design of Integrated Crystallization Systems, Vol. 47, No. 11 *AIChE Journal*, pp. 2472-2492

Zacher, U., Mersmann, A. (1995). The influence of internal crystal perfection on growth rate dispersion in a continuous suspension crystallizer, *Journal of Crystal Growth*, 147, pp.172-180

2

A task-based approach to the design of crystallization processes†

The design of solid state processes and in particular crystallization processes have been the subject of past academic and industrial research. Systematic procedures for designing an integrated crystallization system were developed, considering the interactions between product and process as well as between crystallization and downstream processing. The research presented in this Chapter takes the hierarchical procedure of Bermingham (2000) as the reference. This hierarchical multi-level design procedure covers the whole range from product design to the staging in a crystallization unit, leading to a decomposed sequence of smaller size design problems with increasing amount of detail when proceeding from level to level.

Here, a novel task-based procedure is proposed to improve the conceptual design at the level of a solution crystallization process unit. The aim is to reduce cost of resources and capital, and possibly lead to process intensification. The physical task concept is chosen to facilitate a more synthesis-focused, functional approach, as an alternative to the traditional way of thinking in geometric structures for existing equipment. The synthesis approach is to represent a crystallization unit as a structured set of basic functions (tasks) each of which transforms the physical state of matter from an initial state to some final desired target state by means of physical event(s). These tasks can be connected in a network to accomplish the transformation of the feed into the product within quality specifications. The main thrust in this chapter is to develop the conceptual building blocks for this task-based approach (ontology), along with behavioral models for the tasks. The ontology is a necessary step towards a structure model for generating design alternatives via a superstructure. Since a task network is coupled with behavioral models of physical events, it can also be used in a process-modeling environment for synthesis, analysis and optimization studies.

† Parts of this chapter have been submitted for publication in Industrial & Engineering Chemistry Research (2006)

2.1 INTRODUCTION

The process industry must respond to needs and expectations in society, involving increased sustainability of material cycles, competitive capital productivity, as well as higher customer expectations regarding product functionality and performance. In this respect, crystallization is gaining increasing importance for the process industry with a wider range of structured products (Wintermantel(1999)). The process industry can increase its performance by making better designs, both for products and processes taking a life span perspective. Within such a perspective, the design approach should provide:

- a useful platform for the experienced designer and a means of enhancing the expertise of the less experienced designer;
- methods to enable the capture, storage and reuse of design process knowledge for complex, dynamic and often iterative processes, and flexibility to accommodate new technologies and design tools;
- support for multiple alternative design decisions and guidance on their most appropriate ordering;
- support for the integration of other design tools required for specific design tasks, thus providing an integrated design environment;
- a useful, usable design environment, which is cost effective to install and use.

Any design approach involves the engineering ways and methods by means of which a process design is made as well as the organization and management of the design process. Both contribute significantly to the success of a design approach. For instance, Heller(2004) presents a system, which supports the management of dynamic and inter-organizational design processes by providing a delegation-based approach for coordinating distributed design processes in which multiple enterprises are involved. This is more related to *organizational tasks*. The focus in this chapter will be on the engineering dimension of design. It is assumed that a well-structured engineering design process is also beneficial to the management and organization of the design process.

In the field of chemical engineering for solids processes, systematic design procedures have been developed which mainly focus upon the synthesis and (economic) evaluation tasks of the design process (Rajagopal(1992), Dye and Ng(1995), Berry and Ng(1997)). More dedicated to crystallization, Rossiter and Douglas (1986) and Wibowo(2000, 2001) discuss a systematic procedure for designing an integrated crystallization system by considering the interaction between crystallization and downstream processing. Along this line, Bermingham (2000,2003a) and Westhoff (2002,2004) proposed systematic design procedures for improving the quality of both, the design and the design process of crystallization processes. Their design procedures are focused on the core crystallization process (no down stream) with due attention to the interaction with product design and the consideration of instrumentation and control. These design procedures are hierarchically structured, allowing one to systematically deal with the large number of initial design specifications, design and operational variables and the wide variety of domain knowledge involved, descending from one level to the next one, while increasing the amount of detail.

Parallel to the developments in the design of crystallization processes, more generic improvements have been achieved in the design approaches to chemical manufacturing process in general. These improvements are the result of application experiences in industry as well as of academic research. One of the more remarkable developments is the recent attention to integrated and intensified process units (e.g., for reactive separations). In process design, the conventional unit operations have been traditionally used as standard building blocks. While the dimensions (geometry) of the units can vary from case to case, the underlying processing function and architecture remain invariant. Using such concepts as building blocks prohibits the invention of novel integrated processing operations. In order to achieve such inventions, a finer and more modular building block than a unit operation is needed

(Siirola, 1996) from which such an integrated unit can be synthesized. The chief drawback (weakness) of today's design approaches is their focus on analysis (see Figure 2.1 for the distinction between synthesis and analysis). The synthesis seems to be limited to the selection of existing type of process unit equipment and hardware. The degrees of freedom left to improve the performance of the process plant are the optimization of the operating conditions, the integration of heat and mass exchanges between units and the options for plant-wide control. It is noticed that the selection of the process unit equipment determines the way in which the physical processes are conducted. Ideally, it should be the other way around. Rather the equipment must facilitate the *tasks* that are needed for the unit operation. So, it seems that in current practice, when a process flow sheet is directly composed with conventional process equipment, chances for inventive solutions are missed. This will require a new approach to the process (unit) synthesis step.

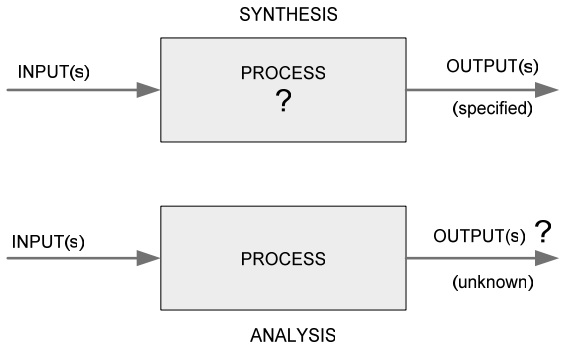

Figure 2.1 Difference between Synthesis and Analysis (after Doherty and Malone, 2001)

This new building block for process synthesis is the *physical task* concept, which is an abstract building block. A physical task aims to accomplish the transition of a target process variable (composition, temperature, phase, ..) from an initial state to a desired state, enabled by suitable physical phenomena. This task concept allows for finer resolution in process synthesis than with the classical unit operations building block. The objective would be to identify relevant tasks and associated physical mechanisms needed to achieve the desired processing objective while satisfying the constraints at hand. The task-based design approach has the credo "*form follows function*" firmly embedded within it. The task-based approach aims to create a wider solution space. This task based concept got a practical boost up in the late 90's when Eastman Chemical Company made its reactive distillation technology for Methyl Acetate (Siirola (1995,1996)). Such a fundamental approach is needed for process integration.

When carrying this perspective over to crystallization processes, we notice that the strength of the design approach developed by Bermingham(2000), extended by Westhoff(2004) with instrumentation and control design levels, is in the careful structuring of the decision making process and in covering the full range of conceptual design. While the design approach of Bermingham(2000) is a significant step forward in mapping out the entire design space and route, their fill-in of the design route is in a sense traditional by a strong focus on the design *analysis* steps. There is room for potential improvement at the synthesis level for a crystallization unit. Their synthesis approach is still based on (a traditional way of) thinking in geometric structures for equipment. A geometric compartment was taken as the basic building block for the synthesis of a multi-compartment unit and the resulting physical behavior is computed. The structuring of the compartments is not yet directly based on a functional approach of what the unit is supposed to do from a physical point of view.

The synthesis of new structures of crystallization processes by means of a task-based approach would be rather ineffective if the behaviour of the new structures could not be easily modelled and analyzed by the aid of predictive simulations. The current state-of-the-art in the modelling of crystallization populations and rate processes effecting the population will allow for a more modular approach to the synthesis step in design.

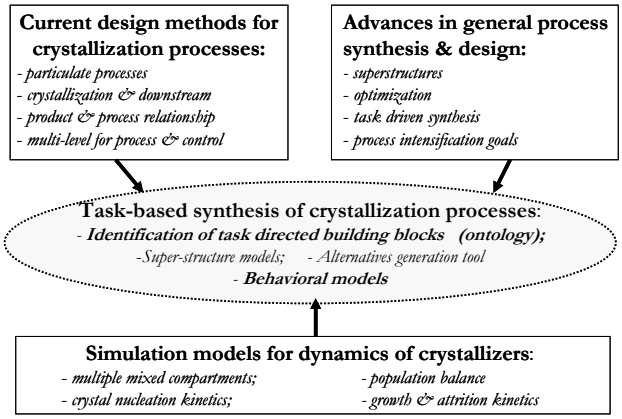

Figure 2.2 Roadmap for the design research in this thesis

The roadmap to the design research in this thesis is shown in Figure 2.2, depicting the influences from crystallization design, developments in process synthesis and in modelling of crystallization processes. The core of the design research will be a procedure for task-based synthesis of a crystallization unit.
It is the author's hypothesis that this generic and abstracted view on physical tasks could be helpful in getting more inventions (e.g. for process intensification). For crystallization process design, the research goal and hypothesis reads as follows:

> "To contribute to the development of a synthesis method for a crystallization ***unit***, with the aim to reduce cost of resources and capital, possibly leading to process intensification. The key assumption is that creative thrust is gained by taking a physical task driven approach, in which the equipment form (structure) and behavior will follow from the required functions. A novel ontology[1] for this design approach is developed, specifying the properties of the conceptual (physical) task-directed building blocks to be used for synthesizing the unit structure and its behavior. "

For crystallization, the task-based approach to be developed in this thesis can be regarded as the first attempt towards *process intensification*[2] in this area. It must be mentioned however, that process intensification is not the main goal of this exercise, but rather it must be visualized as more of a product of this exercise arising due to the prevention of loss of valuable resources like money (cost reduction), mass and energy efficiencies, etc.

Concerning the approach to the development of a physical task-based synthesis it is the hierarchical multi-level approach proposed by Bermingham(2000) and Westhoff(2004) that remains the reference design procedure. It is only the level of process unit design that is being addressed by means of this more fundamental approach, aimed more at getting control over the ordering of the physical events in a crystallization stage. The sections 2.2 and 2.3 review this multi-level design hierarchy and provide an extension at the level of the flow sheet design for a crystallization process in terms of a potential application of superstructures. The main contribution is at the level for a crystallization stage (unit) in section 2.4, where the ontology of the building blocks for a physical task-based synthesis is presented.

---

[1] Ontology is an explicit specification of the conceptualization, in this case of the conceptual building blocks needed for the task-based approach. The term ontology as we use it here is taken from the field of computer science (artificial intelligence) rather than from its original root in philosophy, dealing with the fundamental categories of being or existence. In our situation, the ontology provides the vocabulary for the task-based synthesis.

[2] *Process intensification*, as it is widely understood nowadays, comprises novel equipment, processing techniques, and process development methods that, compared to conventional ones, offer substantial improvements in (bio)chemical manufacturing and processing (Stankiewicz, 2004).

Such a specification of the available building blocks for synthesis by means of an ontological description is a pre-requisite and a first step towards the development of a structure model. A structure model describes how these buildings blocks can be coupled in a generic way. In addition to a structure model, one needs a tool to actually generate alternative structures from it. Such a tool can be based on heuristics and / or using an optimization technique with options to handle logical or discrete decisions. A predictive behavioral model is needed for the computation of the physical behavior of the various alternatives[3]. The scope of section 2.4 is restricted to the ontology and the behavioral models. The development of a structure model and a tool for computer-aided generation of alternative design structures, requiring an extensive effort, is topic of future research (see Chapter 8).

2.2 THE DESIGN HIERARCHY

In structuring the design of a crystallization plant by means of a hierarchical decomposition, three layers in the decomposition can be distinguished: the supply-chain layer[4], the process design layer and the control systems design layer, as shown in Figure 2.3. The supply-chain layer provides the context of the process and control design problems, but is not really a part of it in our approach. The supply chain layer sets the initial design specifications for the final product.
In this section, certain refinements/additions to the process design procedure developed by Bermingham(2000) are suggested, with a more fundamental approach to synthesis at the level of a crystallization unit. The aim is to construct the crystallization process from a subset of basic functions (tasks), which are connected in a network, in such a way so as to achieve the desired product specifications. This allows for the generation of a *superstructure* [5] to arrive at an optimum crystallization process, and a crystallizer configuration to realize this. The logic behind this refinement and the structure coming out of it is discussed in this chapter.

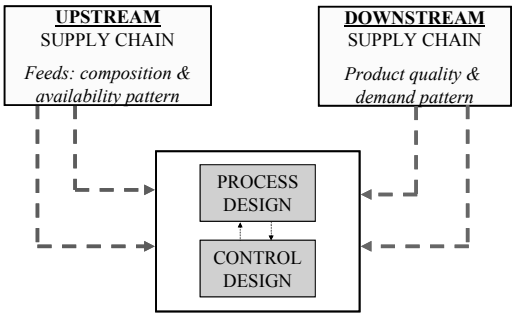

Figure 2.3 Information flow diagram of the design hierarchy

The control design layer, which needs much information from the process design layer, addresses the control aspects for the crystallization process. But, the process and control design layers are interactive, often leading to undesirable design iterations costing time and money. Between two extremes, i.e. strictly sequential or completely parallel design of the process and its control system, there exists a practical intermediate solution (Meeuse, 2002): the control anticipatory mode of process design, where the process dynamics is made to comply with controllability measures within a pre-specified but amenable structure of sensors and actuators. This approach reduces the number of iterations between the process design and control systems design layer.

[3] Since process synthesis presents an inverse problem, the behavioral models may be used many thousand times in an attempt to generate alternative structures. Therefore, it can be wise to limit the computational complexity of the behavioral model to its essential features for the synthesis.
[4] A Layer is a higher stage of aggregation than a Level.
[5] A *superstructure* is a structure in which all process alternative structures of interest are embedded and hence, are candidates for feasible or optimal process flowsheet(s) (Floudas, 1995).

In this chapter, the process design layer is dealt with in detail, with emphasis on a newly developed task-based design approach. The control design layer and supply chain layer are briefly touched upon, for the sake of completeness (refer Appendix A2.1 & A2.2). For a detailed discussion on the integration between the process design and control systems design layer, the reader is referred to Meeuse (2002), who provides many references to publications in this area.

2.3 THE PROCESS DESIGN LAYER

The process design layer follows a hierarchical decomposition that transcends from a product engineering character to a process engineering character. The process design hierarchy consists of one level at which the initial design specifications are formulated and six design levels, as shown in Table 2.1. The design levels are ordered to an increasing amount of detail (or resolution). At the level of the process unit/stage, a ontology for a new physical *task-based design* is developed.

Table 2.1 Design levels in the process design hierarchy

Design Level	Description	Character
0	Initial design specifications - *Process Input/Output Level*	product and process
1	Design of the crystalline *product and product streams*	product synthesis
2	Physical/chemical design of the crystallization *technology*	process technology
3	Block diagram design of the crystallization *process*	process synthesis
4	A task-based approach to the design of a *crystallization stage*	process synthesis and intensification
5	Design of actuators and instrumentation	process engineering
6	Sensitivity analysis with respect to design	process engineering

Design levels 0 – 2 are identical to the design procedure proposed by Bermingham (2000). Hence, these levels will be summarized here for the sake of brevity. At Level 3, an additional step (relative to Bermingham(2000)) is introduced with regards to the possibility of building up *superstructures* for the crystallization process. Level 4 addresses a novel task-based approach to the synthesis of crystallizers. This level aims to provide a wider solution space in arriving at novel crystallizer configurations. Level 5 looks into the possible actuators and instrumentation that may be required to efficiently operate the crystallizer (decided at Level 4) to meet the demands set at Level 0. Finally, Level 6 briefly discusses the overall economic optimization that can be done on the process design layer, before transcending into the control design layer. The results of such an optimization provide cost-optimal settings for the operational variables, being set-points for the control. Thus, in an evolutionary manner, this design procedure leads the user to identify the important crystallization tasks, to identify equipment configurations, to determine the important design variables and the associated safety and economic trade-offs. Heuristics aid the decision making process at relevant stages in the procedure.

Having recapitulated the hierarchical decomposition into 5 levels of increasing detail, the next pertinent question is what should be done in terms of design activities at each level. Actually, the activities in each design level from Levels 1 – 5 can be described by means of a *generic design cycle* (see Figure 2.4). There are seven phases in this design cycle (see Table 2.2), as described by Grievink (2004). Though the ordering of the phases to a large extent represents a 'logical' way of working by designers during the design process, these phases are not necessarily covered in a strictly sequential manner. For instance, if a performance constraint violation emerges in the evaluation phase, it may be necessary to go back to the synthesis phase in order to change the structure to satisfy this constraint. Such kind of iterative progress and interaction is possible between all phases of the design cycle. It is up to the designer to try and minimize these iterations, by identifying all constraints and targets early on (in the scope phase)[6]. For this very reason Figure 2.4, visualizes the phases in a circular arrangement rather than a linear sequence.

[6] Superstructure generation (synthesis) and optimization enables to combine the synthesis, analysis and evaluation phases.

Table 2.2 Phases of the generic design cycle (after Grievink (2004))

Phase	*Description*
1. Scope of design	Define specifications and objects in design space
2. Knowledge about objects[7]	Gather and assess the knowledge that is required
3. Synthesis	Create various structures (spatial, temporal)
4. Analysis	Determine the physical behavior of these structures
5. Evaluation	Determine the performance of these structures
6. Report of design	Document all design decisions and resulting structures
7. Selection	Select suitable designs and propagate to the next space

The first phase at each level is to **identify and specify the design space.** The specifications consist of relevant initial design specifications from level 0 and design specifications propagated from a preceding or upper level. Propagated design specifications are in fact design variables, which are fixed after completion of a previous level. The design space is defined by the available new design variables and operational variables as well as the building blocks for the level under consideration. The new variables and objects are made possible by increasing the resolution, thus achieving a finer measure of detail.
The second phase is to **gather and assess the domain knowledge** that relates the design variables and operational variables to the physical behavior of building blocks. This knowledge may consist of: (a) experimental data on physical, chemical biological phenomena and associated statistical, data driven models, (b) experimental data on practical behavior of objects on various scales (like equipment in laboratory and in plants), (c) first principles models of the physical behavior of objects; models relating performance to operational and design variables, (d) heuristics and guidelines concerning operational experience, etc. If parts of the domain knowledge are considered inadequate, additional experimental and modeling efforts may be required. The tools (graphical and computational) available at a level to aid in the decision-making for design can also be identified along with the domain knowledge. This second phase is an additional attribute to each of the decomposition levels, as proposed by Bermingham (2003).

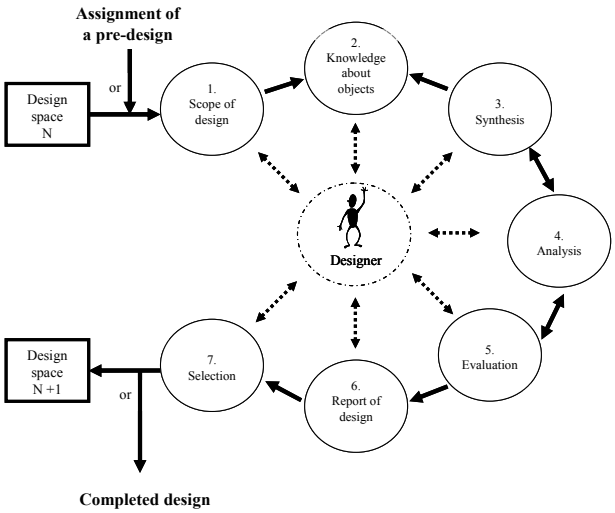

Figure 2.4 The generic design cycle (after Grievink, 2004)

The third phase is the **synthesis** task wherein the designer generates one or more design alternatives, given a set of objects ('building blocks') in the design space and constraints on and targets for desired behavior and performance as defined in the scope. A design alternative is characterized by its structure and by its scale. In this design procedure, design and operational variables that determine the structure will be classified as *discrete*, and those that define the scale as *continuous design and operational variables*. Often, the design alternatives can be systematically ordered in a super-structure. Discrete design variables describe the internal connectivity in the superstructure.
The fourth phase is the **analysis** of the physical behavior of the design alternatives that have been selected in the synthesis phase. The information that is obtained from this phase by means of model-based simulation typically involves a complete overview of numerical values of the states of all streams

[7] The term *object* refers to a building block, which is used for synthesis.

and internal states of objects (steady state or dynamic scenarios); covering the (species) mass and energy balances.
In phase five, the designer must **evaluate the performance of the design alternatives**. The distinction between *performance* and *behavior* is that performance relates to 'values' appreciated by society while behavior refers to 'physical patterns'. Given the physical behavior of the system, this evaluation phase must:

- meet S.H.E.E.T. performance indicators (**S**afety, **H**ealth, **E**nvironment, **E**conomic, **T**echnological) as functions of the design variables and decisions.
- select scenarios of operation and compute performance, using performance models
- evaluate performance against targets and/or constraints set in the scope
- optimize (mathematically) the performance to meet or exceed targets, while satisfying constraints
- identify potential hazards in operation
- identify options for changes in structure and/or scale if the performance does not meet the targets

Next, in phase six, the designer **reports all design decisions**, plus the reasoning behind these decisions, as well as the main results.
Finally, phase seven arrives at the **go/no-go decision** with respect to each of the alternatives. The designer screens and selects from the set of generated alternatives the better candidates that will be propagated unto the next design space, based on their performance in the evaluation phase. Furthermore, information on the design objects and their attributes and any other relevant information on the selected alternatives are transferred to the scope of design of the next design space. If none of the alternatives are eligible for propagation to the next design space, two options remain:

- Generate better options by returning to the 'Synthesis' phase and revising / improving on the design decisions laid down in the 'report of design'
- End the design.

Having outlined the distinctive levels in crystallization process design and the seven generic design phases per level, each of the levels will be reviewed. In particular, attention will be paid to a clear presentation of the specifications, objectives and constraints, the design decision variables as well as an indication of required domain knowledge and available tools per design level, using a sequence of tables. Which information is transferred from one level to the next one will also become clear from these tables.

2.3.1 Level 0 - Initial Design Specifications – Process Input/Output Level

Level 0 basically sets the specifications and requirements for the product quality, process and design process. This level defines the demarcation between the supply chain and process under design, leading to a set of design specifications for the product performance, for the process and a set of specifications for the management of the design work-process. The latter comprises the management of the available resources (time, costs, skills, etc.) and knowledge (technology, information handling/documentation, etc.).

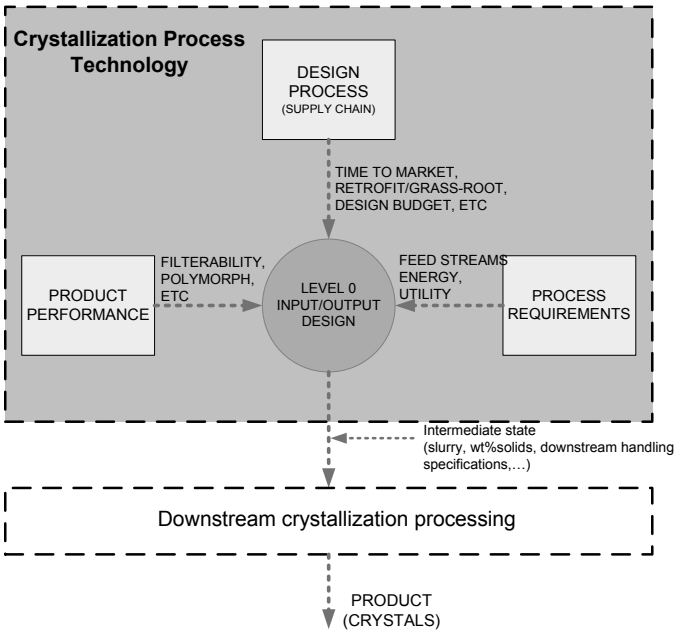

Figure 2.5 Level 0: Information flow with respect to initial design specifications

Although the organization and management of the design work process can have significant impact on the quality of the resulting design, these will not be further discussed, being outside the scope of this thesis. Some of the product performance requirements like *no caking in storage, aesthetic appearance,* etc. can also be directed by the supply chain layer. Table 2.3 provides an overview on Level 0 (Bermingham, 2000). Here, the connection is established between the physical process inputs and outputs linking it to the supply chain. The process itself is seen in an abstract manner from an input-output perspective. A simple input-output information flow diagram for a crystallization process including the downstream process is depicted in Figure 2.5.

Table 2.3 Initial design specifications – Process Input/Output Level

Product performance requirements
Market demands: product quality variability restrictions, prices and elasticity
Customer application: no caking in storage, dissolution rate, mechanical strength, freedom from dust, bulk density or porosity, aesthetic appearance, preferred polymorph, particle size permissible
Downstream handling: filterability, washing-ability, drying-ability, dissolution rate, pneumatic handling, freedom from dust, flow-ability, mechanical strength
In the crystallizer: no flotation, suspendability (off-bottom criterion satisfied)
Process requirements
feed composition, battery limits and conditions, production capacity, yield, energy consumption, stability, reproducibility, resiliency, controllability, availability, SHE considerations, current equipments available, special material requirements (corrosivity), vacuum generation capability
Design process requirements
design budget, time to market, in-house or licensed technology, available skilled design staff, traceability (documentation), explicitness of design decisions, type of design (retrofit/grass-root), collaboration with other industries/universities, market demand, technology available from competitor, the product specification and price from competitor.
Tools
Expert system, Software/Model at disposal, Supply chain modelling tools

2.3.2 Level 1 - Design of the crystalline product and product streams

At this design level (Table 2.4) the aim is to determine which product composition is required to meet the product performance criteria listed in level 0. Essentially, this level transforms the product performance specifications listed in level 0 into more tangible and quantifiable quantities relating to structure and composition, like crystal size distribution (say).

Table 2.4 Design of the crystalline product and product streams

Design specifications Objectives and Constraints		Design Variables	Domain knowledge	Tools
Product:		*Discrete:*		
• Filterability	• SHE considerations	• Polymorphism	• Filterability tests and models: permeability and compressibility	• CERIUS2® (Molecular modelling)
• No caking in storage	• Pneumatic handling	*Continuous:*	• Shear tests	
• No flotation	• Freedom from dust	• Morphology	• Indentation tests	
• Suspendability	• Flow-ability	• Crystal size distribution	• Caking tests	
• Washability	• Mechanical strength	• Purity	• Flowability tests	
• Dryability	• Abrasion resistance	• Maximum inclusion content	• Safety aspects	
• Dissolution rate	• Bulk density or porosity			
• Taste	• Aesthetic appearance			
• Solubility	• Melting point			
	• Thermodynamic Stability			

The second key decision at this level is to decompose between the core crystallization step and the down stream processing. Figure 2.6 depicts this decomposition. As a consequence of the decision to decompose between the core crystallization process step and the downstream processing, the product stream between the core crystallization and the down stream processing must be specified as well in terms of feasible composition and conditions ranges. Setting the specifications for this stream is part of the decision making at the next level (2).
In view of the focus of this thesis on the core crystallization step, the design of the downstream processing will be skipped, while acknowledging its importance for the final product quality (control).
A more comprehensive approach would be to consider the downstream processing jointly with the crystallization process technology section. This leads to better process integration and optimization options, as discussed by Ng(2001). However, such integration and interaction is not completely lost by the present decomposition because it can be covered at the sixth and final level of design, where sensitivity analysis is carried out.

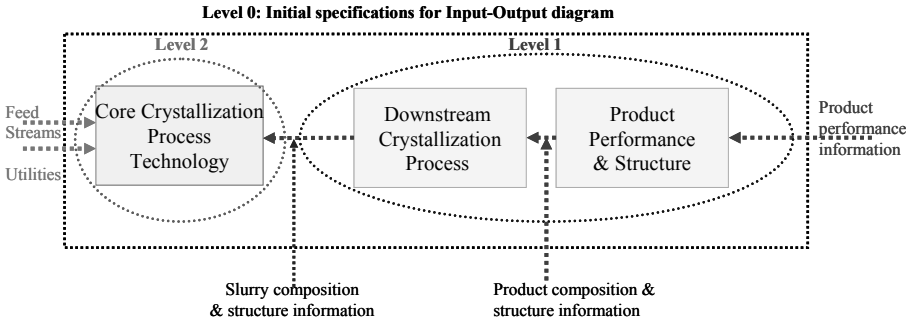

Figure 2.6 Decomposition between the core crystallization step and the down stream processing

2.3.3 Level 2 - Physical/Chemical design of the crystallization technology

The design specifications of level 2 (Table 2.5) are composed of process requirements from level 0 and propagated product composition characteristics from level 1. The design variables at this level mainly involve the chemical species and the mechanisms to carry out and control the core crystallization process. For each design variable, there is a lot of heuristics available. For an extensive discussion on these heuristics, please refer Bermingham (2003).

Table 2.5 Physical/chemical design of the crystallization technology

Design specifications Objectives and Constraints	Design Variables	Domain knowledge	Tools
Process: • Production capacity • Feed composition • Yield • Energy consumption • Availability • SHE considerations *Product:* • Polymorphism • Morphology • Crystal size distribution • Purity • Maximum inclusion content • Allowable range for slurry /fluidized exit product stream solids content • Co-solvents	*Discrete* • Crystallization method • Feed purification • Recrystallization step • Type of solvent(s) • Phase of solvent(s) • Additive(s) • Material of construction • Nucleation targets - primary by seeding - secondary by attrition/collisions *Continuous:* • Pressure range • Concentration solvent(s) • Concentration additive(s) • Temperature range • Solids fraction	• Thermodynamic activity of species/components in solid, liquid and vapor phase • Adsorption (energy) of components/species on the various crystal faces • Scaling or encrustation tendency of components/species • Metastable zone with respect to homogeneous and heterogeneous primary nucleation • Physical properties, e.g. material densities and specific heats • Safety aspects • Degree of corrosivity • Solubility curve • Phase diagrams	• CERIUS2® (Molecular modelling) • OLI®/ASPEN® thermo-dynamics

2.3.4 Level 3 – Block diagram design of the crystallization process

Having defined the output conditions for the materials entering and leaving the core crystallization process, the current level of design addresses the creation of the internal structure of this process. To avoid an excessive amount of detail in synthesizing and analyzing the internal structure, a lumped description is used. Functional blocks are introduced which describe transformations of the physical resources in the process. An effective utilization of such resources in creating the product from the feed is key to the success of a process design. What are the key design decisions at this level and what will be the approach?

First of all the relevant physical resources need to be specified. Such resources are primarily the mass and energy streams, being the main economic cost drivers. Nevertheless, from a fundamental physical perspective one could argue that in addition to matter and energy, the changes in momentum (pumping, compression) should be involved as well. The first simplifying assumption regarding use of resources is that these momentum transformations are relatively less costly than the transformations in the state of mass and energy and, hence will be ignored. Also, the use of any other physical resource, like electrical charge and energy for electrochemical transformations, is believed to be irrelevant in this case.

Another consideration is that the use of thermal energy is much more dominated by changes of thermodynamic phases than by creating a temperature difference. Such phase changes involve evaporation or condensation, solidification or dissolution. So, a distinction is made between thermal operations involving a phase change and those for a temperature change.

The second key specification involves the choices of functional blocks that physically transform the chosen resources, being only material and energy flows. These blocks are the key building blocks in the synthesis of a process block diagram. The rather obvious choices made in this thesis are:

(1) A crystallization block operating on a fluid phase material stream with dispersed solids;
(2) Fluid phase transformation blocks for evaporation and condensation, operating on a material stream and utilizing an energy stream to effect the change.
(3) Heat exchanger to effect temperature change of two streams by heat transfer.

What will be the approach to the design at this level? Ideally, for a rigorous approach to the synthesis of a process block diagram, a complete *ontology* for the functional blocks would be required; describing all

attributes of the functional blocks as well the options for connecting such blocks. Having the ontology, a *structure model* can be developed from which *superstructures* for process synthesis can be derived. Such a development is very research and time intensive. For this reason, it could not be covered in this thesis, where most attention has been given to obtaining new design results at the level of a crystallization unit (level 4). Hence, the contribution at this level is just an informal sketch of the approach.

Functional building blocks and some attributes

Before going into the superstructure synthesis, some 'building blocks' and key attributes that are essential to build up the process block diagram will be briefly introduced here:

- Operation mode – a functional block is batch/continuous/semi-batch
- Sequencing of operation – successive blocks in continuous/batch mode or continuous mode followed by batch, etc.
- Crystallization method – supersaturation generation by evaporation of solvent, cooling or flash-cooling, reactive crystallization, etc.
- Crystallization stages – parallel or serial staging, involving multiple staging;
- heat exchangers, condensers, pumps, etc
- Feed distribution
- Presence of recycles streams or purge streams
- ……

At this level, the functional block is treated as a black-box with no equipment specific details added here. The main principle and thrust here is to come up with alternative designs, to realize the transformation of the feed to the desired product specifications at the optimum use of resources while meeting the economic and technical feasibility of the process.

An overview of the design specifications, design and operational variables and domain knowledge for this level is given in Table 2.6. This is almost identical to Level 3 as discussed by Bermingham (2000).

Having outlined the functional building blocks and the associated design specifications and design decisions variables, the issue arises how to generate alternative process block diagrams.

Again, creating such block diagram structure(s) still involve heuristics, for instance, using the procedure describe by Kramer(1999) in fixing the choices of the functional blocks. Once these blocks have been decided on, the connectivity aspect can be treated. In view of the many options to connect these blocks, the concept of a superstructure has been developed. This concept is quite well known in the chemical engineering design field, just as an example, refer to Kokossis and Floudas (1994). Systematic approaches to synthesis alternatives have been investigated in the development of heat-exchanger network superstructures (Yee and Grossman, 1990; Ciric and Floudas, 1991; Papalexandri and Pistikopoulos, 1994) and reactor networks (Chitra and Govind, 1985; Achenie and Biegler, 1990; Kokossis and Floudas, 1990; Kokossis and Floudas, 1994, Balakrishna and Biegler, 1993). At the end of this thesis research, no applications of superstructure for crystallization process design were published.

Superstructure synthesis

In general, the flow sheet synthesis of the process can be formulated as an optimization over all feasible process structures. In principle, if all different possible approaches to implement some desired physical or chemical change are employed – including all possible different reactor configurations, all possible different separation and purification schemes, techniques, and units, and all interconnections among these potential process units in one gigantic tentative process flow sheet – and then subjected such a superstructure to economic optimization constrained by environmental, safety, reliability and other criteria, the best manufacturing process in terms of both structure and the design of each surviving unit operation would emerge. In the optimization process, inferior units and connections were eliminated.

Table 2.6 Block diagram design of the crystallization process

Design specifications Objectives and Constraints	Design and Operational Variables	Domain knowledge	Tools
Process: • Production capacity • Feed composition • Yield • Energy consumption • Crystallization method • Feed purification • Re-crystallization step • Availability, controllability and responsiveness • SHE considerations • Temperature range • Pressure range • Supersaturation range • Nucleation targets • FDA regulations • Exergy losses • Constraints on economies of scale - utility/energy costs - investment costs *Product:* • Crystal size distribution • Solids fraction • Solvent phase	*Discrete* • Operation mode • Number of crystallization stages, heat exchangers, condensers, etc • Feed distribution (parallel/serial feed) • Recycle structure • Location purge stream(s) , feed stream, seeding point(s) • Parallel or serial staging • Product concentration • Sequence of operation mode • Sequence of crystallization method • Seeding and seeding technique/policy *Continuous:* • Residence time in each stage or batch time • Recycle flow rates • Purge flow rate • Pressure and/or temperature in each stage • Heating/cooling duty or trajectory • Seed amount /size • Heat exchange duty • (pseudo-) Pinch point	• Thermodynamic activity of species/components in solid, liquid and vapor phase • Physical properties, e.g. material densities, specific heats and viscosities • Crystallization kinetics, i.e. rate expressions for the nucleation, growth, attrition, agglomeration and breakage of crystals • Fouling kinetics • Shape factors of the crystalline components • Fire and explosion index • Controllability • Synthesis rules for superstructure generation • MINLP techniques for optimization	• gPROMS® • PROSYN® • ASPEN® • OLI®/ Aspen® for thermo-dynamics • GAMS® for optimiza-tion

With respect to the synthesis of a crystallization process block diagram, Figure 2.7 illustrates just some of the possibilities that could be embedded as alternatives within a superstructure. Here, some of the following variables can be considered quite rigorously.

1. There can be hybrid operation mode in the entire plant i.e. first a continuous process followed by batch crystallization and then again continuous.
2. The feed mode i.e. forward, backward (recycle), mixed and parallel mode of operation can be chosen more rigorously.
3. Similarly there can be a sequence for the crystallization method – first cooling crystallization followed by evaporation etc.
4. The crystallizers can be heat integrated i.e. in the case of evaporative crystallizers; the vapor generated from first crystallizer can be fed as a heat input for the next crystallizer. For this the boiling point elevation and the feasible pressure drop allowed between two subsequent crystallizers have to be taken into account. Their purpose is mainly to minimize operating (mainly energy consumption) and investment costs.
5. In cases (e.g. NaCl), where the crystal production follows from flash evaporation of the aqueous solvent, the heat of condensation of the vapor is partly reused to evaporate the water in the next stage and partly for countercurrent heating of the feed.
6. If a chain of crystallizers is used, it gives a more narrow size distribution than either a number of crystallizers in parallel or a single crystallizer with the same total volume.
7. The superstructure can also give the optimum number of heat integrated/chain of crystallizers.
8. ……

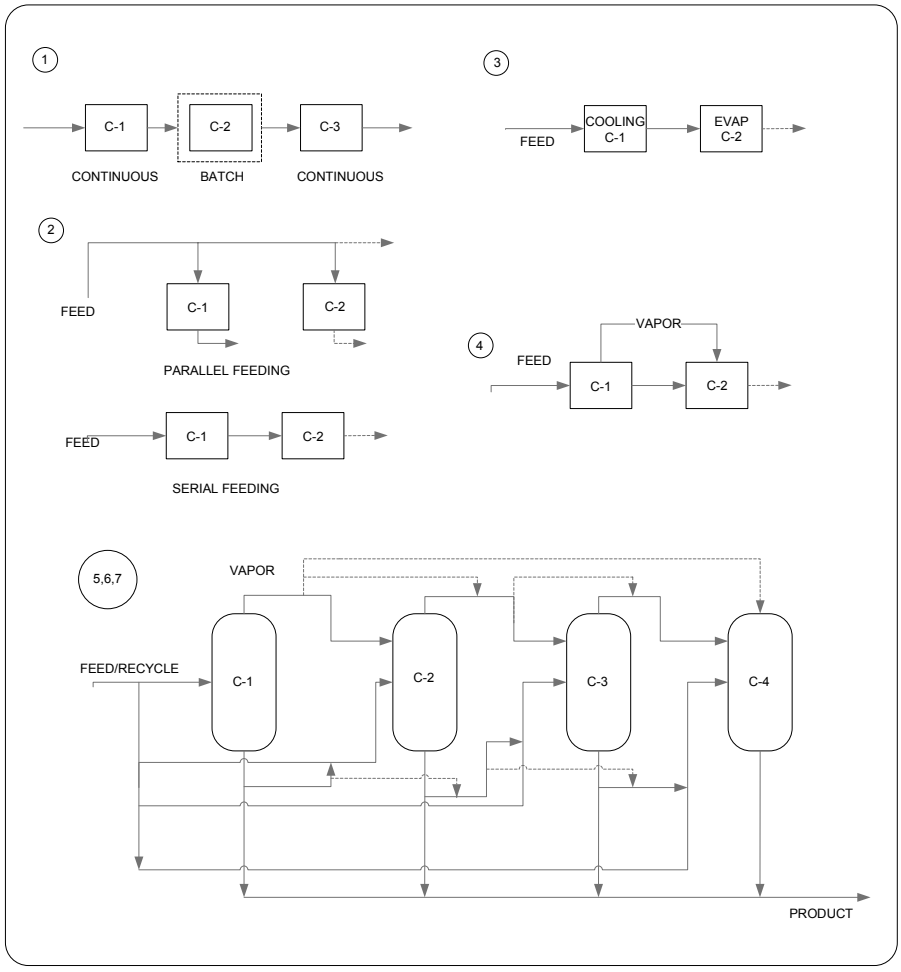

Figure 2.7 Possible alternatives in the form of a superstructure for a crystallization process

The process synthesis target at the block diagram level is to come to a rough first-order assignment of duties and yields to the various building blocks, meeting S.H.E.E.T. specifications for the block diagram as a whole.
Controllability can be taken as a criterion for selection of a configuration both at level 3 and level 4, creating a trade-off between buffering (resilience) in equipment and agile control in response to disturbance patterns. The handling of the discrete design elements in conjunction with the dynamic models and multi-period optimization is still of an overwhelming complexity. Considering the fact that controllability analysis usually requires a dynamic model, it will be considered very briefly after level 4 only, when such models have become available.

Although this block diagram level will generate a superstructure with a number of block diagram possibilities, it must be kept in mind that a rigorous modeling of a crystallization process with focus on product quality is hardly possible at this level, as this would involve the solution of very detailed models, including population balance equations. For this, the designer needs to know the detailed geometric parameters of the crystallization equipment, the intrinsic kinetic parameters, etc., which are not available at this level yet. So, rather than using detailed distributed product composition and quality

parameters, simplified modeling including one or two lumped quality parameters can be used as targets to be met by the process block diagram alternatives.

A few remarks are in order with respect to solving such a superstructure. Solving a superstructure is a difficult optimization problem involving a mixture of continuous, integer, and logical variables and relationships. For a comprehensive introduction to the solution of superstructures and the associated problems, the reader is referred to Floudas (1995). However, MINLP (**M**ixed **I**nteger **N**on **L**inear **P**rogramming) techniques and new mathematical techniques such as generalized disjunctive programming and global optimization (Grossmann (2002)), combined with the tremendous increases in available computing power made possible through large clusters of fast independent processors, give hope that this superstructure optimization approach to chemical process synthesis may be practical in the near future.

Recently, Mendez(2005) demonstrated the practical feasibility of the superstructure approach for crystallization. They present an MINLP optimization model for the synthesis of paraxylene separation processes based on crystallization technology. A superstructure is proposed that considers different alternative designs and operating conditions for the recovery of a high purity paraxylene product from a feed stream containing other xylene isomers and ethylbenzene. The goal is to maximize the overall annual profitability of the process, including capital and operating cost as well as product revenues. Major decisions involve selecting: (a) number of crystallization stages, (b) type, number and size of equipment at each stage and interconnections between unit operations, (c) temperature levels for crystallizers, heat exchangers, refrigeration system and flows in the system, and (d) alternatives for the return of recycles.

So what seems possible is a cost-driven optimization of the superstructure solely based on mass and energy balance considerations. Coupled with heat-integration, an optimization of such a superstructure will result in the optimum process block diagram. This structure will largely govern the superstructure to be elaborated in the next level (level 4) unless there is one big, cost dominating crystallizer that overrides the importance of optimization done at this level. For the time being, the superstructures at both levels will be solved independently.

2.3.5 Level 4 - A task-based design approach to the design of a crystallization stage

Level 3 focused on the block diagram design which may include a chain of crystallizers as one of the possibilities. Level 4 looks at the design of a single crystallizer unit, which is referred to as a 'crystallization stage' here. This involves detailed design of the crystallizer equipment that was treated as a blackbox in Level 3. At Level 4, the features of the incoming feed streams (could be a recycle stream from the downstream of this stage) and the desired features of the product stream must be provided. The corresponding design specifications are listed in Table 2.17 - column 1.
As this is the main innovative part of this chapter, it deserves its own section. Hence, first Level 5 and Level 6 will be introduced before treating Level 4 in greater detail.

2.3.6 Level 5 - Design of actuators and instrumentation

Possible actuators for the crystallization process include product classification, fines classification, impeller frequency, heat input, feed to the crystallizer etc. Actuators may be necessary for the operation of equipment or for better control over the process. Some of the actuators (for eg. type of impeller) influence the decisions taken at a level higher in hierarchy (in level 4). So, if there is an additional actuator required, iteration is unavoidable.

Propeller frequency is regarded as a process actuator due to its evident influence on the product CSD. It influences a variety of phenomena in a crystallizer. Among them there are overall fluiddynamics

(temperature, concentration and supersaturation gradients, crystal suspension, and crystal circulation time), local fluiddynamics and secondary nucleation.
In evaporative crystallization, the heat input determines the rate of solvent removal. Hence, the heat input influences the supersaturation generation rate. The supersaturation being the driving force of crystallization determines the crystal growth rate.
The seed size and mass are recognized as crucial in obtaining the product with certain characteristics. Shape, purity, and origin of seeds play an important role too. The seed crystals should have shape and purity similar to those of the desired product. A discussion on the possible consequences of using the seed crystals of different origin is given by Heffels (1999). The induction time (metastability limit) for primary nucleation can be greatly influenced by the use of ultrasound as an actuating device.

In the design of instrumentations (sensor measurements) in plant wide context, the process variables that can be measured are determined; their number and measurement location/s within the equipment is decided. Essentially, information needed for automatic control and process performance monitoring are established here along with a preliminary Degree of Freedom (DOF) analysis. The manipulated variables (MV), controlled variables (CV), constraints and disturbances are determined. The basic inventory control (level and/or pressure, etc) can be determined at this level. For instance, the liquid level is manipulated with either product flow or feed flow, pressure can be manipulated with heat input in case of evaporative crystallization. The method of measuring and controlling the production rate of product(s) and its quality can be decided.
The design of the overall control design structure in conceptual form is discussed in Appendix A2.1 (The Control Systems Design Layer) and it belongs more within the domain of control design rather than process design. Albeit, it must be kept in mind that these two layers are very much inter-connected in the overall design of a process.

Table 2.7 gives an overview of the design decisions to be taken at this level with respect to the actuators and instrumentation.

Table 2.7 Design of actuators and instrumentation

Design specifications Objectives and Constraints	Design Variables	Domain knowledge	Tools
Process: • Production capacity • Feed composition • Yield • Energy consumption • Availability, controllability and Resiliency • SHE considerations • Crystallization method • Temperature range • Pressure range • Supersaturation range(concentration) • Seed mass/size • Operation mode • Residence time (distribution) • Heat exchange rates • Nucleation targets • No boiling in heat exchanger • No entrainment of droplets by vapor • Type of heat exchanger • Type of condenser • Location of feed pipes • Product removal location • FDA regulations • Controllability aspects • Suspension criterion • Liquid level(s) *Product and feed stream* • Crystal size distribution • Flow (slurry) • Slurry density • Filterability	*Discrete:* • Controlled variables • Sensors (type) (includes measurement devices) o CSD measurement o pressure measurement o temperature sensor (PT-100) o density meter and flow meters o in-line measurement device for concentration determination o off-line measurement of crystal slurry filterability o in-line video images of crystal slurry product stream with a CCD camera • Sensor locations • Data acquisition, storage and retrieval • Manipulated variables • Number of actuators • Passive actuators o Annular zone (fines classification/clear liquor advance) o Baffle(s) o Draft-tube(s) o External/internal heat exchanger o Type of circulation device (impeller/pump/mixer/ vessel) o Seeding technique(s) o Seeding point(s) o Direction of circulation *Continuous:* • Active actuators o Sonic velocity (ultrasound) o Agitation rate (propeller) o Fines removal rate o Seed purity o Fines dissolution rate (Heat input for fines dissolution) o Heat input rate for crystallization o Feed flow rate o Product classification rate	• Thermodynamic activity of species/components in solid, liquid and vapor phase • Physical properties, e.g. material densities, specific heats and viscosities • Crystallization kinetics, i.e. rate expressions for the nucleation, growth, attrition, agglomeration and breakage of crystals • Fouling kinetics • Shape factors of the crystalline components • Fire and explosion index • Controllability • Equipment characteristics • Fluiddynamics • Measurement principles	• gPROMS® • PROSYN® • ASPEN® • OLI®/ Aspen® (thermo-dynamics) • FLUENT®, CFX® (CFD)

2.3.7 Level 6 - Sensitivity analysis with respect to design

Level 6 is devoted to a sensitivity analysis and an optimization of the plant performance. This optimization must compensate for the fact that many design decisions have been made sequentially at different levels. The overall result will definitely be suboptimal. Sensitivity analysis with respect to design decision variables will show how much can be gained potentially. Optimization, not necessarily of the entire flow sheet, but of the more cost-critical sections, is expected to give significant improvements (see for example, Bermingham (2003a,b)). In each design candidate, there will be trade-offs for an economic optimum, involving a simultaneous fine-tuning over numerous design decision variables. Therefore, sections of the flow sheet(s) can be optimized mathematically using mathematical programming techniques. Availability of models is a must at this stage for analysis and optimization studies. If no significant improvements emerge at this level, this design alternative is finished at the process side.

After level 6, the process design layer is complete and the process control part begins. The process sensitivity analysis has revealed which operational variable(s) are crucial to economic performance and should be kept under set-point control. The process control design layer will be a study by itself and is out of scope for research as part of this thesis; hence it is not discussed any further in this chapter. To get an overview on the *process control design layer*, the reader is referred to Appendix A2.1.

2.4 LEVEL 4 - A TASK-BASED APPROACH TO THE DESIGN OF A CRYSTALLIZATION STAGE

The key unit in a crystallization process is the crystallization stage. Such a stage is defined here as an operation in which mother liquor, possibly containing off-spec crystals, is changed into a liquid-solid slurry containing an increased mass fraction of crystalline material. When compared with the input process stream, the properties of this crystalline material in this output process stream have come closer to the product quality specifications. It may require several stages in sequence to achieve the final product quality. At design level 4, the design of a crystallization stage is treated as a conceptual (mental) process in which it must be envisaged what physical events (or phenomena) can be used as vehicles to achieve the change from input to output and how to order these events. For a reproducible design process, it is needed to create a structure in the selection and ordering of the physical events. Hence, a design approach or a methodology is needed. In this section, a novel task-based design approach is introduced, for which the ontology is presented.

2.4.1 Why use a task concept ?

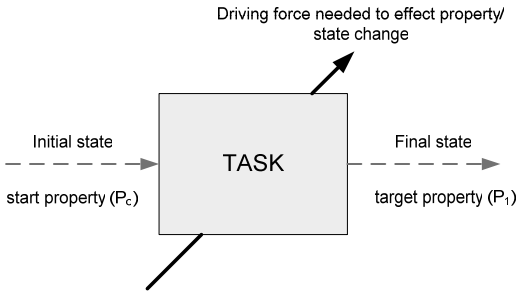

Figure 2.8 Black-box representation of a task

According to Siirola (1995), a natural hierarchy among property differences (and hence tasks) exists: molecular identity, amount, composition, phase, temperature and pressure, form. This hierarchy arises because changing the properties lower in the hierarchy will generally not influence the properties higher in the hierarchy.
A *task* (see Figure 2.8) could be defined as "the elimination of a property difference by means of a physical transformation, where the transformation is driven by a thermodynamic force, like chemical potential difference (say)".
The task based concept got a boost up in late 90's when Eastman Chemical Company made its reactive distillation technology for methyl acetate (Siirola 1995,1996). In this method, the properties of the product and feedstocks are compared. The raw materials are considered to be the initial state and the desired product is the final target state. When property differences exist between the initial state and target state, tasks are required that eliminate these differences.
Although Figure 2.8 is a very simplistic representation of a task, things can get more complex when, for instance:

- simultaneous changes of multiple properties are needed
- multiple driving forces are required
- driving forces can cause unwanted effects on other properties
- multiple feed and products are to be considered
- there are tasks that are very much inter-related and cannot be isolated

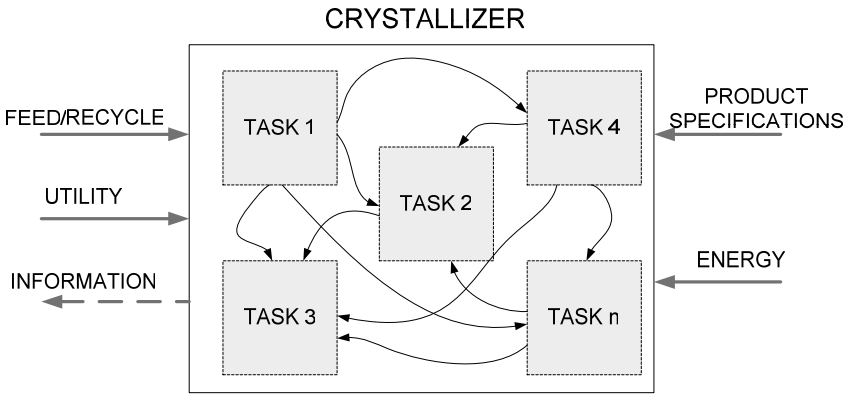

Figure 2.9 A task-network representation in a means-to-an-end fashion

Accounting for these complexities, a *physical task* can be defined as an intentional transformation of the initial state of matter (e.g., a material stream) into a target state by means of physical events (and/or information processes) satisfying constraints on the physical conditions under which such events can take place The phrase 'intentional transformation' implies that the task concept is a mental construct of the human designer, having a specific goal/intent in mind. A physical event is required as the vehicle to accomplish the task in a physical reality.
In the 1930's, chemical engineering was typically based on unit operations approach, which changed to a more fundamental transport phenomenon approach due to the pioneering work of Bird (1960). Even though this gave a deeper understanding of the phenomenon at work in the operations, still most of the synthesis of new processes was based on unit operations as the "basic" building blocks (Ruud,1973). Synthesis involves positioning the process operations in such a way so as to eliminate property differences.

The design methodology adopted here in Level 4 is *task-oriented* aiming to cover a wider ground than the traditional *geometrically-oriented* way of design (i.e. it is synthesis focused in contrast to current design practice which is more analysis focused). This concept is represented in Figure 2.9.
The basic idea here is to arrange these tasks in a "means-to-an-end[8]" fashion to accomplish the transformation from input to output. This is the problem that needs to be solved, for which the tasks will be treated as the building blocks at this level. This would ultimately end up in a network of connections between the tasks, which facilitates the generation of superstructures to give the optimum 'task-network'.
Once all required tasks have been identified, suitable equipment(s) should be designed to realize these tasks which can result in significant savings when multiple tasks are integrated into a single piece of equipment. Such a fundamental approach is expected to contribute to more innovative process synthesis and process integration.

Some variations of the task concept in Chemical Engineering
Papalexandri & Pistikopoulos(1996) proposed a generalized modular representation framework for process synthesis alternatives, based on fundamental mass/heat transfer principles. Such a mass/heat-exchange superstructure module was treated as a building block for entire process flowsheets involving reactors, separations, etc. Here, within the mass/heat-transfer context of process operations, one can distinguish components of interest, the concentration of which in one stream/phase increases, while in

[8] Means to an end can be regarded as a sequence of transformations where each transformation aims to eliminate a property difference.

another stream/phase decreases. Thus, process operations may be viewed as sets of mass (and heat) exchangers between two properly defined sides/streams, a "rich" side (decreasing concentration) and a "lean" side (increasing concentration). This approach again involves the solution of superstructures. Here, the mass/heat-exchange module can be seen a general form of a synthesis unit, i.e. a task.

More recently, Shah & Kokossis (2001, 2002) used the concept of a *task* (for complex distillation sequences) to reduce rather than enlarge the mathematical model and to simplify rather than complicate the optimization. In order to address complex systems effectively, they replace superstructures with *supertasks*[9]. Here, the building blocks are not unit-based but, rather task-based elements. This approach uses simple tasks and hybrid tasks to conceptualize alternatives, wherein the tasks are superimposed to yield different configurations.

Sargent (1998) proposed a general framework for systematic enumeration and evaluation of feasible designs, applied to the synthesis of simple and complex distillation systems, which is in line with the Douglas (1987) philosophy of a target-directed hierarchical approach to process design. Here, the process is represented by a *state-task-network* (STN) wherein the feed(s) to a process typically undergo a series of transformations, creating a number of intermediate *states*, and that a *task* may be defined as a device for transforming material from one set of states to another. Feasible networks can be generated by assigning a purpose/function to each elementary task. Certain *performance models* [10] are assumed to define the resources and conditions required to implement the tasks and *value models* are used to assess the usefulness of the tasks in achieving the overall process objectives. Using this approach, one can organize a depth-first search among the feasible networks which starts from the simplest feasible configurations and is unlikely to need to evaluate the most complex. Hence, unlike the approach of Papalexandri & Pistikopoulos(1996), here the need for a flowsheet superstructure is rendered unnecessary but at the same time, it allows available superstructures to be incorporated as sub-models, if needed.

The task-based approach that will be presented here has elements of the approach used by Papalexandri & Pistikopoulos(1996), Sargent (1998) and Shah and Kokossis(2002), i.e. the task-based synthesis approach allows the designer to think in terms of *physical tasks* to synthesize crystallizer configurations, making use of *behavioral* and *performance models*[11], and at the same time allowing the degree of freedom to choose the complexity needed to optimize the performance involving *superstructures*. One of the reasons to stick with the superstructure approach for the representation of process alternatives is that it provides a basis for the evaluation and optimization of synthesis alternatives, especially with improvements in mathematical programming techniques and computing power.

In a complex unit operation like crystallization, it is unimaginable that a single mechanism governs the process; rather it's the combination of different phenomena in different zones of a crystallizer, which leads to the final product quality. Complementing this case is the inhomogeneity within a crystallizer that gives rise to different local conditions in different regions of the crystallizer. Certain conditions may be optimum for a particular mechanism, which can then be manipulated in order to achieve the final product design specifications.

The state-of-the-art in the design of crystallization processes and crystallization equipment is fairly driven by heuristics and an analysis-oriented way of thinking. This provides enough motivation to treat the crystallization design process(es) from a synthesis point of view, by the formulation of a task-based design procedure.

---

[9] The term *supertask* is analogous to the term *functional building block* used in Level 3 (in this thesis).

[10] Sargent (1998) describes *performance* models as those which define the relationship between input and output streams, together with additional resource requirements, and contains constraints defining the range of feasible operation of the task in question. It enables the designer to decide whether a proposed process is feasible and whether it meets the specified requirements. A *value* model on the other hand assigns a net "value" to the execution of each task which provides a basis for deciding whether the task is useful, and preferable to other tasks performing the same function. At the economic optimization stage, the value models may provide an economic profit measure or atleast a quantitative performance measure, but nevertheless will enable a better decision on the alternatives at hand.

[11] In this thesis, the term behavioral model will be the equivalent of the performance model of Sargent (1998) and the term performance model will be used in place of value model. So, the terms performance and value models differ in terminology from the ones used by Sargent (1998).

In this procedure, the physical crystallization events are the vehicles enabling the implementation of the tasks. Since there is a close link between a task (mental concept) and the associated physical event, the tendency will arise to name the task after the driving physical event. This is all right as long as it is kept in mind that alternative physical events can exist to perform the same task. For example, the task of creating a temperature increase in a gas can be accomplished both by thermal heat transfer and by forming a shock wave.
The objective here would be to identify relevant physical tasks needed to achieve the desired design specifications, making use of the behavioral and performance models, at the same time providing the degree of freedom for the generation of superstructures at appropriate stages in the design hierarchy. The order of task-based design will be as follows:

a) Establishing specifications for the final (product) state and for the initial (feed related) states;
b) Setting up a sequence of physical/chemical tasks in going from initial to final state(s);
c) Identifying the proper (combination of) physical phenomena to perform such tasks;
d) Establishing the internal rate processes to effectuate the tasks and grouping these in (new) operational units; by selecting compatible operating conditions and space-time requirements;
e) Finding spatial arrangements for selected, feasible combinations of tasks in equipment.

2.4.2 Ontology [12] of task-based design for crystallization

An ontological specification of how to represent the objects, concepts and other entities that are assumed to exist in some area of interest and the relationships that hold among them will be discussed in this sub-section. As a result, the decomposition and abstraction of the process are assisted considerably, since the designer is released from inventing and defining adequate elementary and aggregated sub-systems for every design problem. Rather, with a set of generic objects available, it is only required to match one of the pre-defined objects with real process parts, to specify values for the characterizing attributes. Some objects have behavioral and performance models associated with them and the specification of the ontology will also facilitate the modeling process.
To formulate the synthesis problem in a precise and articulate manner, a few concepts – stream, task, connection etc. have to be understood first.

2.4.2.1 Stream

A *stream* is a directed flow connection between a source and a sink of a specific "resource" (matter, energy, and signal). A stream is characterized by its *state* which can be a vector of properties of a stream (*stream vector*). A property difference can be expressed as a difference in the states between two streams. The streams can be used to connect the tasks with each other and serves as a medium for the tasks to interact with its environment (see attribute 'environment' later). The streams can enter/exit a task by means of ports (see attribute '*port* '). Three types of streams can be identified to facilitate communication between different tasks:

- Material stream – The state of this stream is characterized by mass flow M, energy H (intrinsic to the mass), momentum Mo, number of phases, phase ratios, composition per phase,

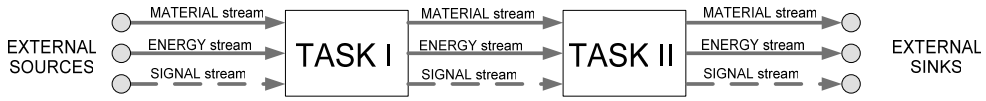

Figure 2.10 Stream flows between tasks

[12] Ontology is defined as a hierarchical structuring of knowledge about things by subcategorizing them according to their essential (or at least relevant and/or cognitive) qualities.

T, P, particle size distribution (for mobile solid particles),.... . This stream can have multiple thermodynamic phases wherein the phases have equal temperature and pressure.

- Energy stream - This stream carries energy (power, electromagnetic flux, etc) only, and no mass or momentum.
- Signal stream - Signal stream is used for electrical and pneumatic transmission of information in a process control system. It is characterized by transmitted quantities and the direction of information flow. This stream has purely information contents (eg. the measured numerical value of a temperature, i.e. it conveys the information required by sensors and actuators).

For conciseness, only *material streams* will be considered here while describing each task. The energy and signal streams are relatively simple to add, because these streams have a scalar rather than a vector feature.

2.4.2.2 Physical Task

A *physical task* is an intentional transformation[13] of the initial state of a stream into a target state by means of physical events (and/or information processes) satisfying constraints on the conditions under which such events can take place. Since there is a close link between task (as the mental concept) and the associated physical event to make the task happen, there will be a natural tendency to name the task after the driving physical event. This is all right as long as it is kept in mind that alternative physical events can exist to perform the same task. Just to list a few examples how a task is named after the event:

- *Agglomeration* is a task for the discontinuous enlargement of a crystal, which is achieved by a change in the crystal size through particle cementation/clustering.
- *Nucleation* refers to the birth of new crystals (embryos), which can result from a spontaneous outburst via primary nucleation or via secondary nucleation (eg. crystal-hardware collisions).
- *Classification* can be visualized as a selective removal of crystals of a certain size from a solid-liquid mixture (say), which can be achieved via particle segregation techniques.
- *Heat exchange* is a task for changing the temperature of a stream, which is achieved by inducing a heat exchange with another object.

A task is endowed with its attributes, which characterize the nature of a task. The formal attributes of any given task are as follows:

1. **Name** – used to identify a task and differentiate them from each other.
2. **Target variable** – the internal state variable(s) that is purposely affected by a given task. For example, if we consider a task such as crystal growth, the target variable here would be the crystal size (L), as ultimately the growth process is contributing to a change in the crystal dimensions. There may arise two limiting situations for the target variable:
    - Non-distributive (uniform over the crystal population)
    - Distributive due to a time history associated with the variable
3. **Duty** – the duty is defined in terms of the desired change in the target variable and the associated amount of resource (mass of a species, energy,….) needed to accomplish that change. For example, to affect a temperature change ΔT on an amount of mass M, the heat duty, $Q = M.C_p.\Delta T$ (assuming no phase change). The effectuation of a duty can result even in associated undesired outcomes. The physical event to perform the duty may have side effects on state variables, other than the target variable, eg. in the boiling zone of an evaporative crystallizer, the desired duty is the generation of supersaturation, but the side-effect (undesired) could be a spontaneous primary nucleation event.

[13] The phrase "intentional transformation" implies that the task concept is a mental construct of the human designer, with a specific goal/intent in mind. The physical event is taken as the vehicle to accomplish the task in a physical reality.

4. **Environment** – the term environment here implies an external world (surrounding) with respect to the task at hand. This task can interact with surrounding tasks in the environment by means of *'ports',* which allow the entry and exit of streams.
5. **Port** – a port essentially acts as the gate that allows/disallows entry or exit for a particular stream into/out of a particular task. Figure 2.11 shows a black-box representation of a task.

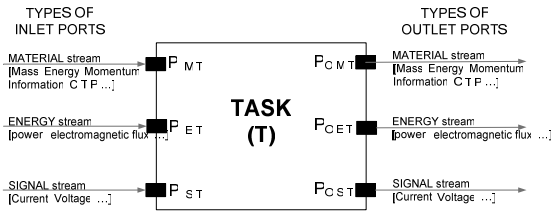

Figure 2.11 Detailed black-box representation of a task

The term $P_{I,M,T}$ represents the inlet (I) port for the material (M) stream for a given task (T). Similarly, all the streams exit the task by means of the outlet ports. It must be mentioned however that there can be multiple instances of the various streams, eg. material stream can be a feed flow, utility stream, product stream, waste stream, etc.. Also, as will be described later, the material stream will first be split into the respective phase streams for which there will be separate ports for the respective phases. This concept of port will be elucidated a bit more later, on the lines of the methodology developed by Marquardt (2004) using the concept of connections.

6. **Event**[14] – a physical event (chosen as a physical vehicle) that can realize the pre-set duty of a given task. This physical event is characterized by one or more physical phenomena, which are endowed with a rate process as well as one or more physical forces driving the rate process. For example, consider the growth of crystals. Due to the difference in chemical potential between the solid and liquid phase, there is a mass transfer from the liquid to the solid phase, thereby the potential difference acting as a driving force for change in crystal size w.r.t. time. Here, mass transfer due to the chemical potential difference can be seen as an event used to carry out the task of crystal growth.
   The physical event can take place only if the corresponding states of the phases remain in feasible domains. Within such domains, the driving forces and rate processes can be active.
7. **Phase system** – the thermodynamic target phase or combination of phases which enable a given physical task to be carried out; it can be solid, liquid or gaseous phase. The presence of multiple phases is often required as a way to create a driving force to make an event happen in a reference phase. To thermally heat a fluid, often another hot fluid is applied to create a temperature difference. Note: In addition to the phase system, one could also introduce a (force) field system, like electro-magnetic and gravitational fields. These fields are universal fundamental physical entities, not linked to any particular phase. However, interactions between a force field and a phase can occur, e.g. heating by induction.
8. **Phase building block** – To perform a task, it is necessary to *construct* a physical event to realize its duty. Often multiple phases are needed to create the event. Each phase is given here its own building block, which facilitates a change in the state variable(s) of the respective material phase stream entering the respective phase building block. The phase building blocks are characterized by thermodynamic state functions and the phase flow regime. This state vector can be defined for each phase as follows:
   S_n^{α} = S [P, E, C, M, φ, α, Mo, (γ, χ, ……..)[15], ň$^{\beta}$, FR[16]….]
   where :P – pressure, E – Enthalpy, C – Concentration, M – Mass, α - Phase concerned, φ - phase ratio, Mo – Momentum, ň$^{\beta}$ – Number density distribution (for solid phase), γ - Internal stress

[14] Physical event is a general term here and can imply a chemical/mechanical/physical phenomenon.
[15] The '……' in this state vector indicates that there are many other quantities that are useful to characterize the solid phase. For many of them, their effect on crystal is poorly understood. Because of this and to reduce the complexity at this stage, it is decided not to discuss about the quantities in the semi- circular brackets hereafter.
[16] The phase flow regime is important as well, for instance, in a given material stream, the liquid phase can be well-mixed while the gas phase shows plug-flow behaviour (eg. rising bubbles)

within crystals (for solid phase), χ - Morphology of crystal (for solid phase), FR – phase flow regime, etc.
The concept of phase building block will be explained in greater detail later.

9. **Behavior** – this describes the evolution of the physical event chosen to perform the task. The description is made by means of a mathematical model of the event. The equations can be constitutive equations, balance equations and/or constraints or they can be just algebraic equations or integro-partial differential equations in time and/or in one or more dependent spatial co-ordinates. The models describing the behavior are consciously kept as simple as possible in the synthesis phase in order to avoid overwhelming computational complexities.
10. **Performance –** performance models essentially give an indication about the usefulness of the task and may provide an economic profit measure or at least a quantitative performance measure. This can be expressed by means of multiple criteria involving safety, health, environmental risks, economic costs, exergy efficiency, responsiveness, etc. It is noted that some performance measures can only be meaningfully expressed at the level of the entire process, because of internal trade-offs to improve overall performance.
11. **Physical constraints** - imposes some limitations on the task either due to quality demands on product or due to safety regulations or to a confined physical domain in which the event will effectively work. The constraints can also be used to favor the target rate process and state variable, while keeping competitive adverse rate processes at bay. For example, the temperature in a crystallizer operated in evaporative mode may not fall below a certain prescribed limit for a certain time period because of the danger of microbial infections.
12. **Time scale of rate events** – The length of time scale at which a phenomenon occurs. For example, supersaturation depletion in a crystallizer is of the order of seconds, whereas mixing can be considered to be almost instantaneous.
13. **Time ordering** – it is the real time at which the task is executed, for example in a batch process, the order (sequence) of the processing of tasks is an important issue and hence, the time ordering aspect must be linked to each task.
14. **Spatial region** – the spatial region limits the geometric boundaries of the task and defines the spatial structure in terms of volume and exchange surface with other regions.
15. **Instance –** A task may have multiple realizations in the spatial and/or temporal domains. The instance is a reference to a particular realization.

The above attributes, though quite comprehensive and minutely detailed, are indispensable to:

- establish physical windows of operation under which a task can be actually carried out;
- establish connectivity options with other tasks and the surroundings;
- capture and articulate expert knowledge on the different tasks involved in a crystallization process

Fundamental understanding of the tasks in terms of its attributes will contribute to a better understanding of process abstraction and model development. Please note that the task-based approach aims primarily at creating a processing structure, with as simple as possible but reliable information, which will also aid analysis and optimization studies.

Example of a task

As an example, the task CRYSTAL GROWTH (see Figure 2.12) (used to denote the growth of crystals) will be used to just illustrate the attributes of a task (see Table 2.8). Figure 2.12 illustrates the transformations occurring within the different phases for task GROWTH. The target variable is the size of crystal and the duty is to have a specified average size (e.g., say 600 micro meter). The inlet port

Figure 2.12 Example of task Crystal Growth

($P_{I,M,GR}$) denotes the entry for the material stream containing crystals suspended in a supersaturated solution. Here, the task is to induce crystal growth of the solid phase, which in turn contributes to depletion in supersaturation in the liquid phase. The gas phase here is a non-entity.[17] At the outlet port ($P_{O,M,GR}$), the material stream contains grown crystals (or crystals with a change in their crystal size) in the solid phase while the liquid stream is depleted in supersaturation.

Table 2.8 Attributes for task *Crystal Growth*

Name	CRYSTAL GROWTH
Target variable	Crystal length (size)
Duty	Increase crystal size (eg. to 600 μm)
Environment	No exchanges except for mass streams through the ports
Port	$P_{I,M,GR}$, $P_{O,M,GR}$
Event	Mass transfer of solute from liquid phase to solid phase due to difference in chemical potential (driving force)
Phase system	Solid / Liquid
Phase building block	Solid phase : growth of crystals (C, M, n, L, μ_s , particle dispersed in liquid) Liquid phase : depletion of supersaturation (C,T, μ_l , well mixed) Gas phase : dummy block (-)
Behavior	Mass transfer rate, intrinsic/net growth rate (eg. $G = k.\Delta C^r$)
Performance	Economic potential, exergy efficiency,….(at the process level)
Physical constraints	Growth rate < 10^{-7} m/s
Time scale of rate events	3 hrs
Time ordering	Dictated by induction time for primary nucleation, eg. 30 min from start
Spatial region	Volume ; no external contact surface, lumped (well-mixed)
Instance	Once, twice, …

Various attributes will be explained in more detail now. Not all attributes will be covered, because some attributes have already been explained well enough in the earlier section.

2.4.2.3 Elucidation of attribute port

The attribute *port*, as defined earlier, acts as a gate that permits entry or exit for a stream into/out of a task. But, this concept of port can also be extended to connections within the task, i.e. to say the connections between the various phase building blocks. This is further explained by using the concept of *connections* as described by Marquardt (Marquardt, 2004). A connection is characterized by the following attributes:

- Phenomenon – physico-chemical phenomenon occurring within the interface.
- Phase properties – characterized by thermodynamic state functions
- Behavior – equations describing the connection.

[17] Here, it is assumed that the supersaturation is achieved either by indirect heating/cooling. If direct heating is provided, say by means of a hot/cold gas stream as in the case of a bubble-column, then the gas-phase no longer remains a non-entity. The inlet stream would then contain dry gas while the outlet stream can be saturated with the solvent. Thus, the vapor phase is important as a way to induce rapid evaporation to keep the supersaturation high for crystal growth.

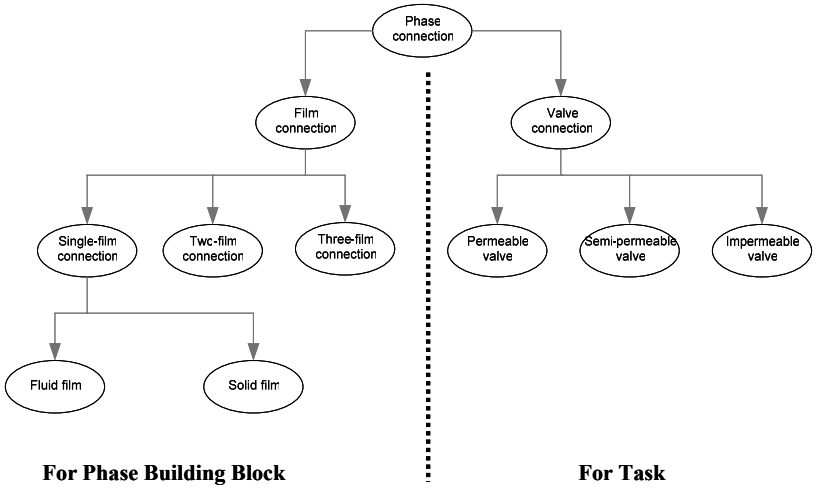

Figure 2.13 Different types of phase connections (Marquardt, 2004)

For instance, if we consider the connection of different material streams, this can be explained by 'phase connection' which is the boundary between volume cells of different tasks. It is based on the flux of any extensive property due to difference in pressure, temperature or chemical potential from the adjacent phase. Diffusion, surface reaction etc. can also occur in the phase connection. The different types of phase connections are given in Figure 2.13. The two types of phase connections are film and valve connections. Film connections are dominated by diffusion and conduction whereas valve connections are dominated by convection. Permeable valve conveys all species in a mixture, semi-permeable conveys only a few species and impermeable blocks any transfer of any extensive quantity.

The phase building blocks within a given task can be connected to each other by means of film connections while the tasks themselves can communicate by means of valve connections, as shown in Figure 2.14. The conditions for phases that are in thermal, mechanical and chemical equilibrium (i.e. same temperature, pressure and chemical potential for phases) have to be defined thus in connections. So now equilibrium is not a property of the spatial region of the task but of a connection. To take into account the disturbances, they must be connected via environment attribute to task. For more details on connections please refer Marquardt (2004). The detailed modelling issues are not discussed here, as the main objective of this work is to provide a framework for the synthesis of different crystallizer configurations using the task-based design approach.

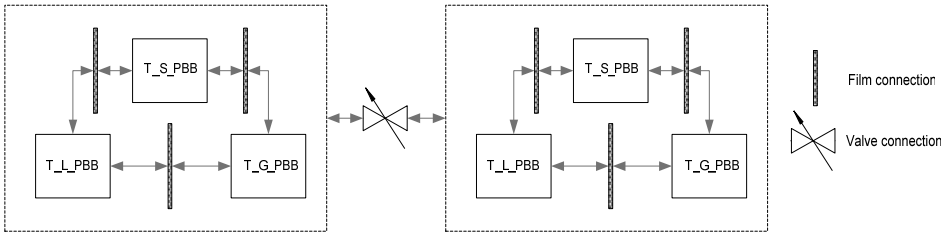

Figure 2.14 Internal and external interactions for a task

2.4.2.4 Concept of phase building block

(a) Structure

It is worthwhile mentioning that in a design context, the *task* is a mental construct to describe an intentional physical/chemical transformation. The *duty* of a task can only be achieved by means of a physical event (which can be visualized as a real-life vehicle that facilitates this realization). An event is characterized by rate processes which are required to change the initial state to the final target state. This is again made possible by the use of one or more driving forces (thermodynamic, mechanical, electrical, gravitational, etc.). Often driving forces emerge from differences between the physical states of two phases that are brought into contact. The introduction of a phase system is almost always needed to create an event with a driving force, apart from homogeneous reactions. Hence, one can *construct* a physical event by combining the relevant thermodynamic phases together, as shown in Figure 2.15, which depicts the concept of a phase building block (PBB) for an arbitrary task.

Here, the material stream (consisting of the different phases) entering a particular task via the inlet port ($P_{I,M,T}$), is split into its respective phase streams. These phase streams are then directed to their respective phase building blocks, via the respective ports for each phase. These material phase streams are characterized by their state variable(s) and the phase building block actually acts as a *sub-task* in effecting a change in these state variable(s). The phase building blocks in the different phases interact with each other by means of *film connections*, as discussed earlier. The respective phase streams exit the task via their respective ports, before being merged together at the outlet port ($P_{O,M,T}$). The advantage of having separate ports for the different phases provides the flexibility to tear the phase streams.

The physical interaction between two or more thermodynamic phases almost always provides the driving force for an event to take place and make a task *happen*. For eg., consider heat transfer (from wall to a fluid phase) or mass transfer (solute diffusion from solvent to solid phase) or momentum transfer (rotating impeller). In all these instances, some potential energy (chemical, gravitational, electrical, etc.) or kinetic energy difference between the different phases creates the driving force to drive the rate events.

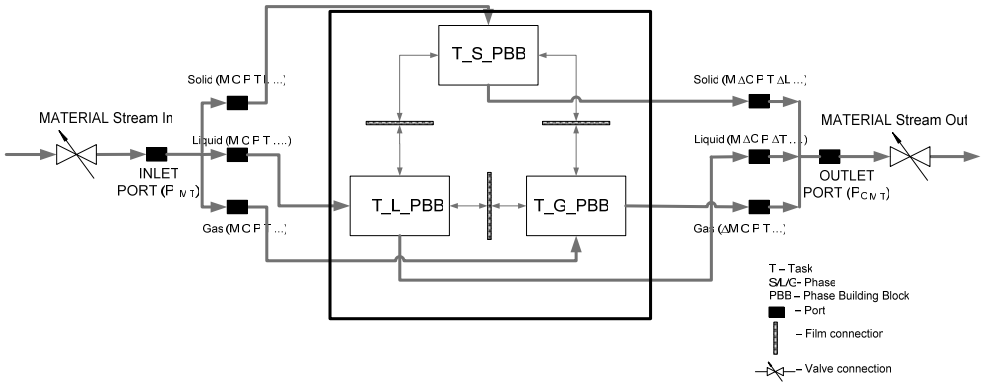

Figure 2.15 Flow of material into a task along with the respective phase building blocks constituting any given task

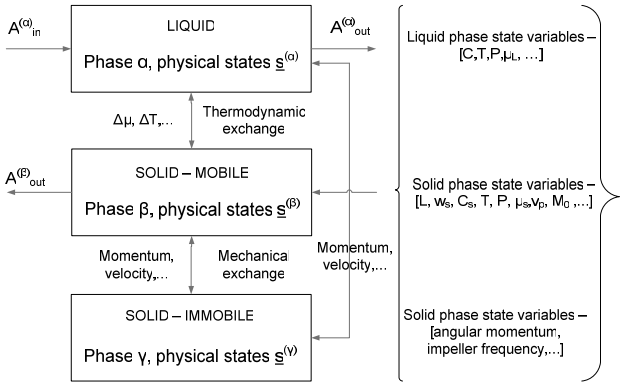

Figure 2.16 Thermodynamic and mechanical exchanges between phases

Figure 2.16 depicts an instance wherein a species A is removed from the liquid (α) phase to the mobile solid (β) phase. This exchange is solely based on thermodynamic considerations. But, there can also be an exchange between the mobile solid phase (β) and the immobile solid phase (γ), which can be purely due to mechanical interactions (eg. particle-foreign body collisions, where the foreign body could be an impeller or just the vessel inner-wall). All these exchanges result in changes to the state variables in the liquid/solid/gas phase, which ultimately provide the realization of a given task.

(b) Task-related design decision variables in a synthesis model for Phase Building Blocks

This section explains the decisions a designer can make in setting up a task and its associated PBBs. Please note that the decisions mentioned here are present in the Level 4 specifications Table 2.17 - column 2 (design variables). In order to explain the role of the design decision variables, a fundamental model for the synthesis is presented. The presented model is not meant to be a compelling template for all synthesis situations of PBBs.

In order to achieve the final target state (eg. desired crystal size/shape, slurry density, etc), the transition conditions must be conditionally controlled with respect to the physical events that can effect the transformation, i.e. the physical event can take place only if the corresponding states of the phases remain in feasible domains wherein the driving forces and rate processes can be rendered active. The first design decision for a PBB is to set a *duty* that specifies a target transfer flow between phases, $\psi_{t\arg et}^{(\alpha,\beta)}$. Often a duty is specified as a fraction of a throughput material flow $F_{t\arg et}^{\alpha}$. :

$$\psi_{t\arg et}^{(\alpha,\beta)} = Duty.F_{t\arg et}^{\alpha} \tag{2.1}$$

Some of the design decision variables that can play a role may be:

- preferred thermodynamic phases (solid, liquid, gas)
- extra driving forces to influence desired fluxes (g, electromotive force,..)
- improved kinetics (fluiddynamic regime, catalyst,…)
- contact modes and areas between phases/walls
- contact times (residence times)

Here, the discrete elements will be the thermodynamic phases, type of force fields, etc. while the continuous variables will be the states of phases, forces, fluxes, etc.

In order to meet a certain specified design duty (eg. a specific product quality defined in terms of a final crystal size (L)), a suitable rate process(es) and driving force(s) must be created. In the theory of non-equilibrium thermodynamics (de Groot and Mazur, 1969), all physico-chemical processes can be described by a combination of driving forces, X and fluxes, ϕ. Sufficiently close to thermodynamic equilibrium, the relation between fluxes and forces can be described by linear relations with phenomenological constants, K.

$$\begin{aligned}\phi_1 &= K_{11}X_1 + K_{12}X_2 + \ldots\ldots\ldots + K_{1n}X_n \\ \phi_2 &= K_{21}X_1 + K_{22}X_2 + \ldots\ldots\ldots + K_{2n}X_n \\ \vdots &\qquad\qquad\qquad \vdots \\ \phi_n &= K_{n1}X_1 + K_{n2}X_2 + \ldots\ldots\ldots + K_{nn}X_n\end{aligned} \tag{2.2}$$

The off-diagonal elements in Equation 2.2 imply that a driving force for one state variable can lead to a flux of another state variable. These cross-effects are especially important for systems in which multi-component mass transfer takes place. The Maxwell-Stefan model is an elaboration of this multi-component transfer.
Thus,

$$\begin{aligned}&\psi^{\alpha\longrightarrow\beta} = \phi(\bar{X}^{(\alpha,\beta)}, \bar{X}^{(\alpha)}, \bar{X}^{(\beta)}; \bar{K}).a^{(\alpha,\beta)}.V^{(\alpha,\beta)} \\ &V^{(\alpha,\beta)} = V^{(\alpha)} + V^{(\beta)} \\ &a^{(\alpha,\beta)} = f(H, M_A) \\ &H = f(v^{\alpha}, v^{\beta}, \varepsilon^{(\alpha,\beta)}) \\ &\bar{X}^{(\alpha,\beta)} = s^{\alpha} - s^{\beta} \\ &\bar{X}^{(\alpha)} = \nabla s^{\alpha};\ \bar{X}^{(\beta)} = \nabla s^{\beta}\end{aligned} \tag{2.3}$$

where:
$\psi^{(\alpha\longrightarrow\beta)}$ - transfer flow from phase α to phase β
K - transport co-efficient,.
a - contacting area,
$V^{(\alpha,\beta)}$ - volume,
H – flow regime
M_A – contact mode of operation
v – superficial velocity,
ε - phase ratio,
s – thermodynamic variable

Here, $\{a, V, H, M_A, v, \varepsilon, s\}$ could be the typical design decision variables. It is known that fluiddynamic flow conditions exert influence on various transport/transfer parameters and phase contact areas ($a^{(\alpha,\beta)}$). At this stage of design, the detailed influences must be ignored to keep the overall synthesis problem manageable. Order of magnitude estimates for transport coefficients and phase contact areas are deemed sufficient. The analysis phase in the design cycle is the appropriate place to make corrections, if significant deviations would occur between the assumed parameters and calculated parameter estimates when fluiddynamics is taken into account.
However, as mentioned earlier, the presence of these driving forces can also give rise to fluxes for some other properties or species (in case of multi-component systems), where the change is not aimed for or desired. If for instance, there are more species ($B^{(\alpha)}, C^{(\alpha)}, \ldots$) in the system in addition to the species $A^{(\alpha)}$, and if $A^{(\alpha)}$ is to be selectively removed into the solid phase as $A^{(\beta)}$, then a possibility is to provide sufficient contact area a to facilitate this removal. The undesired rate processes can be limited (in some cases) by manipulating the design decision variables. This can be very effective in the case of existence of polymorphs or impurities in the system and where the need is to control their ratios or perhaps arrest the formation of the undesired species completely.

Having discussed the design decision variables, next it will be shown how this concept of phase building blocks plays its role in the optimum design during process synthesis. For this purpose, we treat the design problem more from an optimization perspective, where the goal is to manipulate the

design decision variables to minimize a desired objective function (J). The desired objective function could as simple as the ratio of the adverse competitive rates over the rate of change of the target variable. The many design decision variables of a PBB provide enough degrees of freedom for such optimization.
A typical characteristic of such an optimization problem is that it consists of both continuous real-valued design variables, like equipment dimensions, temperatures, pressures, flowrates, etc. and discrete integer-valued design variables, indicating the structure of the process. The discrete design variables are associated with a so-called *superstructure*, which has embedded within it, a large set of feasible process operations and interconnections that are candidates for an optimal process design. Within such an optimization formulation, behavioral models play a key role; hence they are first discussed here and then, the performance models which define the optimization are dealt with.

2.4.3 Behavioral (process) and performance models for task-based design

The models presented in this section are capable of providing a very detailed description of the physical behavior of a crystallization stage. Such amount of detail is certainly essential for the analysis phase of a design. For the synthesis phase, such amount of detail in modelling can be prohibitive in terms of cost of model development and in computational efforts. It is not the computing time as such but rather the human-assisted process of getting the models converged. For the synthesis phase, it is recommended to restrain the modelling to:

- essential components and phases only
- conservation equations with moment approaches to the crystal population
- simplified physical property correlations
- simplified rate equations
- simple fluiddynamic regimes

Before presenting a behavioral model for crystallization with considerable physical-chemical detail, it will be helpful to highlight the generic structure of the model to catch its main features. The model is formulated in a general dynamic form, capturing batch processing as well. To achieve closure of the model (i.e. having as many equations as variables) it needs to be supplemented with design specifications. Generic structure of the behavioral model:

$$\begin{aligned}
\dot{x}(t) &= f(x(t,L),\nabla_L x(t,L),z(t,L),u(t),\sigma_c,\sigma_d), \quad \forall t \in [0,T],\\
0 &= g(x(t,L),\nabla_L x(t,L),z(t,L),u(t),\sigma_c,\sigma_d), \quad \forall t \in [0,T],\\
0 &\le h(x(t,L),z(t,L),u(t),\sigma_c,\sigma_d),\\
0 &= k(x(0,L)) - k_0(L),\\
0 &= l(x(t,L),\nabla_L x(t,L)) - l_0(t), \qquad L = L_1
\end{aligned} \tag{2.4}$$

t - time
L - geometric and / or crystal size coordinate
$x(t,L)$ - state variables ;
$z(t,L)$ - output variables ;
$u(t)$ - time variant input variables;
σ_c - continuous design decision variables (e.g. fluiddynamics, flow regime, axial fluid velocity, volume, contact area between phases, residence time, states of phases, etc) ;
σ_d - discrete design decision variables (type of force fields, number of components, preferred thermodynamic phase, contact mode and areas, etc);
f - (partial) differential equations, covering the conservation equations;
g - algebraic equations, describing physical properties, rate equations, phase equilibria;
h - end-point and path constraints (e.g. 650μm < median crystal size < 675 μm) ;
k - set of initial conditions for the state
k_0 - given initial conditions
l - boundary condition for the geometric and/or the crystal size coordinate L at size $L = L_1$.
l_0 - given boundary condition for the geometric and/or the crystal size coordinate L at size $L = L_1$.

The behavioral model will have *degrees of freedom*[18]. These degrees of freedom must be fixed in order to be able to solve the model. The designer can take away the degrees of freedom by means of some design specifications. These specifications usually involve the required duties of the process unit, as well as a specification of the mode of operation (dynamic or steady state) of the unit.

Design specifications:

$$\begin{aligned} 0 &\le DS(x(t,L),z(t,L),u(t),\sigma_c,\sigma_d) - DS_0, \\ 0 &= p(\sigma_c,\sigma_d), \\ 0 &\le q(\sigma_c,\sigma_d), \\ 0 &= u(t) - U(t), \end{aligned} \tag{2.5}$$

DS - design specification functions;
DS0 - design specification values;
p - equality constraints on decision variables (e.g. vessel temperature = 50^{0}C) ;
q - inequality constraints on decision variables (e.g. $19\ ^0C \le Fines\ \Delta T \le 20\ ^0C$);
U(t) - specified mode of operation of the input variables over time.

Rather than taking away all degrees of freedom of the behavioral model by means of algebraic type of specifications, it is also possible to cast the design problem in the form of an optimization problem. Then, a performance function is introduced which is optimized over the remaining degrees of freedom (see section on Performance Optimization)

2.4.3.1 Specification of a Behavioral (process) model for a crystallization unit

The process (behavioral) models (that include all the above state variables and continuous/discrete design decision variables), needed to build up the relevant fundamental tasks, must always be defined over a domain of independent variables, possibly involving time, geometric (spatial) coordinates and internal coordinates of a crystal particle, like its size. The geometric space can be spatially arranged either in a zero-dimensional (lumped), one-dimensional, two-dimensional or three-dimensional space. The preferred spatial structure is dependent on and determined by the degree of detail one wants for the fluiddynamic description. Here, the fluiddynamics part is deliberately kept simple in the design synthesis by allowing for a few options:

- perfectly mixed phase (0-dimensional)
- counter-current plug flow (1-dimensional)
- co-current plug flow (1-dimensional)
- cross-current plug flow (2-dimensional)

The model to be presented here is applicable to a single perfectly mixed stage. Multiple thermodynamic phases are taken into account, comprising vapor, liquid and solids. The key modeling assumptions are listed in Bermingham(2003a), some of which are briefly given here:

- vapor and liquid phase are in full equilibrium (chemical, thermal, mechanical)
- liquid and solids are in thermal and mechanical equilibrium, not in chemical equilibrium
- a particle population with one or more distributed properties
- the particle distribution can change in time due to rate phenomena
- when phases are not in chemical equilibrium internal fluxes between the phases will arise
- …..

[18] The difference between the number of variables involved in a design and the number of relationships in a design model is called the number of *degrees of freedom* (Sinnot, 1999)

Consider a control volume for a task with volume V, temperature T, pressure P, NC_L components for the solute in the liquid phase, NR_L liquid phase reactions, NP_S solid (crystalline) phases, NI S/L inlet and NO S/L outlet streams and one vapor outlet (which is considered in the solvent mass balance and heat balance equations). It is assumed that each solid phase is created or depleted via one reaction only.

The set of equations that governs the process synthesis of innovative crystallizer configurations will primarily consist of:

- conservative equations of change w.r.t. each phase;
- fluiddynamics
- thermodynamic equations of state w.r.t. each phase;
- rate expressions
- phase equilibrium conditions

These behavioral models that are presented here are for general illustration purpose(s), but can be tailored for any specific task.

I. Conservative equations of change w.r.t. phase (after Bermingham, 2003a)

- **Mass balance**

Mass balance for liquid phase component –solvent

$$\overbrace{\frac{dm_{L,solvent}}{dt}}^{\text{mass rate of accumulation}} = \overbrace{\sum_{k=1}^{NI}\phi_{m,L,solvent,in,k} - \sum_{l=1}^{NO}\phi_{m,L,solvent,out,l} - \phi_{m,V,solvent,out}}^{\text{mass rates in and out via convective transport}} + \overbrace{M_{solvent}\sum_{p=1}^{NR_L}v_{L,p,solvent}\cdot r_p}^{\text{mass production rate due to liquid phase reactions}} + \overbrace{M_{solvent}\sum_{q=1}^{NP_S}v_{S,q,solvent}\cdot[\phi_{mol,grow,q} + \phi_{mol,nucl,q} - \phi_{mol,dis,q}]}^{\text{interphase mass flux due to crystal growth and due to primary nucleation and dissolution at the critical nucleus size}} \quad (2.6)$$

Mass balance for liquid phase component –solute (for $i = 1$ to NC_L)

$$\overbrace{\frac{dm_{L,solute}}{dt}}^{\text{mass rate of accumulation}} = \overbrace{\sum_{k=1}^{NI}\phi_{m,L,solute,in,k} - \sum_{l=1}^{NO}\phi_{m,L,solute,out,l}}^{\text{mass rates in and out via convective transport}} + \overbrace{M_{solute}\sum_{q=1}^{NP_S}v_{S,q,solute}\cdot[\phi_{mol,grow,q} + \phi_{mol,nucl,q} - \phi_{mol,dis,q}]}^{\text{interphase mass flux due to crystal growth and due to primary nucleation and dissolution at the critical nucleus size}} \quad (2.7)$$

Similar expressions can be derived for the vapor phase component(s) if present.

- **Population balance**

Population balance for solid phase q (for $q = 1$ to NP_S)

$$\overbrace{\frac{\partial\left(n_q(L,t)V(t)\right)}{\partial t}}^{\text{number rate of accumulation}} = \overbrace{-V(t)\frac{\partial\left(n_q(L,t)\cdot G_q(L,\sigma)\right)}{\partial L}}^{\text{rate of number gain due to crystal growth}} + \overbrace{\sum_{k=1}^{NI}\phi_{V,in,k}(t)\,n_{q,in,k}(L,t)}^{\text{number rate in}} - \overbrace{\sum_{l=1}^{NO}\phi_{V,out,l}(t)\,n_{q,out,l}(L,t)}^{\text{number rate out}} + \overbrace{(\phi^{+}_{n,q,nucl}-\phi^{-}_{n,q,dis}).V(t)}^{\text{number production rate due to primary nucleation and dissolution at the critical nucleus size}} + \overbrace{(\phi^{\pm}_{n,q,attr}+\phi^{\pm}_{n,q,break}-\phi^{\pm}_{n,q,aggl}).V(t)}^{\text{number production rate due to attrition, breakage and agglomeration}} \tag{2.8}$$

The population balance is in fact a distributed mass balance for the solid or dispersed phase, and is linked to the liquid or continuous phase component mass balances via the crystallisation kinetics. Equation (2.8) represents the conventional form of the population balance equation. Because the solid and liquid phases are in intimate contact, the volume term V represents a pseudo slurry volume.

- **Moment equations**

Though population balance equations (PBEs) are very useful in determining the evolution of the CSD, they add to the modelling complexity at the same time. This can be resolved by transforming the PBE into a moment form for which analytical solutions can be attained that allow the description of the dynamic behavior of crystallizers. The moments (m_j) of a distribution are generally defined as:

$$m_j(t) = \int_0^{\infty} n(L,t).L^j dL \tag{2.9}$$

and can be related to lumped properties of the entire crystal population.

Thus, the partial differential equation in the PBE can be reduced to a set of ordinary differential equations (ODEs) by means of the moment transformation(s).

- **Enthalpy balance** – The dynamics of the temperature are given by the energy balance for the entire system. Here, the energy balanced is simplified into an enthalpy balance by assuming that kinetic energy, potential energy and shaft work can be neglected.

$$\overbrace{\frac{dH(t)}{dt}}^{\text{rate of enthalpy accumulation}} = \overbrace{\sum_{k=1}^{NI}\phi_{H,in,k}(t) - \sum_{l=1}^{NO}\phi_{H,out,l}(t) - \phi_{H,V,out}(t)}^{\text{rate of total enthalpy in and out by convection}} + \overbrace{Q(t)}^{\text{net rate of heat addition}} \tag{2.10}$$

Of course, for continuous crystallization processes, the dynamic terms in all the above equations can be comprised, which can greatly reduce computational times.

II. Fluid-dynamics of slurry

Instead of using equations of momentum, the computational demands can be drastically simplified by making use of (semi-)empirical equations:

- Fluiddynamic regime of operation (flow patterns), eg. annular flow, intermediate slug flow, bubble flow, etc, leading to a fixation of the range and ratio of the superficial velocities of the phases involved;.

- Flow pattern =f(stirrer frequency, superficial velocities of the respective phases ($v^{(\alpha)}$, $v^{(\beta)}$)
- Residence time distribution
- Phase hold-up ($\varepsilon^{(\alpha)}$) = f (physical properties, flow rates,…)
- Specific contact area $a^{(\alpha\beta)}$ between the different phases = f (physical properties, flow rates)
- Pressure drop (Δp)= f (physical properties, flow rates, ε)
- Phase ratios of different species (eg. polymorphic solid phases for same chemical species)
- …..

III. Thermo-physical equations of state w.r.t. phase

- Density (T)
  Solid phase (α): $\rho_s^{\alpha} = K_1 - K_2.T^{\alpha}$; $\left[T_1^0 C \le T \le T_2^0 C \;;\; c_1 \; wt\% \le c \le c_2 \; wt\%\right]$
  Similar expressions can be derived for the liquid and vapor phases as well.

- Solubility (T)
- Specific heat capacity(T)
- Viscosity
- …..

IV. Rate expressions

- Reactions within a given phase; eg. $r_p^{\alpha} = k.C_A^{\alpha}$
- Species mass transfer between phases;
- ……

A few of the kinetic rate terms in the component mass balances and population balances are shown here:

$$\phi_{mol,nucl,q}(t) = \frac{k_v \rho_s}{M_s} V(t) \int_0^{\infty} \phi_{n,nucl}^{+}(L,t) L^3 dL \tag{2.11}$$

$$\phi_{mol,grow,q}(t) = -\frac{k_v \rho_s}{M_s} V(t) \int_0^{\infty} \frac{\partial (n(L,t) G(L,t))}{\partial L} L^3 dL \tag{2.12}$$

$$\phi_{mol,dis,q}(t) = \frac{k_v \rho_s}{M_s} V(t) \int_0^{\infty} \phi_{n,dis}^{-}(L,t) L^3 dL \tag{2.13}$$

- Heat transfer : $Q = UA(T^{\alpha} - T^{\beta})$

- Crystallization kinetics (eg. nucleation, growth, attrition, etc.)
  - Primary nucleation rate = $\xi D C_e S C_0 \left(\frac{k_B T}{\gamma_{ef}}\right)^{1/2} \ln S . exp\left[\frac{-W^*}{k_B T}\right]$; $S = f(\Delta\mu)$
  - Growth rate - $G = K_g a \Delta C^i$; $1 \le i \le 2$

$\frac{1}{K_g a} = \frac{1}{k_d a} + \frac{1}{k_r a}$; a represents the interfacial area per unit volume (m^2/m^3)

where: $G = f(\Delta c, L) = f(\Delta\mu, L)$; and $\Delta\mu = \mu^{\alpha} - \mu^{\beta}$

The mass transfer coefficient (k_d) is given by (Herndl, 1982):

$$\frac{k_d L}{D_{AB}} = 2 + 0.8\left[\frac{\bar{\varepsilon}.L^4}{v_l^3}\right]^{1/5}\left[\frac{v_l}{D_{AB}}\right]^{1/3} \text{ ; where; } \bar{\varepsilon} = \frac{Ne.s_{imp}^3.d_{imp}^5}{V}$$

- …….

V. Phase equilibrium conditions

- Temperature: $T^{\alpha} = T^{\beta} = T^{\xi}$ (liquid, solid and vapor)
- Pressure: $P^{\alpha} = P^{\beta} = P^{\xi}$ (liquid, solid and vapor)
- Chemical potential: $\mu^{\alpha} = \mu^{\beta}$ (liquid and solid)
- ……

The above behavioral equations need to be complemented by design specifications in order to remove some or all degrees of freedom. Some choices for the design specifications are the fixation of the following variables:

$$\left\{L_{target}^{<50>}, \varepsilon, T, P, C, s_{imp}, d_{imp}, ...\right\}$$

Having fixed most degrees of freedom, the model will allow computation of all relevant geometric equipment dimensions, like volume, contact surfaces, etc. Leaving open some degrees of freedom will permit optimization of the performance over the remaining degrees of freedom.
The logic for supporting the task in terms of the various phase interactions may be apparent now. With the presence of multiple phases (phase splitting), there is more scope for manipulating the state-variables (both discrete and continuous). This can be very useful in maximizing the economic potential, for instance. This approach would provide a model-based way of integrating some tasks into a design compartment (explained later), obtaining the duties at minimum efforts while keeping adverse effects from task integration at bay.

2.4.3.2 Performance optimization models for task-based design

The performance optimization contains three parts:

1. Formulating a process out of a task network

Using individual tasks as building blocks, a process unit design problem can be formulated. To illustrate this task-based approach, a helicopter view of this procedure can be seen in Figure 2.17. It shows how a crystallization process is split into tasks (T_1,T_2….T_n) which in turn are made up of **P**hase **B**uilding **B**locks (PBBs). It is emphasized that Figure 2.17 is only one way of visualizing the structure of the task network. A formal and complete characterization of the task network structure would require a full-fledged **structure model** in addition to the behavioral models. Since the development of such a structure model is a very significant effort, it was kept outside the scope of this thesis. Here, just a flavor is given of the physically motivated thinking to create such a task network structure, without aiming to be complete for computational purposes.

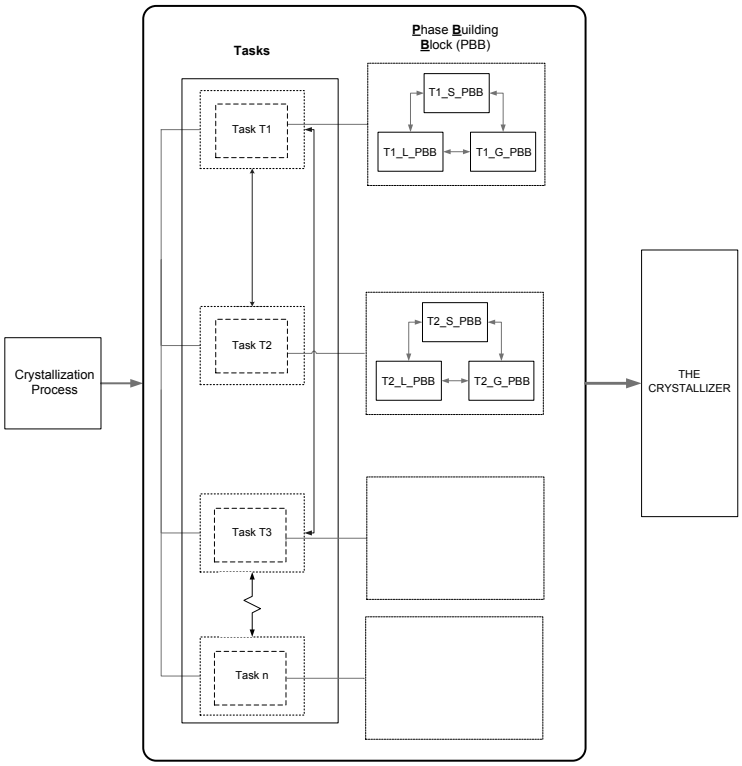

Figure 2.17 Decomposition of a crystallization process in terms of tasks

In the representation of Figure 2.17, only the tasks can be connected with each other by means of streams/connections and not the PBBs in different tasks. This is done to make the task-based design look easy and simple which will definitely simplify issues at the modelling stage. The task-based design procedure will be explained in more (but not exhaustive) detail in the ensuing sections. Here it will suffice to give a few heuristics to connect tasks:

- the key physical events operate well under the same physical state (P,T, composition of phases)
- the driving forces for the task-related events do not interact in a negative sense, when brought into contact
- one or two phases are almost always present in all the tasks; the presence of any other phase is not adverse

This process of connecting different tasks and arranging them in different sequences can generate a large network of alternative process configurations, which ultimately results in a superstructure. Such a task-based superstructure for the overall process can be subjected to Mixed Integer Dynamic Optimization (MIDO) making use of multiple resources (mass, energy, money, etc.) and subject to:

- *Behavioral models* for each task block with constraints
- *Structural models* for connectivity between task blocks
- *Plant wide controllability models* as physical/operational constraints
- *Performance models* with minimum performance constraints

2. Process performance optimization

Here, the process design problem is formulated as an optimization problem. Mathematically the problem can be formulated as a Mixed Integer Dynamic Optimization (MIDO) problem (Bansal, 2000) as follows:

$$\begin{aligned} &\min_{u(t),\sigma_c,\sigma_d,t} J(x(t),z(t),u(t),\sigma_c,\sigma_d,t) \\ &s.t. \quad \dot{x}(t) = f(x(t),z(t),u(t),\sigma_c,\sigma_d), \quad \forall t \in [0,t], \\ &\quad 0 = g(x(t),z(t),u(t),\sigma_c,\sigma_d), \quad \forall t \in [0,t], \\ &\quad 0 \le h(x(t),z(t),u(t),\sigma_c,\sigma_d), \\ &\quad 0 = p(\sigma_c,\sigma_d), \\ &\quad 0 \le q(\sigma_c,\sigma_d), \\ &\quad 0 = x_0 - x(0), \\ &\quad 0 = u_0 - u(0), \end{aligned} \tag{2.14}$$

J - objective function;
x_0 - initial conditions
u_0 - initial values of the input variables.

The objective function J could embed multiple objectives as an economic parameter EP_0, € (annualized capital costs, operational costs, return on investment, etc). The investment costs are functions of the equipment dimensions and type of course.

$$J(EP_0) = \frac{1}{\tau}.(\text{investment cost}) + \beta.(\text{annual operating cost}) \tag{2.15}$$

where τ could be the economical horizon and β is a weighting factor (e.g. correction factor for, say tax).
In addition to process economics, it is also desirable to consider sustainability aspects, such as exergy efficiency and minimal waste losses

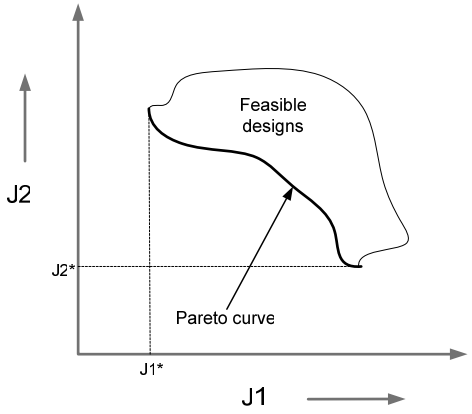

Figure 2.18 Pareto curve for two objectives

In general, each objective function itself can be minimized, but it is not possible to simultaneously minimize both or all of the objective functions. Figure 2.18 shows a typical feasible solution set.
The Pareto solution consists of those designs where one objective can only be improved at the expense of the other objective function. For the designs that do not lie on the Pareto curve, always at least one objective can be improved, without resulting in a negative effect on the other objectives. The designer has to select a single design later by making a trade-off between the various objectives. Rather than doing a Pareto optimization, it is also possible to perform a conventional optimization with a single objective function, while the other objective functions have been reformulated as inequality constraints which must be met.

3. Process design optimization calculations

The numerical optimization techniques that can be employed to find the optimum design embedded in the superstructure can be either gradient based, mixed integer non linear programming techniques (MINLP) (Grossman, 1997, Floudas, 1995) or genetic algorithms (Emmerich, 2000). The main benefit of the optimization-based approaches is that it can really find the optimum solution embedded within the problem statement. However the time required for this is substantial. Especially the formulation of

the problem and the efforts required to get the converged solution from arbitrary initial conditions can be significant. Hence, suitable approximations are needed at appropriate instances to reduce the computational effort and provide a trade-off between enough complexity for design v/s speed and robustness of CPU time.

With this outline of the behavioral models, the task network structure and the features of the design optimization, we have reached the end of the description of the task concept and its attributes. Out of the 15 attributes of any task, the attributes 'name' and 'phase' are already specified when a task is selected. The task attributes: the target variable, (extent of) duty and performance come from a higher level, as well as the ports and time ordering. All remaining attributes are determined by the designer; i.e. event, PBB, behavior, constraints, etc.

2.4.4 Steps in task-based synthesis procedure - a design hierarchy

In view of the many degrees of freedom in the synthesis and the associated combinatorial complexity, a hierarchical structuring of the decision making within level 4 is introduced. This structuring is based on the sequential formation of primary, secondary and tertiary structures, being *tasks* (primary), *compartments* (secondary) and *process unit* (tertiary). A compartment is a spatial region (as meant in attribute 14) in which a combination of tasks can be carried out in parallel (continuous processing mode) or in a sequential mode. Obviously, the operation conditions for effective execution of the tasks must match. A process unit is also a spatial domain entity, being a collection of compartments, which are closely integrated by mass, energy and momentum stream exchanges. A process unit can accomplish the overall transformation from feed streams to target products streams.
In process synthesis, there is always the choice between running different tasks simultaneously in different spatial domains (continuous processing) or by scheduling the tasks sequentially in time for execution in the same spatial domain (batch like operation). For the sake of conciseness, the following explanation will focus on the continuous processing mode. A similar development could be given for the batch mode.
The task-based synthesis methodology will be decomposed into layers of decision-making which is an essential step towards developing a structure model and a model based synthesis and design environment. The proposed hierarchy consists of ten levels as shown in Table 2.9.

Table 2.9 Proposed task-based synthesis hierarchy

Synthesis sub-levels	*Description*	*Domain*
4.1	Identification of tasks for a crystallization process	temporal and spatial
4.2	Selecting phase building blocks for each task	temporal and spatial
4.3	Connection of different tasks	spatial
4.4	Integration of different tasks within a design compartment	spatial
4.5	Connection of different design compartments into process units	spatial
4.6	Operational unit identification	spatial
4.7	Connection of different tasks	temporal
4.8	Integration of different tasks within a design compartment	temporal
4.9	Operational unit identification	temporal
4.10	Connection of different design compartments into process units	temporal

Synthesis sub-levels 4.1 and 4.2 are primarily aimed at identifying the physical mechanisms and building blocks that would constitute the different relevant tasks. These can be spread across the temporal and spatial domain. Levels 4.3 to 4.6 focus on the connection, integration and interaction of these tasks within a spatial domain. Levels 4.7 to 4.10 repeat what has been done in levels 4.3 to 4.6, but within the temporal domain. The split in spatial and temporal domains may be needed when dynamic models cannot be used and when dynamics need to be accounted for in a batch process (say). In this chapter, only levels 4.1 to 4.6 will be discussed in detail, with a brief overview on levels 4.7 to 4.10 which can be found in Appendix A2.3.

2.4.4.1 Sub-Level 4.1 : Identification of tasks within a crystallizer (both temporal and spatial identification)

The first step in task-based design is to identify the relevant tasks to execute the crystallization process (already decided at Level 3). Some of the most generally encountered tasks for a crystallization process are listed in Table 2.10. In an ideal world, one would want the newly born primary nuclei (seeds in case of seeded crystallization), to just undergo *uniform growth* to a pre-defined crystal size and the right morphology, mostly contributing to a very narrow crystal size distribution. In this case, the only tasks that would be needed are *crystal growth* and *supersaturation generation*. But tasks like *secondary nucleation*, *crystal dissolution*, *fines destruction*, etc. will almost always come into play in order to achieve the desired product specifications.

So from a different perspective, mechanisms like secondary nucleation can be considered as 'undesired'[19] effects. But, by carefully manipulating and exploiting these undesired effects to achieve the certain desired design specification(s), they become tasks. In this chapter, all these possibilities will be treated as 'tasks', by acknowledging that a desired task can result in undesired outcomes.

There can be some more tasks as well. For example, consider the downstream operations wherein, if the final product after crystallization is still wet, it has to be dried, which involves changing the temperature of crystal phase which is achieved by means of changing the temperature of fluid surrounding it in a dryer. Also, there can be mother liquor inclusions in the crystalline phase, or phenomenon like growth rate dispersion. These can be very easily incorporated within the task-based design framework. But, for simplicity, it is decided to stick with the very basic tasks needed for the core crystallization process to proceed.

Table 2.10 Commonly occurring tasks for solution crystallization processes

Task	Abbrevi-ation	Change of state	Target variable	Event/Force
Crystal growth	GR	continuous size enlargement of crystal	crystal size	chemical potential difference
Crystal dissolution	GR	continuous size reduction of crystal	crystal size	chemical potential difference
Primary nucleation	PN	new solid phase formation from a clear liquid via • supersaturation generation • ultrasound as actuator	concentration	breaking the metastability barrier
Secondary nucleation				birth of new crystals from the parent crystals :
• *Crystal – Foreign body*	SN-FB	secondary nucleation by attrition	crystal size	contact between crystal-hardware
• *Crystal – Crystal*	SN-CC	secondary nucleation by crystal-crystal collisions	crystal size	contact between crystal-crystal
• *Activated nucleation*	SN-AN	secondary nucleation due to surface breeding/ shearing of secondary nuclei	crystal size	fluiddynamic conditions surrounding the crystal
Agglomeration	AG	discontinuous size enlargement of a crystal	crystal size	chemical bonding, van der Waal's forces
Breakage	BR	discontinuous size reduction of a crystal	crystal size	contact between crystal-hardware
Supersaturation generation	SS	change in solute concentration	concentration	create driving force for crystallization
Classification	CL	particle segregation	density difference	density difference between particles and liquid
Fines Dissolution	FD	destruction of fine particles	crystal size	effecting solubility of fine crystals
Heat Exchange	HX	change in temperature	temperature	effect thermodynamic properties of liquid/solid phase
Mixing (Pump /Circulation device)	MX	uniform conditions	concentration	effect mixing of material/energy streams

[19] These *undesired* effects arise from the side effects of forces needed to carry out the *main* task and create the target rate process and flux. Something is a task **only** if it is an intentional use of a physical event to achieve a target.

2.4.4.2 Sub-Level 4.2 : Selecting phase building blocks (PBB) for each task (both temporal and spatial identification)
Here, each task is being assigned basic building blocks as an attribute. It is possible to define a number of generic phase building blocks, which can be associated with the tasks. So next, it will be shown how the different phase building blocks make up the different tasks listed above. The relevant phase building blocks for the solid, liquid and gas phase are listed in the tables below (Table 2.11, 2.12 and 2.13).

Table 2.11 PBB for the solid phase

PBB	Description	State variables
S_CG	growth of the crystals	C, M, n, L
S_PRIM	generation of primary nuclei	n
S_SN-FB[20]	generation of secondary nuclei by crystal – foreign body collisions	n
S_SN-CC	generation of secondary nuclei by crystal – crystal collisions	n
S_SN-AN	generation of secondary nuclei by activated nucleation	n
S_AGGL	generation of crystal agglomerates	C, M, n, L
S_BREK	generation of fractured particles	n
S_CLA	selective removal of small crystals to increase density of mother liquor	C, M, n
S_PR	selective removal of small crystals ($L>L_F$) from a suspension of crystals	C, M, E, n
S_FR	selective removal of small crystals ($L<L_F$) from a suspension of crystals	C, M, E, n
S_FD	dissolution of fine crystals	C, M, n
S_MIX	mix multiple number density distributions	C , M, P, T, n
S_NOT	dummy phase building block	-

Table 2.12 PBB for the liquid phase

PBB	Description	State variables
L_HEAT	increase in the temperature of the liquid phase	T
L_COOL	decrease in the temperature of the liquid phase	T
L_EVAP	phase change from liquid to vapor phase	C, M,T
L_SPLIT	splitting of the liquid phase into two or more streams	M
L_MIX	mixing of two liquid phase streams	C , M, P, T
L_SGEN	generation of supersaturation	C, T
L_SDEP	depletion of supersaturation	C, T
L_NOT	dummy phase building block	-

Table 2.13 PBB for the gas phase

PBB	Description	State variables
G_HEAT	increase in the temperature of the gas phase	T
G_COOL	decrease in the temperature of the gas phase	T
G_COND	phase change from vapor to liquid phase	C, M, T
G_SPLIT	splitting of the gas phase into two or more streams	M
G_MIX	mixing of two gas phase streams	C , M, P, T
G_PRES	change in pressure of the gas phase	P
G_NOT	dummy phase building block	-

To put the tasks and phase building blocks in perspective, Table 2.14 shows the support of the listed tasks in terms of their respective phase building blocks.

[20] Foreign bodies (impellers, walls, inert solids) could be properly represented as additional solid phases, interacting with the crystalline solids. For sake of conciseness these additional solid phases are lumped with the crystalline solids

Table 2.14 Phase building blocks for common crystallization tasks

Task	Phase Building Block		
	Solid	**Liquid**	**Gas**
Crystal growth	S_CG	L_SDEP	G_NOT
Crystal dissolution	S_CG	L_SDEP	G_NOT
Primary nucleation	S_PRIM	L_SDEP	G_NOT
Secondary nucleation			
• *Crystal –Foreign body*	S_SN-FB	L_NOT	G_NOT
• *Crystal – Crystal*	S_SN-CC	L_NOT	G_NOT
• *Activated nucleation*	S_SN-AN	L_NOT	G_NOT
Agglomeration	S_AGGL	L_SDEP	G_NOT
Breakage	S_BREK	L_NOT	G_NOT
Supersaturation generation	S_NOT	L_EVAP	G_VAP
Classification	S_FR/S_CLA/S_PR	L_SPLIT	G_SPLIT
Fines Dissolution	S_FD	L_SGEN	G_NOT
Heat Exchange	S_NOT	L_HEAT/L_COOL	G_COOL/G_HEAT
Mixing (Pump /Circulation device)	S_MIX	L_MIX	G_MIX

For illustration purpose, the task *primary nucleation* is supported by its respective phase building blocks, as shown in Figure 2.19. The inlet port ($P_{I,M,PN}$) denotes the entry for the liquid material stream containing the supersaturated solution devoid of any solid or gas phase while the outlet port ($P_{O,M,PN}$) indicates the material stream out of the task, containing primary crystals in a liquid (slurry).
The task *primary nucleation* generates primary nuclei (solid phase) from the supersaturated liquid phase. The generation of the new solid phase is depicted by the phase building block PN_S_PRIM which is coupled with the phase building block in the liquid phase, PN_L_SDEP, which results in the depletion of supersaturation in the liquid phase. As there is no activity within the gas phase, it is represented by the dummy phase building block PN_G_NOT.

After the tasks have been supported by its respective phase building blocks, the next step involves the connection of these tasks.

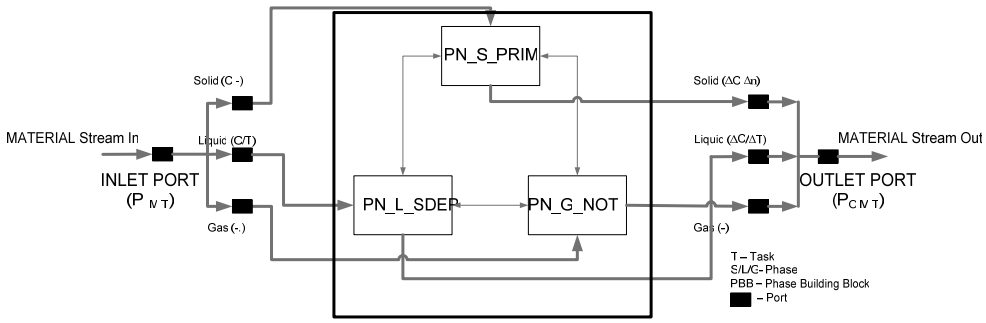

Figure 2.19 Phase building blocks making up a task (here *primary nucleation*)

2.4.4.3 Sub-Level 4.3 : Connection of tasks (spatial connection)

At this level, all the tasks that are considered to be necessary and identified above are connected. Here a superstructure can be generated that takes into account all possible combinations among different tasks. To connect the tasks with each other, certain guidelines are identified. Some of these can be seen as compulsory and some of them flexible (which may be included only to simplify the solution of a superstructure). Just to list a few of these guidelines:

- a task can be connected with any number of other/same tasks provided that the continuity in the state vectors is ensured.
- only the corresponding phase building blocks within a task are connected to each other.
- a task can be repeated many times in spatial domain (using the concept of staging[21]) till the combination has achieved its specified duty. In this case, identical tasks provide a better resolution to carry out a certain mechanism. However, these multiple instances of the same task do differ in some detail with respect to different spatial domains and different duties for the same type of target variable.
- tasks can be arranged in sequence or in parallel.
- no adverse coupling effects between rate events associated with tasks to be connected, i.e. care should be taken to arrange tasks in such a way that the effect caused by one should not negate that of the neighbouring tasks. Physically it is possible to connect such tasks, but from a design perspective, this is nonsensical. For instance, task *growth* cannot be directly connected to task *fines dissolution* as they are two opposing mechanisms, which implies that the effect gained by one task is negated by the other.
- uniform operating conditions and operational restrictions in each task.
- tasks must be carried at the same time instant simultaneously.

As a running example through this chapter (for illustration purpose), let us consider a simple case of evaporative crystallization process for a low viscosity system, in a continuous mode of operation. The requirement is to produce crystals with a narrow CSD with a pre-determined median crystal size. For evaporating the solvent to create supersaturation, heat must be provided to the system. The tasks that would need to be effected in order to achieve a specified design criteria could be as follows:

- generation of particle identities (primary nucleation, secondary nucleation)
- growth to a determined target size
- separation and dissolution of certain finer particles to size zero
- increase of solute concentration
- achieve a certain slurry density

Here, it will be shown how using the tasks identified in section 2.4.4.2, can lead to different possible crystallizer configurations, leading to the generation of a mini-superstructure, as shown in Figure 2.20. Again, it must be mentioned that these are only a fraction of the possibilities that could be included in a superstructure.

Figure 2.20(a) is a very simple representation of how these tasks can be woven together to build up a crystallizer. As was discussed earlier, an ideal crystallization process would favor only the growth of crystals, with no other mechanism hampering this process of uniform growth. Figure 2.20(a) could be a possible representation of such a scenario, wherein:

- the supersaturation generated (task *generation of supersaturation*) can overcome the energy barrier for nucleation
- a spontaneous primary nucleation event (task *primary nucleation*) is triggered
- these newly born embryos start growing (task *growth*)
- uniform distribution in supersaturation and fluiddynamics is ensured by good mixing (task *mixing*)

[21] Staging is a measure to reduce a wide distribution of a target property to an acceptable band-width. Such a distribution can be due to underlying fluiddynamic dispersions leading to residence time distributions of the targeted property.

- the driving force for crystallization, i.e. supersaturation to be achieved is provided by solvent evaporation, driven by a heat exchange system (task *heat exchange*)

But, then in a real-life case, its virtually impossible to avoid associated mechanisms like secondary nucleation[22] (say, due to mixing/circulation which would invoke crystal-foreign body collisions). This possibility is represented by Figure 2.20(b). As a result of secondary nucleation, there would be an inevitable generation of fine particles which could hamper the product design specifications. A possible solution could be to introduce a fines destruction and/or classification systems as shown in Figure 2.20(c),(d). Figure 2.20(d) is an even more detailed representation with respect to certain specific tasks, for eg., the task *secondary nucleation* is a combination of two different types of secondary nucleation mechanisms, viz. attrition and activated nucleation. Also, there are multiple instances of the task *growth*. Although these tasks exhibit the same behavior, they are dictated by different duties to realize the desired product specifications. Figure 2.20(e) shows a uniform distribution of supersaturation within the crystallizer which would contribute to uniform growth conditions.
Thus it has been shown in a simple manner how different tasks can be connected in a number of ways in order to realize the final design specifications. When embedded within a modelling environment, this synthesis approach should make it possible to realize different crystallizer configurations and arrive at alternative crystallizer configurations, close to optimal performance[23], , using optimization techniques.

In the superstructure shown in Figure 2.20, there are instances when a certain task appears successively more than once, eg. the task *growth*. This spatial region is referred to as '*growth-zone*', wherein only growth of crystals should occur. Basically, the *growth-zone* is split up into multiple growth tasks and a distinction has to be made between a task-zone and a task itself. A task-zone can be a tubular flow within a crystallizer whereas a task is treated as a mixed zone, in our example. When a number of such *similar* tasks are connected together we get a tubular flow task-zone. It means that for describing the events in a task-zone, one may require a high resolution involving many tasks.
It's of course possible to have multiple task-zones for eg. for primary nucleation, just as shown for growth. But, this is a decision left up to the designer whether to split a volume cell for a task-zone into multiple volume cells or not. This decision will be strongly based on whether the desired design specifications and targets are achieved or not.
It's again possible, to use a plug-flow constraint on the tasks, but using well-mixed zones as the building blocks for the spatial distribution, makes the computational modelling load a bit more easier. This approach is similar to the compartmental modelling approach of Bermingham (2003) who discusses the advantages of using CSTRs as opposed to PFRs for modelling purposes. All the attributes and guidelines for connecting tasks apply to a task-zone as well.
Just as *similar* tasks can be clubbed together, another possibility is the integration of '*dis-similar*' tasks, which will be discussed in the next section. This situation may arise due to instances within the spatial region where two or more tasks go hand-in-hand and are practically inseparable.

[22] Secondary nucleation can be seen as an adverse event here. But, this very event can also be exploited to control nucleation and growth. Thus, it now becomes a task.
[23] Rather than determining a single optimum configuration it seems more practical (in view of the underlying modeling uncertainties) to establish a feasible set of design solutions, all exceeding a threshold performance.

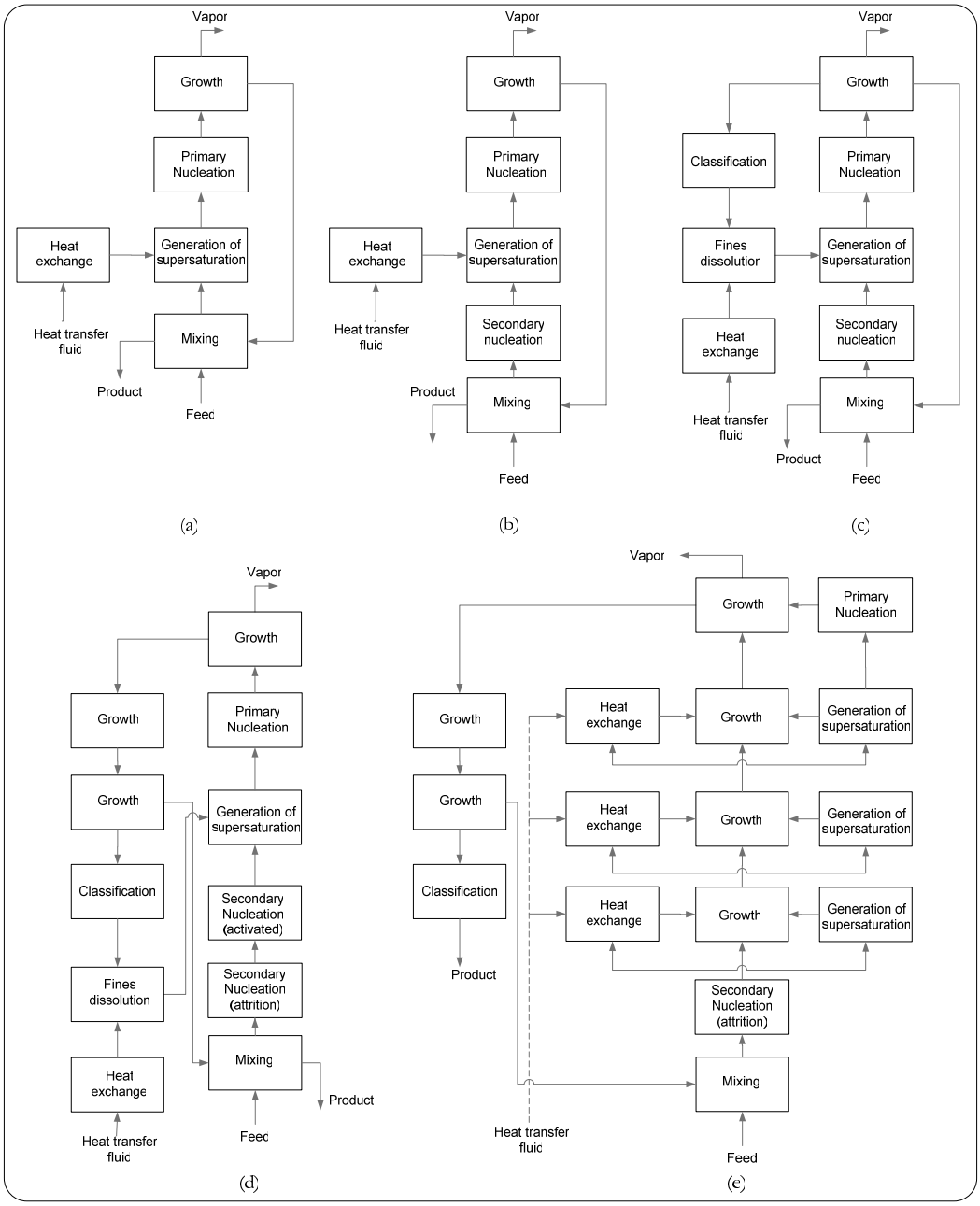

Figure 2.20 The anatomy of a crystallization equipment in the form of a mini-superstructure

2.4.4.4 Sub-Level 4.4 : Integration of tasks in a design compartment (spatial integration)

It's not always necessary to demarcate a specific spatial region for each particular task. On most occasions, there can be multiple tasks co-existing in one region. Then such tasks are integrated together within a spatial region referred to as a *design compartment*. A design compartment inherits all the attributes that hold for a task. In addition, it can be qualified by a few more guidelines that are listed below:

- there are a finite number of design compartments connected to each other.
- the boundaries of a design compartment are defined by the boundaries of the volume and surface of the tasks that it contains.
- the basic building block in a design compartment is still the task.
- a design compartment incorporates a finite number of tasks within it.
- there can be multiple task-zones connected to each other within a design compartment.
- the tasks can be carried out at overlapping processing conditions and comparable time scales.

Care should be taken to avoid as much as possible any adverse coupling effects between rate events associated with tasks to be connected within a design compartment. These rules follow from the ones defined earlier in step 4.3 (for connection of tasks). Again, it is possible that, to describe a design compartment, one may require a high resolution involving sub-design compartments, just like task-zones. Using a similar analogy, there can be a *Design Compartment Zone (DCZ)* which entails multiple design compartments. The final taxonomy in terms of compartmentation will look as follows (Figure 2.21):

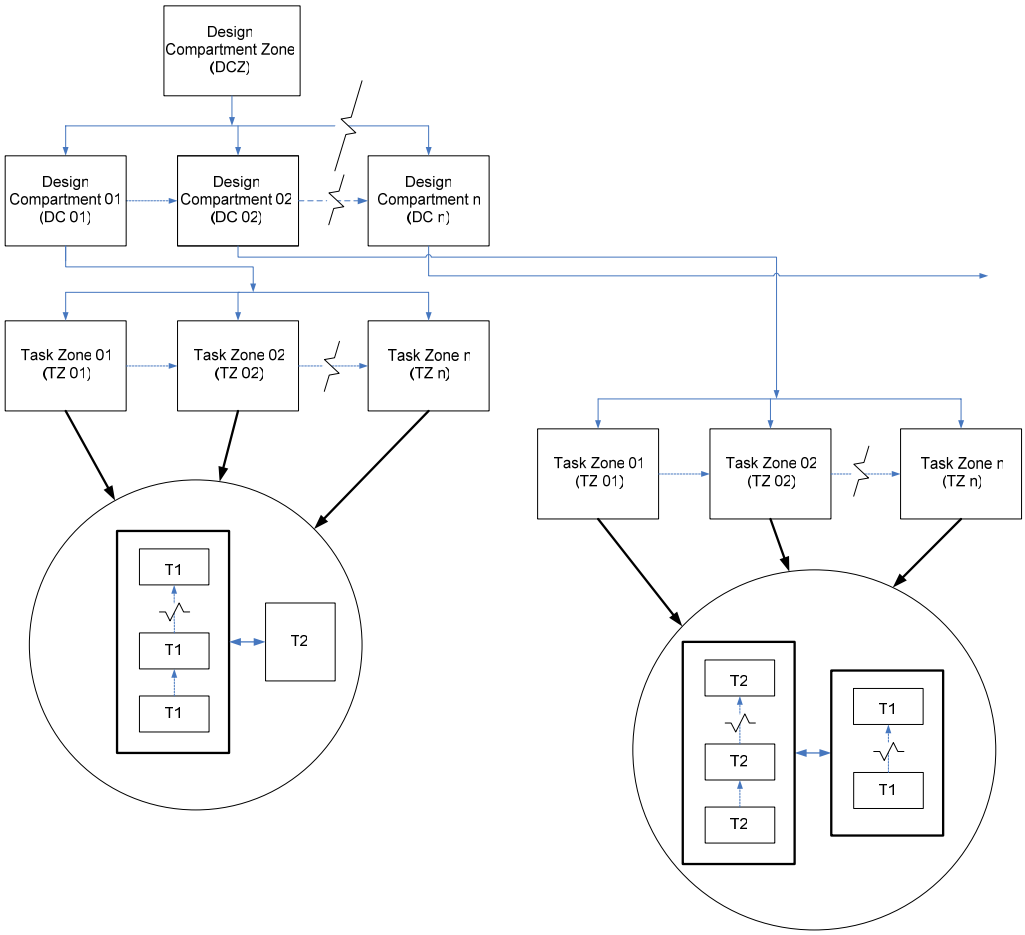

Figure 2.21 Integration of tasks in a design compartment

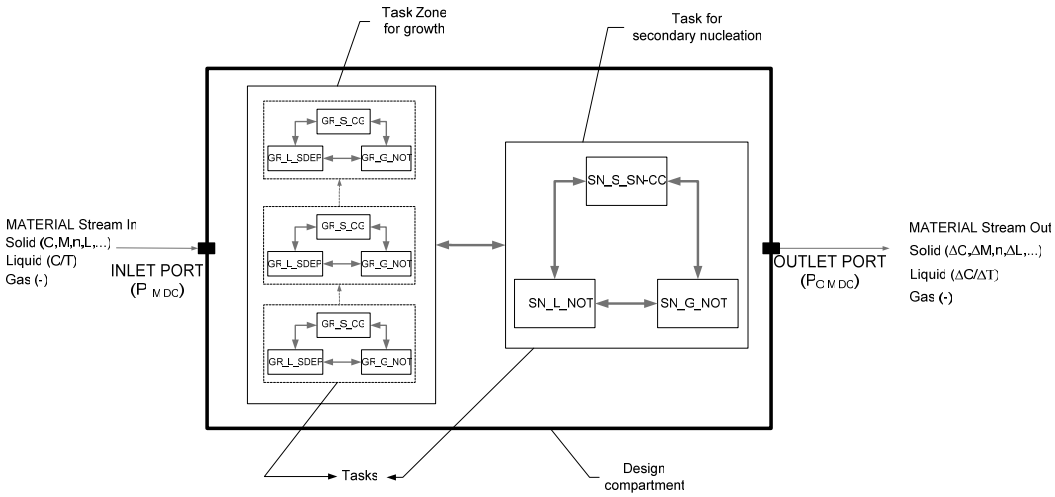

Figure 2.22 Example of co-habiting tasks within a design compartment (here, *crystal growth* & *secondary nucleation*)

Following the taxonomy in Figure 2.21 above drastically simplifies issues for the designer at the modelling stage. To illustrate this particular level, we can consider an instance of a Design Compartment where-in growth and secondary nucleation (crystal-crystal) co-habit. Figure 2.22 shows conceptually what this compartment might look like. This procedure can result in a superstructure wherein the design parameters can include the number of design zones, number of design compartments, number of task-zones, number of tasks, the related structuring and sequencing of these compartments/tasks, etc. But, the arrival at the optimum superstructure is practically feasible only when such a task-based design approach is actually embedded within a modelling environment with optimization capabilities. Due to the numerous tasks involved in a crystallization process, a classification of these tasks in terms of the various design compartments helps to put things in perspective. Table 2.15 gives an account of the strength of occurrence for different tasks within different design compartments.

Table 2.15 Strength of occurrence for tasks within different design compartments

DESIGN COMPARTMENT	TASKS										
	Crystal growth	Nucleation				Agglomeration	Supersaturation generation	Classification	Fines Dissolution	Heat Exchange	Mixing
		Primary	Secondary								
			Crystal – Foreign Body	Crystal – Crystal	Activated						
Boiling Zone	++	++	- -	- -	+/-	- -	++	- -	- -	- -	- -
Annular zone	+/-	- -	-	-	- -	+/-	- -	++	- -	- -	- -
Fines Removal + Heat Exchange	- -	- -	- -	- -	- -	- -	+	- -	++	++	- -
Bulk volume	++	- -	- -	+/-	- -	+/-	+/ -	- -	- -	+/ -	+/ -
Pump /Impeller	- -	- -	++	+/-	-	- -	- -	- -	- -	- -	- -
Feed	- -	- -	- -	- -	- -	- -	+/-	- -	- -	- -	++
Seeding	++	- -	- -	+/-	+/-	+/-	+/-	- -	- -	- -	+/-

+ occurrence is on the higher side
- occurrence is on the lower side

2.4.4.5 Sub-Level 4.5 : Connection of different design compartments into process units (spatial connection)

In this level, all the design compartments (including individual tasks if any) that have been identified in the earlier levels are connected to result in an integrated process unit. It should be noted that some of the design compartments can be the one arising out of integration of tasks and some of the compartments can be just the tasks themselves. This step is very similar to the connection of tasks level and again, a superstructure can be generated that takes into account all possible combinations among different design compartments/zones and tasks. A design compartment helps the designer to identify different spatial regions at an aggregated (higher) level and helps in simplifying the task-based design considerably when modelling comes into play. To connect the design compartments with each other, certain guidelines are identified. Note that most of these guidelines follow from the same logic as those applied for the connection of tasks.

- There can be multiple instances of the same design compartment connected to each other. In this case, they are referred to as Design Compartment Zones (discussed in earlier section).
- Design compartments can be arranged in sequence or in parallel and in forward/backward modes.
- No adverse coupling effects between rate events associated with design compartments to be connected.

For example, applying this level to Figure 2.20(d) will result in a superstructure by itself. For illustration purpose, Figure 2.23 shows a possible solution from the superstructure in the form of a design compartment model.

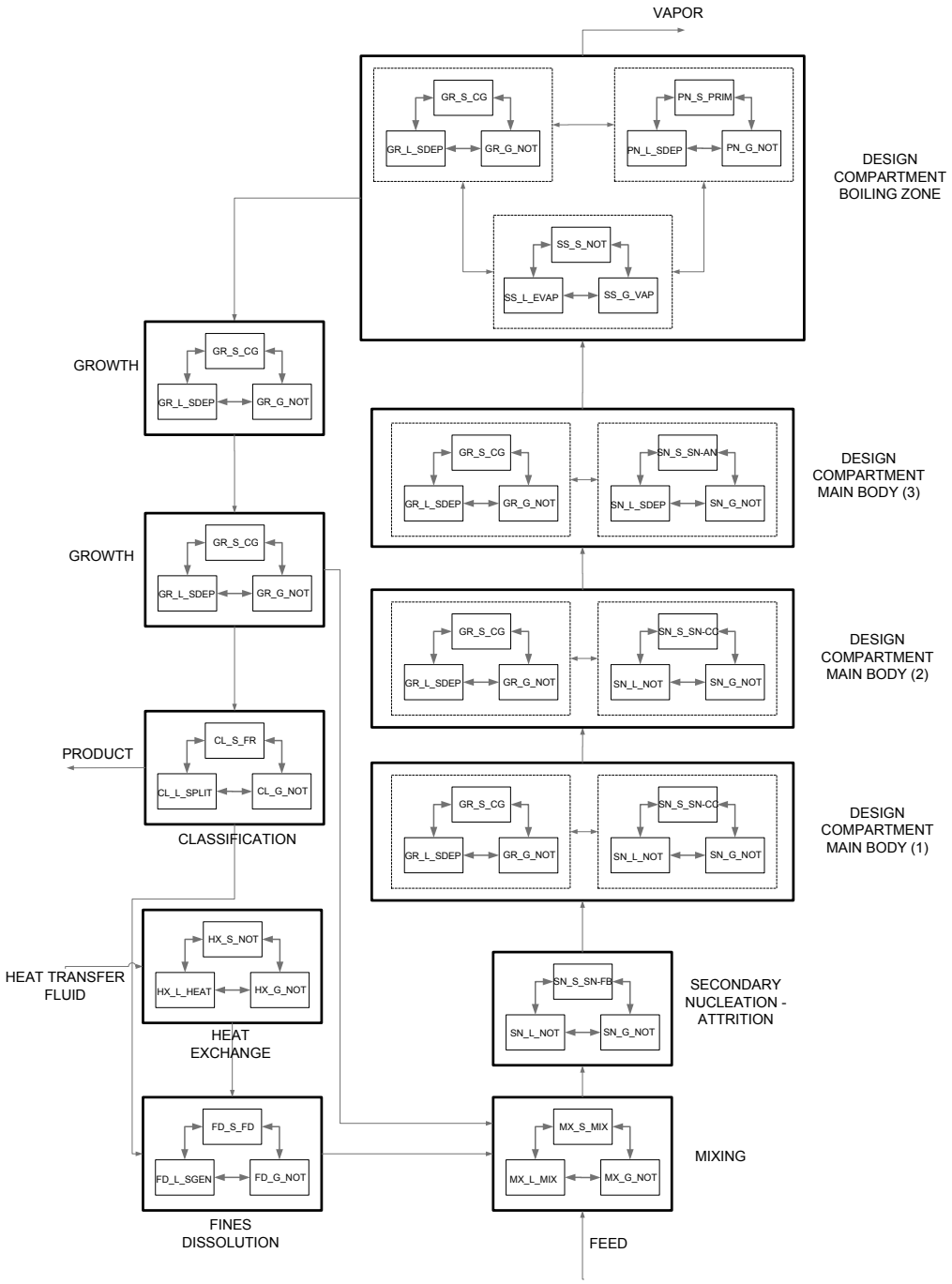

Figure 2.23 A possible alternative (representation) from the superstructure in the form of a design compartment model (in spatial domain)

2.4.4.6 Sub-Level 4.6 : Operational unit identification (spatial domain)

Tasks can be done individually, combined in design compartments or even in design zones. All these ordering of tasks must have a real-life embedding or containment. A containment 'vessel' is needed to separate the task execution from the environment. Such containment for a task, task-zone, design compartment or design zone will be named as an 'operational unit'. It is equivalent with an apparatus or equipment, taking into account it can be new apparatus or equipment that does not exist currently. Existing equipment(s) may or may not be able to conduct the specified task sequence. In that case, the task identification sub-level has to be repeated again. The design variables are typically geometric areas for heat exchange or contact, etc. and the domain knowledge is the characteristics and limitations of each of the operational units. Table 2.16 lists the possible operational units for certain identified tasks.

Table 2.16 Operational units for a crystallization process

TASK	OPERATIONAL UNIT
Crystal growth	Vessel
Primary nucleation	Vessel, Ultrasonic device
Secondary nucleation	Impeller, pump, vessel
Agglomeration	Vessel
Breakage	Vessel, pump, impeller
Supersaturation generation	Vessel, membrane
Classification	Cyclone, centrifuge, vessel (gravity), elutriation leg, T-joint, S/L separator
Heat Exchange	Heat exchanger
Fines dissolution	Vessel(solvent addition), Heat exchanger
Mixing	Vessel, impeller, pump, baffle

Different process units or equipment entities are considered when practical size limitations are met for a particular unit or when operating conditions (P,T, pH, …) require different materials for vessel walls and internals.

2.4.4.7 Sub-Levels 4.7 – 4.10 : Temporal domain

The next steps (4.7 – 4.10) in the task-based design synthesis involve repeating steps (4.3 – 4.6) but for the temporal domain. The advantages of this split in space and time, when applied to superstructure network for crystallizers can be :

- In the task representation, the time dimension can be eliminated from the superstructure at one time instant which means the conceptual thinking is better understood. This freedom of separation between temporal and spatial domain is not achieved otherwise.
- Several tasks can be added / deleted at different times in a network which is not the case with the compartmental modelling approach (Bermingham, 2003b, 1998).
- The approach is independent of the complexities of the equations involved in describing the process which makes it suitable to be applied to task based approach since the 'behavior' attribute of a task can be described in varying degrees of detail.

These steps are not discussed any further here, but an illustration can be found in Appendix A2.3.

2.4.5 Overview of design decisions for design level 4

In Table 2.17, a systematic description of design specifications, design variables and domain knowledge available at this entire process unit synthesis level 4 is given, just as in the case of upper levels.

Since the synthesis focusses on building blocks of crystallization, emphasis is on understanding the process and developing optimal solutions for the same. This can lead to new equipment, existing equipment with some modifications or existing equipment with efficient control strategy. This task-oriented approach is in line with recent fundamental approaches in the chemical process synthesis area. It is the author's opinion that this design concept, when translated into a rigorous modelling tool, will surely pave the way for innovate designs for crystallizer equipments, with probably process intensification as a distant outcome.

Table 2.17 Design Level 4 – A task-based approach to the design of a crystallization stage

Design specifications Objectives and Constraints	Design Variables	Domain knowledge	Tools
Process: • Production capacity • Feed composition • Yield • Energy consumption • Exergy savings • Availability, controllability and Resiliency • SHE considerations • Task Duty (distribution) • Crystallization method • Temperature range • Pressure range • Supersaturation range • Seed amount/CSD • Operation mode • Residence time (distribution) • Heat exchange rates • No boiling in heat exchanger • No entrainment of droplets by vapor • FDA regulations • Suspension criterion • Nucleation targets • Economic potential • Time-to-market • Process intensification criteria *Product:* • Crystal size distribution	*Discrete:* • Tasks (identification/integration/connection) o Crystal growth o Primary/Secondary nucleation o Supersaturation generation o Agglomeration/Breakage o Classification o Fines dissolution o Heat exchange o Mixing o Selection between seeding techniques • Design compartments /zones (identification/integration/connection) o Boiling zone o Annular zone o Fines removal/Heat exchange o Bulk volume o Pump/Impeller o Feed o Seeding • Phase building blocks • Stream and port connections • Feed location • Product removal location • Location of recycled stream • Thermodynamic phase • Fluiddynamic regime of operation • Operational unit identification : o Fines classification and dissolution/clear liquor advance o Product classification o Circulation device (Impeller/Pump/Vessel) o Storage (batch) o Actuator for batch process (like propeller frequency, ultrasound, seeding) o External/internal heat exchanger o Heating whole feed/ partial feed/ fines loop o Type of heat exchanger/condenser o Type of impeller/pump/mixer o Direction of circulation o Baffle/Draft tubes (good mixing) *Continuous:* • Spatial allocation for tasks/design compartments • Temporal allocation for tasks/design compartments • Physical constraint(s) • Solids concentration • Phase ratio • Circulation flow rate • Operating conditions of tasks • Flow rate through compartments • Initial conditions (batch) • Magnitude of recycle stream(s) • Phase velocities • Contact mode(s)/time • Time scale and ordering of rate events	• Thermodynamic activity of species/components in solid, liquid and vapor phase • Physical properties, e.g. material densities, specific heats and viscosities • Crystallization kinetics, i.e. rate expressions for the nucleation, growth, attrition, agglomeration and breakage of crystals • Fouling kinetics • Shape factors of the crystalline components • Fire and explosion index • Controllability • Equipment characteristics • Fluiddynamics • Synthesis rules for superstructure generation • MINLP techniques for optimization	• gPROMS® • PROSYN® • ASPEN® • OLI®/ Aspen® (thermo-dynamics) • GAMS® (optimiza-tion) • FLUENT®, CFX® (CFD)

2.5 CONCLUSIONS & OUTLOOK

The hierarchical design procedure proposed by Bermingham(2000) and Westhoff(2004) has been adopted as a reference for the design research in this thesis. Within this multi-level procedure, the design approaches for flow sheet structure (Level 3) and the crystallization unit (Level 4) have been extended. The extension at level 3 gives a better possibility of delivering the optimum flow sheet for the crystallization process, which can narrow down immensely, the alternatives to be considered for design of crystallization units at Level 4. The design approach at level 4 is enhanced from a synthesis point of view by adopting a task-based design approach.

The task-based design approach is based on the assumption that the process unit under design may be thought of as a collection of physical tasks. It is concerned with the identification, estimation of key design and performance parameters and iterative refinement. This allows the designer to think creatively in selecting specific tasks needed for the crystallization process at hand, which facilitates in generating superstructures that can deliver *the* optimum crystallizer configuration. This method is expected to be applicable to grassroots design as well as to retrofits and to improve (de-bottlenecking) existing process operations.

A task-based approach comprises four constituents, being an explicit specification of the building blocks for the tasks (ontology), a structural model (rules on how to connect tasks), behavioral physical models and synthesis techniques (heuristic, algorithmic) to create alternative networks of tasks. A novel ontological treatment of the physical task concept has been articulated for Level 4, along with an outline of the design decision variables and of the contents of the associated behavioural models. The specification of the conceptual building blocks is the first step towards a structure model, for use by the synthesis technique to generate alternative networks or superstructures.

It will be evident that the task-based framework presented here is still in the first stage of development. It has not yet been applied and critically tested with respect to its effectiveness for generating innovative designs. The next stages of development would involve:

- modelling of the behavioral aspects of the task blocks;
- modelling of structural connectivity of the task blocks and the links with the higher levels of aggregation;
- development of techniques for the generation and optimization of task superstructures

The problems that may be associated with the generation and optimization of superstructures are complex and computationally demanding. Taming the combinatorial complexity arising from the structure model and the computational load of the behavioral models is key to a successful development. The development of parsimonious models for synthesis may be required. Nevertheless, this fundamental and systematic approach merits attention for future work in the area of crystallizer design and optimization.

The successful completion of a computer-aided physical-task based synthesis procedure is an important intermediate milestone. But it is not yet a measure for practical effectiveness. This design approach is similar to a scientific hypothesis that must be tested for credibility by means of proper experiments. The outcome of the experiments, when properly conducted, will give the necessary information to which extent the hypothesis can be maintained or be rejected. The ultimate test for acceptance of the design procedure would be when the application of the synthesis procedure would lead to innovative designs, which will be experimentally tested and which then show validated performances in accord with the initial design specifications. Therefore, we also suggest as further activity the testing and validation of the task-based synthesis and design methodology. The approach presented by Ajah (2004) provides an adequate theoretical background to test the effectiveness of the design procedure by means of an evaluation of design outputs. They suggest that a reliable approach for the testing and validation of a design framework might be composed of a sequence of activities:

0. Given a design procedure,
1. Specify design performance criteria;
2. Select design teams and cases;
3. Test and monitor design process and outputs;

4. Make a theoretical evaluation of design outputs;
5. Construct a design and experimental evaluation of design outputs.

As an example of such theoretical testing, the design method of Bermingham(2000) and extended by Westhoff (2002) for instrumentation and control has been applied to the design of a research crystallization unit (Westhoff, 2004). Hence, future work should also look into testing the viability of this design approach by building small-scale design units.

NOTATIONS

a	contact area	[m^2]
A	heat transfer area	[m^2]
c	molar concentration	[$mole \cdot m^{-3}$]
C	molar concentration	[$mole \cdot m^{-3}$]
C_e	equilibrium concentration (solubility)	[$\# \cdot m^{-3}$]
C_o	concentration of nucleation sites	[$\# \cdot m^{-3}$]
D	diffusion coefficient of solute molecule	[$m^2.s^{-1}$]
D_{AB}	binary diffusion coefficient	[$m^2.s^{-1}$]
DS	design specification functions	[-]
DS_o	design specification values	[-]
d_{imp}	impeller diameter	[m]
E	enthalpy	[J]
f	partial differential equation	[-]
FR	flow regime	[-]
g	algebraic equation	[-]
G	linear crystal growth rate	[$m \cdot s^{-1}$]
h	end-point and path constraints	[-]
H	enthalpy	[J]
H	contact mode	[-]
k	set of initial conditions	[-]
k_o	given initial conditions	[-]
k	rate constant	[$m \cdot s^{-1}$]
k	set of initial conditions	[-]
k_B	boltzmann constant	[$J.K^{-1}$]
k_d	rate constant for diffusion	[$m \cdot s^{-1}$]
k_r	rate constant for surface integration	[$m \cdot s^{-1}$]
k_v	volumetric shape factor	[-]
K_G	overall rate constant	[$m \cdot s^{-1}$]
K	constant	[-]
l	set of boundary conditions	[-]
l_o	given boundary conditions	[-]
L	crystal length	[m]
L	phenomenological constant (say diffusion constant)	[$m^2.s^{-1}$]
m	mass	[kg]
m	moment of a distribution	[-]
M	mass	[kg]
M	molar mass	[$kg \cdot mole^{-1}$]
M_A	flow regime of operation	[-]
M_o	momentum	[$kg.m.s^{-1}$]
n	crystal number density	[$m^{-3} \cdot m^{-1}$]

NC	number of components	[-]
NI	number of solid/liquid inlet streams	[-]
NO	number of solid/liquid outlet streams	[-]
NP	number of phases	[-]
NR	number of reactions	[-]
Ne	newton number or power number	[-]
p	equality constraints on decision variables	[-]
P	pressure	[Pa]
q	inequality constraints on decision variables	[-]
Q	net rate of heat addition	[J.s^{-1}]
r	reaction rate	[mole·s^{-1}]
r	exponent (order of reaction)	[-]
s	thermodynamic variable	[-]
s_{imp}	impeller frequency	[s^{-1}]
S	supersaturation ratio	[-]
t	time	[sec]
T	temperature	[K]
u	time variant input variable	[-]
U	heat transfer co-efficient	[W.m^{-2}.K]
U	specified mode of operation of the input variable over time	[-]
V	volume	[m^3]
w_s	strain energy	[J/mol]
W^*	nucleation work	[J]
X	driving force (say concentration)	[mol.m^3]
x	state variable	[-]
z	output variable	[-]

Greek

ε	porosity	[-]
$\bar{\varepsilon}$	specific power input	[W·kg^{-1}]
γ_{ef}	effective specific surface energy	[J.m^{-2}]
γ	internal stress within crystals	[J/mol]
μ_s	chemical potential of the solid phase	[J.mol^{-1}]
μ_l	chemical potential of the liquid phase	[J.mol^{-1}]
ν_l	kinematic viscosity of the liquid	[m^2·s^{-1}]
ϕ	flux	[mol.m^{-2}.s^{-1}]
ϕ_H	enthalpy flow rate or enthalpy flux	[J·s^{-1}]
ϕ_m	mass flow rate or mass flux	[kg·s^{-1}]
ϕ_{mol}	molar flow rate or molar flux	[mole·s^{-1}]
ϕ_n	number density production rate	[m^{-3}·m^{-1}·s^{-1}]
ϕ_V	volumetric flow rate or volumetric flux	[m^3·s^{-1}]
φ	phase ratio	[-]
ρ_L	material density of the liquid phase	[kg·m^{-3}]
ρ_S	material density of the solid phase	[kg·m^{-3}]
σ_c	continuous design decision variable	[-]
σ_d	discrete design decision variable	[-]
χ	morphology representation	[-]
ξ	coefficient of monomer sticking	[-]

Indices

i	index of a liquid phase component
k	index of a solid/liquid inlet
l	index of a solid/liquid outlet

p	index of a liquid phase reaction
q	index of a solid phase and of the corresponding crystallization reaction

Subscripts/Superscripts

α	liquid phase
β	solid phase
γ	immobile solid phase
L	liquid phase
S	solid phase
V	vapor phase
aggl	agglomeration
attr	attrition
break	breakage
grow	growth
nucl	primary nucleation
aggl	agglomeration
attr	attrition
break	breakage
dis	dissolution
grow	growth

Abbreviations

APC	Advanced Process Control
CSD	Crystal Size Distribution
CSTR	Continuous Stirred Tank Reactor
DCZ	Design Compartment Zone
DNA	Dynamic Nyquist Array
IMC	Internal Model Control
INA	Inverse Nyquist Array
MIDO	Mixed Integer Dynamic Optimization
MINLP	Mixed Integer Non-Linear Programming
MPC	Model Predictive Control
PBB	Phase Building Block
PBE	Population Balance Equation
PDE	Partial Differential Equation
PFR	Plug Flow Reactor
ODE	Ordinary Differential Equation
RTPO	Real Time Process Optimization
SHEET	Safety, Health, Environmental, Economical, Technological

REFERENCES

Achenie, L.K.E. and Biegler, L.T. (1990). A superstructure based approach to chemical reactor network synthesis, *Computers and Chemical Engineering*, 14, pp.23-40

Ajah, A. N ., Swinkels, P.L.J. and Grievink, J. (2004). Towards the Testing and Validation of Novel Conceptual Process Design Frameworks, In C.A. Floudas, & R. Agrawal, (Eds.), *6th Int. Conf. on Foundations of Computer-Aided Design (FOCAPD)*; Discovery Through Product and Process Design. pp. 231-235. Austin, TX, USA: CACHE Corp.

Balakrishna, S. and Biegler, L.T.(1993). A unified approach for the simultaneous synthesis of reaction, energy and separation systems, *Ind.Eng.Chem.Res.*, 32, pp.1372

Bansal, V. (2000). *Analysis, design and control optimization of process systems under uncertainty*, PhD thesis, Imperial College, University of London

Bermingham, S.K., Neumann, A.M., Kramer, H.J.M., Verheijen, P.J.T., van Rosmalen, G.M. and Grievink, J. (2000). A design procedure and predictive models for solution crystallization processes. *AIChE Symp. Series 323*, **96**, pp. 250-264

Bermingham, S.K. (2003a). *A Design Procedure And Predictive Models For Solution Crystallization Processes- Development And Application*, Ph.D. Thesis, Delft University of Technology, the Netherlands, ISBN 90-407-2395-8

Bermingham, S.K., Verheijen, P.J.T. and Kramer, H.J.M. (2003b). Optimal design of solution crystallization processes with rigorous models, *Trans. IChemE*, 81, part A, pp.893-903

Bermingham, S.K., Kramer, H.J.M. and Rosmalen van, G.M. (1998). Towards on-scale crystallizer design using compartmental models, *Computers and Chemical Engineering*, 22, pp.S355-S362

Berry, D.A. and Ng, K.M. (1997).Synthesis of reactive crystallization processes, *AIChE Journal*, 43, pp.1737-1750

Bird R. B., Stewart W. E., Lightfoot E. N. (1960). *Transport Phenomena*, John Wiley & Sons, ISBN 9971-51-142-8

Chitra, S.P. and Govind, R. (1985). Synthesis of optimal serial reactor structures for homogeneous reactions: I and II, *AIChE Journal*, 31, pp.177

Ciric, A.R. and Floudas, C.A. (1991). Heat exchanger network synthesis without decomposition, *Computers and Chemical Engineering*, 15, pp.385-396

Doherty, M.F., and Malone, M.F. (2001). *Conceptual design of distillation systems*, McGraw Hill, Boston

Douglas, J.M. (1987). *Conceptual Design of Chemical Processes*, McGraw Hill, New York

Downs J. J. (2002). Linking Control Strategy design and Model Predictive Control, In Rawlings J. B., Ogunnaike B. A., Eaton J. W. (Editors), Sixth International Conference on Chemical Process Control, *AIChE Sym. Series*, Vol. 98, No 326

Dye, S.R. and Ng, K.M. (1995). Fractional crystallization: design alternatives and tradeoffs, *AIChE Journal*, 41, pp.2427-2438

Emmerich, M., Grötzner, M., Groß, B. and Schütz, M. (2000). Mixed-Integer Evolution Strategy for Chemical Plant Optimization. In: *I. C. Parmee (ed) Evolutionary Design and Manufacture (ACDM 2000)*, pp.53-67

Floudas, C.A. (1995). *Nonlinear and Mixed-Integer Optimization: Fundamental and Applications*, Oxford University Press

Grievink (2004), http://www.dct.tudelft.nl/pse/pageresearch.htm

Groot, S.R. de, and Mazur, P. (1969). *Non-equilibrium thermodynamics*, NHPC, Amsterdam

Grossmann, I. E. (1997). Mixed-integer optimization techniques for algorithmic process synthesis, *Advances in Chemical Engineering*, 23, pp.171 – 286

Grossmann, I.E. (2002). Review of Nonlinear Mixed-Integer and Disjunctive Programming Techniques, *Optimization and Engineering*, 3, pp.227-252

Heffels S. K.; Kind M.(1999).Seeding Technology : An Underestimated Critical Success Factor for Crystallization, Industrial Crystallization, *Proceedings of 14th International Symposium on Industrial Crystallization*, Cambridge

Heller,M., Jäger,D., Schlüter,M., Schneider,R. and Westfechtel,B. (2004). A management system for dynamic and inter-organizational design processes in chemical engineering, *Computers and Chemical Engineering*, Vol.29, Issue 1, pp. 93-111

Kokossis A. C. and Floudas C. A. (1990). Optimization of Complex Reactor Networks I – Isothermal Operation, *Chemical Engineering Science*, Vol. 45, pp.595-614

Kokossis A. C. and Floudas C. A. (1994). Optimization of Complex Reactor Networks II – Non - isothermal Operation, *Chemical Engineering Science,* Vol. 49, No. 7, pp. 1037-1051

Kramer, H.J.M., S.K. Bermingham and van Rosmalen, G.M. (1999). Design of industrial crystallizers or a required product quality. *Journal of Crystal Growth*, 198/199, pp.729-737

Marquardt, W. (2004). RWTH, Aachen University of Technology, Aachen Germany, course notes for course CE 3611 TU delivered at Delft University of Technology, the Netherlands

Meeuse, F.M.,(2002). *On the design of chemical processes with improved controllability characteristics*, Ph.D. Thesis, Delft University of Technology

Mendez, C.A., J. Myers, S. Roberts, J. Logsdon, A. Vaia and Grossmann, I. E. (2005). MINLP model for synthesis of Paraxylene Separation Processes based on Crystallization Technology, *Proceedings ESCAPE-15*, pp.829-834, Barcelona, Spain

Papalexandri, K.P. and Pistikopoulos, E.N. (1996). Generalized modular representation framework for process synthesis, *AIChE Journal*, 42, pp.1010-1032

Papalexandri, K.P. and Pistikopoulos, E.N. (1994). Synthesis and retrofit design of operable heat exchanger networks: I and II, *Industrial Engineering Chemistry Research*, 33, pp.1718

Rajagopal, S., K.M. Ng and Douglas, J.M. (1992). A hierarchical procedure for the conceptual design of solids processes, *Computers & Chemical Engineering*, 16, pp.675-689

Rossiter, A.P. and Douglas, J.M. (1986). Design and optimization of solids processes. I: A hierarchical decision procedure for process synthesis of solids systems. *Chem. Eng. Res. Des.*, 64, pp.175-183

Ruud, D.F., G.J.Powers and Siirola, J.J. (1973). *Process Synthesis*, Prentice-Hall, Englewood Cliffs, NJ

Sargent, R.W.H. (1998). A functional approach to process synthesis and its application to distillation systems, *Computers & Chemical Engineering*, 22, pp. 31-45

Seborg D. E., Edgar T. F., Mellichamp D. A. (2004). *Process Control and Dynamics*, 2nd edition, ISBN 0-471-00077-9, Hoboken Wiley

Shah, P.B. and Kokossis, A.C. (2001). Knowledge based models for the analysis of complex separation processes, *Computers and Chemical Engineering*, Vol. 25, 4-6, pp.867-878

Shah, P.B. and Kokossis, A.C. (2002). New Synthesis Framework for the Optimization of Complex Distillation Systems, *AIChE Journal*, Vol.48, 3, pp. 527-550

Siirola, J. J. (1995). An industrial perspective on process synthesis, 4th Int. Confer. on Foundations of computer-aided process design, *AIChE Symp. Series.*, 91 (306), pp.222 – 233

Siirola, J. J. (1996). Industrial applications of chemical process synthesis, *Advances in Chemical Engineering*, 23, pp.1-92

Sinnot, R.K., (1999). *Coulson and Richardson's Chemical Engineering, Chemical Engineering Design*, Volume 6, 3rd edition, Butterworth Heinemann

Skogestad S. and Postlethwaite I. (1996). *Multivariable feedback control : analysis and design*, ISBN 0-471-94277-4, Chichester: Wiley

Stankiewicz, A. and Moulijn, J.A. (2004). *Re-engineering the chemical processing plant: Process Intensification*, Marcel Dekker Inc., New York

Tousain, R. (2002). *Dynamic optimization in business-wide process control*, Ph.D thesis, Delft University of Technology, The Netherlands

Westhoff, G.M.(2002). *Design and analysis of suspension crystallizers: Aspects of crystallization kinetics and product quality*, PhD Thesis, Delft University of Technology, the Netherlands, ISBN 90-6464-138-2

Westhoff, G.M., Kramer, H.J.M., Jansens, P.J. and Grievink, J. (2004). Design of a multi-functional crystallizer for research purposes, *Chemical Engineering Research and Design*, 82(A7), pp.865-880

Wibowo C. and Ng K.(2000). Unified approach for Synthesizing Crystallization – Based Separation Process, *AIChE Journal*, Vol 46, No. 7, pp.1400-1421

Wibowo,C., Chang,W., Ng, K.M. (2001).Design of Integrated Crystallization Systems, Vol. 47, No.11, *AIChE Journal,* pp.2474-2492

Yee, T.F. and Grossman, I.E. (1990). Simultaneous optimization models for heat integration : II. Heat exchanger network synthesis, *Computers and Chemical engineering*, 14, pp.1165

Zhang, J. and Smith, R. (2004). Design and optimization of batch and semi-batch reactors, *Chemical Engineering Science*, 59, pp.459-478

3

Crystallization mechanisms and process model framework

This chapter discusses the dominant crystallization mechanisms that play a role in solution crystallization processes. An introduction into the thermodynamic aspects of crystallization is also presented. In the second half of this chapter, the process modelling framework developed by Bermingham(2003) is described briefly. This model framework which comprises of population balance equations in addition to mass and energy balances is built within a dynamic modelling tool gPROMS. This process model can be applied for design and optimization purposes and used to predict the relations between crystallizer geometry and operating conditions on one hand and production capacity and crystal quality on the other.

3.1 INTRODUCTION

Crystallization may be defined as a phase change in which a crystalline product is obtained from a solution. Typically, the term solution means a liquid solution consisting of a solvent, which is a liquid, and a solute, which is a solid, at the conditions of interest. Crystallization is employed heavily as a separation technique in the inorganic bulk chemical industry in order to recover salts from their aqueous solution. In the organic process industry, it is also used to recover crystalline product, to refine the intermediary, and to remove undesired salts. In some cases, the desired product can be a non-crystalline liquid phase. Thus, crystallization invariably involves producing, processing and handling of solid phase and can occasionally encounter more than two phases (see Table 3.1, Tavare (1995)).

Table 3.1 Phases in a crystallization process

System	Phases
Two-phase	Liquid $\rightleftharpoons$ Solid
	Gas $\rightleftharpoons$ Solid
Three-phase	Gas $\rightleftharpoons$ Liquid $\rightleftharpoons$ Solid
	Liquid $\rightleftharpoons$ Gel $\rightleftharpoons$ Solid
	Liquid (1) $\rightleftharpoons$ Liquid (2) $\rightleftharpoons$ Solid
	Liquid $\rightleftharpoons$ Solid (1) $\rightleftharpoons$ Solid (2)
Multi-phase	Gas $\rightleftharpoons$ Liquid $\rightleftharpoons$ Liquid $\rightleftharpoons$ Solid $\rightleftharpoons$ Solid

3.2 THERMODYNAMIC ASPECTS AND CRYSTALLIZATION MECHANISMS

Although a lot of research effort has been directed at developing rate models and analytical solutions for the rate processes, the crystallization literature of engineering practice is still largely based on experimental data yielding empirical correlations. Albeit several kinetic events are identifiable in a crystallizer operation, crystallization kinetics in the literature are conveniently characterized in terms of two dominant rate processes occurring in a process of crystallization from solution, viz. crystal nucleation and crystal growth. But, in order for crystallization to begin, the solution must be supersaturated. A supersaturated solution is not in equilibrium. In order to relieve the supersaturation and move towards equilibrium, the solution crystallizes. Once crystallization starts, the supersaturation can be relieved by a combination of nucleation and crystal growth. It is the relation of the degree of nucleation to crystal growth that controls the product crystal size and size distribution, and is, therefore a crucial part of industrial crystallization processes. In the following sub-sections, these mechanisms will be briefly introduced along with a few important ones. Before that, an introduction into the thermodynamic aspects of crystallization is presented.

3.2.1 Supersaturation – Driving force for crystallization

A solution that is in equilibrium with the solid phase is said to be *saturated* with respect to that solid. When the solution contains more dissolved solid than that represented by the saturated condition, then it is said to be *supersaturated* with respect to the dissolved solute. The state of supersaturation is a pre-requisite for all crystallization processes. An appreciable degree of supersaturation may be achieved for many solutions by proper manipulation of operating conditions.

The thermodynamic driving force for the first-order phase transition is given by the difference in chemical potential of the system ($\Delta\mu$) :

$$\Delta\mu \equiv (G_{old} - G_{new})/M \equiv \mu_{old} - \mu_{new} \tag{3.1}$$

Physically, $\Delta\mu$ is the gain in free energy per molecule (or atom) associated with the passage of the phase from the state with higher Gibbs free energy G_{old} to the state with lower Gibbs free energy G_{new} (μ_{old} *and* μ_{new} are, respectively, the chemical potentials of the old and new phases at the corresponding minima). When $\Delta\mu > 0$, the solution is supersaturated, as only then are nucleation and/or growth of the crystals possible. The solution is, respectively, saturated or undersaturated when $\Delta\mu = 0$ or $\Delta\mu < 0$. Using known thermodynamic expressions for μ_{old} (solution) and μ_{new} (crystal phase), one may present $\Delta\mu$ in the form:

$$\Delta\mu = kT \ln S \tag{3.2}$$

Although the fundamental driving force for a crystallization process is the difference in chemical potential between the crystallizing substance in the crystal and in the solution phase, it is common practice to use the supersaturation as the driving force for the process. Among the most common expression of supersaturation are the concentration difference, Δc, the supersaturation ratio, S, and a quantity sometimes referred to as the absolute or relative supersaturation, σ. If c is the solute concentration in solution and c^* is the solute concentration at the given temperature, these quantities are defined as follows:

$$\Delta c = c - c^* \tag{3.3}$$

$$S = \frac{c}{c^*} \tag{3.4}$$

$$\sigma = \frac{\Delta c}{c^*} = S - 1 \tag{3.5}$$

It is essential to quote the other variables like temperature and impurity composition while expressing the supersaturation of a system, since these variables may change substantially the equilibrium saturation concentration of the system.

3.2.2 Solution stability

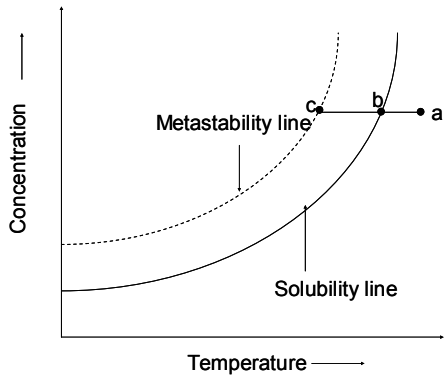

Figure 3.1 Metastability limit as function of temperature

The concept of supersaturation and the existence of the so-called *metastable zone*, are useful in understanding the behavior of a crystallizing system. Ostwald (1897) first introduced the terms *labile* (unstable) and *metastable* supersaturation, referring to supersaturated solutions in which the spontaneous deposition of the solid phase, in the absence of crystallizing solid material, will or will not occur, respectively.

In any crystallization process, supersaturation is the necessary driving force for crystal formation from solution, but at the same time, nuclei are necessary for the deposition of solute material on the crystal lattice surface (growth). The formation of a nucleus from a clear liquid is a statistical process. If within a given time frame no nuclei are

formed, the solution is called metastable. This time is a measure of the ability of a system to remain in the metastable state and can therefore be used to determine the metastability limit. This limit represents the maximum supersaturation below which the solution of the specific compound can stay without losing its metastability. The metastable zone is the region between the solubility line and the metastability limit line. This is illustrated in Figure 3.1. The induction time is infinite at the solubility line but decreases as the metastability line is approached. Consider the line a,b,c to be followed by cooling crystallization. Cooling down the solution from point a to b, at point b the solution is saturated. Cooling down from b to c, the solution becomes supersaturated. At point c the metastability limit is reached and primary nucleation may occur and this is a spontaneous event. Primary nucleation is the formation of a new solid phase from a clear liquid.

3.2.3 Nucleation

The process of nucleation involves the formation of new crystals in a crystallizing environment. The generation of a new crystalline phase from solution, under conditions where a free energy barrier exists, is a process of nucleation from solution. In actual practice, the formation of new crystals may result from any one, or a combination, of different mechanisms as classified in Table 3.2, or by mechanical attrition.

Table 3.2 Nucleation mechanisms – primary and secondary

Primary	Homogeneous	(Solid interface absent)
	Heterogeneous	(In presence of foreign interface)
Secondary		(In presence of crystal interface of the same solute)

Primary nucleation

Primary nucleation occurs in the absence of foreign (crystalline) surfaces. Two types of primary nucleation can be distinguished, viz. homogeneous primary nucleation and heterogeneous primary nucleation. Homogeneous nucleation rarely occurs in practice and that too at very high supersaturation; however it forms the basis of several nucleation theories. Heterogeneous nucleation is usually induced by the presence of dissolved impurities.

Homogeneous nucleation

Homogeneous nucleation (HON) occurs when the clusters of the new phase are in contact only with the old phase and with no other phases and/or molecular species. Nucleation of droplets in the bulk of ideally pure supersaturated vapors is a classical example of HON. The new phase is created due to formation of clusters exceeding the critical size. This critical cluster size is determined by the free enthalpy of crystallization and the surface tension.

The free enthalpy of lattice formation favors the formation and growth of the clusters whereas the surface tension promotes the dissolution of the clusters. At the critical cluster size, the derivative of the total surface free enthalpy is equal to the derivative of the total volume free enthalpy of the cluster, both with respect to size.

Heterogeneous nucleation

Heterogeneous nucleation (HEN) takes place when the old phase contacts and/or contains other phases and/or molecular species. Here, the cluster formation takes place on the surface of a foreign particle thus, lowering the surface energy. The lower surface energy provides a lower energy barrier for nucleation and thus, occurs at lower supersaturation. Hence, heterogeneous nucleation is more likely to occur in industrial processes than homogeneous nucleation, provided that there are sufficient foreign particles present.

Secondary nucleation

Secondary nucleation is a nucleation process that takes place only because of the prior presence of crystals of the material being crystallized. A variety of possible secondary nucleation mechanisms exist and some of these are listed in Table 3.3.

Table 3.3 Types of secondary nucleation mechanisms

Type of secondary nucleation	Cause
Initial breeding	Dust on dry seeds
Dendritic breeding	Breakage of dendritic growth on parent crystals
Polycrystalline breeding	Breakage of agglomerates
Shear nucleation	Fluid shear on growing crystal face
Contact nucleation	Collision breeding: crystal-crystal, crystal-impeller, crystal-vessel internals

The crystal surface at the solid-liquid interface appears to play an important role in all the secondary nucleation processes. Most experimental observations tend to indicate that the secondary contact nucleation (normally referred to as *attrition*) process provides an important source for producing nuclei and that in industrial practice; the secondary nucleation event has a predominant influence on the overall performance (Mersmann (1988), Myerson and Ginde (1993), van der Heijden and van Rosmalen (1993) and Qian and Botsaris (1997)). Contrary to the relatively high supersaturations required for primary nucleation, secondary nucleation already occurs at low to moderate values of the supersaturation. The driving force for attrition is determined by the concentration of the various sized crystals and their relative motion with respect to the pump blades, vessel walls or other crystals. The relative kinetic energy of a collision is determined by the size and relative velocity of the particle, which in its turn is a function of the slurry motion, viscosity and particle inertia (thus particle size). The rate coefficient or resistance for attrition is a function of the shape, surface roughness and mechanical properties of the colliding crystal. The rate coefficient is also indirectly influenced by the supersaturation, which determines factors such as surface roughness and healing of corners and surfaces damaged due to previous collisions. The supersaturation also determines the effective secondary nucleation rate as a result of attrition: it determines the fraction of attrition fragments that actually grow out and thus 'survive'.

In this thesis, secondary nucleation due to attrition (crystal-hardware collisions) and due to fluid shear (activated nucleation) will be mainly considered for simulation and optimization purpose(s). The attrition model as given by Gahn & Mersmann (1999 a,b) is discussed in more detail in section 3.5 and the activated nucleation mechanism proposed by Mersmann (1996) is discussed in section 3.4.

3.2.4 Crystal growth

Nucleation is the beginning of the phase separation process, wherein the solute molecules have formed the smallest sized particles, under the conditions present. The next stage of the crystallization process is for these nuclei to grow larger by the addition of solute molecules from the supersaturated solution. This process is called *crystal growth*.

For growth from solution, the crystal growth process can be roughly divided into two steps: (volume) diffusion of growth units towards the crystal surface and integration of these growth units into the crystal surface. Depending on the rate coefficients of diffusive transport (k_d) and surface integration (k_r), and on the prevailing level of supersaturation, the process will be diffusion-controlled, surface integration-controlled or a combination of both.

The concentration profile perpendicular to the crystal surface for such a two step process is given in Figure 3.2, where c_b = bulk concentration, c_i = concentration at the crystal-solution interface and c^* = equilibrium concentration at the growth site where the growth unit finally becomes incorporated in the crystal surface. For very well soluble compounds such as NaCl and $(NH_4)_2 SO_4$, the surface integration step is in general not rate limiting (Daudey (1987) and Kitamura (1991)), and the growth rate is determined by diffusion through the stagnant film or diffusion layer with thickness δ at the interface. The driving force for diffusion then becomes equal to $c_b - c^*$, since $c_i = c^*$. For poorly soluble

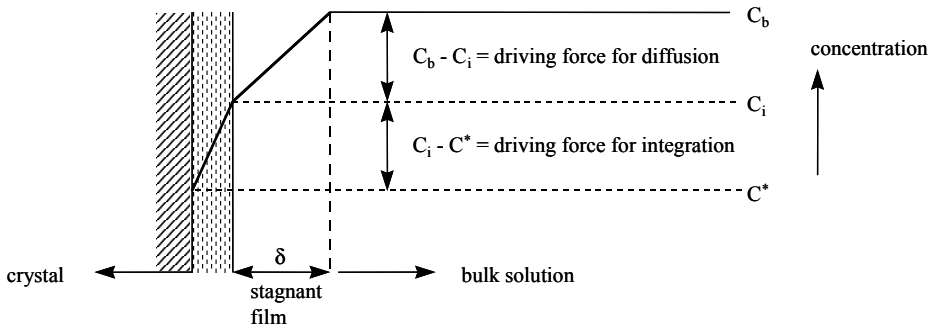

Figure 3.2 Concentration profile perpendicular to the crystal surface during growth

compounds, surface integration is rate limiting, and the driving force for integration then equals $c_b - c^*$, since $c_i = c_b$. For most compounds, however, both steps have to be taken into account in the calculation of their growth rates.

For growth from the melt, transport of heat of crystallization through the bulk phases becomes a third rate limiting step. This is also the case for very concentrated solutions, for example in case of crystallization of a highly hydrated salt, where the solution can almost be treated as a melt.

Mersmann and Kind (1988) have plotted the linear growth rate in industrial crystallizers for a number of salts as a function of the corresponding supersaturations. This plot (see Figure 3.3(a)) shows that easily soluble salts have roughly linear growth rates of 10^{-7} m/s at supersaturation (S) values around 0.01, while slightly soluble salts have linear growth rates of 10^{-9} to 10^{-8} m/s at S values of 10 to 100. Their corresponding mean crystal size varies from about 600 μm for easily soluble salts to 10 μm for slightly soluble salts (see Figure 3.3(b)).

The mechanism explained above considers only the solute species and additional factors such as lattice stress imperfections, crystal size and fluiddynamics have not been taken into account. Several workers

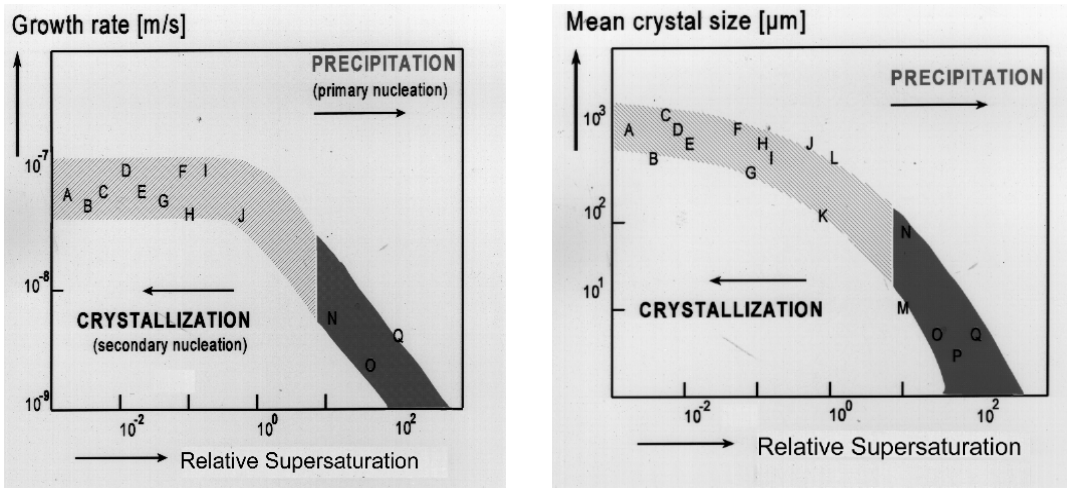

Figure 3.3 Growth rate(a) and mean crystal size(b) versus relative supersaturation (Mersmann and Kind (1988)).

A: KCl, B: NaCl, C: $(NH_2)_2CS$, D: $(NH_4)_2SO_4$, F: Na_2SO_4, G: K_2SO_4, H: $(NH_4)Al(SO4)_2$, I: $K_2Cr_2O_7$, N: $CaCO_3$, O: TiO_2, P: CaF_2, Q: $BaSO_4$

(van der Heijden (1992), O'Meadhra (1995 and Ristić(1990)) have shown that these factors have a pronounced influence on the growth rate of individual crystals. In this context, two prominent theories are distinguished:
Growth Rate Dispersion (GRD): GRD is the phenomenon wherein crystals of the same size and material exhibit a stochastic variation in crystal growth rates, under identical global conditions of supersaturation, temperature and fluiddynamics. This phenomenon may be explained by an increase in the chemical potential of the solid species due to the increased strain content within the crystal lattice. Chapter 7 is devoted to studying this phenomenon of GRD and hence, it is not discussed any further at this point.
Size Dependent Growth (SDG): SDG is defined as a phenomenon whereby crystals of different sizes grow at different rates, under identical conditions of supersaturation, temperature and the overall fluiddynamics. This can happen due to the influence of the crystal size on the local fluiddynamics thereby, altering the diffusion rate, which in turn affects the growth rate.

3.2.5 Crystal dissolution

Crystals will dissolve if the concentration falls below the saturation level, which can happen due to dilution or temperature changes. However, crystal dissolution is not the exact opposite of crystal growth. This is because dissolution does not require surface diffusion and orientation of atoms, ions or molecules and is generally limited by mass transfer, with a first order dependency on supersaturation. The rate coefficient for dissolution is a function of the diffusion coefficient, crystal size and the local fluiddynamics.

3.2.6 Agglomeration

Agglomeration of particles is a reversible process which involves transport and collision of the particles, interaction of the particles, rupture of aggregates and cementation of aggregates into stable agglomerates. The modelling of these four steps separately is difficult, especially while they occur simultaneously. The agglomeration rate is therefore mostly described with one size dependent function, the so called *agglomeration kernel* (β). The rate at which particles agglomerate in a crystallization or precipitation system is mainly dependent on the following process variables:

- the (local) energy dissipation
- the supersaturation of the fluid phase
- the number and the size distribution of the particles.

In addition, the agglomeration process will be affected by a number of material properties, surface charge, hardness) and process conditions (temperature, viscosity). Agglomeration is an important mechanism in the sub-micron range and in particular for sparingly soluble systems. When enough surface area is present in the system, the agglomeration process can be neglected for all practical purposes (for moderately and easily soluble compounds).

3.3 PRIMARY NUCLEATION THEORY OF KASHCHIEV

3.3.1 Critical nucleus size for primary nucleation

There is a competition between the two opposing terms constituting the Gibbs free energy of a pre-nucleus (cluster) as seen in Figure 3.4. On the one hand, each solute entity added to a cluster reduces its free energy. However, on the other hand, the surface increment of the cluster surface leads to a positive contribution of free energy. Both terms are dependent on the number of solute entities building up the cluster and thus also the size of the cluster. The Gibbs free energy shows a maximum at a certain critical cluster size. The clusters smaller than the critical size will dissolve and the clusters larger than

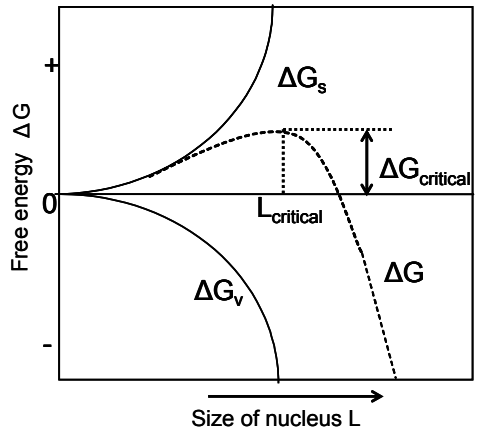

Figure 3.4 Plot of the volume (ΔG_v) and surface energy (ΔG_s) and the resulting total free energy (G) as a function of cluster size (L) (Mullin, 1993)

the critical size will grow out. The critical nucleus size is given by a modified Gibbs-Thomson equation (Dirksen & Ring, 1991) in the form:

$$L_{crit} = \frac{2\gamma M}{3\rho_s RT \ln S} \tag{3.6}$$

γ is an important parameter in the physical chemistry of surfaces in general and in the classical nucleation theory in particular. It should be mentioned that the critical nucleation length L_{crit} is not constant, but moves as a function of the supersaturation, S. A rough estimate of the γ value can be obtained with the aid of the Stefan-Skapski-Turnbull formula (Kashchiev, 2000):

$$\gamma = \beta\lambda / v_0^{2/3} \tag{3.7}$$

where $\beta \approx 0.2$ to 0.6 is a numerical factor, and λ (in Joules) is the molecular heat of dissolution. Since λ and the solubility C_e are approximately related by $C_e = (1/v_0)\exp(-\lambda / kT)$, Equation 3.7 leads to:

$$\gamma = (\beta kT / v_0^{2/3}) ln[1/v_0 C_e(T)] \tag{3.8}$$

These equations apply to homogeneous nucleation mechanisms. In order to apply the above equations to heterogeneous primary nucleation, γ needs to be corrected for. In distinction to Homogeneous nucleation (HON), however, the effective excess energy of the cluster for Heterogeneous nucleation (HEN) is not merely the cluster total surface energy, but contains additional energy terms. These allow for the changed total substrate surface energy after the appearance of the cluster on the substrate and, in 2D HEN, for the total edge energy of the cluster periphery. For 3D HEN of caps, γ is replaced by an effective specific surface energy γ_{ef} (J/m^2) defined as :

$$\gamma_{ef} = \psi.\gamma \tag{3.9}$$

where: ψ is the heterogeneity factor ; $0 < \psi < 1$.
Thus, it can be said that the heterogeneously formed nucleus requires less work for it's formation because of an effective reduction of the specific surface energy γ of the nucleus/old phase interface. In Equation 3.8, β takes the following values (Kashchiev,2003): $\beta = 0.514$ for spherical clusters and $\beta = 0.414$ for cubic clusters

3.3.2 Nucleation work

The formation of crystals in liquid solutions begins with nucleation. This is the process of fluctuational appearance of nanoscopically small molecular clusters of the new crystalline phase. The size of a cluster can be characterized by the number n of molecules constituting the cluster. The clusters of size $n=n^*$, which stay in unstable equilibrium with the ambient solution, are called nuclei (or critical nuclei), and the smaller ($n < n^*$) or the larger ($n > n^*$) clusters are subnuclei or supernuclei, respectively. Since only the supernuclei can grow spontaneously to macroscopic sizes, the nucleation rate J giving the number of supernuclei generated in the system per unit time and per unit volume or area is an important kinetic characteristic of the nucleation process. Also, knowing J is necessary for the comprehensive description

of other processes involving nucleation, such as, for instance, mass crystallization and nucleation-mediated crystal growth. The cluster constituted of n^* molecules (or atoms) is called the *nucleus* (sometimes *critical nucleus*), and the energy barrier W^* to the phase transition is known as *nucleation work*. The work W (in Joules) to form a cluster of $n = 1, 2, 3, \ldots$ molecules can be found by thermodynamic considerations, since it is defined as the difference between the free energy of the system in its final and initial states, *i.e.* after and before the cluster formation. In assembling n solute molecules into an n-sized cluster, the work $-n.\Delta\mu$ would be gained if the cluster were just a part of the bulk crystal. Then $W(n)$ would merely be equal to $-n.\Delta\mu$. However, $W(n)$ contains an additional energy term accounting for the presence of an interface between the cluster and the ambient solution and for the difference of the cluster properties from those of the bulk crystal. Thus, most generally, $W(n)$ is written down as (Kashchiev, 2000):

$$W(n) = -n\Delta\mu + \phi(n) \tag{3.10}$$

where ϕ (in Joules) has the physical significance of effective excess energy of the cluster. While $\Delta\mu$ in this expression is given by Equation 3.2, the determination of the $\phi(n)$ dependence is one of the hardest problems in nucleation theory and requires model considerations. In finding this dependence, a distinction is made between homogeneous and heterogeneous nucleation. Homogeneous nucleation (HON) occurs in the volume of ideally pure solutions, *i.e.* solutions constituted of solvent and solute molecules only.

According to the classical nucleation theory, $\phi(n)$ is merely equal to the cluster total surface energy $A_c(n)$ where γ (J/m^2) is the specific surface energy of the cluster/solution interface, and $A_c(n) = (36\pi v_0^2)^{1/3} n^{2/3}$ is the area of the cluster surface (v_0 (m^3) is the volume occupied by a molecule in the cluster). Hence, from Equations 3.2 and 3.10, it follows that:

$$W(n) = -nkT \ln S + (36\pi v_0^2)^{1/3} \gamma n^{2/3} \tag{3.11}$$

Although v_0 and γ characterize nanoscopically small clusters, the classical nucleation theory approximates their values by those corresponding to a macroscopically large crystal: v_0 is calculated from $v_0 = M/\varrho N_A$ (M (g/mol) is the crystal molecular weight, ϱ (kg/m^3) is the crystal density, N_A is Avogadro's number), and γ is considered as an appropriate average of the specific surface energies of the crystal faces present in the equilibrium form of the crystal.

Figures 3.5 and 3.6 show the effect of cluster size on the work needed for cluster formation, for different supersaturation levels. As seen from the Figure 3.4, the negative "volume" term and the positive "surface" term in Equation 3.11 result in a maximum of $W(n)$ at $n = n^*$. Physically, the value $W^* \equiv W(n^*)$ of this maximum is the energy barrier to nucleation. The cluster of n^* molecules is the nucleus, and W^* is the nucleation work. These two basic quantities in the theory of nucleation are readily obtained from Equation 3.11 with the help of the condition $\left(\frac{dW}{dn}\right)_{n=n^*} = 0$ for maximum.

It can be seen in Figure 3.5 that a nucleation work of 156kT is needed to form the critical nucleus (for cubic clusters), which consists of 300,000 molecules. For spherical clusters, the corresponding nucleation work increases to 300kT to form the critical nucleus which now is made up of 600,000 molecules. Thus, we see a factor 2 increase with change in the cluster shape. Figure 3.6 shows the effect of increased supersaturation levels on W^* and n^*. As expected, it is seen that with increasing supersaturation, the work needed for cluster formation is brought down.

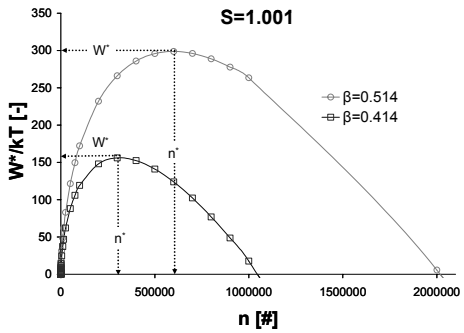

Figure 3.5

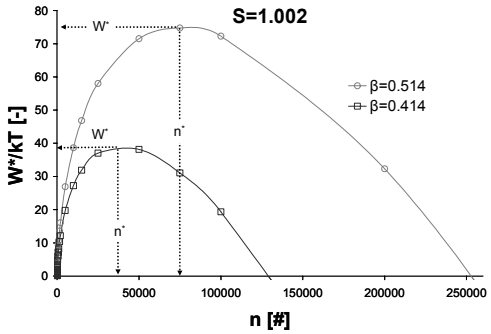

Figure 3.6

Nucleation work as a function of cluster size and cluster shape. Increased supersaturation levels decrease the energy barrier and thus, drive the nucleation work down.

3.3.3 Equilibrium concentration of nuclei

The equilibrium concentration C_n (m^{-3} or m^{-2}) of n-sized clusters in a solution can be obtained by considering the system as an ideal mixture of clusters of all sizes. It then follows (see, *e.g.* (Kashchiev, 2000)) that C_n obeys the Boltzmann-type formula $C_n = C_0 \exp(-W(n)/kT)$. Accordingly, the equilibrium concentration $C^* \equiv C_n$ of nuclei is given by (Kashchiev, 2000):

$$C^* = C_0 \exp(-W^*/kT) \tag{3.12}$$

Here C_0 is the concentration of nucleation sites in the system and, like C^*, is in m^{-3} or m^{-2} for volume or surface nucleation occurring, respectively, in the bulk of the solution or on a substrate.
In HON, every molecule in the solution provides a nucleation site so that, to a good approximation (Kashchiev, 2000):

$$C_0 = 1/v_0 \approx 10^{28} - 10^{29}\, m^{-3} \tag{3.13}$$

This approximation parallels Nielsen's $C_0 = 1/v_s$ in which v_s is the volume of a solvent molecule in the solution.
For HEN on N_a nucleation-active centres in the volume V of the solution $C_0 = N_a/V$. Analogously, for HEN on a substrate with N_a active centres on the substrate surface $C_0 = N_a/A_s$, A_s being the area of this surface. When the substrate is free of nucleation-active centres, C_0 equals the concentration of adsorption sites on the substrate surface, *i.e.* $C_0 = 1/a_0 \approx 10^{19}\, m^{-2}$ (Kashchiev, 2000).

3.3.4 Nucleation mechanism

As is generally agreed, nucleation occurs by the Szilard mechanism of successive attachments and detachments of single molecules (monomers) to and from the clusters of various size n = 1, 2, 3, …. Accordingly, the chain "reaction" of cluster formation can be schematized as

$$[1] \Leftrightarrow [2] \Leftrightarrow ... \Leftrightarrow [n-1] \Leftrightarrow [n] \Leftrightarrow [n+1] \Leftrightarrow ..., \Leftrightarrow$$

where $[n]$ denotes a cluster of n molecules. The nucleation kinetics are, therefore, governed by the frequencies $f(n)$ (s^{-1}) and $g(n)$ (s^{-1}) of monomer attachment to and detachment from an n-sized cluster,

respectively. At constant temperature and supersaturation, these frequencies are time-independent and nucleation can proceed in stationary regime. The process is then characterized by the stationary nucleation rate J ($m^{-3}s^{-1}$ or $m^{-2}s^{-1}$) which is the time-independent frequency of transformation of the nuclei (the n^*-sized clusters) into the smallest supernuclei (the clusters of size $n^* + 1$). Hence, if $Z(n)$ (m^{-3} or m^{-2}) is the time-independent stationary concentration of n-sized clusters, in conformity with the above "reaction" scheme, J is the difference between the frequency $f(n^*)Z(n^*)$ of all $n^* \rightarrow n^* + 1$ transitions per unit volume or area of the system and the frequency $g(n^* + 1)Z(n^* + 1)$ of all $n^* + 1 \rightarrow n^*$ ones; i.e.

$$J = f(n^*)Z(n^*) - g(n^* + 1)Z(n^* + 1) \tag{3.14}$$

With $f^* \equiv f(n^*)$, this expression can be given the familiar form (Kashchiev, 2000) upon ignoring the $g(n^* + 1)Z(n^* + 1)$ term, replacing the stationary concentration $Z(n^*)$ of nuclei by their equilibrium concentration C^* from Equation 3.12 and introducing the so-called Zeldovich factor z to compensate for the resulting error, gives:

$$J = zf^*C^* = zf^*C_0 \exp(-W^* / kT) \tag{3.15}$$

As shown by Zeldovich (Kashchiev (2003)), z is approximately given by :

$$z = [(-d^2W / dn^2)_{n=n^*} / 2\pi kT]^{1/2} \tag{3.16}$$

so that (*e.g.* Kashchiev(2000)) for HON ($\gamma_{ef} = \gamma$) or 3D HEN of caps ($\gamma_{ef} < \gamma$)

$$z = (W^* / 3\pi kTn^{*2})^{1/2} = \frac{3\Delta\mu^2}{4\left(\pi k_B T a^3 \gamma_{ef}^3\right)^{1/2}} = \Delta\mu^2 / (64\pi^2 kT)^{1/2} v_0^{3/2} \gamma_{ef} \tag{3.17}$$

where;

$$a = \left(36\pi v_0^2\right)^{1/3} \tag{3.18}$$

3.3.5 Monomer attachment frequency

In nucleation kinetics, the transition frequencies (f^*) play the same central role as that of the nucleation work $W(n)$ in the thermodynamics of nucleation. Monomer attachment to the clusters is controlled by mass and/or heat transfer. Heat transfer may be important when the heat required for or released during attachment must be conducted sufficiently quickly to or away from the cluster. Mass transport is always needed and it usually occurs by three mechanisms:

- diffusion of molecules towards the cluster
- direct impingement of molecules upon the cluster surface
- transfer of molecules across the cluster/old phase interface

Here, the attachment controlled only by mass transport will be considered, since this kind of control is most often encountered in practice. Two types of mechanisms for monomer attachment are described below.

3.3.5.1 Volume-Diffusion Control (VDC)

Diffusion of molecules from the volume of the old phase towards the cluster surface can control monomer attachment to the clusters, eg. in nucleation in liquid or solid solutions.
Assumption: every arrival of molecule at the nucleus surface results in attachment

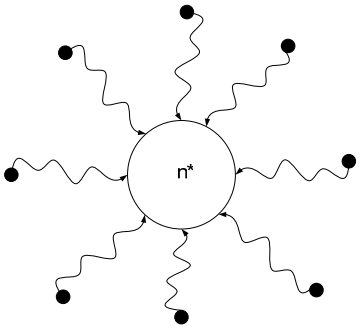

Figure 3.7 Volume Diffusion Control mechanism

Equation 3.15 shows that the determination of the nucleation rate requires knowledge not only of the nucleation work W^* and the concentration C_0 of nucleation sites, but also of the attachment frequency f^* of monomers to the nucleus. In both HON and HEN of crystals in solutions, monomer attachment usually occurs by diffusion of solute in the volume of the solution towards the nucleus or by transfer of solute across the nucleus/solution interface.

When attachment is controlled by volume diffusion, f^* is the product of the incoming diffusion flux j^* of monomers to the nucleus surface and the area A^* of this surface. In the case of HON, for a spherical nucleus of radius $R^* = (3v_0\, n^*/4\pi)^{1/3}$, j^* is readily obtained as $j^* = DC/R^*$ upon solving the corresponding diffusion problem and, since then $A^* = 4\pi R^2$, the resulting formula for f^* reads (Kashchiev, 2000):

$$f^* = \xi(48\pi^2 v_0)^{1/3} DCn^{*1/3} = (512)^{1/3} \frac{\pi\xi DCv_0\gamma_{ef}}{k_B T \ln S} \tag{3.19}$$

where;

$$f^* = \xi . j . A^* \; ; \; 0 < \xi \leq 1 \tag{3.20}$$

$$j = DC\left[\frac{4\pi}{3v_0 n^*}\right]^{1/3} \tag{3.21}$$

$$n^* = \frac{8c^3 v_0^2 \gamma_{ef}^3}{27\Delta\mu^3} = \frac{8c^3 v_0^2 \gamma_{ef}^3}{27(k_B T \ln S)^3} \tag{3.22}$$

$$A^* = c . v_0^{2/3} n^{*2/3} \tag{3.23}$$

$$A = z . f^* . C_0 \tag{3.24}$$

Equation 3.24 unveils the physical meaning of the pre-exponential factor: it is the product of z, f^* and C_0 and is thus, an essentially kinetic quantity accounting for the concrete kinetic (f^*) and spatial (C_0) peculiarities in each particular case of nucleation.

Typically, $0.01 < z < 1$, $f^* = 1$ to 10^{12} s^{-1} and $C_0 = 10^{15}$ to 10^{29} m^{-3} or 10^{10} to 10^{19} m^{-2} for nucleation in the volume of the old phase or on a substrate, respectively. Thus, in most cases, $A = 10^{13}$ to 10^{41} $m^{-3}s^{-1}$ or , $A = 10^8$ to 10^{31} $m^{-2}s^{-1}$. Besides, the smaller values are indicative for the presence of active centre, seeds, etc. in the system and/or for a lower frequency of monomer attachment to the nuclei.

$$\therefore A = \xi DCC_0 \left(\frac{k_B T}{\gamma_{ef}}\right)^{1/2} \ln S = \xi DC_e S C_0 \left(\frac{k_B T}{\gamma_{ef}}\right)^{1/2} \ln S \tag{3.25}$$

where;

$$S = \frac{C}{C_e} = \frac{C}{C_{sat}} \tag{3.26}$$

Here D (m^2/s) is the monomer diffusion coefficient, C is the monomer concentration in the bulk of the solution, C_e (m^{-3}) is the solubility.

3.3.5.2 Interface-Transfer Control (ITC)

Transfer of molecules across the cluster/old phase interface can control their attachment to the clusters mostly in nucleation of liquids or solids in condensed phases (eg., melts, solutions, etc).

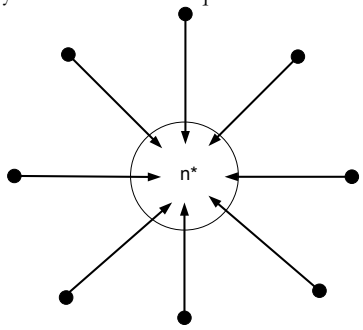

Figure 3.8 Interface Transfer Control mechanism

In attachment controlled by interface transfer, the molecule to be attached is in immediate contact with the condensed-phase cluster and can join the cluster by making a random jump over a distance comparable with it's molecular diameter d_0 which is given by $d_0 \approx (6v_0/\pi)^{1/3}$. The probability for such a jump is characterized by it's jump frequency.

Assumptions:

- Diffusivity at the interface is the same as in the bulk,
- every transfer of molecule across the interface results in attachment

Under the assumption that the probability for such a jump is proportional to D and that the monomer sticking coefficient is unity, $f^* = DC/d_0$ so that, as again $f^* = j^*A^*$, for HON of spheres f^* is given by (Kashchiev, 2000). Now,

$$f^* = \xi w d_0 A^* \tag{3.27}$$

$$w = w_0 \exp(-E_a / kT) \tag{3.28}$$

$$E_a = -kT \ln\left(\frac{D}{d_0^2 w_0}\right) \tag{3.29}$$

$$\therefore A = 6^{5/3} \xi w C_e S C_0 d_0 \pi^{1/3} \left(\frac{k_B T}{\gamma_{ef}}\right)^{-1/2} v_0^{5/3} \tag{3.30}$$

3.3.6 Primary nucleation model

Employing the above expressions for z, f^*, C_0 and W^* in the general Equation 3.15, which is valid for any kind of one-component nucleation allows determination of the supersaturation dependence of the stationary rate J of HON of spherical or HEN of cap-shaped crystals in solutions. Indeed, the use of Equations 3.17, 3.19, 3.20, and 3.24 yields the familiar formula of the classical nucleation theory (Kashchiev, 2000):

$$J = A.\exp\left[\frac{-W^*}{k_B T}\right] \tag{3.31}$$

$$W^* = \frac{4c^3 v_o^2 \gamma_{ef}^3}{27\Delta\mu^2} \tag{3.32}$$

For Volume Diffusion Control

$$J = \xi D C_e S C_0 \left(\frac{k_B T}{\gamma_{ef}}\right)^{1/2} \ln S . exp\left[\frac{-W^*}{k_B T}\right] \tag{3.33}$$

For Interface Transfer Control

$$J = 6^{5/3} \xi w C_e S C_0 d_0 \pi^{1/3} \left(\frac{k_B T}{\gamma_{ef}}\right)^{-1/2} v_0^{5/3} . exp\left[\frac{-W^*}{k_B T}\right] \tag{3.34}$$

3.4 SURFACE/ACTIVATED NUCLEATION MECHANISM OF MERSMANN

Mersmann(1996) proposes an activated secondary nucleation mechanism, which is called *surface nucleation*. The equations used to describe surface nucleation are based on 2D surface nucleation of steps (Dirksen ,1991) which is a mechanism used for the description of crystal growth. Mersmann proposes that some of these growth units can be released from the surface and grow out to 3D-nuclei.

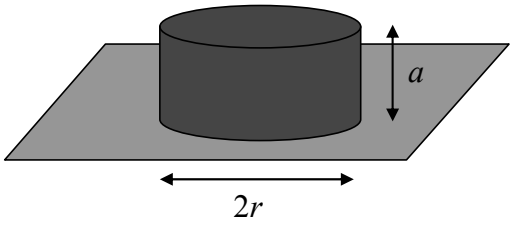

Figure 3.9 Cylindrical embryo on flat crystal surface

The theory deals with the formation of embryos on parent crystals. The shape of the embryos is often assumed to be cylindrical. Figure 3.9 shows the dimensions of a cylindrical embryo. The height of an embryo *a* corresponds to the height of one growth unit (i.e., atom or molecule). The Gibbs free energy change for nucleation of a cylindrical embryo on a flat surface of a parent crystal is given by Equation 3.35. The molecular volume *v* of the embryo is estimated by a^3.

$$\Delta G_r = -\left(\frac{\pi r^2 a}{v}\right) kT \ln(S) + 2\pi r \gamma_e \tag{3.35}$$

The first term corresponds to the change in free energy due to the volume change of the embryo, while the second term results from the change in the length of the edge of the embryo. The first term is negative, while the second is positive. γ_e represents the edge free energy, which has the dimension J/m. Both terms in Equation 3.35 are a function of radius *r*. Similar as in primary nucleation; there exists a maximal value of the Gibbs free energy change, which occurs at the critical cluster size:

$$r_S^* = \frac{\gamma_e a^2}{kT \ln(S)} \tag{3.36}$$

The number of molecules in a critical cluster is:

$$n^* = \frac{a\pi(r_S^*)^2}{v} = \frac{\gamma_e^2 a^2 \pi}{(kT \ln(S))^2} \tag{3.37}$$

And the value of the Gibbs free energy at this maximum is:

$$\Delta G^* = \pi \frac{\gamma_e^2 a^2}{kT \ln(S)} \tag{3.38}$$

The height of the embryo a can be replaced by the molecule diameter d_m. The crystal density ρ_c can be used to make a rough estimate of the molecular diameter.

$$a \approx d_m \approx \left(\rho_c N_A\right)^{-1/3} \tag{3.39}$$

The edge energy is an unknown quantity for ammonium sulphate. The product of the interfacial energy and the molecular diameter is a frequently used approximation for the edge energy:

$$\gamma_e \approx \gamma_{CL} d_m \tag{3.40}$$

The rate of cylinders created on the surface per square meter per second is a function of the maximum Gibbs energy. An expression for this rate is available from 2D surface nucleation of steps (Dirksen, 1991):

$$B_S = \frac{D}{d_m^4} \exp\left[-\frac{\Delta G^*}{kT}\right] \tag{3.41}$$

Substitution of Equations 3.38 to 3.41 leads to:

$$B_s = \frac{D}{d_m^4} \exp\left[-\frac{\Delta G^*}{kT}\right] = \frac{D}{d_m^4} \exp\left[-\frac{\pi \gamma_{CL}^2 d_m^4}{(kT)^2 \ln(S)}\right] \tag{3.42}$$

The dimension of B_s is number of embryos per m^2 crystal surface per second. Two final steps are required to come to an expression, which has the dimension of nuclei per unit volume of solution per second.

Firstly, not all cylinders on the surface will create nucleation in the solution. Only a fraction E of the cylindrical embryos is removed and therefore only this fraction causes nucleation in the solution. So E represents the fraction of surface nuclei that is removed from the surface to become a volume nucleus (Mersmann, 1996). The value of E is not known and is a parameter. Secondly, the surface nucleation rate is proportional with specific surface area. The final formula for surface nucleation is:

$$B_{surf} = E a_v B_S = \frac{E a_v D}{d_m^4} \exp\left[-\frac{\pi \gamma_{CL}^2 d_m^4}{(kT)^2 \ln(S)}\right] \tag{3.43}$$

Mersmann substitutes an equation for the interfacial energy into the final equation for the surface nucleation rate.

$$\gamma_{CL} \approx \frac{kT}{3d^2{}_m} \ln\left(\frac{c_c}{c_{sat}}\right) \tag{3.44}$$

As a result the final equation as given by Mersmann(1996) is:

$$B_{Surf} = \frac{Ea_v D}{d_m^4} \exp\left(-\frac{\pi}{9} \frac{\left[\ln\left(c_c / c_{sat}\right)\right]^2}{\ln\left(S\right)}\right) \tag{3.45}$$

The interfacial energy is eliminated from the final equation. The estimate described by Equation 3.44 has been tested for 58 inorganic systems (Mersmann, 1990). The mismatch between the calculated and the experimental determined interfacial energy is on average 21%. From Equation 3.45, it is no longer clear that there is so much uncertainty inside the exponential term and it is therefore advised to use Equation 3.43.

3.5 KINETIC MODEL OF GAHN & MERSMANN

For the systems considered in this thesis, mechanisms like agglomeration have little or no impact on the process dynamics and the product quality. The chief contributors which influence the crystallization process in terms of the process behavior and also the final product quality specifications (for inorganic systems like $(NH_4)_2SO_4$), are crystal growth and secondary nucleation. To this extent, the only fundamental model derived from first principles is the secondary nucleation model developed by Gahn and Mersmann (1999a,b).

The secondary nucleation and growth model framework proposed by Gahn and Mersmann (1999a,b) contains a more physical basis than any previous work, thus reducing the number of kinetic parameters significantly. Also, the parameters have a physical significance thus, making the model more predictive in nature from a design perspective. The secondary nuclei (eg. for ammonium sulphate crystals) are assumed to be generated by crystal-impeller collisions which fall under the contact nucleation mechanism (attrition) category. Here, the attrition resistance of a crystalline substance is related to it's mechanical properties. The model framework of Gahn and Mersmann can be seen as a synthesis of three sub-models (see Figure 3.10):

1. a procedure to determine the total number of crystals colliding per second with the faces and edges of the impeller blades, and the corresponding impact energy per collision (Mersmann (1988); Ploß (1989));
2. a relation between the impact energy and the attrition volume produced due to a single collision of a crystal corner with a hard, flat surface and the resulting number and size distribution of resulting attrition fragments (Gahn(1997)); and
3. a relation to derive the growth rate of the fragments formed by the attrition process (van der Heijden (1992); Zacher (1995); Gahn (1997)).

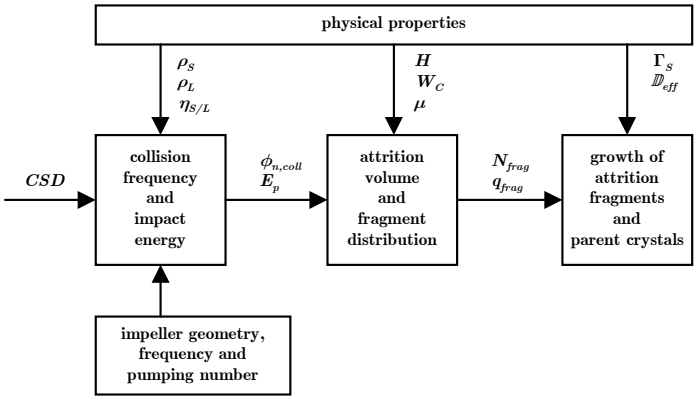

Figure 3.10 Model structure of the framework of Gahn and Mersmann (1999a) (after Bermingham, 2003)

3.5.1 Collision frequency and impact energy

The collision frequency and impact energy of a crystal with the impeller is calculated using the model developed by Pohlish and Mersmann (1988), Ploβ and Mersmann (1989) and Sangl (1991). This model which provides an approximation for the complex two-phase flow pattern in the vicinity of the impeller and applicable for propellers, pitched-blade turbines and axial pumps, determines the total number of crystals colliding per second with the edge and face of the impeller blades, and the corresponding impact energy of the collision. It is assumed that the slip velocity of the crystal equals zero and there is no radial flow velocity component. The probability and impact velocity of a collision are calculated for each: the edge and face of the blade impeller. This is done by dividing the impeller into a number of segments (j) along the impeller radius. The relative velocity and impact velocity are both a function of the impeller radius. The axial velocity of a crystal is calculated from the volumetric flow rate through the draft tube. Thus, the model assumes that a crystal follows the macroscopic flow pattern of the liquid phase around the impeller. For the calculation of the collision frequency, three main aspects are considered:

i. the frequency of the crystals moving towards the impeller
ii. the probability that a crystal is on a streamline moving towards the impeller ($\eta_{geo,edge/blade,j}$)
iii. the probability that a crystal that is on such a streamline collides with the impeller ($\eta_{edge/blade}$ = target efficiency)

The collision rate of crystals of size, L, with the face and the edge of the impeller blade at radial position, j, is given by:

$$\varphi_{n,coll,edge/face,j} = n.\varphi_{V,dt}\ \eta_{coll,edge/face,j} \tag{3.46}$$

The collision probability of a crystal (η_{coll}) with the impeller is approached by using the target efficiency. The probability that a crystal collides with the impeller is equal to:

$$\eta_{coll,edge/blade,j} = \eta_{geo,edge/blade,j} \cdot \eta_{target,edge/blade,j} \tag{3.47}$$

The collision efficiencies, $\eta_{coll,edge}$ and $\eta_{coll,blade}$ are measures for the chance of a crystal of size, L, being on a streamline towards and actually colliding at radial position, j, with the impeller edge and blade(face) respectively.

The target efficiency is given by:

$$\eta_{target,edge/blade} = \left(\frac{\psi_{edge/blade}}{0.32 + \psi_{edge/blade}} \right)^{2.1} \tag{3.48}$$

The Stokes number in Equation 3.48 is given by:

$$\psi_{edge/blade} = \frac{(\varrho_s - \varrho_l).v_{rel}.L^2}{18.\eta_L.T_{edge/blade}} \tag{3.49}$$

Equation 3.48 is used to calculate the target efficiency for the flow around and the edge and the blade. The geometric efficiency in Equation 3.47 is calculated, according to Equation 3.50, by the ratio of the projected area perpendicular to the axial flow direction of the segments of the impeller and the cross-sectional area of the draft tube.

$$\eta_{geo,edge/blade,j} = \frac{4.T_{edge/blade}.N_{blade}.\Delta r_j}{\pi.D_{dt}^2.\sin a_j} \tag{3.50}$$

Prior to the impact of a crystal with the impeller a laminar boundary layer has to be displaced. Therefore, the actual collision velocity will be lower than the relative velocity. It is assumed that the ratio between the actual and the relative collision velocity is equal to the target efficiency (Ploβ and Mersmann, 1989).
From this point onwards, the calculations are identical for the edge and face of the impeller blades. The collision impact energy, W_p, is calculated using the following equation:

$$W_{p,edge/blade,j} = \frac{1}{2} \varrho_s \, k_v \, L^3 \, v_{coll,edge/face,j}^2 \tag{3.51}$$

3.5.2 Attrition volume and fragment distribution

Removed attrition volume
The collision of a crystal with an impeller can take place with its faces, edges, or its corners. However, the crystal corners probably produce the most attrition fragments, because the stress of the collision can be localized in a smaller crystal area then when it collides with the edge or face. It was shown that rounded-off crystals show less attrition than ideally shaped crystals (Chianese (1993), Chianese (1996), Ó Meadhra (1995) and Gahn (1996). In this model, only the collisions between the impeller and the crystal corner is taken into account, with the assumption that the crystal corner is a cone. A collision between a crystal with the impeller results in a so-called plastic deformation of the cone tip and an elastic stress field in the cone (see Figure 3.11).

The abraded(attrited) volume, V_{attr}, removed from a parent crystal as a result of a single collision with an impeller is related to the impact energy of the collision, W_p, of the crystal via a number of material properties, viz hardness, H, shear modulus, μ, and effective fracture surface energy, Γ/K_r.
The effective fracture surface energy is the most difficult property that can be measured experimentally (Gahn and Mersmann, 1999a) and can be related to the critical work of indentation for crack formation, W_C:

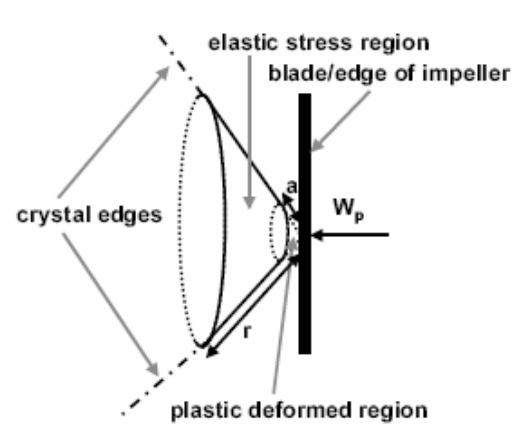

Figure 3.11 Assumed geometry of the plastically deformed and elastic stress zone (a = radius of plastically deformed region, r = radius from the cone of the crystal), after Westhoff(2002)

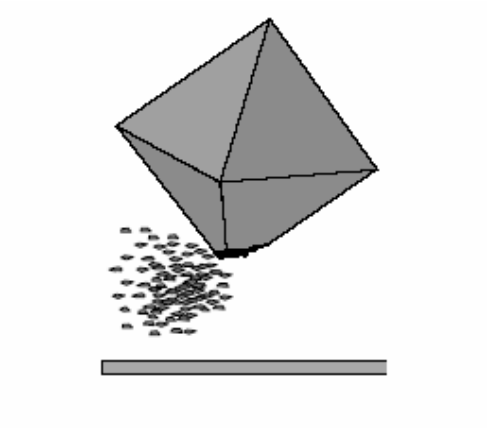

Figure 3.12 Attrition fragments generated after crystal-impeller collision, after Westhoff(2002)

$$\frac{\Gamma}{K_r} = \frac{1}{10}\frac{W_C^{1/3} H^{5/3}}{\mu} \tag{3.52}$$

This material property is the most uncertain model parameter and Gahn and Mersmann (1999a) therefore attribute any observed deviations between model predictions and experimental results to this material property.
In order for an impact to cause fracture and to remove material from a crystal, the impact energy must exceed a certain minimum impact energy. This energy is solely a function of the material properties and thus a constant for a given substance:

$$W_{p,min} \approx 64\frac{\mu^3}{H^5}\left(\frac{\Gamma}{K_r}\right)^3 = \frac{64}{1000}W_C \tag{3.53}$$

Combining Equations 3.51 and 3.53 shows that the required minimal collision velocity is only a function of crystal length for a given substance:

$$v_{coll,min}(L) \approx \sqrt{128\frac{\mu^3}{\varrho_s k_v L^3 H^5}\left(\frac{\Gamma}{K_r}\right)^3} = \sqrt{\frac{128}{1000}\frac{W_C}{\varrho_s k_v L^3}} \tag{3.54}$$

The attrition volume resulting from a single collision, at a given radial position(r) is given by:

$$\begin{aligned} V_{attr}(L,r) &= C\,E_p^{4/3}(L,r) && W_p(L,r) \geq W_{p,min} \\ V_{attr}(L,r) &= 0 && W_p(L,r) < W_{p,min} \end{aligned} \tag{3.55}$$

where C is the attrition constant, which is defined as:

$$C \approx \frac{2}{3}\frac{H^{2/3}}{\mu}\frac{K_r}{\Gamma} = \frac{20}{3}\frac{1}{W_C^{1/3}H} \tag{3.56}$$

Number and distribution of fragments
The attrition volume removed from a parent crystal consists of a plastically and an elastically deformed part. The attrition fragments from the plastically deformed volume have such a high internal stress content, that these are assumed to dissolve instantaneously. The total number of attrition fragments in the elastically deformed part, N_{frag}, and their normalized number density distribution, $q_{frag}(L)$, are given by the following two equations:

$$N_{frag}(L,r) \approx \frac{\pi}{21}\frac{H^{1/2}}{k_v\mu^{3/4}}\left(\frac{K_r}{\Gamma}\right)^{3/4}\left(L_{frag,min}^{-2.25} - L_{frag,max}^{-2.25}(L,r)\right)W_p(L,r) \tag{3.57}$$

$$\begin{aligned} q_{frag}\left(L,r,L_{frag}\right) &= \frac{2.25L_{frag}^{-3.25}}{L_{frag,min}^{-2.25} - L_{frag,max}^{-2.25}(L,r)} \quad L_{frag,min} \le L_{frag} \le L_{frag,max}(L,r) \\ q_{frag}\left(L,r,L_{frag}\right) &= 0 \qquad\qquad L_{frag} < L_{frag,min} \vee L_{frag} > L_{frag,max}(L,r) \end{aligned} \tag{3.58}$$

The size of the smallest attrition fragments is only a function of material properties:

$$L_{frag,min} = \frac{32}{3}\frac{\mu}{H^2}\frac{\Gamma}{K_r} = \frac{32}{30}\left(\frac{W_C}{H}\right)^{1/3} \tag{3.59}$$

Whereas the size of the largest attrition fragments is also determined by the magnitude of the impact energy:

$$L_{frag,max}(L,r) = \frac{1}{2}\left(\frac{H^{2/3}}{\mu}\frac{K_r}{\Gamma}\right)^{1/3}W_p^{4/9}(L,r) = \frac{1}{2}\left(\frac{10}{W_C^{1/3}H}\right)^{1/3}W_p^{4/9}(L,r) \tag{3.60}$$

3.5.3 Growth of attrition fragments and parent crystals

Driving force
The secondary nuclei generated via attrition contain a certain amount of strain within their crystal lattices in the form of elastic deformation. The plastically deformed attrition fragments are assumed to dissolve instantaneously due to their high internal stress. The strain in the crystal lattice increases their chemical potential and consequently the solubility of the attrited fragment, c^*_{real}, in comparison to the solubility, c^*, of an ideal, stress free crystal.

$$c^*_{real}(L) = c^* \exp\left(\frac{\Gamma_S}{RTL}\right) \tag{3.61}$$

The resulting driving force for crystallization, Δc,(L) is now given as:

$$\Delta c(L) = c - c^*_{real}(L) \tag{3.62}$$

where the parameter, Γ_S, is the surface related energy increase.

The reduction in the driving force due to the increased chemical potential will lead to reduced growth rates and can even cause dissolution of certain highly strained fragments. The growth of the crystals can be described as a two-step process, as described earlier in section 3.2.4, combining a diffusion step from the bulk to the interface followed by a surface integration step. A size-dependent growth rate equation can then be given as:

$$\frac{G(L)}{2k_d(L)} = \frac{\Delta c(L)}{c_s} + \frac{k_d(L)}{2k_r c_s} - \sqrt{\left(\frac{k_d(L)}{2k_r c_s}\right)^2 + \frac{k_d(L)}{k_r c_s}\frac{\Delta c(L)}{c_s}} \quad ; \Delta c(L) > 0 \tag{3.63}$$

where, k_d is the mass transfer coefficient, k_r the surface integration rate constant and c_s the molar concentration of the crystallizing substance. In case of a negative driving force, the dissolution rate assuming diffusion controlled becomes:

$$\frac{G(L)}{2k_d(L)} = \frac{\Delta c(L)}{c_s} \quad ; \Delta c(L) \leq 0 \tag{3.64}$$

The mass transfer coefficient can be calculated using a Sherwood type relation developed by Herndl (1982):

$$k_d(L) = \frac{D_{AB}}{L}\left[2 + 0.8\left(\frac{\bar{\varepsilon}L^4}{\upsilon_L^3}\right)^{1/5}\left(\frac{\upsilon_L}{D_{AB}}\right)^{1/3}\right] \tag{3.65}$$

The mean specific power input of the impeller follows from:

$$\bar{\varepsilon} = \frac{Ne\, N_{imp}^3 D_{imp}^5}{V} \tag{3.66}$$

Thus, there are two unknown parameters that stem from this model framework, viz. the k_r and Γ_s, which need to be determined experimentally. Alternatively, these will be determined via parameter estimation studies, using experiments done on semi-industrial scale crystallizers.

3.6 PROCESS MODELLING FRAMEWORK

In this sub-section, the process modelling framework developed by Bermingham(2003a) is described briefly. For a more comprehensive overview on these models, the reader is referred to Bermingham(1998, 2003a,b). This model framework, built within a dynamic modelling tool gPROMS[1], can be applied for design and optimization purposes and used to predict the relations between crystallizer geometry and operating conditions on one hand and production capacity and crystal quality on the other. This process model consists of rigorous kinetic models and a framework providing resolution in 1) external co-ordinates representing the geometric space of the crystallizer vessel, in 2) internal crystal co-ordinates such as size, shape and internal energy, and in 3) the time co-ordinate.
The modelling architecture is chosen such as to account for the spatial distribution of process conditions inside the crystallizer, eg. CSD, energy dissipation and supersaturation. This is achieved using a compartmental modelling approach which enables a rough separation of the *local* intrinsic kinetics and the *overall* fluiddynamics, which also allows for a computationally feasible description of the process dynamics as well as a more detailed description of the CSD.

[1] Process Systems Enterprise Ltd, Bridge Studios, 107a Hammersmith Bridge Rd., London, UK

The scope of this process modelling framework covers a wide variety of crystallization processes which can be classified as follows:

1. Crystallization method (cooling, flash-cooling or evaporative).
2. Operation mode (batch, semi-batch or continuous).
3. Configuration (single or multiple stage); and
4. Crystallizer type (stirred vessel, DT, DTB, FC or Oslo).

Here, a brief overview is presented on the simulation framework that is built within a dynamic modelling environment (gPROMS).

3.6.1 Compartmental model

Compartmental modelling is a technique that comprises the division of the crystallizer into a number of units with well-defined flow patterns (plug flow, perfectly mixed) and was introduced to treat non-ideal flow and mixing problems. The non-ideal flow problem is dealt with by introducing a network of coupled units that have ideal flow characteristics. The objective is to find the combination of interconnected units that best reproduces the measured residence time distribution.

A compartmental model is characterized by the structure and the connectivity of the compartments. The individual compartments are all described using the same equations of conservation, physical and thermodynamic property relations, kinetic rate expressions and parameters. The differences in the compartments are purely a result of varying process conditions. The use of a compartmental model introduces additional model parameters to the process (number and volume of compartments, fluxes between compartments). The compartments must have negligible internal gradients in supersaturation, crystal size distribution, and energy dissipation. A more comprehensive overview on why such an approach was taken as opposed to CFD (say) is given by Bermingham(1998, 2003a,b). An input-output diagram of a single-compartment model is depicted in Figure 3.13.

Here, an arbitrary number of inlet streams (NI) and outlet streams (NO) respectively, enter and exit the compartment. Each flow is characterized by component mass flow rates (ϕ_m), crystal number densities (n) and an enthalpy flow rate (ϕ_H). The vapor flow (ϕ_V), present in each compartment but zero in most compartments, is described by a mass flow rate ($\phi_{m,V,out}$) and enthalpy flow rate only ($\phi_{H,V,out}$). The states in a compartment are the mass quantities of each component, crystal number densities (i.e. CSD) and enthalpy. The heat input of a compartment can be positive (heating), negative (cooling) or zero.

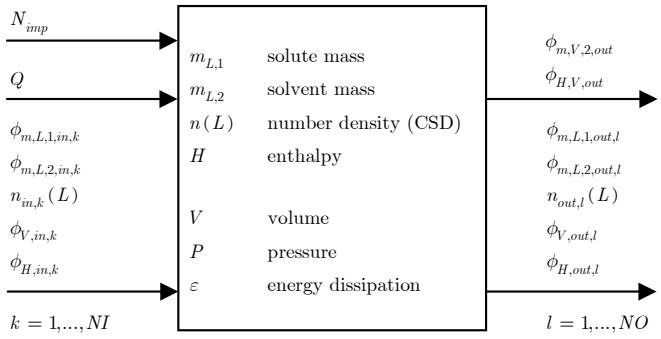

Figure 3.13 Compartment model - variables and structure (after Bermingham,2003)

3.6.2 Conservative equations of state

The equations of conservation consist of the mass balances for the liquid phase components, population balance(s) for the solid phase(s) and the enthalpy balance. The population balance is in fact a distributed mass balance for a solid or dispersed phase, and is linked to the liquid or continuous phase component mass balances via the crystallization kinetics.

Population balance

The population balance equation (PBE) describes the time evolution of the crystal size distribution due to kinetic processes such as crystal growth, attrition, agglomeration, birth and death. The concept of population balances was introduced to the field of crystallization by Randolph and Larson (1962).
The PBE is encountered in many forms. The amount of particles can be expressed in terms of number, volume or mass densities, whereas particle size is usually expressed in terms of length or volume. Volume is typically used for particle size when agglomeration and/or breakage play an important role, because these crystallization mechanisms must obey volume conservation. Furthermore, the PBE can easily be extended to include external co-ordinates (Randolph and Larson, 1988). The PBE for a uniformly mixed volume, with the amount and the size of particles expressed in terms of number density and particle length respectively, can be written as follows:

$$\overbrace{\frac{\partial\left(n_q(L,t)V(t)\right)}{\partial t}}^{\text{number rate of accumulation}} = \overbrace{-V(t)\frac{\partial\left(n_q(L,t)\cdot G_q(L,\sigma)\right)}{\partial L}}^{\text{rate of number gain due to crystal growth}} + \overbrace{\sum_{k=1}^{NI}\phi_{V,in,k}(t)n_{q,in,k}(L,t)}^{\text{number rate in}} - \overbrace{\sum_{l=1}^{NO}\phi_{V,out,l}(t)n_{q,out,l}(L,t)}^{\text{number rate out}} + \overbrace{(\phi^{+}_{n,q,nucl}-\phi^{-}_{n,q,dis}).V(t)}^{\substack{\text{number production rate due to}\\ \text{primary nucleation and dissolution}\\ \text{at the critical nucleus size}}} + \overbrace{(\phi^{\pm}_{n,q,attr}+\phi^{\pm}_{n,q,break}-\phi^{\pm}_{n,q,aggl}).V(t)}^{\substack{\text{number production rate due to}\\ \text{attrition, breakage and agglomeration}}} \tag{3.67}$$

Initial condition:

$$n(L,t=0)=n_0(L) \tag{3.68}$$

The initial condition can be used to express a trivial situation such as a clear liquid (no crystals) or a size distribution of seed crystals (often used in batch processes).

Boundary conditions for the population balance

The classical boundary condition with respect to crystal size for the population balance equation is:

$$n(L=0,t)=\frac{B_0(t)}{G(L=0,t)};\ G(L)\geq 0 \text{ for all L} \tag{3.69}$$

This boundary condition is applicable and sufficient when the crystal growth rate is positive for all crystal sizes. B_0 denotes the birth rate of crystals with size zero.
If the growth rate is negative for all sizes, a boundary condition at infinite length is required and sufficient:

$$n(L=\infty,t)=0;\ G(L)<0 \text{ for all L} \tag{3.70}$$

For a more comprehensive discussion on the numerical discretization for the solution of the partial differential equations, the reader is referred to Bermingham(2003).

Energy balance

The energy balance accounts for the dynamics of the temperature and can be easily transformed into an enthalpy balance assuming that the kinetic energy, potential energy and shaft work are negligible. This results in the following balance:

$$\overbrace{\frac{dH(t)}{dt}}^{\text{rate of enthalpy accumulation}} = \overbrace{\sum_{k=1}^{NI}\varphi_{H,in,k}(t) - \sum_{l=1}^{NO}\varphi_{H,out,l}(t) - \varphi_{H,V,out}(t)}^{\text{rate of total enthalpy in and out by convection}} + \overbrace{\dot{Q}(t)}^{\text{net rate of heat addition}} \tag{3.71}$$

Initial condition:

$$H(t=0) = H_0 \tag{3.72}$$

Mass balance

The liquid phase component mass balance for the solvent is given by:

$$\overbrace{\frac{dm_{L,solvent}}{dt}}^{\text{mass rate of accumulation}} = \overbrace{\sum_{k=1}^{NI}\varphi_{m,L,solvent,in,k} - \sum_{l=1}^{NO}\varphi_{m,L,solvent,out,l} - \varphi_{m,V,solvent,out}}^{\text{mass rates in and out via convective transport}} + \overbrace{M_{solvent}\sum_{p=1}^{NR_L}\nu_{L,p,solvent}\cdot r_p}^{\text{mass production rate due to liquid phase reactions}} + \overbrace{M_{solvent}\sum_{q=1}^{NP_S}\nu_{S,q,solvent}\cdot[\varphi_{mol,grow,q} + \varphi_{mol,nucl,q} - \varphi_{mol,dis,q}]}^{\text{interphase mass flux due to crystal growth and due to primary nucleation and dissolution at the critical nucleus size}} \tag{3.73}$$

Initial condition:

$$m_{L,solvent}(t=0) = m_{L,solvent,0} \tag{3.74}$$

Assuming that the vapour flow only consists of the solvent, the liquid phase component mass balance for the solute is given by:

$$\overbrace{\frac{dm_{L,solute}}{dt}}^{\text{mass rate of accumulation}} = \overbrace{\sum_{k=1}^{NI}\varphi_{m,L,solute,in,k} - \sum_{l=1}^{NO}\varphi_{m,L,solute,out,l}}^{\text{mass rates in and out via convective transport}} + \overbrace{M_{solute}\sum_{q=1}^{NP_S}\nu_{S,q,solute}\cdot[\varphi_{mol,grow,q} + \varphi_{mol,nucl,q} - \varphi_{mol,dis,q}]}^{\text{interphase mass flux due to crystal growth and due to primary nucleation and dissolution at the critical nucleus size}} \tag{3.75}$$

Initial condition:

$$m_{L,solute}(t=0) = m_{L,\,solute,0} \tag{3.76}$$

Kinetic terms present in both the mass balances and population balance
The kinetic rate terms in the component mass balances and population balance are coupled by the following three equations:

$$\phi_{mol,nucl}(t) = \frac{k_v \rho_s}{M_s} V(t) \int_0^\infty \phi^+_{n,nucl}(L,t) L^3 dL \tag{3.77}$$

$$\phi_{mol,grow}(t) = -\frac{k_v \rho_s}{M_s} V(t) \int_0^\infty \frac{\partial (n(L,t) G(L,t))}{\partial L} L^3 dL \tag{3.78}$$

$$\phi_{mol,dis}(t) = \frac{k_v \rho_s}{M_s} V(t) \int_0^\infty \phi^-_{n,dis}(L,t) L^3 dL \tag{3.79}$$

The expressions for the number density fluxes, $\phi^+_{n,nucl}$, $\phi^\pm_{n,attr}$ and $\phi^-_{n,dis}$, and the growth rate, G, follow from the kinetic models treated earlier in sections 3.2, 3.3 and 3.5.

3.6.3 Classification model

The ratio of the crystal number density in a certain outlet stream and in the compartment is defined as the classification function of that stream:

$$h_{out}(L) = \frac{n_{out}(L)}{n(L)} \tag{3.80}$$

The introduction of a classification function allows one to have compartments which are well mixed internally but not necessarily with respect to the outlet streams. The latter only refers to the crystal size distribution; the temperature and liquid phase composition of the outlet stream are always set equal to the temperature and composition within the compartment. Such a classification function can be given by:

$$h_{out}(L) = 1 + \frac{U_{slip}(L) - U_{sup,out}\left(1 - \frac{\varepsilon_{out}}{\varepsilon}\right)}{U_{sup,out}} = \frac{U_{slip}(L)}{U_{sup,out}} + \frac{\varepsilon_{out}}{\varepsilon} \tag{3.81}$$

where the particle slip velocity, U_{slip}, is given by an equation proposed by Barnea and Mizrahi (1973):

$$U_{slip}(L) = \left(\frac{-B(L) + \sqrt{B(L)^2 + AC(L)}}{C(L)} \right)^2 \tag{3.82}$$

where parameters A, B and C are defined as follows:

$$A = \sqrt{a_1}$$
$$B(L) = 0.5\sqrt{a_2}a_4 \tag{3.83}$$
$$C(L) = \sqrt{a_2}a_3$$

and α_1, α_2, α_3 and α_4 are given by:

$$a_1 = g\frac{\varrho_S - \varrho_L}{\varrho_S + \varrho_L}$$
$$a_2(L) = \frac{3}{4}\frac{1+(1-\varepsilon)^{1/3}}{(\varrho_S + \varrho_L)L^2\varepsilon} \tag{3.84}$$
$$a_3(L) = 0.63\sqrt{L\varrho_L}$$
$$a_4 = 4.80\sqrt{\eta_L}\exp\left[\frac{5}{6}\frac{1-\varepsilon}{\varepsilon}\right]$$

3.7 THERMODYNAMIC AND PHYSICAL PROPERTIES

Equations and values for the thermodynamic, physical and mechanical properties used within this framework are given in Appendix A3.1.

NOTATIONS

a	height of surface nucleus	[m]
a_v	specific surface area	[$m^2.m^{-3}$ solution]
a_0	concentration of adsorption sites on the substrate surface	[m^2]
A^*	area of the nucleus surface	[m^2]
A_c	area of the cluster surface	[m^2]
A_s	area of the substrate surface	[m^2]
B	size dependent birth rate	[$\#.m^{-4}.s^{-1}$]
B_0	birth rate at lower size limit	[$\#.m^{-3}.s^{-1}$]
B_s	birth rate	[$\#.m^{-2}.s^{-1}$)]
B_{surf}	surface nucleation rate	[$\#.m^{-3}.s^{-1}$)]
c	concentration	[$kg.m^{-3}$]
$c^*_{real}(L)$	saturation concentration of crystals of size L	[$kg{\cdot}m^{-3}$]
c_c	crystal density	[$kg.m^{-3}$]
c_S	concentration in solid phase	[$kg{\cdot}m^{-3}$]
c_s	concentration of the solid phase	[$kg.m^{-3}$]
c_w	solubility	[kg solute. kg $solution^{-1}$]
c_{ps}	specific heat capacity of the solid phase	[$kJ.kg^{-1}.K^{-1}$]
c_{pl}	specific heat capacity of the liquid phase	[$kJ.kg^{-1}.K^{-1}$]
C_e	equilibrium concentration (solubility)	[$\#.m^{-3}$]
C_0	concentration of nucleation sites	[$\#.m^{-3}$]
c^*, C_{sat}	saturation concentration	[$kg.m^{-3}$]
C^*	equilibrium concentration of nuclei	[$\#.m^{-3}$]
d_m	molecular diameter	[m]
d_0	diameter of a molecule	[m]
D	diffusion coefficient of solute molecule	[$m^2.s^{-1}$]
D	size dependent death rate	[$\#.m^{-4}.s^{-1}$]
D_{AB}	binary diffusion coefficient	[$m^2.s^{-1}$]
D_{dt}	diameter of draft tube	[m]
D_{eff}	effective diffusivity	[$m^2.s^{-1}$]

D_{imp}	impeller diameter	[m]
e	edge of the impeller blade	[m]
E_p	impact energy of collision	[J]
E	removal efficiency surface nucleation	[-]
E_a	activation energy for interface transfer	[J]
f	face of the impeller blade	[m]
f, f^*	attachment frequency of molecules to the nucleus	[s^{-1}]
g	detachment frequency of molecules from the nucleus	[s^{-1}]
g	gravitational acceleration	[$m.s^{-2}$]
G	linear growth rate function	[$m.s^{-1}$]
G	gibbs free energy	[J]
G_{old}	gibbs' free energy (old phase)	[$kg.J.mol^{-1}$]
G_{new}	gibbs' free energy (new phase)	[$kg.J.mol^{-1}$]
h	classification function	[-]
H	enthalpy	[J]
H	hardness	[$N{\cdot}m^{-2}$]
H_v	Vicker's hardness	[$N{\cdot}m^{-2}$]
j^*	diffusion flux of monomers to the nucleus surface	[# $.m^{-2}.s^{-1}$]
J	primary nucleation rate	[$\#.m^{-3}.s^{-1}$]
k ,k_B	Boltzmann constant	[$J.K^{-1}$]
k_d	mass transfer coefficient	[$m.s^{-1}$]
k_r	integration rate constant	[$m^4.mol^{-1}.s^{-1}$]
k_a	surface shape factor	[-]
k_v	volume shape factor	[-]
K_r	radial efficiency factor in crack formation	[-]
L	crystal length	[m]
L_{frag}	crystal length of attrition fragment	[m]
L	crystal length	[m]
L_{crit}	critical nucleus size	[m]
L_{init}	initial crystal length	[m]
m	mass	[kg]
M	molecular weight	[$kg.mol^{-1}$]
n	population number density	[$\#.m^{-4}$]
n	number of molecules constituting the cluster	[#]
n^*	number of molecules constituting the critical cluster	[#]
n_L	population number density at a certain size	[$\#.m^{-4}$]
N_{blades}	number of impeller blades	[-]
N_a	nucleation-active centres	[#]
N_A	avogadro's number	[$1.mol^{-1}$]
NC	number of components	[-]
Ne	Newton number or power number	[-]
N_{frag}	number of fragments from a single collision	[-]
NI	number of solid/liquid inlet streams	[-]
N_{imp}	impeller frequency	[s^{-1}]
NK	number of compartments	[-]
NO	number of solid/liquid outlet streams	[-]
NP	number of phases	[-]
N_{pump}	pumping capacity or discharge coefficient	[-]
NR	number of reactions	[-]
P	pressure	[Pa]
q_{frag}	normalized number density distribution	[-]
Q	specific heat input	[$kW.m^{-3}$]
r_p	reaction rate	[$mole{\cdot}s^{-1}$]
r	radius of cluster	[m]
r^*_s	radius of critical cluster	[m]
r	radial position on impeller	[m]
r^*	critical cluster size	[m]
R	universal gas constant	[$J.mol^{-1}.K^{-1}$]
S	supersaturation ratio	[-]

t	time	[s]
t_{ind}	time in which clusters coagulate to nuclei	[s]
T	characteristic length	[m]
T	temperature	[K]
U_{slip}	particle slip velocity	[m.s^{-1}]
U_{sup}	superficial velocity	[m.s^{-1}]
v_o	molecular volume	[m^3]
v_s	volume of a solvent molecule in the solution	[m^3]
v	molecular volume in cluster	[m^3]
v_{coll}	collision velocity	[m.s^{-1}]
V	volume of the solution	[m^3]
V	crystallizer volume	[l]
V_m	molecular volume	[m^3]
V_{attr}	attrition volume from a single collision	[m^3]
w, w_0	random jump frequency	[s^{-1}]
w_s	strain energy/chemical potential difference	[J.mol^{-1}]
W	nucleation work	[J]
W_C	critical work of indentation for crack formation	[J]
W_P	impact energy of collision	[J]
z	zeldovich factor	[-]

Greek

α	blade angle	[rad]
β	numerical factor	[-]
$\varepsilon, \bar{\varepsilon}$	specific power input	[W·kg^{-1}]
ε	energy of interaction between crystal surface and embryo	[J]
ε	fraction of total volume occupied by continuous phase	[-]
η_l	dynamic viscosity of the liquid	[N.m^{-2}.s]
$\eta_{L/S}$	apparent dynamic viscosity of the slurry	[N.m^{-2}.s]
η_{coll}	collision efficiency	[m^{-1}]
η_{geom}	geometric target efficiency	[m^{-1}]
η_{target}	target efficiency	[m^{-1}]
γ, γ_{cl}	specific surface energy of the cluster/solution interface	[J.m^{-2}]
γ_e	edge free energy	[J.m^{-1}]
γ_{ef}	effective specific surface energy	[J.m^{-2}]
Γ	fracture surface energy	[J.m^{-2}]
Γ_S	surface related energy increase or condition of deformation	[J.m.mol^{-1}]
λ	molecular heat of dissolution	[J]
μ	shear modulus	[N.m^{-2}]
$\Delta\mu$	supersaturation	[J]
μ_{old}	chemical potential (old phase)	[J]
μ_{new}	chemical potential (new phase)	[J]
ν_l	kinematic viscosity of the liquid	[m^2·s^{-1}]
ν	stoichiometric coefficient matrix	[-]
$\phi_{n,coll}$	crystal collision rate at a certain radial position	[m^{-1}.m^{-1}.s^{-1}]
ρ_c	crystal density	[kg.m^{-3}]

ρ_s	material density of solid phase	[kg.m^{-3}]
ρ_l	material density of liquid phase	[kg.m^{-3}]
ρ_v	vapor density	[kg.m^{-3}]
σ	relative supersaturation	[-]
ψ	heterogeneity factor	[-]
ψ	Stokes parameter	[-]
τ	residence time	[s]
ξ	coefficient of monomer sticking	[-]

Indices

i	index of a liquid phase component
j	index of a compartment
k	index of a solid/liquid inlet
l	index of a solid/liquid outlet
p	index of a liquid phase reaction
q	index of a solid phase and of the corresponding crystallization reaction

Superscripts/subscripts

Δ	difference
$*$	equilibrium
in	flow into the crystallizer/compartment
out	flow out of the crystallizer/compartment
$aggl$	agglomeration
$attr$	attrition
$break$	breakage
dis	dissolution
$edge$	edge of the impeller blade
$face$	face of the impeller blade
$grow$	growth
$nucl$	primary nucleation
L	liquid phase, i.e. the continuous phase
S	solid phase, i.e. the dispersed phase
V	vapor phase

Abbreviations

CSD	Crystal Size Distribution
DT	Draft Tube
DTB	Draft Tube Baffle
FC	Forced Circulation
GRD	Growth Rate Dispersion
HEN	Heterogeneous primary nucleation
HON	Homogeneous primary nucleation
ITC	Interface Transfer Control

PBE Population Balance Equation
SDG Size Dependent Growth
VDC Volume Diffusion Control

REFERENCES

Barnea, E. and Mizrahi, J. (1973). A generalised approach to fluid dynamics of particulate systems. *Chemical Engineering Journal.*, 5, pp.171-189

Bermingham, S.K. (2003a). *A Design Procedure And Predictive Models For Solution Crystallization Processes- Development And Application*, Ph.D. Thesis, Delft University of Technology, the Netherlands, ISBN 90-407-2395-8

Bermingham, S.K., Verheijen, P.J.T. and Kramer, H.J.M. (2003b). Optimal design of solution crystallization processes with rigorous models, *Trans. IChemE*, 81, part A, pp.893-903

Bermingham, S.K., Kramer, H.J.M. and Rosmalen van, G.M. (1998). Towards on-scale crystallizer design using compartmental models, *Computers and Chemical Engineering*, 22, pp.S355-S362

Chianese A., Di Berardino, F. and Jones, A.G. (1993). Chemical Engineering Science, 48, pp.551-558

Chianese A., Sangl, R.G. and Mersmann, A.B. (1996). On the size distribution of fragments generated by crystal collisions, *Chem. Eng. Comm.*, 146, pp.1-12

Daudey, P.J. (1987). *Crystallization of ammonium sulphate.* PhD Thesis, Delft University of Technology, The Netherlands

Dirksen, J.A. and Ring, T.A. (1991). Fundamentals of Crystallization: Kinetic Effects on Particle Size Distributions and Morphology. *Chemical Engineering Science*, Vol. 46, No. 10, pp.2389-2427

Gahn, C. (1996). The effect of impact energy and the shape of crystals on their attrition rate, *Journal of Crystal Growth*, 166, pp.1058-1063

Gahn, C. and Mersmann, A. (1997). Theoretical prediction and experimental determination of attrition rates. *Trans IChemE.*, 75(A), pp.125-131

Gahn, C. (1997). *Die Festigkeit von Kristallen und ihr Einfluß auf die Kinetik in Suspensions-kristallisatoren*, PhD thesis, München University of Technology, Herbert Utz Verlag Wissenschaft, München, Germany

Gahn, C. & Mersmann, A. (1999a). Brittle fracture in crystallization processes Part A: Attrition and abrasion of brittle solids, *Chemical Engineering Science*, 54, pp.1273-1282

Gahn, C. & Mersmann, A. (1999b). Brittle fracture in crystallization processes Part B: Growth of fragments and scale-up of suspension crystallizers, *Chemical Engineering Science*, 54, pp.1283-1292

Heijden, A.E.D.M and van der Eerden, J.P. (1992). Growth rate dispersion: The role of lattice strain, *Journal of Crystal Growth* , 118, pp.14-26

Heijden, A.E.D.M. van der and van Rosmalen, G.M. (1993. Industrial Mass Crystallization, In: *Handbook of Crystal Growth*, Vol.2a, D.T.J.Hurle, editior, North-Holland, Amsterdam, The Netherlands

Jager, J. (1990). *Control of industrial crystallizers – the physical aspects*, PhD Thesis, Delft University of Technology, The Netherlands

Kashchiev, D. (2000). *Nucleation: Basic Theory with Applications,* Butterworth-Heinemann Ltd. Oxford, U.K.

Kashchiev, D. & van Rosmalen, G.M. (2003). Review: Nucleation in solutions revisited, *Cryst. Res. Technol.*, 38, No.7–8, pp.555–574

Kitamura, M. and Endo, H. (1991). Growth process of ammonium sulphate crystals produced by secondary nucleation in stirred-tank crystallizer, *Journal of Chemical Engineering of Japan*, 24, 5, pp.593-599

M.Kind and Mersmann, A. (1990). On Supersaturation during mass crystallization from solution, *Chem. Eng. Technol.,* 13, pp.50-62

Myerson, A.S. and Ginde, R.(1993). In: *Handbook of Industrial Crystallization*, Chapter 2, Edited by Myerson, A.S., Butterworth-Heinemann, Boston, USA

Mersmann, A. (1990).Calculation of interfacial tension, *Journal of Crystal Growth*,, 102, pp.841-847

Mersmann, A. (1996). Supersaturation and nucleation, *Trans. Inst. Chem. Eng. A.*, 74, pp.812-820

Mersmann, A. (1988). Design of crystallizers. *Chemical Engineering and Processing*, 23, pp.213-228

Mersmann, A., Sangl, R., Kind, M. and Pohlisch, J. (1988). Attrition and secondary nucleation in crystallizers. *Chem. Eng. Technol.*, 11, pp.80-88

Mersmann, A. (1995). Fundamentals of Crystallization. In A. Mersmann (Ed.), *Crystallization Technology Handbook*, Marcel Dekker, New York, USA. pp. 1-78

Mersmann, A. and Rennie, F.W. (1995). Design of Crystallizers and Crystallization Processes. In A. Mersmann (Ed.), *Crystallization Technology Handbook*, Marcel Dekker, New York, USA. pp. 215-326

Neumann, A.M.(2001).*Characterizing industrial crystallizers of different scale and type.* PhD Thesis, Delft University of Technology, Delft, the Netherlands, ISBN 90-6464-882-4

Ó Meadhra, R. (1995). *Modelling of the kinetics of suspension crystallizers – a new model for secondary nucleation.* PhD Thesis, Delft University of Technology, the Netherlands, ISBN 90-407-1190-9

Ostwald, W. (1897). Studien über die bildung und umwandlung fester körper, *Zeitschrift für Physilische Chemie*, 22, pp.289-330

Ploβ, R., Tengler, T. and Mersmann, A. (1989). A new model of the effect of stirring intensity on the rate of secondary nucleation. *Chem. Eng. Technol.*, 12, pp.137-146

Qian, R. and Botsaris, G., (1997). A new mechanism for nuclei formation in suspension crystallizers: the role of interparticle forces, Chemical Engineering Science, vol. 52, No. 20, pp.3429-3440

Randolph A.D. and Larson, M.A. (1962).Transient and steady-state size distributions in continuous mixed suspension crystallizers, *AIChE Journal*, 8, 5, pp.639-645

Randolph, A.D. and M.A. Larson (1988). *Theory of Particulate Processes*, *Second Edition*, Academic Press, San Diego, USA

Ristić,R.I., Sherwood, J.N., Shripathi, T. (1990). Strain variation in the growth sectors of potash alum single crystals and its relationship to growth rate dispersion, *Journal of Crystal Growth*, 102, pp.245-248

Sangl, R.G. (1991). *Mechanischer Abrieb von Kristallen als Beitrag zur sekundaeren Keimbildung,* PhD Thesis, TU München, Germany

Tavare, N.S. (1995). *Industrial Crystallization : Process Simulation Analysis and Design*, Plenum Press, New York, USA

Westhoff, G.M.(2002). *Design and analysis of suspension crystallizers: Aspects of crystallization kinetics and product quality*, PhD Thesis, Delft University of Technology, the Netherlands, ISBN 90-6464-138-2

Westphal, G.H. and Rosenberger,F. (1978). On diffusive-advective interfacial mass transfer, *Journal of Crystal Growth*,43, pp.687-693

Zacher, U. (1995). *Die Kristallwachstumsdispersion in einem kontinuierlichen Suspensions-kristallisator*, PhD thesis, München University of Technology, Germany

4

Experimental study of the effect of process actuators in fed-batch processes - analysis and model validation†

Fed-batch experiments were performed for the evaporative unseeded crystallization of ammonium sulphate from water in a 75L Draft Tube and 1100L Draft Tube Baffle crystallizer. The heat input, mixing conditions and fines removal rate were selected as the primary actuators for the process. During the experiments, the process actuators were kept at constant levels or were varied stepwise and their effect on the final product quality of the batch was studied. The study reveals a significant influence of the actuators on the initial start-up and dynamic behavior of the process, especially the effect of the propeller frequency and the fines removal rate. The heat input was found to be less critical in affecting the overall process dynamics in fed-batch processes. Dynamic parameter estimation studies showed that the kinetic parameters for surface integration rate constant (k_r) and the surface-related energy increase (Γ_s) are strongly correlated. The parameter sets obtained give a reasonable fit with experimental data when used to test the descriptive and predictive quality of the rigorous crystallizer models, for varying process conditions.

† Parts of this chapter have been submitted for publication in AIChE Journal (2006)

4.1 INTRODUCTION

In recent years, the importance of fine chemicals and specialty high-value-added materials have increased in the competitive chemical industry. Consequently, an increasing proportion of capital investment on research and development of such specialty products is being made at the expense of conventional large tonnage commodity products. Many specialty chemicals, such as pharmaceuticals, agrochemicals, pigments, dyestuffs, catalysts, zeolites, proteins and food products, involve crystallization or precipitation as a crucial part of their manufacture, and usually require batch or semi-batch processing because of their low tonnage capacity. High product purity and specific crystal size and habit may be desirable in many instances.
Batch crystallization from solution is a key process step in the production of pharmaceuticals, fine chemicals, biochemical, food additives, and bulk products. This is due on the one hand to its ability to achieve high product purity, and on the other hand to the fact that the qualities and size distribution of the crystals have a significant influence on the downstream processing and the commercial value of the product itself.
The crystallizer operation can be significantly affected with regards to the final product quality or changes in feed composition or even external process disturbances. To understand the effect of such circumstances on the plant operation and control, one needs sufficient knowledge on the underlying mechanisms influencing the process dynamics. An extensive overview on continuous experimental results is given by Neumann (Neumann, 2001), for the evaporative crystallization of ammonium sulphate from water, for a wide-range of operating conditions in crystallizers of different scale and type. Here, the thrust is on gaining more knowledge on the crystallization of ammonium sulphate from water in batch processes. Two semi-industrial scale crystallizers, viz. a 75L Draft Tube and 1100L Draft Tube Baffle crystallizer will be employed to perform unseeded crystallization experiments at varying process conditions and using different actuators. The gathered experimental data will be used as a basis to provide a quantitative and qualitative description of the process dynamics and the effects on the final product quality. Further, parameter estimation studies will be explored to test the applicability of the rigorous crystallization models for it's predictive and descriptive capabilities.

4.2 (SEMI-) INDUSTRIAL SCALE CRYSTALLIZERS

In the chemical industry, a wide variety of batch and continuous crystallizer configurations are in use. Within the last thirty years or so the technical means to measure nucleation in operating equipment have been developed that have given a new insight into the design of crystallization equipment, with the result that modern crystallization designs are far more flexible in terms of their ability to control crystal product size and size distribution than earlier equipment. Also, within the last few decades, electronic instruments have been developed that make possible the continuous on-line measurement of particle size distribution and other operating variables required for the operation and control of industrial crystallizers.
The crystallization equipment ranges from apparently simple designs like solar ponds (used to obtain sodium chloride from sea water), agitated vessels, or thermo-syphon crystallizers (in which mixing occurs through natural convection), to more complex designs. Despite this variety in available crystallizer configurations, the majority of them can be divided into three basic crystallizer types: Draft Tube (DT) agitated designs including the Draft Tube Baffle (DTB) agitated configuration, Forced Circulation (FC) and the Fluidized Bed (FB) units. The latter is also referred to as Oslo type crystallizer.
For the development of batch crystallization technology and the validation of the rigorous crystallization models, two different crystallizer configurations have been employed for research purpose, at the Laboratory for Process Equipment, Delft University of Technology:

- Draft Tube crystallizer with an operating volume of 75 litres
- Draft Tube Baffle crystallizer with an effective volume of 1100 litres

Both these units are operated in a fed-batch mode as evaporative-type crystallizers and the system studied is the crystallization of ammonium-sulphate from water. The 75L DT crystallizer was commissioned by Westhoff(2002) and this crystallizer was adapted for fed-batch experimental runs. So, also the 1100L DTB crystallizer, which was re-commissioned by Neumann(2001), was also adapted for fed-batch experimental runs. The core design and basic construction of these two crystallizers have remained the same since they were originally commissioned.
In the following sub-sections, a brief description is given for both these plants and also the associated measurement and control details.

4.2.1 75L Draft Tube crystallizer plant

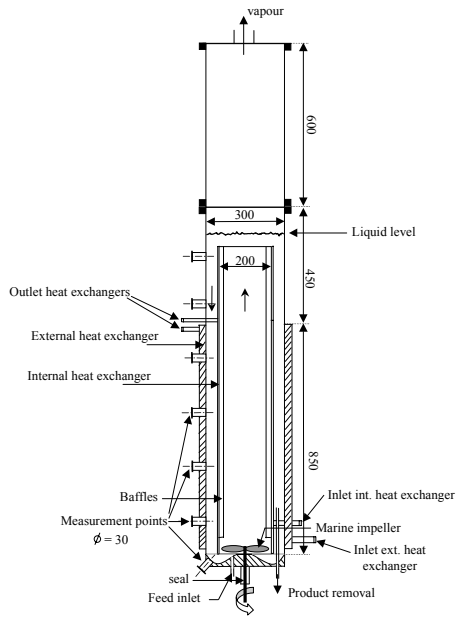

Figure 4.1 Schematic sketch of the 75-litre DT crystallizer at Delft University of Technology, after Westhoff(2002)

The 75L DT crystallizer is a simple agitated vessel with a draft-tube inside. The DT agitated units are the most widely used in the chemical industry for suspending solids in liquids. This is due to their simple nature, but moreover due to the fact that the mixing generated in such units provides an optimal combination of maximum particle suspension and minimal power input.
A schematic drawing of the 75-litre DT crystallizer is given in Figure 4.1. This crystallizer can be operated in a fed-batch or continuous mode. The crystallizer body is a cylindrical vessel having a height of 1.9m and an internal diameter of 0.3m with a flat head and a contoured base, which increases the suspension flow velocity when it passes the base of the vessel. This aids in reducing sedimentation at the bottom of the crystallizer. The nominal liquid volume in the crystallizer is 75 litres. The entire body is made up of stainless steel, SS304. The crystallizer is fitted with a draft-tube (height 1.15m and internal diameter 0.2m). The draft-tube not only enables better defined flow conditions within the crystallizer but, also acts as a heat-exchanger. The draft-tube acts as an internal heat-exchanger, while a jacket mounted around the crystallizer acts as the external heat-exchanger. The effective height of both heat exchangers is 0.85m. Hot water is used to provide the heat for evaporation of the solvent.
A marine-type propeller with a diameter of 0.19m (check exact specifications in Appendix A4.1) is used to pump the suspension through the draft-tube upwards to the boiling zone. The propeller frequency can be varied up to 775 rpm. The feed point of the crystallizer is located just under the marine impeller to enable a proper mixing of the inlet stream with the suspension in the crystallizer. Four baffles are mounted in the draft-tube (length = 1.013 m, diameter = 0.025 m) to reduce the rotational momentum produced by the propeller and to divert it to the axial direction. The centre of the product removal pipe is located in the down-coming zone, 0.20 m from the wall of the body of the crystallizer. The top part of the crystallizer body is connected to a condenser to remove the solvent that is evaporated. All parts of the crystallizer, piping and vessels are insulated to prevent encrustation due to the formation of cold spots that may serve as a growth surface for crystal material.

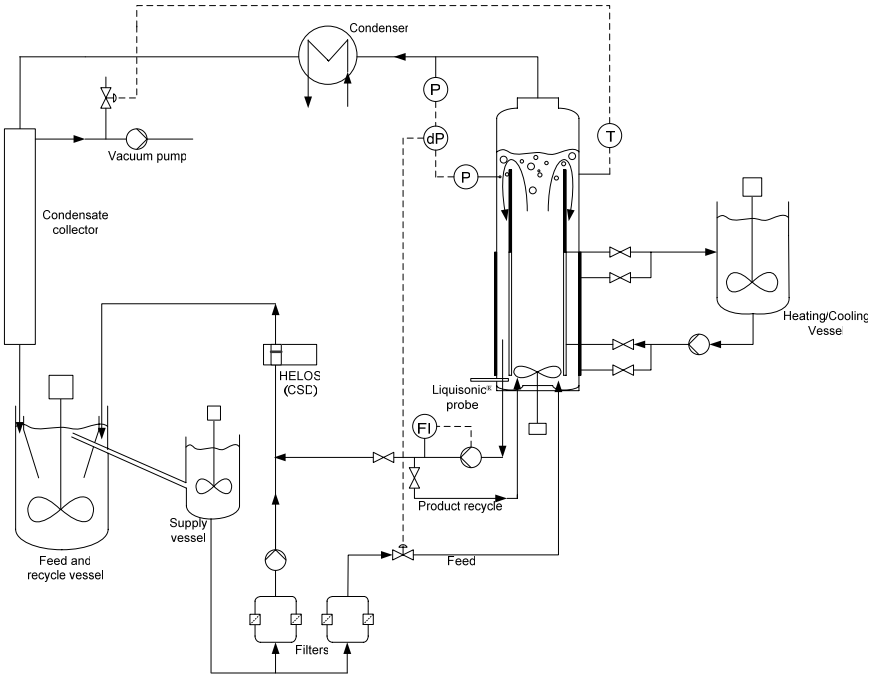

Figure 4.2 Simplified process scheme of the 75L DT crystallizer plant; solid lines represent process lines, dotted lines represent control loops

There are five measurement points located on the lower section of the crystallizer, where different kinds of measurement probes can be inserted, for eg. the LiquiSonic® 20 probe (SensoTech, Germany) was inserted at the lowest hole which is used to record the supersaturation at which primary nucleation is instantiated.

Process description

The process flowsheet for the 75L DT crystallizer plant is shown in Figure 4.2. Although the study is on batch crystallization, it is not possible to realize a true batch process as some amount of the product material is lost in sampling and measurement of the crystal size distribution. The removal of a small product flow needed for on-line sampling is compensated a supply of fresh saturated feed from the feed tank. Also, this serves in maintaining the volume and hence, the liquid level in the crystallizer constant, due to the loss of solvent via evaporation.

The plant is made up of two main parts, the first is the crystallizer reactor itself while the second is the area containing the ancillary equipment for feed preparation, solution storage and the hot water vessels. The crystallizer is integrated into this experimental set-up with pumps, recycle streams, buffer vessels, piping, instrumentation, measurement devices, etc. DSM technically pure ammonium sulphate using water as solvent, is used as the model material for the crystallization experiments.

Feed is supplied to the crystallizer from the feed preparation tank (Feed Vessel), by means of a membrane pump. This feed preparation tank is fed from an overflow line connected to the top section of a settler, which is located in the recycle vessel (Buffer vessel 1). This vessel which is maintained at 50^0C recycles product slurry, clear mother liquor used for CSD measurement and condensed water vapor. The temperature in the feed preparation tank is raised up a further 2^0C to ensure a crystal-free feed into the crystallizer. Possible dust and other impurities are removed by means of Millipore filters that are built in the feed line. The filter system is mounted double, so that during continuous operation the filters can be changed. Vacuum in the crystallizer is maintained at approximately 100-120 mbar.

Heat for crystallization is supplied via the internal heat exchanger (draft-tube) and the external heat-exchanger (crystallizer body). Heating is done using hot water with a temperature of approximately 80^0C. The evaporated solvent in the form of vapor at the top of the crystallizer, is removed as condensate in a condenser. An air-driven membrane pump is used to recycle this condensate back to the recycle vessel. This water recycle essentially closes the material balance of the overall system. A rinse water system using water as the medium at approximately 80^0C is present, with inputs at different locations in the process flowsheet. Rinse water is useful to remove scaling, which causes blockage of the tubes and also to clean the system after the experiments. A Watson-Marlow hose pump is used to remove the product for sampling purpose. It pumps a continuous product stream out of the crystallizer which is recycled back to the crystallizer. But, every two minutes, a product sample is sent to the HELOS CSD measurement device. The product removal and sampling system will be explained in a bit more detail in the ensuing sections. The Watson-Marlow pump is placed 3m below the liquid level of the crystallizer to obtain enough suction pressure. The dilution stream (saturated, crystal free) and the product stream are collected in a 200L buffer vessel.

4.2.2 1100L Draft Tube Baffle crystallizer plant

Figure 4.3 depicts a simplified flow sheet of the 1100L DTB crystallizer plant. The process description is exactly similar to the one presented for the 75L DT crystallizer. The new addition to this crystallizer is essentially the introduction of an external annular zone wherein the fine crystals can be selectively removed. This can be used as an effective actuator in controlling the process dynamics and the final product quality and CSD. For a more comprehensive description on this crystallizer, the reader is referred to Neumann (2001). For the sake of brevity, a brief description of the 1100L DTB crystallizer as given by Neumann (2001) is summarized here.

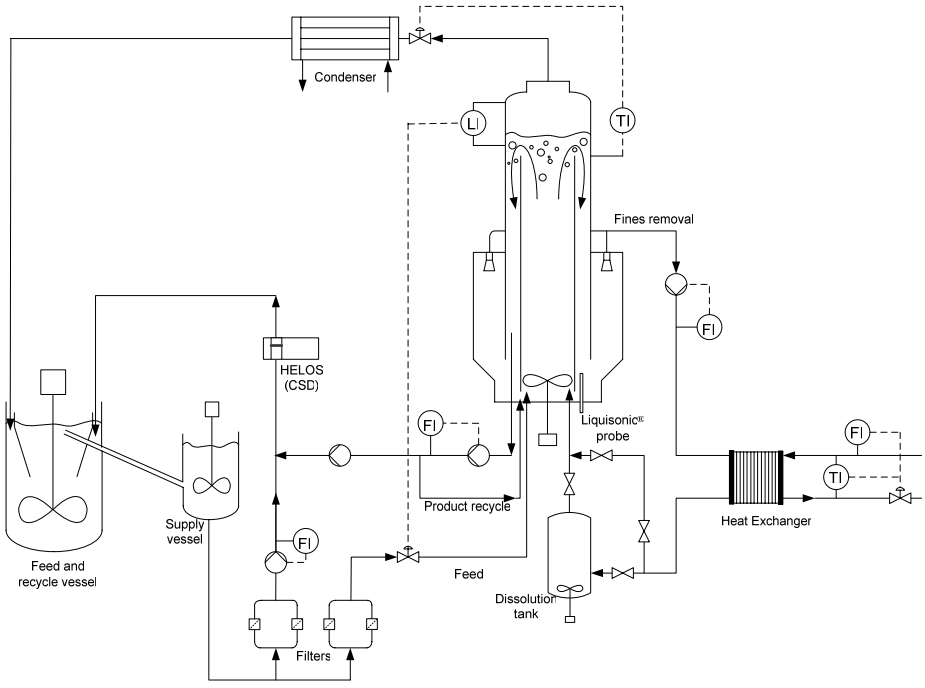

Figure 4.3 Simplified process scheme of the 1100L DTB crystallizer plant; solid lines represent process lines, dotted lines represent control loops

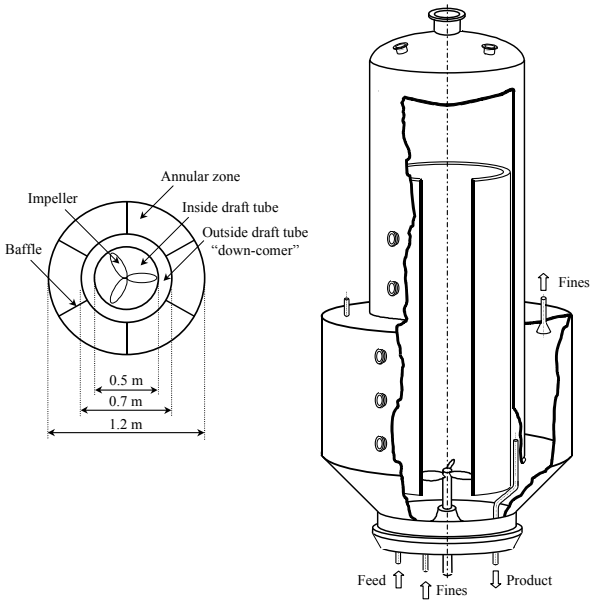

Figure 4.4 Top down, cross sectional view of the 1100-litre DTB crystallizer (left), schematic drawing of the same crystallizer (right), after Neumann(2001)

The crystallizer is a draft tube baffle evaporator-type crystallizer that can be operated either in a fed-batch or a continuous mode. A schematic view of the 1100L DTB crystallizer is depicted in Figure 4.4. The crystallizer body is a cylindrical vessel with a dished head and a contoured base. The body has a total height of 4 m and an outer diameter of 0.7 m; its effective volume is estimated to be 1100L. The lower part of the crystallizer body is surrounded by an annular zone with a height of 1.5 m, an outer diameter of 1.2 m and a total volume of approximately 775L. The hull that separates the annular zone from the crystallizer body is a so-called skirt baffle. The crystallizer body is equipped with a draft tube with a height of 2.3 m and a diameter of 0.5 m. A marine-type propeller with a diameter of 0.484 m (exact specifications are given in Appendix A4.1) is used to circulate the contents of the crystallizer through the draft tube upwards to the boiling zone. The maximum propeller frequency is 370 r.p.m. and the corresponding superficial fluid velocity was measured to be 1.1 m/s. All process streams enter the bottom section of the crystallizer in the vicinity of the propeller. The top part of the crystallizer body is connected via air driven valves to two condensers. All parts of the crystallizer, piping and vessels are constructed from stainless steal (SS316) and are insulated.

Annular Zone

The annular zone surrounding the crystallizer body has a cross-sectional area of 0.746 m^2. Large baffles divide this zone across the entire height into six equally spaced, independent compartments. From the top of each compartment, a so-called fines flow is removed via a withdrawal tube (see Figure 4.4). The bottom of each compartment has an open connection to the crystallizer body. The relatively large cross-sectional area in combination with a low fines removal rate (up to 3.5 l/s) leads to a low vertical upward velocity inside the compartments. Due to this low velocity, the annular zone will act as a settling zone in which small crystals are separated from larger crystals by gravitational forces. Larger crystals will subsequently return to the crystallizer body whereas small crystals are removed with the fines flow.

The partition of the annular zone in compartments is made to 1) prevent the generation of a swirl in the annular zone due to the rotation of the propeller and to 2) de-couple to a certain extent the fines removal rate and the vertical upward velocity in the compartments; thus increasing the flexibility of the system.

Sampling locations

In order to access the inside of the crystallizer from the outside for the purpose of local sampling or in-line measurements, flange connections are made in the crystallizer hull at five different height locations. Where necessary, corresponding holes are made in the skirt baffle and in the draft tube

respectively. To prevent shortcut streams through the holes when no local measurement or sampling is performed, sealing rods are implemented.

Fines Removal and Dissolving System

Due to the low upward superficial velocity in the annular zone, classification occurs as a result of gravitational forces/settling. As a result, the fine particles can be selectively removed from the main body, via six equally spaced withdrawal points located at the top of the annular zone of the crystallizer. The fines removal and dissolving system has a dual use:

- to remove and partially dissolve small crystals in order to decrease the overall crystal surface area.
- supply the required heat for evaporation of the solvent and

This decrease in surface area leads to higher growth rates and thus to an increased median crystal size L_{50}. As shown by Eek (1995) this system can be used as an effective actuator to control the dynamic start-up behavior of the CSD in the crystallizer. In the current configuration, the fines flow rate can be varied in the range of 1 to 3.5 l/s. The upper limit has to be maintained to avoid cavitation in the withdrawal tubes and the lower limit to avoid cavitation at the re-entry location. Next, the stream passes through a plate heat exchanger in which the necessary heat for the crystallization process is added to the system. The temperature increase of the fines flow is determined by the set heat duty and the fines flow rate. The resulting temperature increase of the fines flow leads to dissolution of crystals. The plate heat exchanger is fed with water of 90 °C from a hot water supply vessel. The degree of fines dissolution is not only determined by the level of undersaturation present after the heat exchanger, but also by the volume between the heat exchanger and the crystallizer inlet. The volume of this part of the fines loop is referred to as the fines dissolution loop volume. Together with the fines withdrawal rate, this volume determines the time available for dissolution. In this configuration, the fines dissolution loop volume can be varied between 0.020 and 0.240 m^3 with the use of a dissolution vessel. The fines flow is subsequently fed back to the crystallizer either directly or via this dissolving vessel.

Product Removal and Dilution System

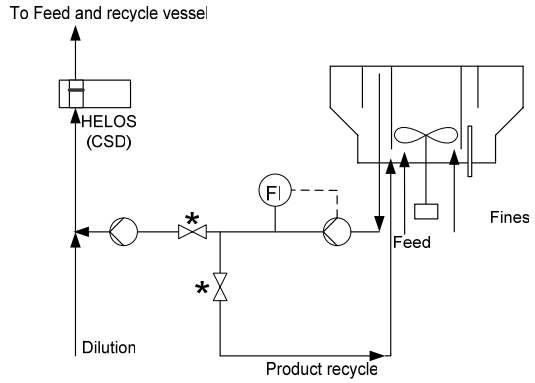

Figure 4.5 Product removal and dilution system of the 1100-litre DTB crystallizer

Product is continuously removed from the down-comer of the crystallizer, in the direction of the internal circulation flow, by means of a progressive cavity pump situated at the ground floor of the plant (see Figure 4.5).

After passing through the product removal pump, at regular time intervals, a part of this product stream is injected into a dilution stream of saturated crystal-free mother liquor. The resulting diluted product sample is transported through an on-line laser diffraction measurement system, HELOS, to measure the CSD. By using this dilution technique the original product solid concentration of approximately 11 vol.% can be lowered to a solid concentration of approximately 1.5 vol.%; the maximum solid concentration which avoids multiple scattering and thus enables an accurate measurement using the laser diffraction measurement systems.

4.3 MONITORING AND CONTROL SYSTEM

This section briefly describes the control system used for the plant operation of the 75L and 1100L DTB crystallizers. A Honeywell Scan9000 DCS system using a SCAN3000 PC-based visualization tool is used to monitor and control the following process variables (Neumann, 2001):

Liquid level
The liquid level in the crystallizer is maintained at the set point by manipulating the feed flow into the crystallizer. The level is determined from the measured pressure difference between the upper part and top of the crystallizer (DTB) and the top part and half-way of the crystallizer (DT).

Temperature
- The temperature in the crystallizer is controlled by a master-slave-loop from the measured pressure in the top part of the crystallizer and solution/suspension temperature in the system controlling the valve near the vacuum pump.

Heat input
The heat input supplied to the crystallizer is controlled:
- By manipulating the valve of the hot water flow towards the internal and external heat exchanger (DT).
- By manipulating a valve in the hot water feed of the heat exchanger. By measuring the flow rate of the fines flow and the temperature increase across the external plate heat exchanger, the current heat input is calculated (DTB).

Fines flow (DTB)
The control loops maintain a constant fines flow rate by manipulating the speed of the fines pump.

4.4 MEASUREMENT SYSTEMS

4.4.1 CSD measurement device – HELOS Vario

When dealing with particle size and size distribution measurement systems, one has to realize that the size of a particle is strongly related to its shape. The particle size to be determined is always based on the definition of a size parameter with specific dependencies on particle shape. For instance, if the particle under consideration is spherical then the diameter or radius is an accurate single number index of size. For irregularly shaped particles such as crystals, however, it is not possible to describe unambiguously its size using a single number. The size for a non-spherical particle is therefore usually presented as an equivalent sphere diameter, which is assigned on the basis of length, surface area, volume or some other property (e.g. sedimentation velocity).

Laser Diffraction Spectroscopy
Laser diffraction spectroscopy is an ensemble scanning method, which implies that the size distribution is deduced from the interaction between an assembly of particles and the incident laser radiation. At present, the technique is probably the most widely used technique for sizing particles (Brown & Weatherby(1987), Ulrich & Lühman(1992)). The main reason for this is that it can be applied to various kinds of particulate systems, it is fast, offering a wide measuring range, relatively accurate and that it can be operated without calibration.
The forward laser light scattering measurement system is given schematically in Figure 4.6. The He-Ne laser light beam is directed onto the flow cell with the crystal slurry and diffracted. A Fourier transform lens focuses the scattered light onto a detector. An integrated intensity pattern is obtained from the detector. The obscuration signal is measured with a separate detector and forms a measure of the particle concentration in the measured volume. To deduce the size distribution from the measured

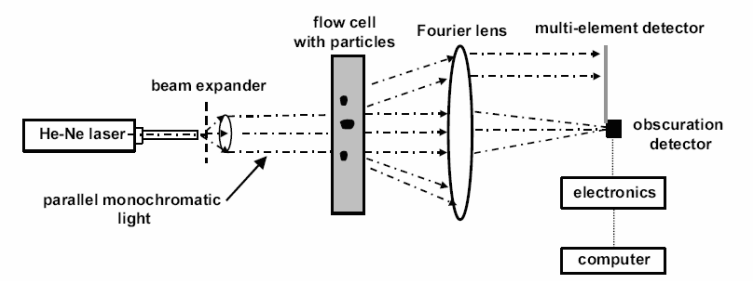

Figure 4.6 Principle of forward laser light scattering measurement system

intensity pattern, a scatter model is required which describes the diffraction of the light by the particles, and a deconvolution procedure.

The HELOS Vario laser diffraction measurement device is an on-line measurement instrument manufactured by Sympatec, Germany. The diffraction device can be equipped with a number of lenses (focal distances of 500, 1000 and 2000 mm). To discretize the size domain, 31 size classes are used. To reconstruct the crystal size distribution, the HELOS software makes use of the Fraunhofer theory and the Phillips-Twomey inversion method. An optical flow cell has a window diameter of 42 mm and a path length of 3.5 mm. The flow cell was placed between the receiver and transmitting unit. Each measurement takes about 10 seconds with a background measurement performed prior to each measurement.

For discussion of the experimental results and also for parameter estimation studies and model validation, the evolution of the CSD is captured in the form of 10, 25, 50, 75 and 90% quantiles. These measures, symbolically denoted as L_{10}, L_{25}, L_{50}, L_{75} and L_{90}, are defined as the crystal size for which respectively 10, 25, 50, 75 and 90% of the observed volume density distribution has a size smaller than or equal to this value.

4.4.2 Supersaturation measurement device - LIQUISONIC®

In general, the techniques for supersaturation measurement are based on either direct analysis, eg. evaporation to dryness or indirect determination of some property of the system that is related to the solute concentration. Properties frequently chosen for indirect measurement are electrical conductivity, refractive index, density or the speed of sound in the solution and the viscosity of the solution. Omar and Ulrich(1997, 1999) proposed a technique which makes use of the fact that the speed of ultrasonic waves propagating through a fluid depends on the elastic (adiabatic compressibility) and the inertial(density) properties of the fluid.

$$V = \frac{1}{\sqrt{B_{ad} \cdot \varrho}} \tag{4.1}$$

Assuming constant pressure, both properties are a function of temperature and concentration. Measuring concentration with the help of the velocity of sound is based on a very simple principle - the time it takes an ultrasonic signal to travel the distance between a transmitter and a receiver in a liquid is measured. Since this distance is constant, the velocity of sound propagation can be determined by measuring the time the signal needs for covering this distance. Together with the temperature, the time makes it possible to calculate the concentration.

The LIQUISONIC® probe manufactured by Sensotech, Germany is one such ultrasonic probe that can be used to measure the supersaturation inline. The tip of this probe (sensor) looks like a tuning fork and comprises the measurement volume between the two branches. Low frequency longitudinal ultrasonic waves (2 MHz) are used, thus avoiding ultrasonic induced nucleation due to the formation

and collapse of cavities. This probe can measure the speed of sound propagating through the liquid media with a precision of ± 0.2 m/s while the temperature is measured with a precision of ± 0.1 ^{0}C.

4.5 PRODUCT QUALITY CHARACTERIZATION FOR UN-SEEDED FED-BATCH RUNS - 75L DT CRYSTALLIZER

The 75L DT crystallizer was operated in the fed-batch evaporative mode. The process temperature was controlled at 50^{0}C by the pressure (~100 mbar). Initially, the crystallizer is filled with a crystal-free, saturated solution of $(NH_4)_2SO_4$ solution at 50^{0}C. The loss of solvent by evaporation is compensated by a continuous feed supply to the crystallizer. The vapor from the top is sent to a condenser. The CSD was monitored online using the HELOS(Sympatec, Germany) laser scattering device. To facilitate this online measurement, very small amounts of product sample were sent to the CSD measuring device at periodic intervals. The supersaturation at which primary nucleation is instantiated was recorded by means of the ultrasonic device – LiquiSonic® 20 (SensoTech, Germany). Table 4.1 lists the standard process conditions for the experimental runs.

Table 4.1 Process conditions for the 75L DT crystallizer

Standard operating conditions	Value	Unit
Crystallizer volume (V)	75	[litre]
Temperature (T)	50	[^{0}C]
Specific heat input (Q)	120	[kW/m^3]
Propeller frequency	450	[rpm]
Feed density (ρ_s)	1248	[kg/m^3]
Seeding policy	Unseeded	-
Product removal rate	0.042	[l/min]

The propeller frequency and heat input were used as actuators to study the effect on the dynamic CSD. These experimental runs will be used to study not only the effect on product quality in the same crystallizer, but will be used for comparison (of scale and type effects) with experiments done in the 1100L DTB crystallizer, under similar process conditions. An overview of the tested process conditions and results are listed in Table 4.2.

Table 4.2 Process operating parameters for the 75L DT crystallizer

Experiment	Heat input (kW/m^3)	Propeller frequency (rpm)	L50 (μm) at batch-time ~8000 sec
DT_c2	120	450	550
DT_c3	120	**577**	442
DT_c4	120	**657**	414
DT_c5	**100**	450	495
DT_c6	**75**	450	503
DT_c7	120	**309**	550
DT_c9	**130**	450	498

***Values in bold are the actuators used for that particular experiment**

It must be mentioned that the supersaturation values for these experiments could not be measured accurately by the LIQUISONIC® probe. This was primarily due to the presence of air bubbles which distorted the exact measurement of the supersaturation at the primary nucleation point.

4.5.1 Impeller frequency as actuator

Mixing is an important factor affecting batch crystallization. On one hand, sufficient mixing is required to maintain crystals in suspension, to assure an adequate rate of energy transfer and to achieve

uniformity of suspension properties throughout the crystallizer. On the other hand, the effect of mixing on batch crystallization is largely system-dependent.

Table 4.3 Process operating parameters for impeller frequency as actuator

Experiment	DT_c2	DT_c3	DT_c4	DT_c7
Heat input (kW/m^3)	120	120	120	120
Propeller frequency (rpm)	450	577	657	309
Specific power input (W/kg)	0.5	1.06	1.56	0.16
Mean velocity in draft tube (m/s)	0.54	0.69	0.78	0.37
Tip speed (m/s)	4.4	5.6	6.4	3.0
Internal volumetric flow rate (m^3/s)	0.017	0.022	0.025	0.012
Turnover time (sec)	4.4	3.5	3.1	6.5
L50 (μm) at batch-time ~8000 sec	550	442	414	550

As seen from Figure 4.8, an increasing specific power input contributes to a reduction in the median crystal size, albeit the trend for DT_c7 and DT_c2 cannot be discriminated very well.

Figure 4.7 shows the effect of the impeller frequency on the median crystal size (L_{50}), on a given crystallizer when all other operating conditions are maintained at their default values (see Table 4.1). Please note that it is a limitation with the current laser-diffraction CSD measurement device (HELOS-Vario, Sympatec) to detect the newly born fresh crop of primary nuclei. In addition, the CSD measurements require low solids concentration in order to ensure a reliable measurement. For this purpose, the dilution ratio is varied appropriately but this ratio should not be too low also, as this would inevitably lead to plugging problems.

Based on the experience with continuous crystallization processes in DTB crystallizers (Neumann, 2001), it was expected that the median size would decrease with increase in the propeller frequency. For a given crystallizer, the time between two successive crystal-impeller collisions (for a particular crystal) and the corresponding collision energy will change as a function of the propeller speed. The time between two successive collisions is related to the turnover time and the chance of a collision per propeller pass. The collision energy will increase with increasing propeller speed whereas the time between two successive collisions will decrease. The overall attrition rate is thus, expected to increase. Under constant operating conditions, the median crystal size should thus, decrease.

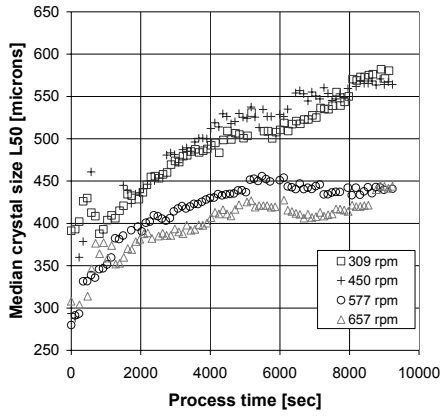

Figure 4.7 Dynamic start-up behavior of the median crystal size (L_{50}) using propeller frequency as actuator

NOTE: The CSD data has been synchronized w.r.t. the point at which primary nucleation is instantiated.

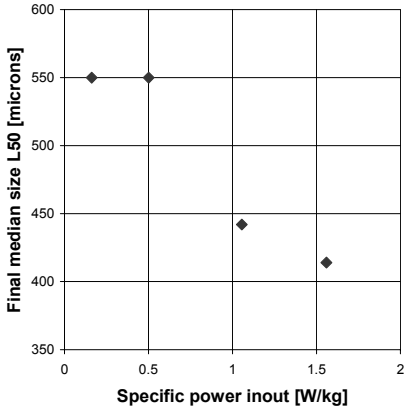

Figure 4.8 Effect of the specific power input on the median crystal size at end of batch

This generally expected trend is observed in Figure 4.7 and Figure 4.8, can be attributed to the increased attrition rates with increasing impeller frequency. This is mainly due to the reduction in the turnover times with increasing impeller frequencies, as shown in Table 4.3: 309 rpm (6.5 sec), 450 rpm (4.4 sec), 577 rpm (3.5 sec), 657 rpm (3.1 sec).

4.5.2 Heat input as actuator

The effect of varying heat inputs (production rates) on the product quality was studied, especially to check it's influence on the start-up dynamics. Under identical operating conditions as listed in Table 4.2, varying the heat input essentially varies the production rate. The heat for crystallization is provided by means of the draft-tube which acts as an internal heat-exchanger and a jacketed external heat-exchanger on the main body of the 75L crystallizer. This ensures that there is a uniform distribution of the heat throughout the crystallizer, thus avoiding any possible hot-spots.
From Figure 4.9, it can be deciphered that the magma density increases with an increasing heat input into the system, but apparently the heat input doesn't seem to have any influence on the CSD. For all the three heat inputs studied (75 kW/m^3, 100 kW/m^3 and 130 kW/m^3), the dynamics of the process is hardly any different.

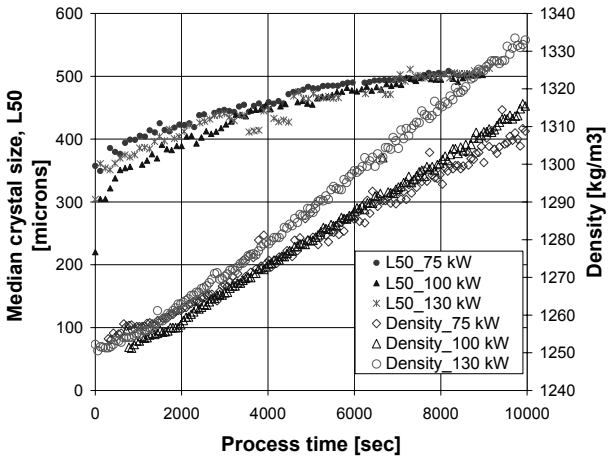

Figure 4.9 Dynamic start-up behavior of median crystal size (L_{50}) and the slurry density using heat input as actuator

NOTE: The CSD data has been synchronized w.r.t. the point at which primary nucleation is instantiated.

These results can be explained as a consequence of the combined effect of two counteracting mechanisms that essentially render the heat input as an ineffective actuator. The resulting increase in the magma density due to increasing heat input contributes to:

- increased growth rates (G) which result in an increase in the median crystal size.
- increased secondary nucleation rates, resulting in an increase in the crystal surface area available for growth which would in turn deplete the supersaturation thus, contributing to a lower median size.

These are two opposing mechanisms which cancel out the effect on the evolution of the median crystal size, as depicted in Figure 4.9. This result is not in line with those observed for continuous experiments by Neumann (2001) for a 22L DT crystallizer, but very much in line with the conclusions of Mullin (1993) and Eek (1995). Neumann (2001) reports a decrease in the median crystal size with an increase in the production rate, which suggests that secondary nucleation via attrition is the dominant mechanism. But, for a fed-batch process, this is probably not as dominant, as is the case here.

Thus, it can be concluded that the heat input doesn't play a significant role in the dynamics of the process and the product quality remains virtually unaffected.

4.6 PRODUCT QUALITY CHARACTERIZATION FOR UN-SEEDED FED-BATCH RUNS - 1100L DTB CRYSTALLIZER

The 1100L DTB crystallizer was also operated in the fed-batch evaporative mode, under similar process conditions, as described for the 75L DT crystallizer. In addition, segregation between coarse and fine particles is realized in the annular zone, from where the fine particles are selectively removed and sent to a heat-exchanger for fines destruction. This fines flow is then, returned back to the crystallizer after passing through a 240L fines dissolution vessel. The CSD was monitored online using the HELOS(Sympatec, Germany) laser scattering device and the supersaturation was recorded by means of the LiquiSonic® 20 (SensoTech, Germany) probe. All experiments were started from the same initial conditions as regards temperature, solute concentration: 50°C, an ammonium sulphate/water solution saturated at that temperature and no solids. The standard operating conditions for the experimental runs are listed in Table 4.4.

Table 4.4 Process conditions for the 1100L DTB crystallizer

Standard operating conditions	Value	Unit
Crystallizer volume (V)	1100	[litre]
Temperature (T)	50	[^{0}C]
Specific heat input (Q)	100	[kW/m^3]
Propeller frequency	320	[rpm]
Fines removal rate	2	[l/s]
Feed density (ϱ_s)	1248	[kg/m^3]
Seeding policy	Unseeded	-
Product removal rate	0.042	[l/min]

The propeller frequency, heat input and fines removal rate were used as actuators to study their effect on the dynamic CSD. Excitation runs were also performed to determine optimal process trajectories to arrive at a pre-determined final crystal size. An overview of the process conditions and results are listed in Table 4.5.

Table 4.5 Process operating parameters

Experiment	Heat input (kW/m^3)	Propeller frequency (rpm)	Fines flow rate (l/s)	Supersaturation at primary nucleation point [-]	L50 (µm) at end of batch-time / step input
DTB_c19	100	320	**3**	1.0118	540
DTB_c20	100	320	**2.5**	1.0124	647
DTB_c24	100	**270**	2	1.0143	743
DTB_c25	100	**370→270**	2	1.0124	400→624
DTB_c27	100	**370→320→270**	2	1.0135	438→485→628
DTB_c29	100	**320**	2	1.0139	510
DTB_c31	**75**	320	2	1.0118	525
DTB_c32	**125**	320	2	1.0133	547

***Values in bold are the actuators used for that particular experiment**

Data obtained from the LIQUISONIC® probe for experiment DTB_c20 is depicted in Figures 4.10 and 4.11. Figure 4.10 shows the dynamic sonic velocity data along with the standard deviation. It is seen that around t=1000 s, there is a steep change in the slope of the sonic velocity and the same is observed for the standard deviation as well. This measurement in the standard deviation plot is taken as the point where the primary nucleation event is instantiated. This is also confirmed by visual observation in the crystallizer during the experimental run. The sonic velocity reading at this point is approximately 1962 m/s and when it is converted to supersaturation (see Figure 4.11), the value is at which the primary nucleation event occurs is around 1.0124.

Omar and Ulrich(1999) have shown the successful application of the ultrasonic probe for concentration measurement even in the presence of crystals. In order to do this, the crystals were filtered from the probe using a mesh, to avoid causing interference in the concentration measurement.

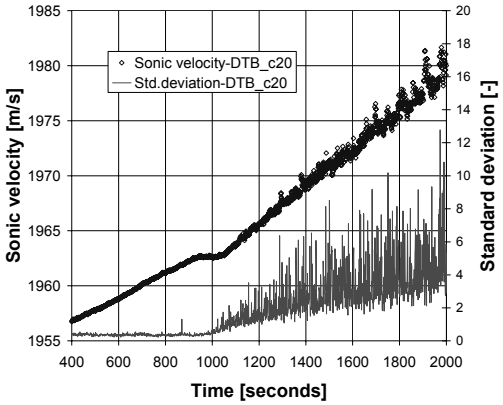

Figure 4.10 Sonic velocity and standard deviation

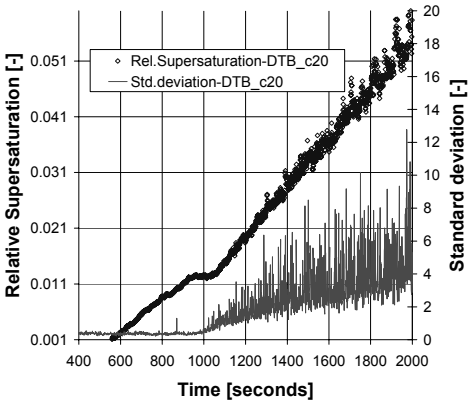

Figure 4.11 Supersaturation and standard deviation

Measurements using the Liquisonic® probe, indication the primary nucleation event

Unfortunately, such an arrangement was not done for the experimental runs conducted here, due to which the evolution of the true supersaturation profile cannot be gathered from this data. However, this data is still very useful in getting an idea about the influence the initial conditions can have on the evolution of the dynamic CSD, as will be discussed in the ensuing sections.

4.6.1 Impeller frequency as actuator

Unlike the results obtained for the 75L DT crystallizer using propeller frequency as actuator, the 1100L DTB fed-batch experiments (Figure 4.12) do not present a very clear trend for the effect of different impeller frequencies on the dynamics of the process.
Figure 4.12 shows the effect of the impeller frequency on the median crystal size (L_{50}), on a given crystallizer when all other operating conditions are maintained at their default values (see Table 4.4). It's clearly perceptible that an increase in the specific power input need not necessarily decrease the median crystal size. As seen from Figure 4.12, the turnover time (attrition rate) is not the sole criterion that decides the growth behavior of the crystals.

Besides the effect on the attrition rates, the impeller frequency will also influence the mass transfer coefficient (Equation 4.2) and the supersaturation distribution within the bulk volume as it affects the mixing of the superheated fines stream coming from the heat-exchanger.
The mass transfer coefficient (k_d) is given by (Herndl, 1982):

$$\frac{k_d L}{D_{AB}} = 2 + 0.8\left[\frac{\bar{\varepsilon}.L^4}{\nu_l^3}\right]^{1/5}\left[\frac{\nu_l}{D_{AB}}\right]^{1/3} \tag{4.2}$$

where;

$$\bar{\varepsilon} = \frac{Ne.s_{imp}^3.d_{imp}^5}{V} \tag{4.3}$$

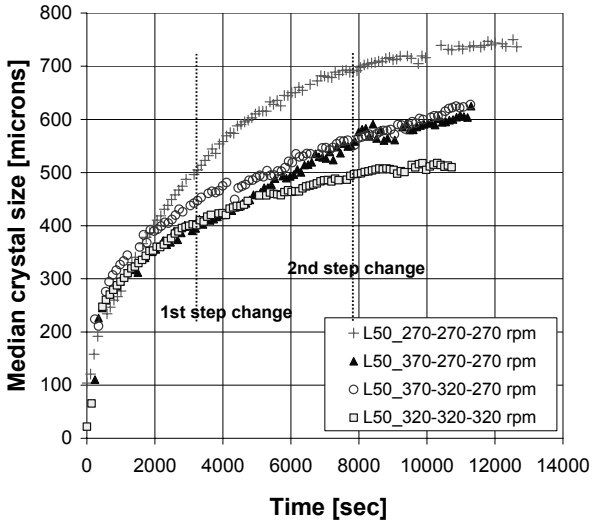

Figure 4.12 Dynamic start-up behavior of median crystal size (L_{50}) using impeller frequency as actuator

NOTE : The first step change was made 45 min (2700 sec) after the first nuclei were detected. The second step change was done 1 hour after the first one (6300 sec). The CSD data has been synchronized w.r.t. the point at which primary nucleation is instantiated.

Mersmann (1992) give an expression for the growth rate $G = G(\Delta c, L)$ for surface integrated (integration rate constant k_r) and diffusion limited (mass transfer coefficient $k_d(L)$) crystal growth, where $G(k_d, k_r)$. The influence of higher specific power inputs ($\bar{\varepsilon}$) on the mass transfer coefficients is negligible ($k_d \propto \bar{\varepsilon}^{1/5}$), as seen from the values in Table 4.6. But, the growth rate is not only diffusion-controlled (k_d) but also integration-controlled (k_r). Hence, the effect of a change in the mean specific power input on the crystal growth rate should be very limited.

But, as seen from Figure 4.12, clearly the initial start-up behavior (initial CSD) is significantly influenced by the specific power input ($\bar{\varepsilon}$) where, the crystal growth rates are lower at higher frequencies. A point that deserves attention here is the mode of heat input into the crystallizer. For the 75L DT crystallizer, the heat for crystallization is provided by the draft-tube which acts as an internal heat exchanger and an external heat exchanger that acts as a jacket around the main crystallizer body. But, in the 1100L DTB crystallizer, the heat for crystallization is provided by the returning stream from the fines dissolution tank, back into the main crystallizer body.

Table 4.6 Effect of specific power input on the hydrodynamics within the crystallizer

Propeller frequency (rpm)	Tip speed (m/s)	Internal circulation velocity (m/s)	Turnover time (s)	Mean specific power input, $\bar{\varepsilon}$ [W/kg]	$\bar{\varepsilon}^{1/5}$
270	6.9	0.84	6.7	0.9	0.98
320	8.1	1.00	5.5	1.5	1.08
370	9.4	1.15	5	2.3	1.18

NOTE: The mean specific power input, $\bar{\varepsilon}$, was calculated using a power number of 0.4

Higher impeller speeds contribute to better mixing of this returning fines stream with the bulk volume. This eliminates possible hot-spots of very high supersaturation and distributes it more uniformly. On the other hand, lower specific power inputs can result in very high nucleation rates (primary nuclei) due to localized high supersaturation levels. In a batch process, all the crystals produced remain in the crystallizer. Hence, the number of nuclei formed in the initial phase can prove decisive for the development of the CSD. A lower number density (low primary nucleation rates) at start-up will contribute to a very sharp rise in the L_{50} in the beginning, resulting in high secondary nucleation rates and vice-versa. This reasoning could also explain the difference in start-up behavior for DTB_c25 and DTB_c27.

Further, excitation (disturbance) experiments were performed to check the effect of changing impeller frequency on the process dynamics and the final product quality. A decrease in the impeller frequency after a certain batch-time was expected to increase the final median size. This was indeed the case for

both the step-inputs done. But, if a comparison is made between the experiment performed at 270 rpm and the step-inputs, it is clearly seen that the effect of step-input is limited. Apparently, the frequency at the initial phase has a much stronger impact than changes in the impeller speed later in the batch. To further analyze the effect of excitation signals on product quality, step-inputs wherein the frequency is increased after a certain batch-time are needed.
Concluding, it can be said that the initial distribution for the crystal population that results from the primary nucleation event has a very strong influence on the development of the CSD during the latter part of the batch process. Hence, excitation signals done after this primary population starts growing, will produce limited effect on the final CSD. But, this again needs to be confirmed by experiments by increasing the specific power input after the first crop of primary nuclei is born.

4.6.2 Fines removal as actuator

In the operation of industrial crystallizers, one would usually want to avoid the fines (i.e. small crystals) since they cause difficulties in downstream processing equipment (eg., filtration) and affect both product quality and process economics. Excessive fines may also require a relatively long batch run time to achieve the desired final size of the product crystals.
The fines removal system includes a fines classifier and a fines dissolver. Fines classification can be achieved in the annular zone of the DTB crystallizer, based on differences in settling velocities of the crystals. The production yield can be maximized by selectively removing a large number of fines with a low total crystal mass from the annular zone of the crystallizer. This is measured in terms of the classification function and the cut-size, L_{cut}. The cut-size (L_{cut}) is defined as the particle size for which the probability that a particle does not survive the fines trap is 50%.
The overall fines removal efficiency (performance) as discussed by (Neumann, 2001) depends on the following factors:

- the design specifications of the annular zone (eg. height, surface)
- the operating conditions (fines removal rate)
- the efficiency of the subsequent fines destruction stage (temperature increase, residence time, etc.)

The cut-sizes have been determined experimentally by Neumann(2001) wherein the experimental and calculated cut-sizes and classification functions were in reasonable agreement. With regards to the efficiency of the fines destruction, Neumann(2001) has reported that for a fines loop residence time of more than 100 seconds, all fine crystals removed from the annular zone are subsequently destroyed. But, this is not necessarily the case for all defined operating conditions with regards to the fines removal rate.
The experimental settings and selected characteristic quantities are listed in Table 4.7. All other operating conditions were kept at their default value as listed in Table 4.4.

Table 4.7 Experimental characteristics for fines removal as actuator

Experiment	Fines removal flow rate (l/s)	Fines residence time in main body (s)	Cut size of fines classification (μm)	Fines dissolution loop volume (l)	Fines residence time in dissolution loop (s)
DTB_c29	2	550	80	240	120
DTB_c20	2.5	440	90	240	96
DTB_c19	3	367	100	240	80

The influence of the fines removal rate on the evolution of the CSD is depicted in Figure 4.13, which shows that it can be a very effective and significant actuator. The fines flow rate was varied between 2 l/s and 3 l/s. Any operation above 3 l/s was found to give operational problems related to the plugging of process lines, which therefore limited the fines removal rate to the upper limit of 3 l/s.

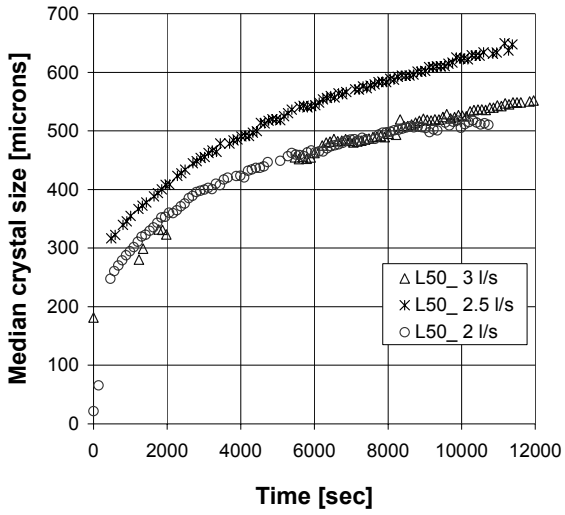

Figure 4.13 Dynamic start-up behavior of median crystal size (L_{50}) using fines removal as actuator without bypassing the fines dissolution tank

NOTE: The CSD data has been synchronized w.r.t. the point at which primary nucleation is instantiated.

A fines removal system essentially ensures the removal and destruction of fine crystals. This results in a decrease in the specific crystal surface area for supersaturation depletion, which implies that the median size will obviously increase as the fines removal rate is increased. This is indeed the case when the fines flow is increased from 2 l/s to 2.5 l/s as seen from Figure 4.13. But, when the fines removal rate is increased further (3 l/s), it is seen that the L_{50} actually drops vis-à-vis the L_{50} for 2.5 l/s. This observation is for the latter development of the CSD, whereas the difference in the initial start-up behavior is attributed to the stochastic nature of the primary nucleation event. This is a very complex phenomenon that is observed here and is very difficult to pinpoint what could be exactly the cause for this strange behavior.

One possibility as discussed by Bermingham (2003) (for a continuous crystallization process), could be due to two opposing effects. An increase in the fines removal rate:

- increases the number of fines removed per unit of time (which increases the L_{50}) ,
- simultaneously contributes to a reduced temperature increase of the fines flow in the dissolution loop (which decreases the driving force for dissolution)

As the fines flow rate is increased from 2 l/s to 2.5 l/s, the first effect is clearly observed, leading to an increase in the median size. But, on further increasing the fines flow rate to 3 l/s, the second effect comes into play and is more dominant, which results in a decrease in the median crystal size. These counter-acting mechanisms seem to be the only likely hypothesis that support the experimentally observed behavior.

Concluding, these results present evidence that selective fines destruction can be a viable technology for batch-operated crystallizers that could allow significant manipulation of the CSD.

4.6.3 Heat input as actuator

Figure 4.14 shows the influence of the heat input on the median crystal size. The trend observed here for the heat input as an actuator is exactly in lines with the discussion for the 75L DT crystallizer. The heat input doesn't play a significant role in the dynamics of the process and the product quality remains virtually unaffected. Apart from the discussion as was done for the 75L DT crystallizer, the difference here is the mode of heat input into the crystallizer. Here, the returning fines stream provides the heat for crystallization but at the same time can greatly affect the driving force for dissolution.

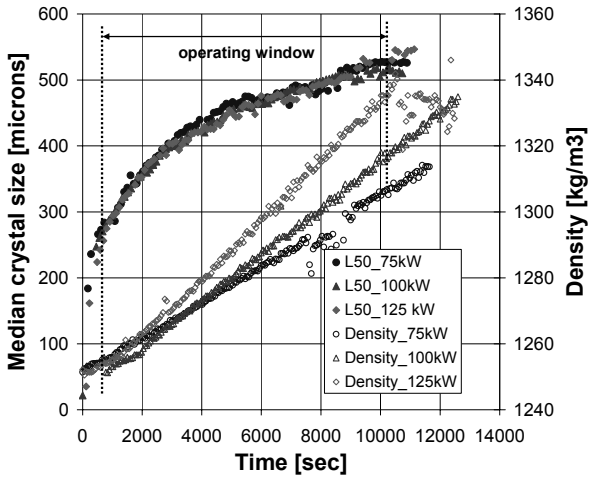

Figure 4.14 Dynamic start-up behavior of median crystal size (L_{50}) using heat input as actuator

NOTE: The CSD data has been synchronized w.r.t. the point at which primary nucleation is instantiated.

An increase in the heat flux across the fines dissolution loop would subsequently increase the temperature difference across the fines removal system, which in the studied cases are : 18^0C(125 kW/m^3), 15^0C (100 kW/m^3) and 12^0C (75 kW/m^3). This would result in more dissolution of the fines with a higher temperature difference across the fines removal system. To understand the effect of this temperature difference, CSD measurements of the fines stream re-entering into the crystallizer are needed, which was not possible due to the unavailability of a dedicated CSD measurement device on this fines return line.

4.7 SCALE-UP AND CRYSTALLIZER TYPE EFFECTS: 75L DT VS 1100L DTB

In order to test the scale-up effects and also the effect of different crystallizer types on the dynamic behavior of the CSD and the final product quality, fed-batch experiments were performed on the 75L DT and 1100L DTB crystallizers, under standard operating conditions as listed in Table 4.8. The criterion for scale-up was based on similar specific power inputs and similar propeller tip speeds, which are generally accepted as a good measure of scale-up. Several criteria can be chosen with respect to the impeller speed, viz. a constant impeller tip speed, a constant power input or an impeller speed which enables a well-mixed suspension criterion.

The experiments chosen for the study are DT_c3 and DT_c4 for the 75L DT crystallizer and DTB_c24 and DTB_c32 for the 1100L DTB crystallizer. The following comparisons were made to test the scale-up and type effects:

1. Similar specific power input (W/kg)
   - DT_c3 vs DTB_c24
   - DT_c4 vs DTB_c32
2. Similar propeller tip speed (m/s)
   - DT_c4 vs DTB_c24

It can be argued for the case of DT_c3 vs DTB_c24 that the operating conditions are not exactly the same, viz. the heat input into the crystallizer is 120 kW/m^3 for the 75L DT experiment, while it is 100 kW/m^3 for the 1100L DTB experiment. But, as it has been understood from the earlier sections, the heat input doesn't seem to have any influence on the process dynamics. Hence, these comparisons can be safely made. The process operating conditions and certain experimental characteristics are listed in Table 4.8.

Table 4.8 Process operating parameters for analysis of scale-up and type effects

Characteristics	DT_c3	DT_c4	DTB_c24	DTB_c32
Crystallizer type	Draft-tube	Draft-tube	Draft-tube baffle	Draft-tube baffle
Crystallizer volume [l]	75	75	1100	1100
Fines flow [l/s]	-	-	2	2
Heat input [kW/m^3]	120	120	100	125
Propeller frequency [rpm]	577	657	270	320
Tip speed [m/s]	5.6	**6.4**	**6.9**	8.1
Mean specific power input [1] [W/kg]	**1.06**	**1.56**	**0.9**	**1.5**
Axial velocity in draft tube [m/s]	0.69	0.78	0.84	1.0
Internal volumetric flow rate [m^3/s]	0.021	0.025	0.165	0.1964
Turnover time [s]	3.5	3.1	6.7	5.6
Supersaturation at primary nucleation point[2] [-]	-	-	1.0122	1.0133
L_{50} at end of batch [μm]	442	453	743	547

[1]Estimated using a power number 0.4; [2]Recorded using Liquisomic® device

The comparison between these set of experiments is again made on the basis of the dynamic trend of the median crystal size (L_{50}), as depicted in Figures 4.15, 4.16 and 4.17. It's clearly perceptible that the start-up behavior and the progression of the L_{50} is very different when the experiments are done in these two crystallizers, under identical operating conditions. All other operating conditions remaining the same, this difference in the dynamic behavior can result only due to differences arising from the scale of operation and the type of crystallizer employed. There are two distinct parts in the dynamic CSD plots (Figures 4.15, 4.16 and 4.17) which can be clearly discriminated:

- the initial dynamic start-up behavior
- the later or final evolution of the dynamic CSD

The initial dynamic start-up behavior is governed mainly by the supersaturation at which the energy barrier is overcome to trigger the primary nucleation event. Later on, the evolution of the CSD is mainly dictated by the scale of operation and the type of crystallizer.

In case of DT_c3 and DT_c4, the initial crystals (for the median size) that are detected by the CSD measurement device (HELOS) is in the range of 250 – 300 μm, whereas for the DTB_c24 and DTB_c32, the first detected nuclei is in the range of 50 – 100 μm. This could be a measurement lapse that smaller nuclei passed undetected in the case of the 75L DT experiments. But, this possibility is ruled out as all the experimental runs on the 75L DT crystallizer showed a very high initial median crystal size (~ in the 250 – 300 μm range).

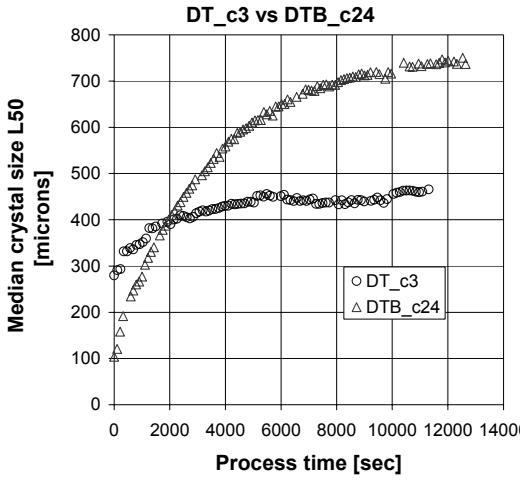

Figure 4.15

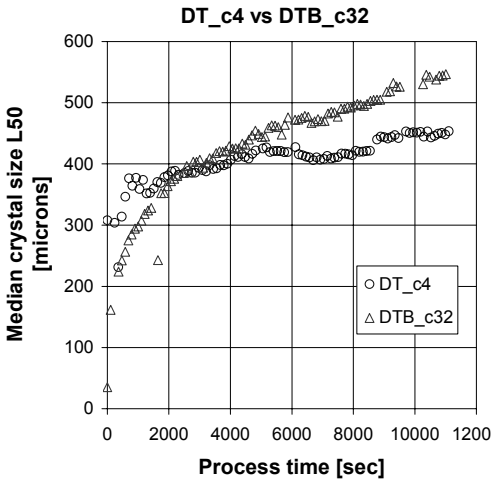

Figure 4.16

Effect of crystallizer scale and type (DT vs. DTB) : Dynamic start-up behavior of the median crystal size (L_{50}) for similar specific power input

Another hypothesis could be the difference in supersaturation between the two crystallizers, at which the primary nucleation event is instantiated. It could be possible that this supersaturation value at induction time is higher in the case of the 75L crystallizer than in the 1100L DTB crystallizer. Unfortunately, this could not be verified due to measurement problems with the supersaturation measurement device (LIQUISONIC®) for the 75L DT crystallization experiments. The consequence in this case would imply that the primary crop of crystals grow at a much accelerated pace in the 75L crystallizer, and by the time they are detected by the CSD measurement device, they have already reached a very large crystal size. But this fast initial growth consumes the supersaturation much faster than in the case of the DTB crystallizer, due to which there is a decline in the growth rate after a certain time.

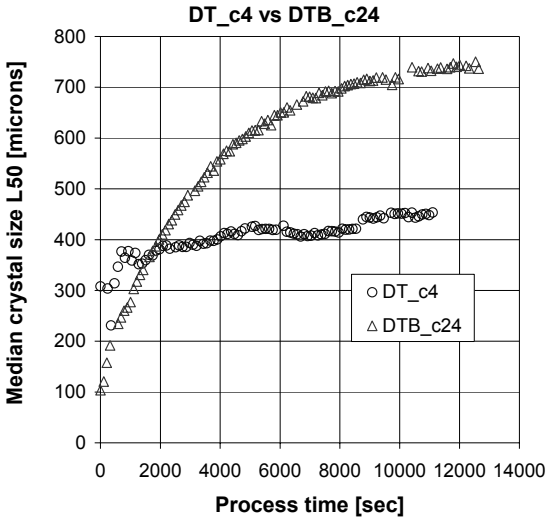

Figure 4.17 Effect of crystallizer scale and type (DT vs. DTB) : Dynamic start-up behavior of the median crystal size (L_{50}) for similar propeller tip speed

For the DTB crystallizer on the contrary, there is a much gradual increase in the L_{50} due to moderate growth rates and after a certain time (~2000 – 3000 seconds after start-up), the L_{50} goes above that for the DT crystallizer (see Figures 4.15 4.16 and 4.17). The reduced final median crystal size for the 75L DT crystallizer vis-à-vis the 1100L DTB crystallizer can be attributed to the difference in scale of operation, to be more precise the turn-over times, which is 3.5 seconds(DT_c3) and 3.1 seconds(DT_c4) for the 75L DT crystallizer and 6.7 seconds(DTB_c24) and 5.6 seconds (DTB_c32), for the DTB crystallizer. A reduced turn-over time implies more frequent crystal-impeller collisions, which in turn increases the secondary nucleation rate via attrition. Also with increase in the scale of operation, the propeller frequency usually drops (which is the case for the 1100L DTB crystallizer). This can shift the secondary nucleation mechanism, more away from crystal-hardware collisions to crystal-crystal interactions within the crystallizer. This can lead to different stress imperfections within the secondary nuclei thus, contributing to different growth patterns as compared to the 75L DT crystallizer, where the higher velocity interactions between the crystal and impeller may render the secondary nuclei in a more stressed condition, thus retarding it's healing process even more.
Another effect that supports the higher median crystal size for the 1100L DTB crystallizer is the influence of the fines removal system. As there is a continuous removal and destruction of fine particles from the annular zone of the DTB crystallizer, the specific crystal surface exposed to the system decreases, thus contributing to higher average growth rates. This would, as expected, contribute to an increase in the median crystal size, as opposed to the 75L DT crystallizer.

Concluding, it can be said that at low specific power input (Figure 4.15), the difference in process dynamics is quite significant with scale-up, for.eg. the difference in the final median crystal size is nearly 300 μm. On the contrary at higher specific power input (Figure 4.16), this difference is significantly reduced with the final median size differing only about 100 μm. Hence, scale-up criteria based on just the specific power input or the propeller tip speed does not really hold well for these types of crystallizers. However, it must also be kept in mind that the study presented here, not only involves a scale-up effect, but also the difference in the type of equipment which makes these kinds of comparisons even more complex.

4.8 DYNAMIC MODELLING AND PARAMETER ESTIMATION

The experiments performed on the 75L DT and 1100L DTB crystallizers will be used to estimate certain unknown kinetic parameters which occur in the simulation framework. The rigorous crystallizer models, which are discussed in section 3.5 of Chapter 3, encompass two unknown kinetic parameters: the surface integration rate constant k_r (Equation 4.4) and the condition for deformation Γ_s (Equation 4.5) which appear in the growth equation proposed by Gahn & Mermsann (Gahn & Mersmann, 1999b). Here, the growth of ammonium sulphate crystals is assumed to be both integration and diffusion-controlled.

$$\frac{G(L)}{2k_d(L)} = \frac{\Delta c(L)}{c_s} + \frac{k_d(L)}{2k_r c_s} - \sqrt{\left(\frac{k_d(L)}{2k_r c_s}\right)^2 + \frac{k_d(L)}{k_r c_s}\frac{\Delta c(L)}{c_s}} \tag{4.4}$$

$$\Delta c = c - c_{sat}.\exp\left(\frac{\Gamma_s}{RTL}\right) \tag{4.5}$$

Dynamic parameter estimation studies using in-built parameter estimation tools within gPROMS[1] will be used to determine these kinetic parameters to provide the best fit with experimental data. Parameter estimation attempts to determine values for the unknown parameters, θ, in order to maximize the probability that the mathematical model will predict the values obtained from the experiments. Assuming independent, normally distributed measurement errors, ε_{ijk}, with zero means and standard deviations, σ_{ijk}, this maximum likelihood goal can be captured through the following objective function (Process Systems Enterprise Ltd., 2005):

$$\varphi = \underbrace{\frac{N}{2}\ln(2\pi)}_{\text{constant term}} + \frac{1}{2}\min_{\theta}\left\{\sum_{i=1}^{NE}\sum_{j=1}^{NV_i}\sum_{k=1}^{NM_{ij}}\left[\underbrace{\ln(\sigma_{ijk}^2)}_{\text{variance term}} + \underbrace{\frac{(\tilde{z}_{ijk}-\hat{z}_{jk})^2}{\sigma_{ijk}^2}}_{\text{weighted residual term}}\right]\right\} \tag{4.6}$$

where

N	:	total number of measurements taken during all the experiments.
θ	:	set of model parameters to be estimated.
		the acceptable values may be subject to given lower and upper bounds, i.e. $\theta^L \le \theta \le \theta^U$.
NE	:	number of experiments performed.
NV_i	:	number of variables measured in the i^{th} experiment.
NM_{ij}	:	number of measurements of the j^{th} variable in the i^{th} experiment.
σ_{ijk}^2	:	variance of the k^{th} measurement of variable j in experiment i.
$\tilde{z}_{ijk}$	:	k^{th} measured value of variable j in experiment i.
$\hat{z}_{jk}$	:	k^{th} (model-)predicted value of variable j in experiment i.

The flowsheeting program gPROMS was used for dynamic simulation studies, using the parameters obtained from the parameter estimation studies. This simulation and modelling framework involves the solution of the typical conservative equations involving mass and energy balances alongwith the population balance equations to predict the evolution of the dynamic CSD. For a more comprehensive overview on the models used, please refer to Chapter 3 of this thesis.

[1] Process Systems Enterprise Ltd, Bridge Studios, 107a Hammersmith Bridge Rd., London, UK

4.8.1 Parameter estimation studies on crystallizers of different scale and type

The dynamic CSD measurements from experiments DT_c3 and DT_c4 (for 75L crystallizer) and DTB_c24 and DTB_c29 (for 1100L crystallizer) were chosen for parameter estimation studies, as these experimental data were found to be the most reproducible and reliable. The parameter estimation was treated as a two-step process for both the crystallizers:

- estimation of initial conditions for the liquid fraction and supersaturation at start-up
- estimation of the kinetic parameters (k_r and Γ_s)

4.8.1.1 75L DT crystallizer

The initial conditions are very important as they greatly influence the evolution of the CSD and also the final product quality. Hence, the first step in the parameter estimation study is to estimate the initial liquid fraction and the initial supersaturation. Although technically pure ammonium sulphate from DSM was used for the experiments, trace amount of impurities and dust particles being present in the feed tank are virtually unavoidable. The initial liquid fraction was estimated to be 0.99 while the initial supersaturation was found to be 8.36795. 10^{-4}. Using these results as input in the second step of the parameter estimation, the remaining kinetic parameters, viz. k_r and Γ_s were estimated. Table 4.9 gives an overview of the results obtained from these parameter estimation studies.

Table 4.9 Parameter estimation results for 75L DT crystallization experiments

	DT_c3		DT_c4	
Kinetic parameter	Estimate and standard deviation	Relative standard deviation (%)	Estimate and standard deviation	Relative standard deviation (%)
k_r $[m^4/mol.s]$	$(6.965\pm 0.191).10^{-4}$	2.74	$(5.270\pm 0.130).10^{-4}$	2.53
Γ_s $[J.m/mol]$	$(3.338\pm 0.014).10^{-5}$	0.43	$(3.122\pm 0.014).10^{-5}$	0.44

The relative standard deviations for the two parameters can be considered very much acceptable for the experiments studied. As seen from the 95% confidence ellipsoids in Figure 4.18(a) and (b) there is clearly a very high cross-correlation between these two parameters. Also, the confidence ellipsoids for the two different experiments do not lie in the same region, i.e. they do not overlap. The estimated correlation factor between k_r and Γ_s is -0.9781 for experiment DT_c3 and -0.9775 for experiment DT_c4. This implies that there is no unique parameter set which would satisfy both these experimental data. These results are very much in agreement with those discussed by Bermingham(2003) for the case of continuous crystallization experiments performed on a 22L DT crystallizer.

Bermingham (2003) discusses possible reasons for this disagreement between the two kinetic parameter sets obtained from different experiments. This is attributed to mainly two shortcomings:

- Omission of an explicit attrition source for the external circulation pump
- Lack of correct information for certain material properties such as shear modulus, Vicker's hardness, critical work for indentation, etc.

Figure 4.19 and Figure 4.20 show the fit of the simulated data with the experimental data, using parameters obtained from the parameter estimation results. The measured CSD transients, viz. the quantiles (L_{10}, L_{50} and L_{90}) are used as a means to validate the crystallizer models. Overall, it can be gauged that the simulations give a reasonably good fit with the plant data over the range of dynamic crystal sizes. But, as seen from Figure 4.19 and Figure 4.20, the fit of the L_{90} isn't as good as those of the L_{10} and the L_{50}. This significant deviation in the L_{90} can be attributed to the increasing measurement noise at higher crystal size measurements.

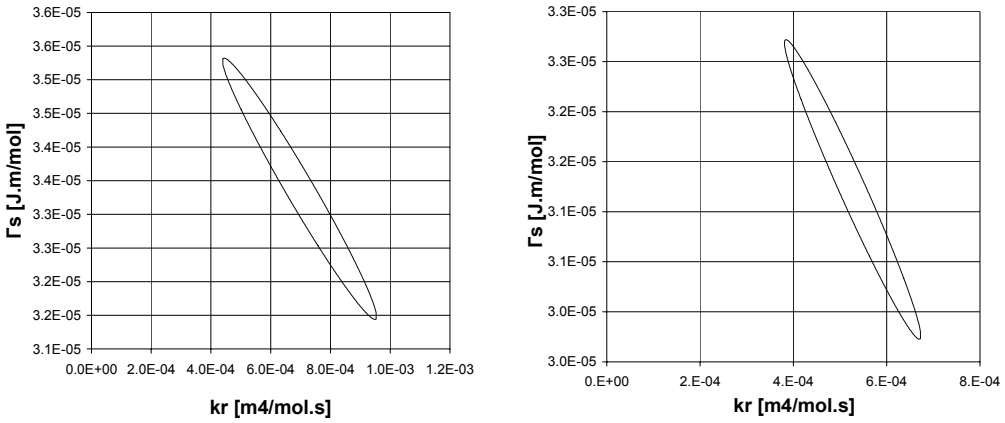

Figure 4.18 Confidence ellipsoids for k_r and Γ_s estimated using data from experiments (a) DT_c3 and (b) DT_c4

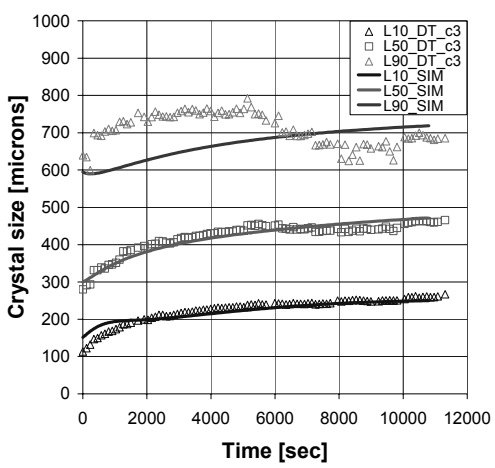

k_r = 6.965.10^{-4} m^4/mol.s, Γ_s=3.338.10^{-5} J.m/mol (LF=0.99, Sigmainit=8.37.10^{-4})

Figure 4.19

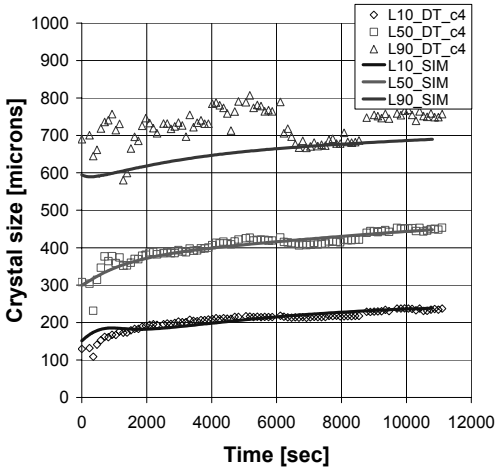

k_r = 5.270.10^{-4} m^4/mol.s, Γ_s=3.122.10^{-5} J.m/mol (LF=0.99, L0_1=300,L0_2=100,Sigmainit=4.10^{-4})

Figure 4.20

Fit of simulated data with experimental data, using parameters obtained for the same experiments from parameter estimation results

Next, the predictive capability of the model is tested by using the kinetic parameters obtained from experiment DT_c4. Two experiments were chosen for this study, viz.

- DT_c2 (75L DT) for testing the effect of a different operating condition on the same crystallizer
- DTB_c29 (1100L DTB) to test the effect of a different crystallizer scale and type under similar operating conditions

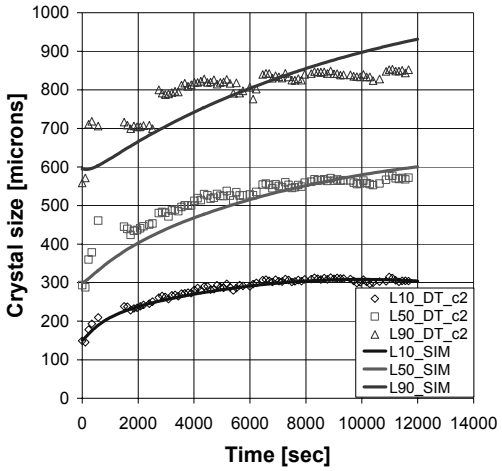

k_r = 5.270.10^{-4} m^4/mol.s, Γ_s=3.122.10^{-5} J.m/mol
(LF=0.99, L0_1=300,L0_2=100,Sigmainit=4.15.10^{-5})

Figure 4.21

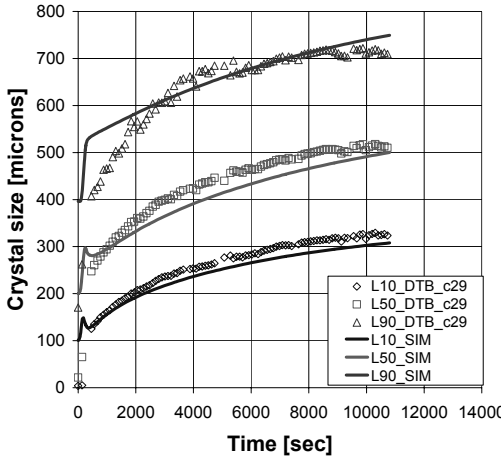

k_r = 5.270.10^{-4} m^4/mol.s, Γ_s=3.122.10^{-5} J.m/mol
(LF=0.99, L0_1=200,L0_2=100,Sigmainit=2.10^{-5})

Figure 4.22

Fit of simulated data with experimental data (using parameters obtained from parameter estimation result of experiment DT_c4) for experiment DT_c4 (75L DT) and DTB_c29 (1100L DTB)

The initial conditions were determined again separately for the experiments DT_c2 and DTB_c32. Figure 4.21 and Figure 4.22 give an indication of the predictive and descriptive capabilities of the model. In both these instances, the model gives a reasonably good prediction of the evolution of the dynamic CSD which implies that the parameter set obtained from one set of experiments can be used for scale-up and design purposes. It is acknowledged that the dynamics especially with regards to the initial start-up behaviour is not captured very well and there are still deficiencies in the model which need to be included, for instance:

- the inclusion of a primary nucleation event to describe the start-up dynamics of the process more accurately
- inclusion of other secondary nucleation mechanisms like crystal-crystal collisions, surface nucleation, etc. which might play a more active role in the case of DTB crystallizers
- accurate determination of certain material properties as discussed earlier.

4.8.1.2 1100L DTB crystallizer

As seen from Figure 4.22, the process dynamic start-up behavior is not captured very well when using the kinetic parameters obtained from a 75L crystallizer. Hence, to further improve upon this result, a parameter estimation study is carried out for the 1100L DTB crystallizer experiments. The results are presented in Table 4.10.

Table 4.10 Parameter estimation results for 1100L DTB crystallization experiments

	DTB_c24		DTB_c29	
Kinetic parameter	Estimate and standard deviation	Relative standard deviation (%)	Estimate and standard deviation	Relative standard deviation (%)
k_r *[m^4/mol.s]*	(3.033± 0.202).10^{-5}	6.65	(1.449± 0.107).10^{-5}	7.39
Γ_s *[J.m/mol]*	(5.454± 0.101).10^{-4}	1.85	(2.752± 0.064).10^{-4}	2.34

As observed in the case of the 75L experiments, here too the kinetic parameters, k_r and Γ_s are very highly correlated (see Figures 4.23 (a) and (b)) with correlation factors of -0.9989 (DTB_c23) and

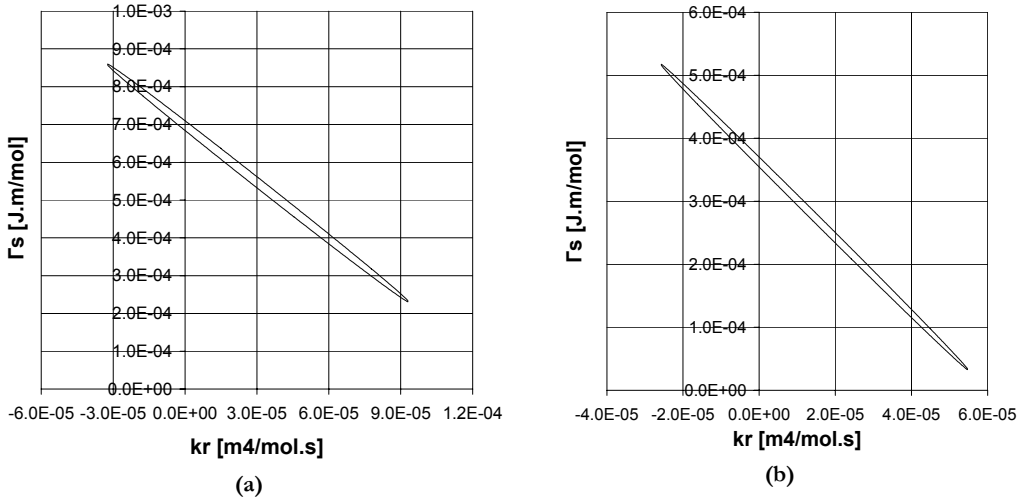

Figure 4.23 Confidence ellipsoids for k_r and Γ_s estimated using data from experiments (a) DTB_c24 and (b) DTB_c29

-0.9994 (DTB_c29) respectively. Also, a check with the parameter values for the 1100L and 75L estimation studies show that the difference is by an order of magnitude.

Using these new parameters, dynamic simulations were performed for the 1100L DTB crystallization experiments. As seen from Figures 4.24 and 4.25, the model gives a very reasonable description of the process dynamics, especially for the L_{10} and the time-averaged median crystal size. A huge improvement is seen with regards to the description of the start-up behavior (compare for instance, Figure 4.25 with Figure 4.22).

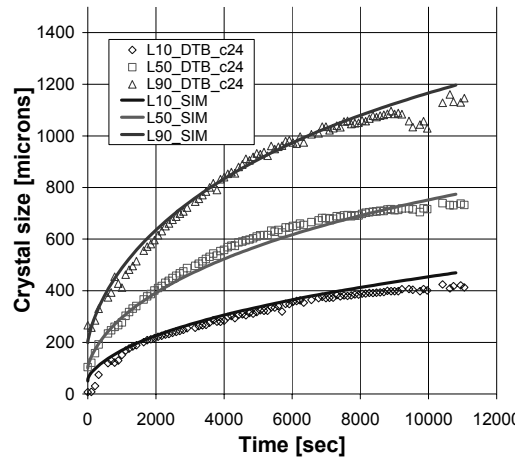

k_r =3.033.10^{-5} m^4/mol.s, Γ_s=5.454.10^{-4} J.m/mol
(LF=0.99, L0_1=100,L0_2=100,Sigmainit=8.37.10^{-4})

Figure 4.24

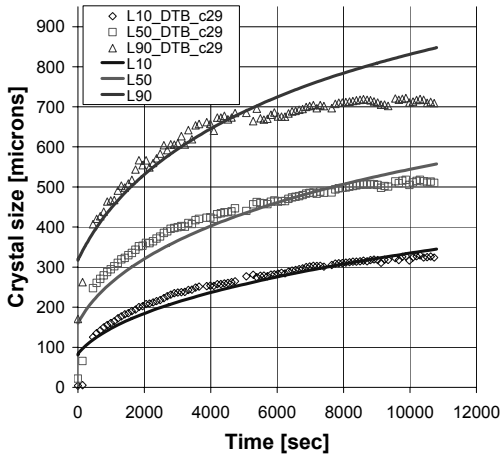

k_r =1.449.10^{-5} m^4/mol.s, Γ_s=2.752.10^{-4} J.m/mol
(LF=0.99, L0_1=160,L0_2=160,Sigmainit=2.10^{-4})

Figure 4.25

Fit of simulated data with experimental data, using parameters obtained for the same experiments from parameter estimation results

4.9 CONCLUSIONS

The study on fed-batch crystallization experiments performed on crystallizers of different scale and type, reveals a significant influence of the actuators (for example, the propeller frequency and fines removal rate) on the product quality and the process dynamics. The heat input was found to be not so critical in affecting the overall process dynamics in fed-batch processes. This result contradicts that of Neumann(2001) for continuous crystallization processes, where he observed that the heat input can be an effective actuator and that an increase in the heat input contributed to reduced median crystal sizes. This might point to secondary nucleation assuming a more dominant role for systems like ammonium-sulphate.

One of the important conclusions from the experiments on the 1100L DTB crystallizer is that the initial conditions have a huge impact on the evolution of the process dynamics, for batch crystallization processes. This is particularly important with regards to the feed purity which can affect the first primary nucleation event, which ultimately decides the initial distribution for the crystal population. This just shows that batch crystallization via seeding techniques can play a very effective actuator in realizing the desired product specifications. Seeding techniques must be investigated in the future to arrive at a blueprint for the optimal operation and control of industrial crystallization processes.

The effects of crystallizer type and scale show a huge impact on the process dynamics and also the final product crystal size, especially at low specific power inputs. This can be a result of different crystallization mechanisms coming into play (for instance, secondary nucleation via crystal-crystal contact alongside crystal-impeller contact) with increase in the scale.

Modelling of these data using the rigorous crystallizer models have shown that the models give a reasonable prediction and description of the process dynamics, also when applied to scale-up studies. Dynamic parameter estimation studies using the experimental data indicate that the two kinetic parameters from the model of Gahn and Mersmann (1999b), k_r and Γ_s, are highly correlated. The parameter estimates were analyzed with respect to different experimental data which suggested that there is no unique parameter set, which can be used confidently for scale-up and design purposes. The reliability and precision of the estimates were investigated by giving the 95% confidence interval. So, it is suggested to re-visit these models, which will be the subject of Chapters 5 and 6 (albeit currently applied to the study of continuous crystallization processes), where multiple nucleation mechanisms will be incorporated into the crystallizer model framework.

As a recommendation to future work, extending the systems studied to other than inorganic systems will be a huge plus for model validation, to test the applicability and potential of such rigorous models to arrive at a more general modelling framework.

NOTATIONS

c	concentration	[kg.m^{-3}]
c_s	concentration of the solid phase	[kg.m^{-3}]
c_{sat}	saturation concentration	[kg.m^{-3}]
d_{imp}	impeller diameter	[m]
D_{AB}	binary diffusion coefficient	[m^2.s^{-1}]
G	growth rate	[m·s^{-1}]
k_d	rate constant for diffusion	[m·s^{-1}]
k_r	rate constant for surface integration	[m·s^{-1}]
L	crystal length	[m]
L_{50}	median crystal size	[m]
R	universal gas constant	[J.mol^{-1}.K^{-1}]
T	temperature	[K]
s_{imp}	impeller frequency	[s^{-1}]
Ne	newton or power number	[-]

v_l	kinematic viscosity of liquid	[$m^2.s^{-1}$]
V	volume of crystallizer	[m^3]

Greek

$\bar{\varepsilon}$	specific power input	[$W \cdot kg^{-1}$]
Γ_s	surface related energy increase	[$J.m.mol^{-1}$]

Abbreviations

CSD	Crystal Size Distribution
DT	Draft Tube
DTB	Draft Tube Baffle
FB	Fluidized Bed
FC	Forced Circulation

REFERENCES

Bermingham, S.K. (2003). *A Design Procedure And Predictive Models For Solution Crystallization Processes- Development And Application*, Ph.D. Thesis, Delft University of Technology, the Netherlands, ISBN 90-407-2395-8

Brown D.M., and E.J. Weatherby, (1987). Practical problems of on-line monitoring of crystal growth using laser diffraction, *Proceeding of the 10th Symposium on Industrial Crystallization*, Bechyně, September 21st-25th, Czechoslovakia

Eek, R.A., Dijkstra, S. and van Rosmalen,G.M. (1995). Dynamic modeling of suspension crystallizers using experimental data, *AIChE Journal*, 41 (3), pp.571-584

Gahn, C. & Mersmann, A. (1999a).Brittle fracture in crystallization processes Part A: Attrition and abrasion of brittle solids, *Chemical Engineering Science*, 54, pp.1273-1282

Gahn, C. & Mersmann, A. (1999b). Brittle fracture in crystallization processes Part B: Growth of fragments and scale-up of suspension crystallizers, *Chemical Engineering Science*, 54, pp.1283-1292

Mersmann,A., Angerhöfer, M., Gutwald, T., & Sangl, R. (1992). General prediction of median crystal sizes, *Separation Technology*, 2, pp. 85-97

Mullin, J.W. (1993). Crystallization. 3rd Edition. Butterworth-Heinemann Ltd. Oxford, U.K.

Neumann, A.M.(2001).*Characterizing industrial crystallizers of different scale and type.* PhD Thesis, Delft University of Technology, Delft, the Netherlands, ISBN 90-6464-882-4

Omar, W. and Ulrich, J. (1997). Application of ultrasonics in the control of crystallizations process, *Proceedings of the Crystal Growth of Organic Materials 4*, Ulrich, J. editor, pp.294-301, Shaker Verlag, Aachen, Germany

Omar, W. and Ulrich, J. (1999). Application of ultrasonics in the online determination of supersaturation, *Cryst.Res.Technol.*, 34, pp.379-389

Process Systems Enterprise Ltd. (2005), *gPROMS Advanced User Guide*, London, UK

Ulrich J. and Lühmann, J. (1992). Anpassung eines Laser-Beugungsspektrometers für den Einsatz in der Technischen Kristallisation, *Chem. Ing.Techn.*, 64, nr. 11, pp.1022-1024

Westhoff, G.M.(2002). *Design and analysis of suspension crystallizers: Aspects of crystallization kinetics and product quality*, PhD Thesis, Delft University of Technology, the Netherlands, ISBN 90-6464-138-2

5

Modelling of the sustained cyclic behavior in DTB crystallizers (using two population balances) – Part 1†

A novel approach is introduced here to improve the description of the dynamic behaviour of industrial crystallizers using a two population balance model to discriminate between primary and secondary nuclei. A heterogeneous primary nucleation model (Kashchiev, 2000) is implemented in a rigorous crystallizer model framework to capture the sustained oscillatory behavior observed in industrial draft-tube baffle (DTB) crystallizers for the crystallization of well-soluble compounds. The distinction between primary and secondary nuclei in the modelling framework is realized by using two different growth rates within the dispersed phase. The total crystal population is split up into two distinct and interacting populations, one representing the primary (no strain) population of crystals and the other the secondary (strained) population. Such a two-population balance model exhibits the sustained cyclic response for a 1100L DTB crystallizer, for an ammonium-sulphate water system. Including the degree of heterogeneity (ψ) and the two parameters; surface integration rate constant (k_r) and condition for deformation (I_y^*) from the growth model, the primary nucleation model framework has three unknown parameters which are fitted using measured transients from experiments performed on pilot-plant crystallizers. The effect of the heterogeneity factor (ψ) on the dynamics of the process, suggests that the parameter ψ is very sensitive and hence, plays a very critical role in predicting the start-up and dynamics of the process. Validation of the model with experimental data , for the continuous evaporative crystallization of ammonium-sulphate from water, in 1100L DTB and 75L DT crystallizers, show that the inclusion of a primary nucleation event definitely increases the descriptive capability of the model, thus justifying it's inclusion as a critical factor. The simulation results give a very good description of the start-up phase of the crystallizer operation, the dynamics of the process as well as the final steady-state values.

† Parts of this chapter have been published in Journal of Crystal Growth (2005), 275, e1373–e1381 and parts have been submitted for publication in AIChE Journal (2006)

5.1 INTRODUCTION

Although crystallization is one of the older unit operations in the chemical industry, the design and operation of crystallization processes still pose many problems. Many plants produce crystals, which do not satisfy the defined quality specifications. The current market need is to operate crystallization and downstream processes in an optimal and cost-efficient manner, in strongly fluctuating market conditions, at the same time meeting stringent product quality specifications. In addition, a major problem with many continuous industrial crystallization processes is the occurrence of crystal size distribution (CSD) oscillations (Eek, 1995), inspite of the fact that the system might be at steady-state as regards the energy and material balances. The dynamics in the CSD can be a result of disturbances (feed changes, blockages, utility failures), changes in operating conditions (start-up, shut-down, grade changes), or simply the fact that the process is open loop unstable (Bermingham, 2003). With a cycling CSD periodically, an excessive number of fine crystals will be present in the product, which can severely hamper solid-liquid separation processes further downstream (eg. filtration) and can result in equipment fouling, caking, etc. All these problems and bottlenecks can cause significant production losses and lower the yield.

Despite the importance of crystallization, there is a relative lack of systematic design procedures and predictive models to overcome the before-mentioned problems and to design crystallizers for flexible product specifications in multi-purpose plants. A simulation tool enabling optimization and experimental design for a wide range of crystallization processes will maximize the added value in production by enabling market responsive plant operation. The main challenge here, in the design of industrial crystallizers is to predict the influence of crystallizer geometry, scale, operating conditions and process actuators on the process behavior and product quality. This challenge stems from a lack of physical understanding of the relevant kinetic processes occurring within the crystallizer.

An extensive study has been done on the development of a rigorous model framework for a wide range of crystallization processes and crystallizers (Bermingham, 1998, 2003a,b). These predictive crystallizer models give a reasonable prediction of the median crystal size and the overall dynamic trend, but exhibits one significant shortcoming: the inability to predict the very pronounced and in some cases even sustained oscillations of the product CSD (Neumann, 2001) in the 1100L DTB crystallizer, when using kinetic parameters obtained from an experiment performed on a 22L draft-tube (DT) crystallizer. At this stage, it is not clear whether this inability is a result of the uncertainties surrounding the parameter estimates or whether it is intrinsic to the kinetic model. The kinetic parameters investigated were the surface integration rate constant k_r and the surface related energy increase Γ_s , from the growth model of Gahn and Mersmann (1999b).

As suggested by Farrell (1995), the sustained oscillatory behavior observed in the 1100L DTB crystallizer could arise due to the locally distributed supersaturation within the crystallizer, which reaches it's peak in the boiling zone. The consequence could be a spontaneous primary nucleation event here. Primary nucleation requires relatively high supersaturation levels and regions with poor mixing properties can have a locally higher supersaturation, say for example, the boiling zone of the crystallizer. It has been confirmed that high supersaturation levels are present in foam layers of industrial evaporative crystallizers and as a result excessive crystal scaling is often found at the liquid level on the vessel wall. The state-of-the-art rigorous crystallization models (Bermingham, 2003a,b) however, do not account for a birth and growth rate expression for primary nuclei, which is considered a liability at this point.

The evolution of the CSD in an industrial crystallization process can be described using population balance equations and the appropriate mass and enthalpy balance equations combined with the equations describing the relevant kinetic phenomena. In continuous crystallization processes of well soluble compounds, eg. the evaporative crystallization of ammonium – sulphate from water, it is generally assumed that secondary nucleation and growth rate are the dominant kinetic phenomena (Bermingham(2003a), Gahn and Mersmann (1999a,b)). In this model, the secondary nuclei are formed as a result of collisions of the crystals with the impeller (attrition) and are characterized by the presence of a certain amount of lattice strain which severely affect the growth behaviour of these nuclei.

For the present study, a primary nucleation model (Kashchiev, 2000) is added to get a better description of the initial start-up of the crystallization process and to study the possible, periodically occurring primary nucleation in the boiling zone of the crystallizer. The strategy developed here is to use a two – population balance model in order to discriminate between two different nucleation mechanisms. A heterogeneous primary nucleation model is implemented in the rigorous crystallizer model framework along with an attrition model for secondary nucleation (Gahn and Mersmann, 1999ab). What is important to realize here is that these primary nuclei, will most likely not contain a strained lattice (assumption) and must therefore be described with a different growth function. So, it is of critical importance to distinguish between primary and secondary nuclei in the modelling framework. This is made possible by using two different growth rates within the dispersed phase. To realize this, the total crystal population is split up into two distinct populations, one representing the primary (no strain) population of crystals and the other the secondary (strained) population.

5.2 PRIMARY NUCLEATION MODEL

The primary nucleation mechanism based on the classical nucleation theory (discussed in Chapter 3) will be employed here for model analysis and simulation work. The reader is referred to Chapter 3 to have a more detailed overview on the specifics of the mechanisms and the model derivations. The rate expressions used are summarized below:

For Volume Diffusion Control

$$J = \xi D C_e S C_0 \left(\frac{k_B T}{\gamma_{ef}} \right)^{1/2} \ln S . exp\left[\frac{-W^*}{k_B T} \right] \tag{5.1}$$

For Interface Transfer Control

$$J = 6^{5/3} \xi w C_e S C_0 d_0 \pi^{1/3} \left(\frac{k_B T}{\gamma_{ef}} \right)^{-1/2} v_0^{5/3} . exp\left[\frac{-W^*}{k_B T} \right] \tag{5.2}$$

5.3 MODEL ANALYSIS

As seen from Equation 5.1 and Equation 5.2, there is often no knowledge at all of the values of important parameters in the formula for J such as the specific surface energy (γ_{ef}), the sticking coefficient (ξ), the number of active centres on the substrate (C_o), etc. Most of the empirical parameters are fixed using educated guesses (refer Appendix A5.1), leaving just the degree of heterogeneity (ψ) as a model parameter. A quick sensitivity analysis helps in identifying the relevant mechanism and critical model parameters, for the evaporative crystallization of ammonium-sulphate from water.

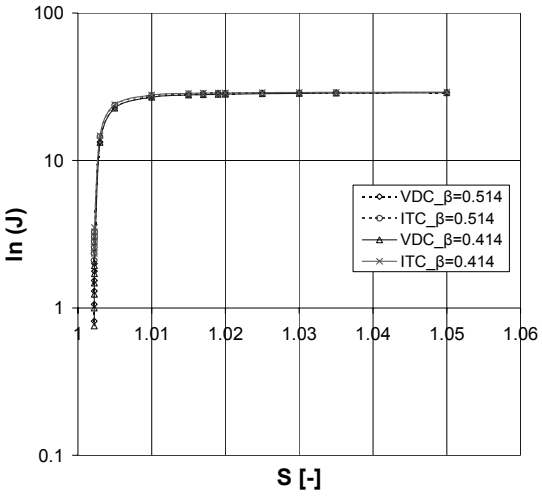

Figure 5.1 Primary nucleation rate vs Supersaturation for volume-diffusion control (VDC) and interface-transfer control (ITC) mechanisms ; for $\beta = 0.514$ and 0.414

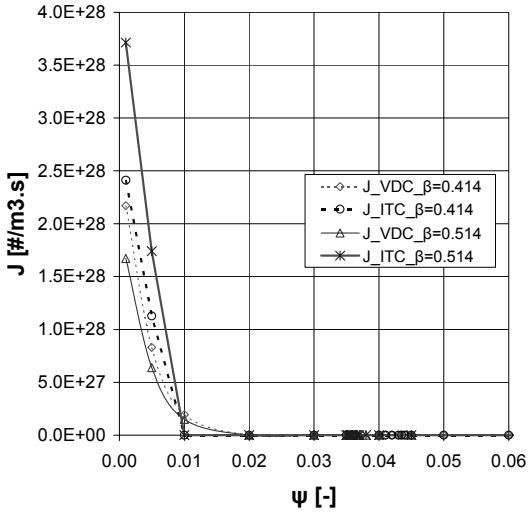

Figure 5.2 Effect of heterogeneity factor on primary nucleation rate for volume-diffusion control (VDC) and interface-transfer control (ITC) mechanisms ; for $\beta = 0.514$ and 0.414

Figure 5.1 shows how the primary nucleation rate (J) behaves as a function of supersaturation, for different mechanisms and shape of clusters. In case of well soluble salts like ammonium-sulphate, it really doesn't matter which rate expression is used for determining the primary nucleation rate. In a very narrow S range (~ S=1.002 to 1.0021), there is an explosive surge in J, which suggests that there exists a critical supersaturation for the nucleation of ammonium sulphate crystals in their solution and below this threshold value; the nucleation process is practically arrested. It is precisely this feature of the nucleation process which is the physical reason for which a supersaturated system can remain for a certain, in some cases, practically infinitely long time, in metastable equilibrium.

The parameter ψ ($0 < \psi < 1$) determines the heterogeneity of the system. The limiting cases of HEN are described by $\psi < 1$ and for these, $\gamma_{ef} < \gamma$. Obviously, the limit $\psi = 1$ corresponds to HON, for then $\gamma_{ef} = \gamma$. Figure 5.2 depicts the trend of the primary nucleation rate (J) as a function of the heterogeneity factor. As seen in the figure, the primary nucleation rate is very sensitive to the value of ψ. A certain threshold value of ψ is needed to get countable number of primary nuclei, which is ~ 0.02 here, where the J-curve cuts the X-axis.

J is a very steep function of ψ, which implies it can really influence the dynamics of a process significantly, as will be shown in the dynamic simulations on a 1100L DTB and 75L DT crystallizer.

As seen from the formulae for J (Equations 5.1 and 5.2), the real difficulties come up when these formulae are used for quantifying the stationary nucleation rate in concrete systems under concrete conditions. This is due to poor or often no knowledge at all of the values of important parameters in the formula for J such as the specific energy (γ_{ef}), the binding energy (E), the sticking coefficient (ξ), the number of active centres on the substrate (N_a), etc. So, educated guesses

need to made to fix most of these parameters, unless of course if there is ample experimental data that can be used for parameter estimation studies.

5.4 APPROACH – TWO INTERACTING NUCLEATION MECHANISMS

In this section, the implementation of the primary nucleation model in the rigorous crystallizer model framework is presented. The strategy used here is a two-population balance model approach which accounts for two interacting nucleation mechanisms in the dispersed phase.
It is important to distinguish between primary and secondary nuclei in the modeling framework. The secondary nuclei that are formed during the crystallization process are mainly due to the attrition process. Such crystals are believed to have a strained crystal lattice that includes structural defects. In contrast, crystals originating from primary nucleation are assumed to have a perfect structured lattice. Due to this assumption, primary crystal nuclei do not have a strained lattice.

The growth of crystals is considered to be a two step process, a diffusion step followed by an integration step of the solute to the crystal lattice (Mersmann,1992). Mersmann gives an expression for the growth rate $G = G(L)$ for surface integrated (integration rate constant k_r) and diffusion limited (mass transfer coefficient $k_d(L)$) crystal growth:

$$\frac{G(L)}{2k_d(L)} = \frac{\Delta c(L)}{c_s} + \frac{k_d(L)}{2k_r c_s} - \sqrt{\left(\frac{k_d(L)}{2k_r c_s}\right)^2 + \frac{k_d(L)}{k_r c_s}\frac{\Delta c(L)}{c_s}} \tag{5.3}$$

The mass transfer rate coefficient which is size dependent, can be calculated using a Sherwood type relation developed by Herndl (1982):

$$k_d(L) = \frac{D_{AB}}{L}\left[2 + 0.8\left(\frac{\bar{\varepsilon} L^4}{\upsilon_L^3}\right)^{1/5}\left(\frac{\upsilon_L}{D_{AB}}\right)^{1/3}\right] \tag{5.4}$$

Crystals formed by primary nucleation will have a crystal growth rate as defined in Equation 5.3 using the well-known definition of the driving force as given by Equation 5.5:

$$\Delta c = c - c_{sat} \tag{5.5}$$

The attrition process also leads to the formation of new nuclei (secondary) which will have a certain amount of strain energy embedded within their crystal lattice. This strain energy arises due to the impact of collisions of the crystals with a foreign body like the impeller or the crystallizer vessel wall. The newly created surface caused by the formation of an attrition fragment is proportional to the elastic strain energy stored in the volume of this fragment (Rittinger's law). Assuming that a constant portion of this strain energy, $\wp$, is stored in the fragment in the form of irreversible deformation, the chemical potential and consequently the solubility of this fragment, c^*_{real}, is increased in comparison with the solubility, c_{sat}, of an ideal, stress free crystal(Van der Heijden and van Eerden, 1992).

$$c^*_{real} = c_{sat}.\exp\left(\frac{w_s}{RT}\right);\ \text{where;}\ w_s = \frac{\Gamma_s}{L} \tag{5.6}$$

where :

$$\Gamma_s = \wp.2.\frac{\Gamma}{K_r}.\frac{1}{c_s}\ ;\quad 0 < \wp < 1$$

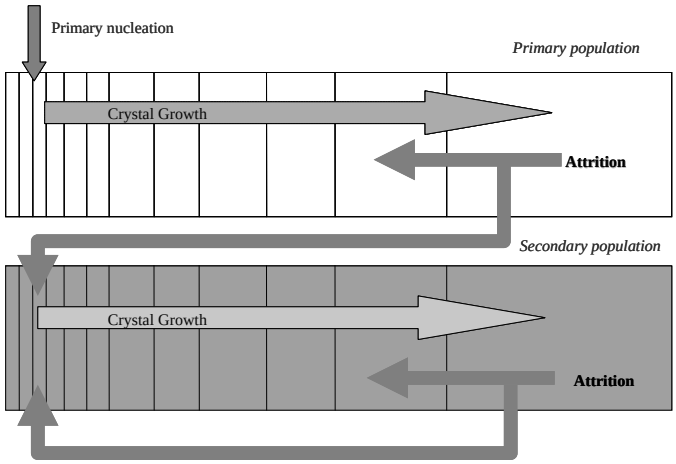

Figure 5.3 Crystal growth for nuclei and strained crystals using two populations (after Mitrovic, 2002)

Γ_s is considered to be a constant for a given substance and k_r for a given substance, purity of the solution and temperature. These two parameters can be determined from experimental data. The driving force for growth (for these secondary nuclei) is corrected for the presence of this strain by:

$$\Delta c = c - c^*_{real} = c - c_{sat}.\exp(\frac{w_s}{RT}) \tag{5.7}$$

This results in two different populations of crystals with a different growth rate as shown in Figure 5.3, one representing the primary population of crystals and the other the secondary population. Thus, two interacting populations have been introduced into the dispersed phase. The so-called primary population contains crystals formed due to primary nucleation for which the driving force from Equation 5.5 is applicable. Crystals colliding with the stirrer produce a large amount of small attrition fragments and one large remaining crystal. The small attrition fragments are stressed due to the crystal stirrer collision and are, therefore, transferred to the secondary population. The large remaining crystal is kept in the primary population. In the secondary population the crystals dissolve or grow depending on their size, which is determined by Equation 5.6. The growing crystals in the secondary population are again subject to the attrition process. The fragments and the large remaining crystal formed in the secondary population are now kept within this population, since the attrition parts, the fragments and the remaining crystal, contain a certain amount of strain energy.

5.5 TWO- POPULATION BALANCE MODEL

The evolution of the CSD in an industrial crystallization process can be described using population balance equations (PBEs) and the appropriate mass and enthalpy balance equations combined with the equations describing the relevant kinetic phenomena. The concept of population balance equations was introduced to crystallization by Randolph in 1962 (Randolph and Larson, 1988) and it accounts for the number balance of crystals and their change in size.
The PBE for a uniformly mixed volume, with the amount and the size of particles expressed in terms of number density and particle length respectively, can be expressed in the conventional form as follows:

$$\overbrace{\frac{\partial(n(L,t)V(t))}{\partial t}}^{\text{number rate of accumulation}} = \overbrace{-V(t)\frac{\partial(n(L,t)\cdot G(L,t))}{\partial L}}^{\text{rate of number gain due to crystal growth and dissolution}} + \overbrace{\sum\phi_{V,in}(t)n_{in}(L,t)}^{\text{number rate in}} - \overbrace{\sum\phi_{V,out}(t)n_{out}(L,t)}^{\text{number rate out}} + \overbrace{[B(L,t)-D(L,t)]V}^{\text{birth and death of crystals}} \tag{5.8}$$

The terms in this unsteady state equation represent different contributions to the number balance on a differential increment L to $L+dL$ in the crystal size coordinate. Thus, the first term on the left hand side represents the accumulation of numbers in the size increment. The first term on the right hand side represents the net flux of particles through the increment by crystal growth, the second and third terms represent the net addition of particles in the incremental size range from flows entering or leaving the crystallizer respectively, while the last two terms represent the birth and death/destruction of crystals directly into the size range under consideration by processes such as nucleation, agglomeration, breakage or attrition.
The number density is given as a function of both, characteristic length L and time

$$n = n(t, L) \tag{5.9}$$

The above PBE (Equation 5.8) takes the conventional form for the two interacting populations as follows (here the volume is assumed to be constant):
For the primary population:

$$\frac{\partial n_p(t,L)}{\partial t} = -\frac{\partial G_p(L)n_p(t,L)}{\partial L} + B_p(L) - D_p(L) + \frac{\mathbf{\Phi}_f}{V}n_p(t,L) - \frac{\mathbf{\Phi}_p}{V}n_p(t,L) \tag{5.10}$$

For the secondary population:

$$\frac{\partial n_s(t,L)}{\partial t} = -\frac{\partial G_s(L)n_s(t,L)}{\partial L} + B_s(L) - D_s(L) + \frac{\mathbf{\Phi}_f}{V}n_s(t,L) - \frac{\mathbf{\Phi}_p}{V}n_s(t,L) \tag{5.11}$$

where; G_p is given by Equations 5.3 and 5.5; G_s is given by Equations 5.3 and 5.7.

The source and sink terms relating to secondary nucleation via attrition (discussed in section 3.5 in Chapter 3), is depicted in Figure 5.4. This net source term, $\phi^{\pm}_{n,attr}$, is composed of three terms, which relate to the various steps of the attrition process: a sink term for the parent crystals that are subject to attrition, $\phi^{-}_{n,attr}$, a source term reflecting the birth of a single crystal, slightly smaller than the parent crystal, $\phi^{+}_{n,attr,1}$, and a source term for the attrition fragments, $\phi^{\pm}_{n,attr,2}$.

$$\varphi^{\pm}_{n,attr}(L) = -\varphi^{-}_{n,attr}(L) + \varphi^{+}_{n,attr,1}(L) + \varphi^{+}_{n,attr,2}(L) \tag{5.12}$$

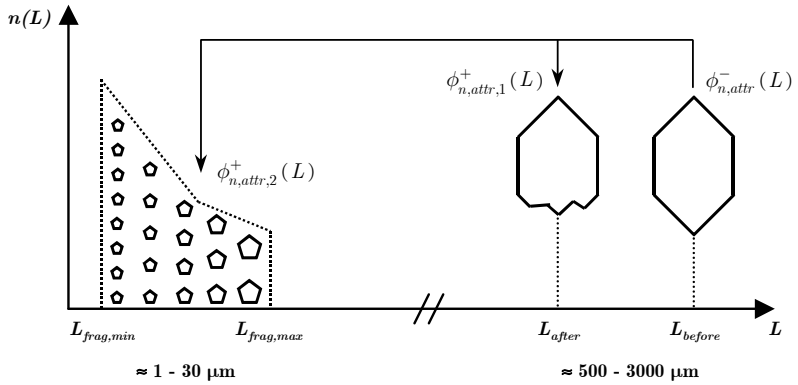

Figure 5.4 Relationship between the attrition related sink and source terms in the population balance equation (after Mitrovic, 2002).

As explained in Figures 5.3 and 5.4, now the birth and death terms for the primary population, $B_p(L) - D_p(L)$, in Equation 5.10 is given by:

$$B_p(L) - D_p(L) = -\varphi^{-}_{n,attr,p}(L) + \varphi^{+}_{n,attr,1,p}(L) \tag{5.13}$$

and that for the secondary population, $B_s(L) - D_s(L)$, in Equation 5.11 is given by:

$$B_s(L) - D_s(L) = -\phi^{-}_{n,attr,s}(L) + \phi^{+}_{n,attr,1,s}(L) + \phi^{+}_{n,attr,2,p}(L) + \phi^{+}_{n,attr,2,s}(L) \tag{5.14}$$

Agglomeration of crystals is not considered here. Suitable initial and boundary conditions need to be defined for the above PBEs.
As stated in the earlier section, the appropriate growth equation is used to discriminate between the primary and secondary population of crystals. Another important aspect is to apply the appropriate boundary condition for the two different classes of population.

Initial Condition
The initial condition can be used to express a trivial solution such as a clear liquid (no crystals) or a size distribution of seed crystals. In this case, we try to go as close as possible to a clear solution.

$$\text{Ideally, } n(L,t=0) = 0 \tag{5.15}$$

Boundary conditions
The classical boundary condition (B.C.) with respect to crystal size for the PBE is:

$$n(L=0,t) = \frac{B_0(t)}{G(L=0,t)} \; ; G(L) \geq 0 \; \forall L \tag{5.16}$$

This B.C. is applicable and sufficient when the crystal growth is positive for all crystal sizes. B_o denotes the birth rate of crystals at the lower limit of the size domain. At the lower limit of the size domain:
$B_0 = J$ (primary population) ; where J is the primary nucleation rate as given by Equation (5.1)
$B_0 = 0$ (secondary population)

If the growth rate is negative for all sizes, a B.C. at infinite length is required and sufficient:

$$n(L=\infty,t) = 0 \; ; G(L) < 0 \; \forall L \tag{5.17}$$

Hence, the appropriate B.C. must be applied for the size interval, depending on whether there is positive or negative growth rate.

5.6 DYNAMIC SIMULATIONS

In order to test and validate the two-population balance model approach, dynamic simulations studies are performed on (semi-) industrial scale crystallizers, viz. a 1100L DTB crystallizer (Figure 5.5) and a 75L DT (Figure 5.6) crystallizer. The Volume-Diffusion Control mechanism is chosen for the birth of the primary nuclei. The dynamic flowsheeting program gPROMS[1] was used as the modelling tool for this work .The dynamic form of the PBE is a PDE and thus needs to be reduced to a set of DAEs to be solved numerically. To this end, numerical methods belonging to the family of the Method of Lines are frequently used. A comprehensive overview on various numerical methods proposed for solving PBEs can be found in Kumar and Ramkrishna (1996). Based on the general crystallizer model developed by Bermingham(1998, 2003a,b), the finite volume method is used here for the solution of the PBEs. The finite volume method is known to be robust for highly convective PDEs such as the PBE, even when the sign of the convective term changes (eg. from growth to dissolution).

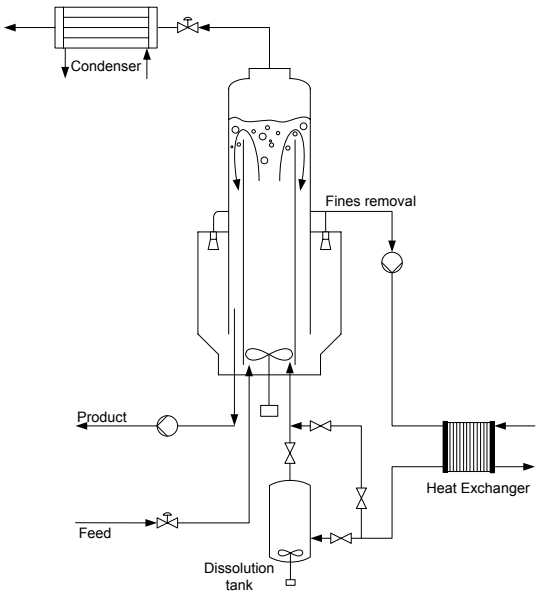

Figure 5.5 Schematic sketch of the 1100L DTB crystallizer set-up

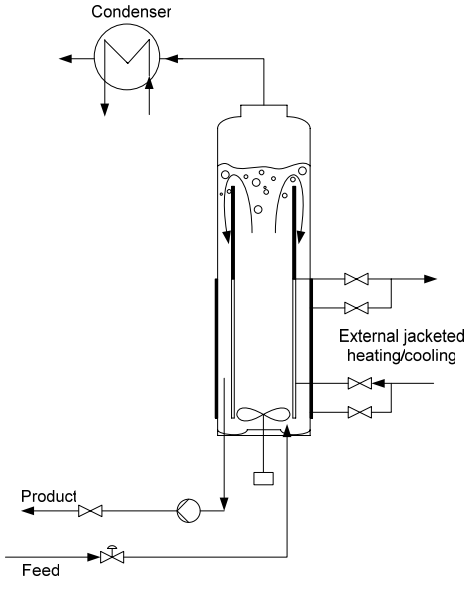

Figure 5.6 Schematic sketch of the 75L DT crystallizer set-up

[1] Process Systems Enterprise Ltd, Bridge Studios, 107a Hammersmith Bridge Rd., London, UK

Table 5.1 Overview of settings for simulations in a 1100L DTB and 75L DT crystallizer

Process/Simulation parameters	**1100L DTB**				**75L DT**		
Temperature [^{0}C]	50						
Impeller frequency[rpm]	370				400,577,657		
Fines removal rate [l.s^{-1}]	2				-		
Volume specific heat input [kW.m^{-3}]	120						
Feed temperature [^{0}C]	50						
Feed density [kg.m^{-3}]	1248						
Product residence time [s]	4500						
Kinetic parameters							
Γ_s [J.m.mol^{-1}]	5.10^{-4}				$2.5.10^{-5}$		
k_r [m^4.mol^{-1}.s^{-1}]	3.10^{-5}				1		
Ψ[-]	SIM9P	SIM11P	SIM66P	SIM10	SIM59	SIM44,49,54	SIM46
	0.033	0.1	0.031	-	0.03	0.045	-

As discussed earlier in section 5.3, lack of precise knowledge on experimental data to estimate the important parameters in the primary nucleation rate expression, makes the exact prediction of the primary nucleation rate J difficult. Table A5.1 in Appendix A5.1 lists the values for the different parameters which were fixed. Based on the outcome of the sensitivity analysis, only the degree of heterogeneity, ψ, is used to fit the CSD transients. In addition to the parameter ψ, from the growth model of Gahn and Mersmann (Gahn and Mersmann, 1999a,b), there are two unknown kinetic parameters as well, the surface integration rate constant k_r and the condition for deformation Γ_s, as given in Equation 5.3 and 5.6 These three parameters are fitted using measured transients from experiments performed on pilot-plant crystallizers. The experimental data set (DTB03) for the 1100L DTB crystallizer is taken from Neumann (2001). The process conditions for the experiments and the settings used for the dynamic simulations are listed in Table 5.1. For model validation, the CSD experimental data, viz. the L_{10}, L_{50} and the L_{90} will be used as a basis.

5.6.1 Single compartment model (1100L DTB)

The 1100L DTB crystallizer is treated as a single compartment model without any provision for a fines dissolution zone. This is not a realistic case and this also renders the crystallizer as a uniformly well-mixed vessel without accounting for any possible hot-spots in localized regions. Hence, this single-compartment model is used as an exploratory case-study to check the sensitivity of the model parameter(s) on the process dynamics.

Figure 5.7 and Figure 5.8 bring out the sensitivity of the heterogeneity parameter ψ. A very small change in it's value from 0.033 (Figure 5.7: SIM9P) to 0.031 (Figure 5.8: SIM66P) produces orders of magnitude difference in the primary nucleation rate J. Also, this effect is translated to the final CSD with respect to the amplitude and phase of oscillations. A decrease in the heterogeneity parameter contributes to lower crystal sizes, increases the amplitude of oscillation (marginally) and produces a shift in the phase of oscillations. For instance, the median crystal size (L_{50}) goes down from the 600-900 micron range (Figure 5.9: SIM9P) to the 500-850 micron range (Figure 5.9: SIM66P).

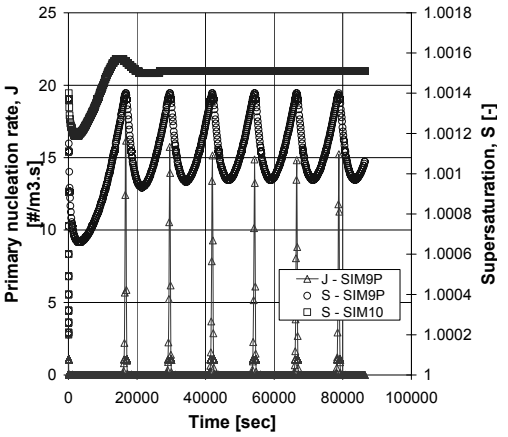

Figure 5.7
k_r = 3.10^{-5} m^4/mol.s, Γ_s=5.10^{-4} J.m/mol
ψ =0.033(SIM9P)

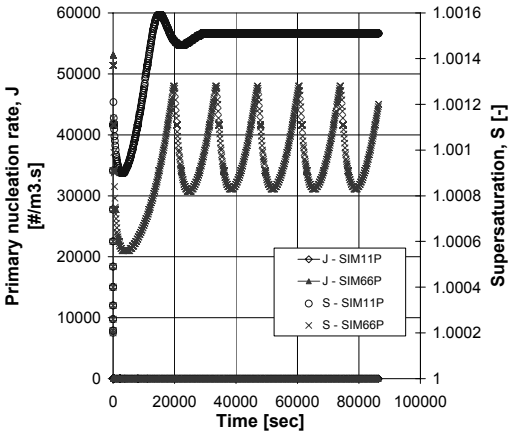

Figure 5.8
k_r = 3.10^{-5} m^4/mol.s, Γ_s=5.10^{-4} J.m/mol
ψ =0.1(SIM11P) and ψ =0.031(SIM66P)

Dynamic profiles of primary nucleation rate and supersaturation

What is interesting to see in Figure 5.7 (SIM9P) is the periodic primary nucleation burst which is thought to give rise to this oscillatory response. The same behavior is also observed in Figure 5.8 (SIM66P) [the scale on the graph doesn't show this clearly, though].
Figure 5.7 (plot for SIM10) shows the dynamic response of the supersaturation profile when the simulations are performed discounting primary nucleation, i.e. basically using a single-population balance model. As expected, there is no observed cyclic behavior in the supersaturation.

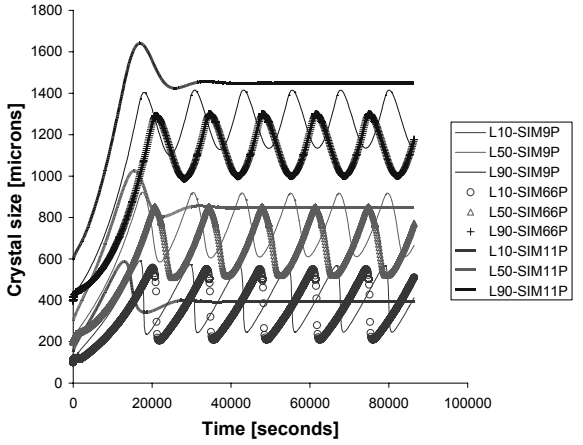

Figure 5.9 Simulated quantiles for SIM9P, SIM66P and SIM11P. Model validation using data from 1100L DTB crystallizer experiment (Neumann, 2001)

The simulations SIM9P (Figure 5.7 & Figure 5.9) & SIM66P (Figure 5.8 & Figure 5.9) show the effect on the dynamic response once a 'primary' nucleation expression is incorporated. The sustained oscillatory behavior is obvious here as seen from the dynamic response of the supersaturation profiles and the quantiles (L_{10}, L_{50}, L_{90}). An important remark at this point is regarding the value of ψ (0.033) for SIM9P and (0.031) for SIM66P which is an order of magnitude lower than physical reality. An expected range for the value of ψ for primary nucleation would be : $0.1 < \psi < 0.18$; for the system ammonium-sulphate. This is primarily because of the low supersaturation values (in the order of 1.001) simulated by the model. So, it can be argued whether this is indeed primary nucleation or some form of secondary nucleation mechanism that is triggered at such low supersaturation levels.
Again just to illustrate the effect on the process dynamics when ψ is increased to 0.1, SIM11P in Figure 5.9 shows that the sustained cyclic response is lost as a result. This is primarily because the value of ψ

(0.1) is so high that the energy barrier for primary nucleation cannot be overcome. Hence, no oscillations occur as the metastability limit is not exceeded. Figure 5.8 clearly shows that the primary nucleation rate in this case is zero which in turn results in hardly any dynamic behavior for the supersaturation profile.

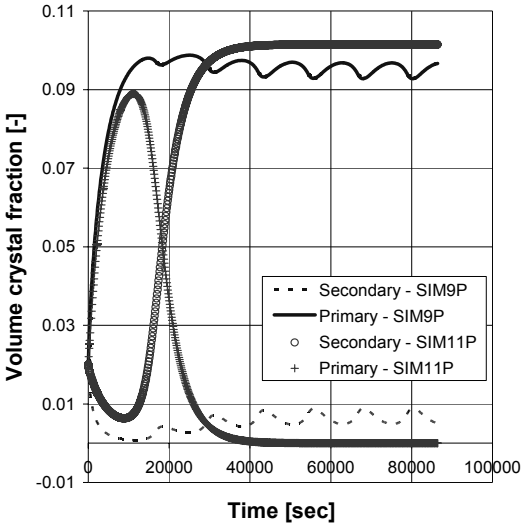

Figure 5.10 Distribution of crystals over the secondary and primary populations. Primary population clearly dominates the secondary class of crystals.

Another interesting aspect is to check the amount of crystals in the respective populations. Figure 5.10 shows the respective volume crystal fractions in the secondary and primary classes for SIM9P and SIM11P.

SIM9P shows that the crystal fraction in the primary class is very high as compared to the secondary class. Actually the primary population is dominating the secondary population over the entire process time. This is not in line with literature data (O'Meadhra (1995)) wherein secondary nucleation due to attrition is considered to be the dominant nucleation mechanism for the evaporative crystallization of ammonium-sulphate from water. So, the observation in Figure 5.10 is somewhat counter-intuitive because one would expect the other way round.

One factor that could contribute to this (unrealistic ?) distribution between the primary and secondary population could be the relatively high values of Γ_s . This results in the dissolution of more attrited fragments which arrive in the secondary population, thus contributing to a lower fraction of surviving secondary nuclei as opposed to the unstrained primary nuclei. If this is not the case, then it could be an artifact of the simulation or from another perspective, this could as well be a matter of fact that primary nucleation plays a more dominant role in determining the process dynamics here.

Nevertheless, what is interesting in Figure 5.10 is the transfer of crystals from the primary to the secondary class for SIM9P. Both the curves are complementary to each other. This is essentially responsible for the oscillatory behavior observed in the 1100L DTB crystallizer.

SIM11P throws more light into why periodic nucleation bursts give rise to the sustained oscillatory behavior as observed for the quantiles for SIM9P (see Figure 5.9). In SIM11P, the primary population practically dies out after some time as there is no primary nucleation being triggered at periodic intervals. This would be the same as in the case of a one-population balance model (SIM10). As a result, there is no corresponding oscillatory behavior observed for SIM11P as shown in Figure 5.9.

In a single compartment model as studied here, the supersaturation is distributed over the entire volume of the crystallizer. As a result, the global supersaturation value is much lower (~ 1.0012 – 1.0015) as seen in Figures 5.7 and 5.8. This in turn contributes to unrealistic values for ψ (<0.1). At such low supersaturation, secondary nucleation is expected to play the dominant role. For the system ammonium sulphate, primary nucleation is expected to occur at much higher supersaturation (in the region of ~ 1.01). Hence, it is important to treat this crystallizer not as a single compartment but, instead of a number of compartments with certain areas having higher superaturation than the bulk zone. This segregation in supersaturation can be achieved using compartmentation of the crystallizer, which will be the subject of sections 5.6.3 and 5.6.4. A compartmental model may also assure realistic values for ψ, simply because of the fact that with higher supersaturation levels in certain localized

region(s) of the crystallizer, the energy barrier to nucleation in these compartment(s) can be significantly reduced to effect a primary nucleation event.
Before that, section 5.6.2 briefly touches upon the effect of inclusion of a primary nucleation event for a 75L draft tube crystallizer, which is still treated as a single compartment.

5.6.2 Single compartment model (75L DT)

The simulations presented for the 1100L DTB crystallizer in the earlier section were performed using a one-compartment model without a fines dissolver, which essentially renders it as a DT crystallizer. Continuous evaporative crystallization experiments performed on a 75L DT crystallizer have shown no oscillatory behavior for the system ammonium sulphate - water (Menon, 2005). Hence, the two-population balance model using a single compartment for the crystallizer body is used to validate these experiments. The process and simulation conditions are as listed in Table 5.1. Figure 5.11 and Figure 5.12 are simulations performed for the 75L DT crystallizer, with and without the two-population balance model respectively. Validation of these models with experimental data shows that the inclusion of a primary nucleation event increases the descriptive capability of the model, thus justifying it's inclusion as a critical factor.

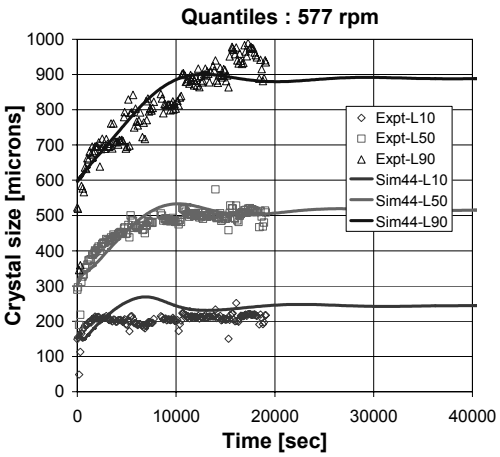

Figure 5.11 Two-population balance model
k_r = 1 m⁴/mol.s, Γ_s=2.5.10⁻⁵ J.m/mol, ψ =0.045

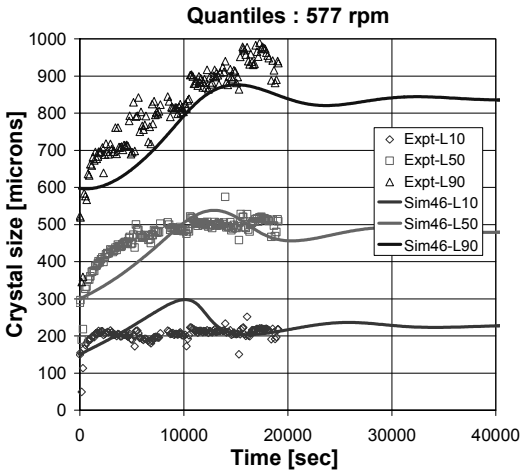

Figure 5.12 Single-population balance model
k_r = 1 m⁴/mol.s, Γ_s=2.5.10⁻⁵ J.m/mol

Quantiles of the crystal size distribution[2]

[2] The smooth lines indicate the simulated results for the quantiles (L_{10},L_{50},L_{90}) and the points indicate the quantiles for the experimental data.

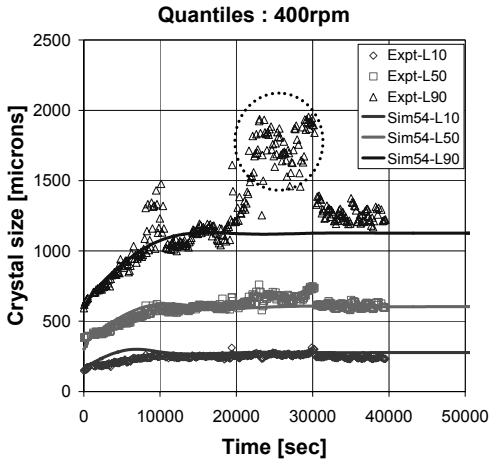

Figure 5.13

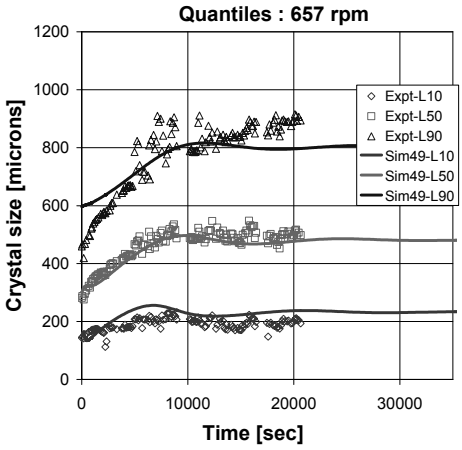

Figure 5.14

Quantiles of the crystal size distribution for SIM54(Figure 5.13) and SIM49(Figure 5.14)[3]
k_r = 1 m^4/mol.s, Γ_s=2.5.10^{-5} J.m/mol, ψ =0.045

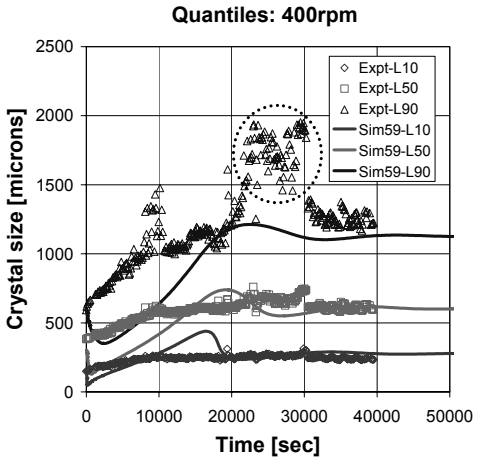

Figure 5.15 Quantiles of the distribution for SIM59,
k_r = 1 m^4/mol.s, Γ_s=2.5.10^{-5} J.m/mol, ψ =0.03

The simulations done at different stirrer frequencies (Figure 5.11, Figure 5.13, Figure 5.14) are able to predict the experimental data reasonably well. The simulation results give a very good description of the start-up phase of the crystallizer operation, the dynamics of the process as well as the final steady-state values. Thus, the two-population balance model shows a good predictive capability for different process conditions. SIM59 shown in Figure 5.15 illustrates the effect of the heterogeneity parameter ψ when it's value is set at 0.03. This shows the sensitivity of the heterogeneity parameter ψ in influencing the process dynamics.

5.6.3 Multi-compartment model without fines dissolver (1100L DTB)

Using a single compartment model for the 1100L DTB crystallizer, it was shown that it is possible to induce the oscillatory behavior. But, a strange observation in those simulations is the triggering of the primary nucleation event at extremely low supersaturation levels (~ 1.001). At such low supersaturations for ammonium-sulphate, the nucleation is mainly due to secondary nucleation. Hence, in order to test our hypothesis, a compartmental modelling approach is investigated, to see if it's

[3] The scattered experimental data(shown by the dotted circle) are a result of erroneous measurements for L_{90}.

possible to achieve higher supersaturation levels, especially in the boiling zone of the crystallizer which consequently can spark off a primary nucleation event.

The compartmental modelling approach accounts for the spatial distribution of process conditions, such as the supersaturation, energy dissipation and CSD, throughout a crystallizer. This approach provides a rough separation of the *local* intrinsic kinetics and the *overall* hydrodynamics, which also allows a description of the process dynamics. All compartments in a *compartmental* model are described with the same *compartment* model, i.e. the same equations of conservation, physical and thermodynamic property relations, kinetic rate expressions and parameters. Differences between compartments with respect to nucleation, growth, dissolution, attrition, breakage and aggregation rates are therefore purely a result of varying process conditions.

To justify the use of a compartmental modelling approach, compartmental models must be set up such that the compartments contain no or negligible internal gradients in supersaturation, energy dissipation and CSD. Considerable gradients may of course exist between the various compartments. The magnitude of these gradients is influenced by the kinetics and material properties of the material to be crystallized, the geometry of the crystallizer vessel and the operating conditions. For a more comprehensive overview on compartmental modelling, please refer to Bermingham (1998, 2003).
Figure 5.17 depicts a very simple compartment model of the 1100L DTB crystallizer (Figure 5.16). In addition to the propeller (mixing compartment), the crystallizer is split into four compartments that include a feed zone (1), two bulk compartments (2 and 4) and a boiling zone (3) at the top. The characteristics of the different compartments are listed in Table 5.2.

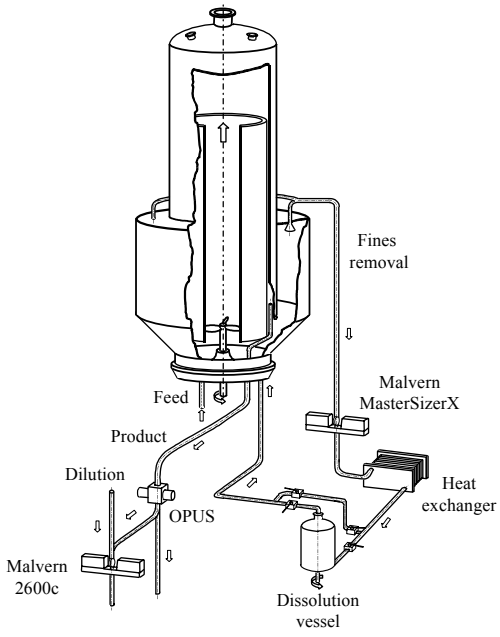

Figure 5.16 1100L DTB crystallizer at Delft University of Technology

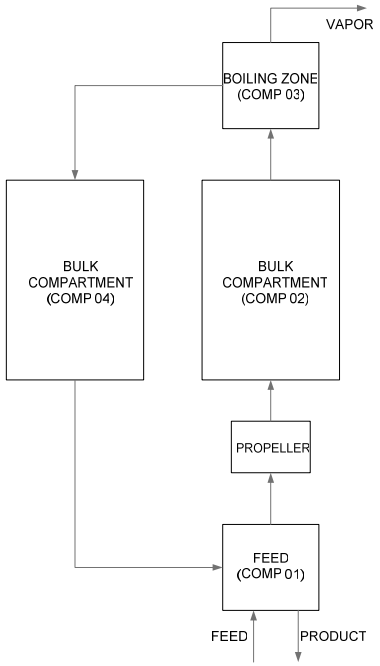

Figure 5.17 Four compartment model without a fines dissolver for the 1100L DTB crystallizer

Table 5.2 Compartment details for multi-compartment model without fines dissolver (1100L DTB crystallizer)

Compartment	Location	Volume	Description
1	Bottom Zone	$5/100 * V_{MB}$	Target for feed and fines return
2	Main Body	$45/100 * V_{MB}$	
3	Boiling Zone	$5/100 * V_{MB}$	Top compartment (highest supersaturation)
4	Main Body	$45/100 * V_{MB}$	
Kinetic parameters (SIM_MC4_1)			
Γ_s [J.m/mol]	4.10^{-3}		
k_r [m^4/mol.s]	2.10^{-7}		
Ψ[-]	0.135		

MB = Main body

Using a compartmental approach, it is possible to achieve very high supersaturation levels in the boiling zone, which triggers off a primary nucleation event here, as depicted in Figure 5.18; and this occurs at regular intervals. The supersaturation level (~1.012) which sparks off the primary nucleation is in reasonable agreement with experimental observation (Menon, 2005), wherein the primary nucleation event was recorded using the LIQUISONIC® probe (SensoTech, Germany). It is worthwhile pointing out that the corresponding value of the heterogeneity parameter, ψ , which is 0.135 here, is also more realistic. The primary nucleation was observed to be instantiated within the supersaturation range of 1.006~1.014. This periodic fresh crop of primary crystals gives rise to a dynamic trend for the supersaturation, which when translated into the CSD, produces an oscillatory response as well (see Figure 5.20). Figure 5.20 shows the fit between the simulated quantiles and experimental data. The smooth lines indicate the simulation results (two-population model) and the dots are the experimental data. Figure 5.19 shows the volume crystal fractions for the two populations. Just as observed for the single compartment model (see Figure 5.10), the primary class of crystals dominates the secondary class.

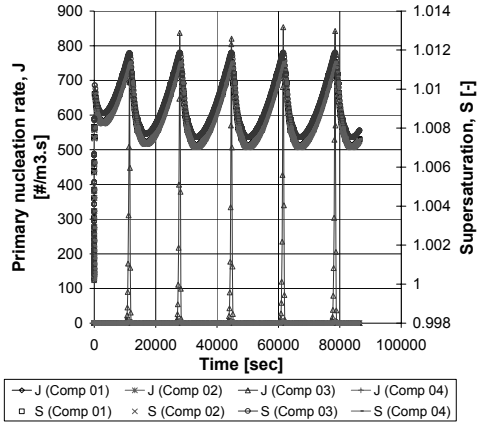

Figure 5.18 Dynamic profiles of primary nucleation rate and supersaturation in different compartments for a four-compartment model without fines dissolution.

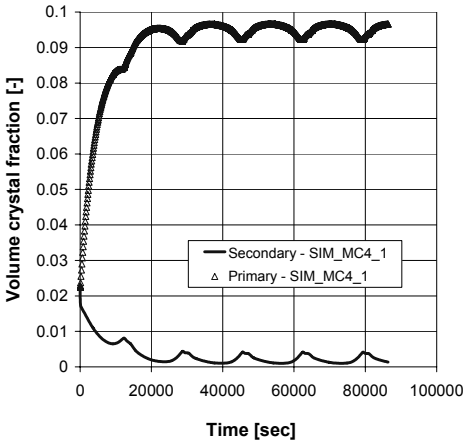

Figure 5.19 Distribution of crystals over the secondary and primary populations. Here again, the primary population clearly dominates the secondary class of crystals.

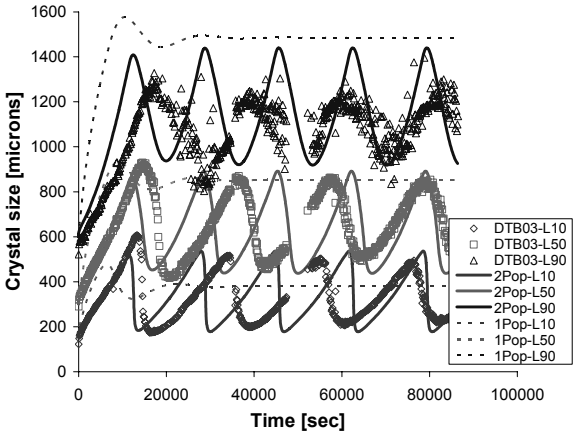

Figure 5.20 Simulated quantiles portraying the process dynamics for single-population (1Pop-SIM10) and two-population (2Pop-SIM_MC4_1) balance models. Model validation shown for a 1100L DTB crystallizer experiment (Neumann, 2001)

Comparison of the simulations using a four-compartment model (Figure 5.20) with a single-compartment model (Figure 5.9) shows an improved description of the dynamics when a multi-compartment model is taken into account. Here, the number of peaks have dropped from six (Figure 5.9) to five (Figure 5.20) and the amplitude of oscillation has also increased. In fact as seen in Figure 5.20, the amplitudes are in very close agreement to the experimental data, especially for the case of the L_{10} and the L_{50}. As for the single population balance model (1Pop), there is an initial hump in the quantiles which subsides and the L_{50} reaches a steady-state value of around 850 microns, after nearly six to seven residence times. And more significantly, there is no oscillatory behavior observed.

5.6.4 Multi-compartment model with fines dissolver (1100L DTB)

In view of the encouraging results using a multi-compartment model, a fines dissolver system is also added into the modeling framework, as depicted in the three-compartment model in Figure 5.21. The main body is split into a bulk compartment (COMP 01) and a boiling zone at the top (COMP 02) with the fines dissolution as the third compartment (COMP 03). The characteristics of these compartments are listed in Table 5.3.

Table 5.3 Compartment details for multi-compartment model with fines dissolver (1100L DTB crystallizer)

Compartment	*Location*	*Volume*	*Description*
1	Main Body	$95/100 * V_{MB}$	Bulk compartment
2	Boiling Zone	$5/100 * V_{MB}$	Top compartment (highest supersaturation)
3	Fines Dissolution	V_{FD}	Fines dissolution tank
Kinetic parameters (SIM_FR70)			
Γ_s [J.m/mol]	10.10^{-3}		
k_r [m⁴/mol.s]	3.10^{-7}		
Ψ [-]	0.14		

MB = Main body
FD = Fines Dissolution loop

Figure 5.22 illustrates the segregation achieved between compartments with respect to primary nucleation rate as a result of varying process conditions, i.e. the supersaturation levels in the various compartments. The primary nucleation event is instantiated only in the boiling zone (COMP 02) at a supersaturation value of around 1.0125 while the low supersaturation (1.0105) in the bulk compartment (COMP 01) circumvents this nucleation event. Actually the first nucleation event occurs at a supersaturation of 1.013 where the nucleation rate is ~ 22000 #/m^{3}s. The next successive periodic nucleation bursts happen at slightly lower supersaturations (1.0125), corresponding to which the nucleation rate drops to ~ 2000 #/m^{3}s. The number of nuclei generated here is enough to avoid any further depletion of supersaturation and thus, sustain the oscillatory behavior.

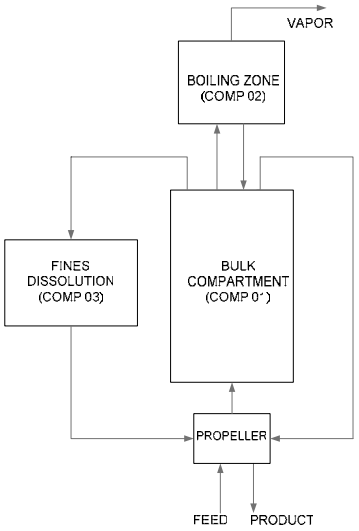

Figure 5.21 Three compartment model with fines dissolver for the 1100L DTB crystallizer

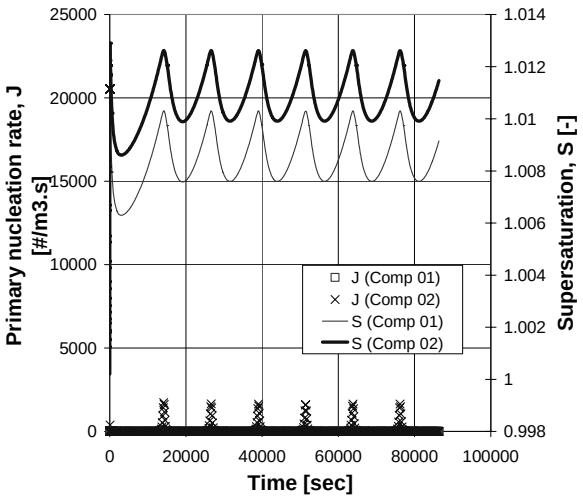

Figure 5.22 Dynamic profiles of primary nucleation rate and supersaturation in different compartments for a three-compartment model with fines dissolution

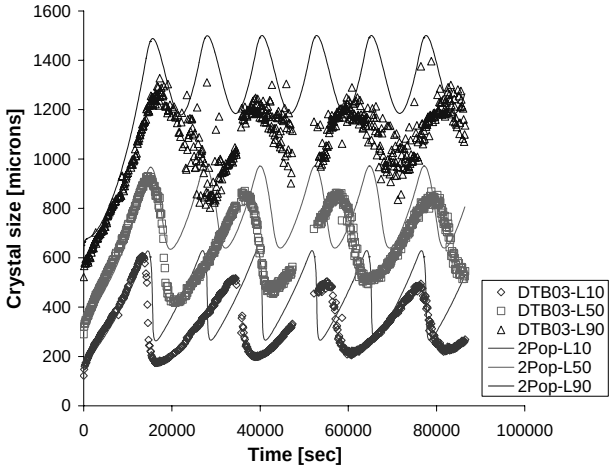

Figure 5.23 Simulated quantiles for the multi-compartment two-population balance model (2Pop – SIM_FR70) describing the process dynamics for a 1100L DTB crystallizer experiment

Figure 5.23 depicts the fit of the quantiles with the experimental data which shows that this multi-compartment model does exhibit the sustained cyclic behavior, but with some mismatch with regards to the phase and amplitude of oscillations. Numerous parameter combinations were tried out but, still it did not yield a better dynamic behavior. Parameter estimation studies using this two-population balance model have not yet been realized in view of the huge computational effort required; using advanced dynamic optimization tools within gPROMS. Future work should be aimed at resolving the computational difficulties for parameter estimation purposes, which should enable a better description of the cyclic behavior using a compartmental modelling approach.

5.7 CONCLUSIONS

This chapter presents a novel approach to simulate the dynamic behavior of industrial crystallizers using a two-population balance model, accounting for two interacting nucleation mechanisms in the

dispersed phase. Apart from the attrition model of Gahn and Mersmann (1999a,b), a heterogeneous primary nucleation model was selected to describe the primary nucleation event.

The primary nucleation expression involves a number of unknown parameters. A sensitivity analysis of the effect of the heterogeneity factor (ψ) on the dynamic behavior of the simulations shows that the primary nucleation rate, J is a very steep function of ψ thus, rendering it as a critical parameter in the simulation model framework. A moderate change in it's value can result in varied dynamics in the system under consideration.

The two-population balance model was mainly aimed at reproducing the oscillatory behavior observed in case of the 1100L DTB crystallizer and to test the predictive and descriptive capability of continuous experiments performed on a 75L DT crystallizer. Simulations were performed with varying combinations of the parameters k_r and Γ_s (Gahn's growth model) and ψ (primary nucleation model). The validity of this model has been demonstrated by comparing the model predictions with the experimental data and the results show that the inclusion of a primary nucleation event definitely increases the descriptive capability of the model, thus justifying it's inclusion as a critical factor.

The single compartment models show that the value of ψ needed to trigger a primary nucleation event is too low and unrealistic ($\psi < 0.1$). This primarily arises because of the low global supersaturation values within the crystallizer, which essentially drive the energy barrier for nucleation much higher and result in very low values for ψ.

The multi-compartment models improved on the value of ψ (0.135 – 0.14) making it a more realistic value, to trigger primary nucleation for the system ammonium sulphate. Here it is possible to create higher supersaturation levels in certain localized region(s) of the crystallizer, say the boiling zone. Hence, the energy barrier to nucleation in these compartment(s) can be significantly reduced to effect a primary nucleation event. The multi-compartment simulations without a fines dissolver give a good description of the start-up phase of the crystallizer operation, the dynamics of the process as well as the final steady-state values for the quantiles. However, simulations using a multi-compartment model with fines dissolution have not yielded an exact fit with the oscillatory behavior.

One of the main observations from the one-compartment and multi-compartment simulations, which was counter-intuitive, was the distribution of the crystals over the primary and secondary populations, wherein the primary class was found to be the more dominant population of the two. This could be explained due to the high values of Γ_s which results in the dissolution of more attrited fragments which arrive in the secondary population, thus contributing to a lower fraction of surviving secondary nuclei.

An important assumption made in this study is that primary nuclei are devoid of any strain. This assumption may not be completely valid as laboratory experiments have shown that growth rate dispersion is also present in primary nuclei (Valcic (1975), Davey (1979) and Garside and Ristic (1983)). It remains to be ascertained whether the distribution of nuclei between the primary and secondary population changes, if this argument of accounting for certain amount of strain in the primary nuclei is incorporated. If this is not the case, then it could be an artifact of the simulation or from another perspective, this could as well be a matter of fact that primary nucleation plays a more dominant role in determining the process dynamics here.

One of the main shortcomings at this point is the huge computational effort needed in realizing dynamic parameter estimation studies using the two-population balance model. This is an important aspect to be realized within the model development phase, so that the values for k_r, Γ_s and ψ can be more or less fixed for a wide range of process conditions and crystallizer type(s).

The most important conclusion from this chapter is that an activated nucleation mechanism like the primary nucleation model of Kashchiev(2000) which has a strong dependency on supersaturation plays a very important role in realizing the sustained cyclic behavior observed in DTB crystallizers. A secondary nucleation mechanism alone is not enough to realize this process dynamics.

An interesting aspect to look into would be implementing other nucleation models from literature (having a strong supersaturation dependence) to compare with the primary nucleation model of Kashchiev(2000). The subsequent chapter addresses this issue with regards to the study of secondary nucleation models having relatively strong supersaturation dependence.

NOTATIONS

A	kinetic parameter (pre-exponential factor)	[[# .m^{-3}.s^{-1}]
A_c	area of the cluster surface	[m^2]
A_s	area of surface of substrate	[m^2]
A^*	area of the nucleus surface	[m^2]
B	size dependent birth rate	[#.m^{-4}.s^{-1}]
B_o	birth rate at lower size limit	[#.m^{-3}.s^{-1}]
c	concentration	[kg.m^{-3}]
c	shape factor	[-]
C	monomer concentration	[#.m^{-3}]
C	concentration	[kg.m^{-3}]
c_s	concentration of the solid phase	[kg.m^{-3}]
C_e	equilibrium concentration (solubility)	[#.m^{-3}]
C_0	concentration of nucleation sites	[#.m^{-3}]
C_n	equilibrium concentration of n-sized clusters in a solution	[#.m^{-3}]
C_{sat}	saturation concentration	[kg.m^{-3}]
C^*	equilibrium concentration of nuclei	[#.m^{-3}]
d_0	diameter of a molecule	[m]
D	diffusion coefficient of solute molecule	[m^2.s^{-1}]
D_{AB}	binary diffusion coefficient	[m^2.s^{-1}]
D	size dependent death rate	[#.m^{-4}.s^{-1}]
E_a	activation energy for interface transfer	[J]
f, f^*	attachment frequency of molecules to the nucleus	[s^{-1}]
g	detachment frequency of molecules from the nucleus	[s^{-1}]
G	growth rate function	[m.s^{-1}]
G_{old}	gibbs' free energy (old phase)	[kg.J.mol^{-1}]
G_{new}	gibbs' free energy (new phase)	[kg.J.mol^{-1}]
j^*	diffusion flux of monomers to the nucleus surface	[# .m^{-2}.s^{-1}]
J	primary nucleation rate	[#.m^{-3}.s^{-1}]
k ,k_B	boltzmann constant	[J.K^{-1}]
k_d	mass transfer coefficient	[m.s^{-1}]
k_r	integration rate constant	[m^4.mol^{-1}.s^{-1}]
K_r	efficiency	[-]
L	crystal length	[m]
L_{crit}	critical nucleus size	[m]
L_{frag}	crystal length of attrition fragment	[m]
L_{init}	initial crystal length	[m]
L_{50}	median crystal size	[µm]
M	molecular weight	[kg.mol^{-1}]
n	population number density	[#.m^{-4}]
n	number of molecules constituting the cluster	[#]
n_L	population number density at a certain size	[#.m^{-4}]
N_a	nucleation-active centres	[#]
N_A	avogadro's number	[1.mol^{-1}]
Q	specific heat input	[kW.m^{-3}]
R	universal gas constant	[J.mol^{-1}.K^{-1}]
S	supersaturation ratio	[-]
t	time	[s]
T	temperature	[K]
v_o	molecular volume	[m^3]
v_s	volume of a solvent molecule in the solution	[m^3]
V	volume of the solution	[m^3]
V	crystallizer volume	[l]
w, w_0	random jump frequency	[s^{-1}]
w_s	strain energy/chemical potential difference	[J.mol^{-1}]
W	nucleation work	[J]
z	zeldovich factor	[-]

Greek letters and superscripts/subscripts

β	numerical factor	[-]
Δ	difference	[-]
ε	specific power input	[W·kg^{-1}]
γ	specific surface energy of the cluster/solution interface	[J.m^{-2}]
γ_{ef}	effective specific surface energy	[J.m^{-2}]
Γ	fracture surface energy	[J.m^{-2}]
Γ_S	surface related energy increase or condition of deformation	[J.m.mol^{-1}]
λ	molecular heat of dissolution	[J]
μ_s	chemical potential of a molecule in the solution	[J]
μ_c	chemical potential of a molecule in the bulk of the crystal phase	[J]
μ_{old}	chemical potential (old phase)	[J]
μ_{new}	chemical potential (new phase)	[J]
$\Delta\mu$	supersaturation	[J]
ν_l	kinematic viscosity of the liquid	[m^2·s^{-1}]
ϕ_f	volumetric flow of feed into crystallizer	[m^3.s^{-1}]
ϕ_n	number density production rate	[m^{-3}.m^{-1}.s^{-1}]
ϕ_p	volumetric flow of product out of crystallizer	[m^3.s^{-1}]
ρ_s	crystal density	[kg.m^{-3}]
σ	relative supersaturation	[-]
ψ	heterogeneity factor	[-]
φ	effective excess energy of the cluster	[J]
τ	residence time	[s]
ξ	coefficient of monomer sticking	[-]
$*$	equilibrium	[-]
$attr$	attrition term	[-]
in	flow into the crystallizer/compartment	[-]
out	flow out of the crystallizer/compartment	[-]
p	primary population of crystals	[-]
s	secondary population of crystals	[-]

Abbreviations

CSD	Crystal Size Distribution
COMP	Compartment (of crystallizer)
DAE	Differential Algebraic Equation
DT	Draft Tube
DTB	Draft Tube Baffle
FD	Fines Dissolution (compartment of crystallizer)
HEN	Heterogeneous primary nucleation
HON	Homogeneous primary nucleation
ITC	Interface Transfer Control
MB	Main Body (of crystallizer)
PBE	Population Balance Equation

PDE	Partial Differential Equation
VDC	Volume Diffusion Control
1Pop	Single population balance model
2Pop	Two population balance model

REFERENCES

Bermingham, S.K. (2003a). *A Design Procedure And Predictive Models For Solution Crystallization Processes- Development And Application*, Ph.D. Thesis, Delft University of Technology, the Netherlands, ISBN 90-407-2395-8

Bermingham, S.K., Verheijen, P.J.T. and Kramer, H.J.M. (2003b). Optimal design of solution crystallization processes with rigorous models, *Trans. IChemE*, 81, part A, pp.893-903

Bermingham, S.K., Kramer, H.J.M. and Rosmalen van, G.M. (1998). Towards on-scale crystallizer design using compartmental models, *Computers and Chemical Engineering*, 22, pp.S355-S362

Davey, R.J., Ristic, R.I. and Zizic, B. (1979). The role of dislocations in the growth of ammonium dihydrogen phosphate crystals from aqueous solutions, *Journal of Crystal Growth*, 47, pp.1-4

Dirksen, J.A. and Ring, T.A. (1991). Fundamentals of Crystallization: Kinetic Effects on Particle Size Distributions and Morphology. *Chemical Engineering Science*, Vol. 46, No. 10, p2389-2427

Eek, R.A., Dijkstra, S. and van Rosmalen,G.M. (1995). Dynamic modeling of suspension crystallizers using experimental data, *AIChE Journal*, 41 (3), pp.571-584

Farrell, R.J., Belokovskiy, A., Bennett, D. (1995). Simulated oscillations and control strategy for an ammonium sulfate DTB crystallizer, *AIChE Annual Meeting*, Miami beach, Florida, Nov.12-17, 1995, Paper 12e

Gahn, C. & Mersmann, A. (1999a). Brittle fracture in crystallization processes Part A: Attrition and abrasion of brittle solids, *Chemical Engineering Science*, 54, pp.1273-1282

Gahn, C. & Mersmann, A. (1999b). Brittle fracture in crystallization processes Part B: Growth of fragments and scale-up of suspension crystallizers, *Chemical Engineering Science*, 54, pp.1283-1292

Garside, J. and Ristic, R.I. (1983). Growth rate dispersion among ADP crystals formed by primary nucleation, *Journal of Crystal Growth*, 61, pp.215-220

Heijden, A.E.D.M. & Van der Eerden, J.P. (1992). Growth Rate Dispersion: The role of lattice strain, *Journal of Crystal Growth*, 118, pp. 14-26

Kashchiev, D. (2000). *Nucleation: Basic Theory with Applications,* Butterworth-Heinemann Ltd. Oxford, U.K.

Kashchiev, D. & van Rosmalen, G.M. (2003). Review: Nucleation in solutions revisited, *Cryst. Res. Technol.*, 38, No.7–8, pp.555–574

Kumar, S. and Ramkrishna, D. (1996). On the solution of population balance equations by discretization--I. A fixed pivot technique, *Chemical Engineering Science,* Volume 51, Issue 8, pp.1311-1332

Kumar, S. and Ramkrishna, D. (1996). On the solution of population balance equations by discretization--II. A moving pivot technique, *Chemical Engineering Science,* Volume 51, Issue 8, pp.1333-1342

Menon, A.R., Kalbasenka, A.N., Kramer, H.J.M., Jansens,P.J. (2005). Characterization of final product quality in unseeded fed-batch crystallization processes of inorganic salts in crystallizers of different scale and type., *Proceedings of the International Symposium on Industrial Crystallization* (ISIC16), 143-148, Dresden, 11-14 September, Germany

Menon, A.R., Kramer, H.J.M., Grievink, J., Jansens, P.J.(2005). Exploring multiple nucleation mechanisms to capture the dynamics in industrial crystallizers. *Proceedings of the 7th World Congress of Chemical Engineering (WCCE7),* Glasgow, July 2005, United Kingdom

Mersmann,A., Angerhöfer, M., Gutwald, T., & Sangl, R. (1992). General prediction of median crystal sizes, *Separation Technology*, 2, pp. 85-97

Mitrovic, A.(2002). *Population Balance based Modeling, Simulation, Analysis and Control of Crystallization Processes*, PhD Thesis, University of Stuttgart, Germany

Mullin, J.W. (1993). Crystallization. 3rd Edition. Butterworth-Heinemann Ltd. Oxford, U.K.

Neumann, A.M.(2001).*Characterizing industrial crystallizers of different scale and type.* PhD Thesis, Delft University of Technology, Delft, the Netherlands, ISBN 90-6464-882-4

Ó Meadhra, R. (1995). *Modelling of the kinetics of suspension crystallizers – a new model for secondary nucleation.* PhD Thesis, Delft University of Technology, the Netherlands, ISBN 90-407-1190-9

Randolph, A.D. & Larson, M.A. (1988). *Theory of particulate processes,* second edition, Academic Press, San Diego, USA

Valcic, A.V. (1975). Influence of dissolution on the growth rates of saccharose crystals, *Journal of Crystal Growth*, 30, pp.129-136

6

Modelling of the sustained cyclic behavior in DTB crystallizers (using two population balances) – Part 2[†]

Two secondary nucleation mechanisms with a dependency on supersaturation, viz. the embryo coagulation secondary nucleation (ECSN) and the surface nucleation models, have been analyzed to explain the sustained cyclic behavior in DTB crystallizers. A two-population balance strategy(Menon,2005) was adopted to discriminate between competing nucleation mechanisms. The models equipped with the ECSN mechanism were not able to describe the oscillatory behavior as the dependence of ECSN on supersaturation turned out to be too weak. Surface nucleation yielded much better results and compartmental modelling approach using a two-compartmental model has been used to simulate a 1100L DTB crystallizer with a boiling zone that has a locally higher supersaturation. The surface nucleation bursts could exclusively be located into the boiling zone and the simulation results give a very good description of the start-up phase of the crystallizer operation, the dynamics of the process as well as the final steady-state values. This proves that even a small spatial region like the boiling zone can have a large influence on the dynamic behavior of evaporative crystallizers. Extension to a three compartmental model with a fines dissolver gave less severe oscillations.

[†] Parts of this chapter have been submitted for publication in Chemical Engineering Science (2006)

6.1 INTRODUCTION

One explanation for the observed oscillatory behavior of industrial crystallizers is periodic primary nucleation events taking place in the boiling zone of the crystallizer (Farrell, 1995). Primary nucleation is, by definition, the process of fluctuational appearance of nanoscopically small molecular clusters of the new crystalline phase (Kashchiev, 2000). It has already been shown by Menon (2005) that periodic primary nucleation bursts are able to describe the sustained oscillations in DTB crystallizers. The probability of periodic primary nucleation events occurring after the first nucleation event is not entirely convincing, however multiple primary nucleation events are observed in the case of precipitation systems where the supersaturations are an order of magnitude higher than in the case of solution crystallization of inorganic salts. Whether such a possibility can occur in the case of solution crystallization of ammonium-sulphate from water has still not been confirmed. Hence, in this study, secondary nucleation mechanisms have been analyzed to explain the sustained cyclic behavior in DTB crystallizers. A selection criterion for these mechanisms is a steep dependency on supersaturation.

The first mechanism is embryo coagulation secondary nucleation (ECSN) which is based on the existence of clusters as postulated in classical nucleation theory, on the existence of long-range attractive forces between particles and on the theory of rapid coagulation of colloids. The second mechanism is referred to as surface nucleation which is based on two-dimensional nucleation of steps on the surface of a crystal, which is a widely accepted mechanism for crystal growth. Nucleation takes place when surface nuclei are released into the solution.

Experimentally, many researchers have observed that the metastable limit of clear solutions is higher compared to solutions in which crystals are present (Qian(1996) & Nyvlt(1970)). These observations imply that mechanisms like homogeneous and heterogeneous primary nucleation need to overcome larger energy barriers to trigger nucleation events, whereas the secondary nucleation mechanisms are activated at lower supersaturation levels.

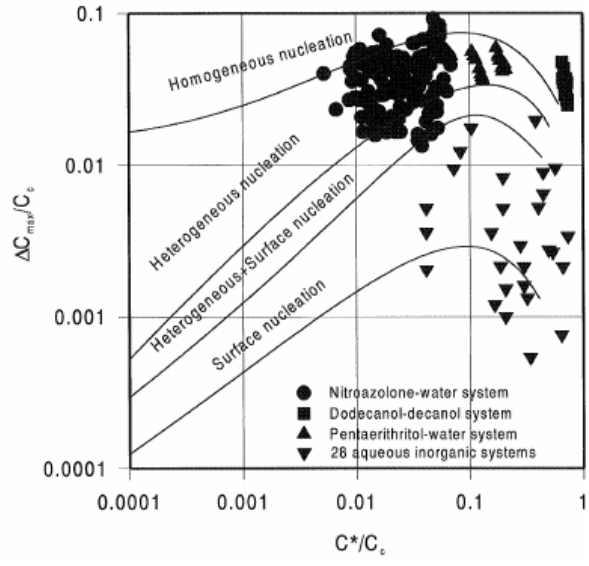

Figure 6.1 Dimensionless metastable supersaturation against the dimensionless solubility (after Kim, 2001)

Kim & Mersmann(2001) plot the nucleation rates for different systems, for primary nucleation (homogeneous and heterogeneous) and secondary nucleation (activated mechanism like surface nucleation), for different rates with the dimensionless supersaturation on the y-axis and the dimensionless solubility on the x-axis. The supersaturation is made dimensionless by dividing it by molar crystal density c_c.

Figure 6.1 shows the regions in which the different nucleation mechanisms are dominating. Below the surface nucleation region, attrition is the dominant nucleation mechanism. Attrition is not an activated nucleation mechanism hence, the nucleation rate of attrition increases only moderately with supersaturation. At higher supersaturation, the dominant mechanism becomes surface nucleation which is an activated mechanism, especially for the aqueous inorganic systems. Here, the nucleation rate strongly increases with supersaturation. As soon as a shower of nuclei is produced, the supersaturation drops significantly and may fall back to attrition-dominated region. According to Mersmann, this is an explanation for the oscillatory behavior observed in industrial crystallizers. Then,

there is an area in which heterogeneous or surface nucleation is dominant. In this area, the dominant mechanism is determined by the surface properties and concentration of foreign particles or the number of crystals that are present. In the highest supersaturation region, homogeneous nucleation is the dominant mechanism, which is observed mainly for the organic systems.
It is entirely conceivable that there are multiple nucleation mechanisms in different regions of the crystallizer that affect the dynamics of a crystallization process. Hence, in addition to a secondary nucleation mechanism via attrition (Gahn & Mersmann, 1999a), the above proposed activated nucleation mechanisms, viz. ECSN and surface nucleation, are implemented into the two-population balance model for a 1100L Draft Tube Baffle (DTB) crystallizer, one population balance for the unstrained and one for the strained crystals. This approach is necessary, because nuclei which originate from attrition are assumed to contain some internal lattice strain, while nuclei created by activated nucleation mechanisms are assumed to be strain-free. This approach is exactly similar to the one described in Chapter 5. Hence, for the sake of brevity, the two-population balance model will not be discussed here. Rather, the focus in this chapter will be more on the analysis of these nucleation theories and it's impact on predicting the sustained oscillatory behavior in the 1100L DTB crystallizer.

6.2 EMBRYO COAGULATION SECONDARY NUCLEATION

Qian and Botsaris (Qian, 1997) propose the Embryo Coagulation Secondary Nucleation (ECSN) mechanism. ECSN is based on the existence of clusters as postulated in classical primary nucleation theory (Kashchiev, 2000), on the existence of long-range attractive forces between particles and on the theory of rapid coagulation of colloids. Clusters below the critical size are called embryos and above are called nuclei. The existence of embryos has been verified by several experiments and forms the basis of the classical primary nucleation theory. Figure 6.2(a) shows embryos in solution. In Figure 6.2(b), a large seed crystal is introduced. These large crystals attract embryos by Van der Waal's forces which results in a high concentration of embryos in a pre-ordered layer, adjacent to the crystal surface (Figure 6.2(c)). This high concentration of embryos around the surface in turn leads to coagulation and nucleation occurs when the coagulated clusters exceed the critical nucleus size (Figure 6.2(d)). The nuclei are then removed from the layer to the bulk by, for example, fluid-shear or collision (Figure 6.2(e)). The major difference between primary nucleation and ECSN is that in primary nucleation, the coagulation of clusters is neglected. This is justified due to the low concentration of clusters.

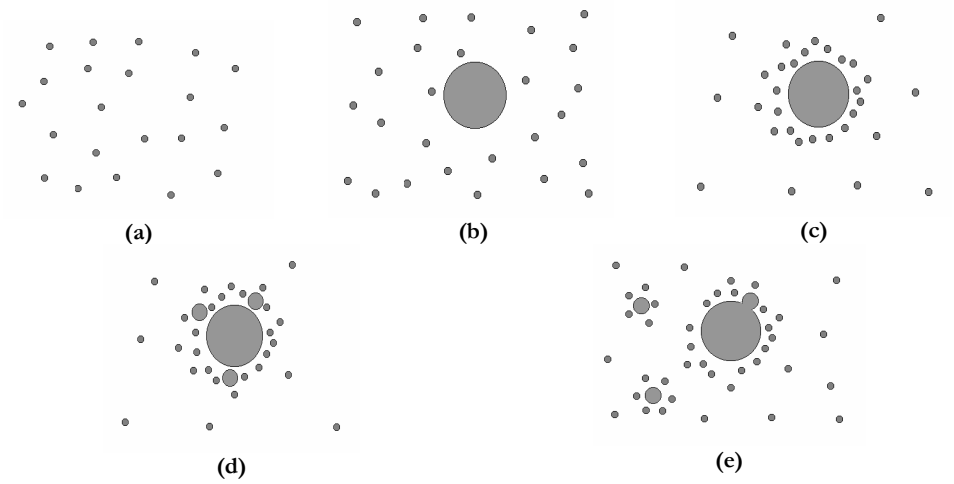

Figure 6.2 (a-e) Schematic representation of embryo coagulation nucleation mechanism

6.2.1 Attractive forces and cluster concentration in surface layer

The presence of parent crystals creates Van der Waals forces of attraction between crystals and embryos. These attractive forces are present due to dipole-dipole interactions. For single molecules, the dipole-dipole interactions depend inversely on the sixth power of the distance between the molecules and are therefore classified as short-range. For macroscopic bodies, the summation of dipole-dipole interactions leads to an inverse dependency on the distance by first or second power. The exact power depends on the geometry under consideration. Therefore the interaction is classified as long-range and as a result, clusters concentrate near parent crystals.

The energy of interaction between a slab (the crystal surface) and a small sphere of radius r (the embryo) is a function of the distance x between the two bodies:

$$\varepsilon = -\frac{A_{131} r}{6x} \tag{6.1}$$

A_{131} is the Hamaker constant of two particles of material 1 in medium 3, x is the distance between the two surfaces and r is the radius of the small sphere. Equation 6.1 can be seen as a potential field surrounding each particle. The free energy difference of formation of a cluster with size g contains one additional term compared to that for primary nucleation, due to the attractive forces between crystals and embryos.

$$\Delta G_g = (4\pi)^{1/3} \gamma_{CL} (3 g V_m)^{2/3} - kTg \ln(S) - \frac{A_{131}}{6kT} \frac{r_g}{x} \tag{6.2}$$

The cluster concentration in the surface layer follows from the cluster concentration in a clear solution. The cluster concentration in the surface layer around a crystal is given by:

$$n_g' = n_g \exp\left[\frac{A_{131}}{6kT} \frac{r_g}{x}\right] \tag{6.3}$$

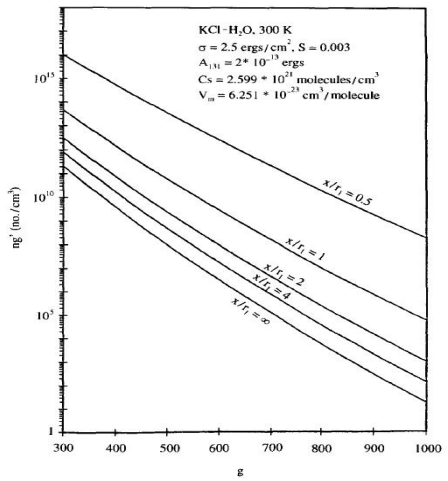

Figure 6.3 Cluster concentration versus cluster size for various distances to the surface for KCl in water. The bulk concentration n_g corresponds to the line $x/r_1=\infty$ (Qian, 1997)

At infinite distance, the cluster concentrations equal the concentrations in clear solution. The cluster radius of a g-mer r_g is substituted by:

$$r_g = r_1 g^{1/3} \tag{6.4}$$

where r_1 is the radius of a solute molecule. This leads to:

$$n_g' = n_g \exp\left[\frac{A_{131}}{6kT} \frac{r_1}{x} g^{1/3}\right] \tag{6.5}$$

Qian(1997) plots the cluster concentration near the crystal surface against the cluster size for various distances x. The system under consideration is potassium chloride in water. Figure 6.3 reveals the strong influence of distance on the cluster concentration. Very close to the surface (x/r_1=0.5) the model predicts an increase of almost a factor 100,000 in cluster concentration. One can no longer speak of a diluted system and therefore coagulation of the clusters has to be taken into account.

6.2.2 Rapid coagulation theory

The theory of rapid coagulation is valid if attractive forces between particles are dominating. Repulsive forces resulting from electrical charges can be neglected, because of the high ionic strength in electrolyte solutions in industrial crystallizers. The domination of attractive forces therefore leads to coagulation. The rate of coagulation is:

$$-\frac{dn}{dt} = \frac{4kT}{3\eta} n^2 \tag{6.6}$$

n stands for the concentration of particles in the suspension and η is the viscosity. From this equation, one can calculate the time in which the concentration of particles is halved:

$$T_c = \frac{3\eta}{4kT} \frac{1}{n_{t=0}} \tag{6.7}$$

The induction time t_{ind} is the time required for all g-mers to become critical g-mers with size g^*. The induction time is estimated by:

$$t_{ind} \approx T_c \frac{g^*}{g} = \frac{3\eta}{4kT} \frac{1}{n_g'} \frac{g^*}{g} \tag{6.8}$$

The assumption made to derive Equation 6.8 is that a cluster of size g does only coagulate with other clusters of size g to form a new cluster of size $2g$.

6.2.3 Nucleation rate according to the ECSN model

The local nucleation rate per unit volume of the crystallizer can be described by:

$$\left(B_{ECSN}\right)_{local} = \frac{n_g'}{t_{ind}} \frac{g}{g^*} = \left(\frac{4kT}{3\eta}\right)\left(\frac{g}{g^*}\right)^2 \left(n_g'\right)^2 \tag{6.9}$$

ECSN takes only place in a small layer around the surface. This layer is assumed to have a thickness of $2r_g$, therefore the nucleation rate is:

$$B_{ECSN} = \left(B_{ECSN}\right)_{local} 2r_g a_v \tag{6.10}$$

in which a_v is the surface area per unit volume of suspension.
Combination of the presented equations finally leads to the following nucleation rate for the ECSN mechanism:

$$B_{ECSN} = K[\ln(S)]^6 \exp[2g\ln(S)] \tag{6.11}$$

where:

$$K = \frac{3}{128\pi^2}\left(\frac{3}{4\pi}\right)^{1/3}\left(\frac{n_1^2}{\eta}\right)\left(\frac{1}{V_m}\right)^{11/3}\left(\frac{1}{\gamma_{CL}}\right)^6 (kT)^7 a_v g^{7/3} \exp\left[\frac{A_{131}}{3kT}\frac{r_1}{x} g^{1/3} - 2(36\pi)^{1/3}(V_m)^{2/3}\frac{\gamma_{CL}}{kT} g^{2/3}\right] \tag{6.12}$$

6.2.4 Sensitivity Analysis – ECSN mechanism

Qian and Botsaris (Qian, 1997) indicate three parameters in the ECSN model - g, x/r_1 and a_v.. The specific surface area a_v can easily be calculated from the volumetric crystal hold up and the second moment of the crystal size distribution, whereas g and x/r_1 are both parameters. For ammonium sulphate, the third parameter is the Hamaker constant (A_{131}) for which no data is available in literature. The Hamaker constant A_{131} and the distance x are present in Equation 6.12 as a ratio. Therefore, they have opposite effects on the nucleation rate. Shorter distances (x) increase the cluster concentrations and triggers ECSN at lower supersaturation values. A higher Hamaker constant leads to higher attractive forces and thus, results in higher cluster concentrations and nucleation at lower supersaturation. The following range has been determined from literature data (Bergstrom,1997) for other inorganic salts for the Hamaker constant of ammonium sulphate:

$$0.31 \cdot 10^{-20}\, J < A_{131} < 8.0 \cdot 10^{-20}\, J \tag{6.13}$$

The range for the distance x has been determined from the sensitivity analysis. At distances above $x/r_1=8$, the attractive forces are too low and cluster concentrations are approximately equal to bulk concentrations. The lower limit has been set at $x/r_1=0.5$. Distances smaller than the half of the molecular radius are unrealistic. Therefore, the following range has been used:

$$0.5 \le x / r_1 \le 8 \tag{6.14}$$

Details on how each parameter and on how the interfacial energy effects the cluster concentrations and the ECSN nucleation rate are presented in Appendix A6.2.

The size of the coagulating clusters (g) is the third parameter. Plots in which the cluster concentration is plotted against the cluster size (like Figure 6.3) give an indication for the value of g. Theoretically, the range for the value is:

$$1 \le g \le g^* \tag{6.15}$$

Qian and Botsaris make an assumption that the interfacial energy of clusters is much lower than the interfacial energy of crystals. This assumption leads to high cluster concentrations, even at large cluster sizes. Figure 6.4 and Figure 6.5 show the ECSN rate of ammonium sulphate for interfacial energy of 6.76 mJ/m^2 and for 1.68 mJ/m^2. The first value is the interfacial energy for crystals while the second value is just four times lower. The ECSN rates are plotted at 50ºC and for a specific surface area of 1000 m^2/m^3. Figure 6.5 clearly indicates that a lower interfacial energy results in a larger value for the coagulating size g. The dependency of the ECSN mechanism on supersaturation is stronger for lower interfacial energy. This makes sense since cluster concentrations are much higher for lower interfacial energy.

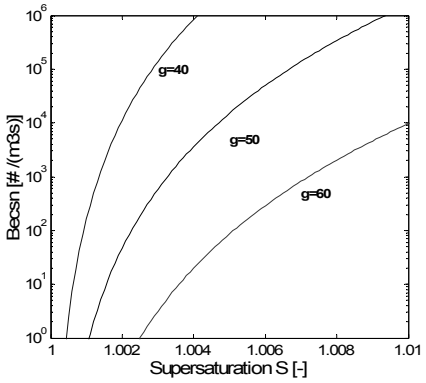

Figure 6.4 ECSN rate for different values of cluster size for A_{131}=4e-20 J, x/r_1=1 and γ_{CL}=6.76 mJ/m^2

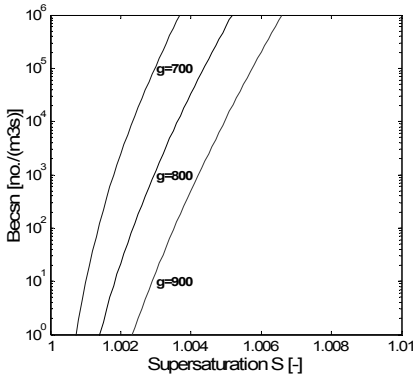

Figure 6.5 ECSN rate for different values of cluster size for A_{131}=4e-20 J, x/r_1=1 and γ_{CL}=1.68 mJ/m^2

6.2.5 Is ECSN Realistic?

The underlying concepts of the ECSN mechanism cannot be questioned :

- The existence of sub-critical embryos
- The existence of inter-particle forces between clusters and crystals due to dipole-dipole interactions

A lot of assumptions have been made to come to a usable set of equations. The main assumptions are:

- Interfacial energy is constant and not a function of cluster size
- Clusters have a low interfacial energy than crystals
- Only attractive forces act between cluster and/or crystals
- Clusters of size g only coagulate with other clusters of size g in order to form a cluster of size $2g$
- The layer thickness in which nucleation takes place has a thickness of $2r_g$.

All these assumptions can be questioned. But especially the second one is critical, as lowering the interfacial energy has a drastic effect on the cluster concentrations and on the cluster sizes. Assuming a lower interfacial energy pushes the mechanism in the right direction.
The removal mechanism of nuclei is unclear. Coagulation takes place very close to the surface and the distance to the surface is smaller than the molecular diameter, in the order of nanometers. The mechanism describes the fact that clusters are attracted into the Van der Waals field. Therefore, it is not possible for a cluster to escape the Van der Waals field, certainly not after it has exceeded the critical nucleus size. Botsaris argues that removal might be enhanced by fluid-shear and collisions. According to mass and heat transfer theories, there is a film layer present around a particle, which is in the order of microns. The film layer is stagnant and therefore removal by fluid-shear is not likely to happen.
The derivation of the cluster concentrations in the surface layer is also questionable. The energy of interaction between a large crystal and an embryo (Equation 6.1) is added to the nucleation work (Equation 6.2). This is not the case as the energy of interaction should only have a concentrating effect and should not influence the nucleation work at all.
It can be concluded that the basic concepts of ECSN are very strong, except for the removal mechanism of nuclei and the assumptions made in the mathematical description which can also be questioned.

6.3 SURFACE NUCLEATION

Mersmann(1996) proposes an activated secondary nucleation mechanism, which is called *surface nucleation*. The equations used to describe surface nucleation are based on 2D surface nucleation of steps (Dirksen,1991) which is a mechanism used for the description of crystal growth. Mersmann proposes that some of these growth units can be released from the surface and grow out to 3D-nuclei.

6.3.1 Theory

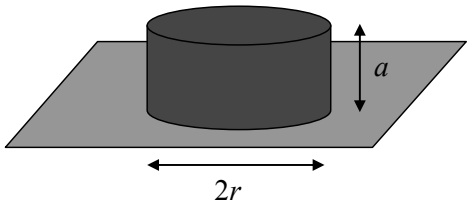

Figure 6.6 Cylindrical embryo on flat crystal surface

The theory deals with the formation of embryos on parent crystals. The shape of the embryos is often assumed to be cylindrical. Figure 6.6 shows the dimensions of a cylindrical embryo. The height of an embryo a corresponds to the height of one growth unit (i.e. atom or molecule). The Gibbs free energy change for nucleation of a cylindrical embryo on a flat surface of a parent crystal is given by

Equation 6.16. The molecular volume v of the embryo is estimated by a^3.

$$\Delta G_r = -\left(\frac{\pi r^2 a}{v}\right) kT \ln(S) + 2\pi r \gamma_e \tag{6.16}$$

The first term corresponds to the change in free energy due to the volume change of the embryo, while the second term results from the change in the length of the edge of the embryo. The first term is negative, while the second is positive. γ_e represents the edge free energy, which has the dimension J/m. Both terms in Equation 6.16 are a function of radius r. Similar as in primary nucleation, there exists a maximal value of the Gibbs free energy change, which occurs at the critical cluster size:

$$r_S^* = \frac{\gamma_e a^2}{kT \ln(S)} \tag{6.17}$$

The number of molecules in a critical cluster is:

$$n^* = \frac{a\pi (r_S^*)^2}{v} = \frac{\gamma_e^2 a^2 \pi}{(kT \ln(S))^2} \tag{6.18}$$

And the value of the Gibbs free energy at this maximum is:

$$\Delta G^* = \pi \frac{\gamma_e^2 a^2}{kT \ln(S)} \tag{6.18}$$

The height of the embryo a can be replaced by the molecule diameter d_m. The crystal density c_c can be used to make a rough estimate of the molecular diameter.

$$a \approx d_m \approx \left(c_c N_A\right)^{-1/3} \tag{6.19}$$

The edge energy is an unknown quantity for ammonium sulphate. The product of the interfacial energy and the molecular diameter is a frequently used approximation for the edge energy:

$$\gamma_e \approx \gamma_{CL} d_m \tag{6.20}$$

The rate of cylinders created on the surface per square meter per second is a function of the maximum Gibbs energy. An expression for this rate is available from 2D surface nucleation of steps (Dirksen, 1991):

$$B_S = \frac{D}{d_m^4} \exp\left[-\frac{\Delta G^*}{kT}\right] \tag{6.21}$$

Substitution of Equations 6.18 to 6.21 leads to:

$$B_s = \frac{D}{d_m^4} \exp\left[-\frac{\Delta G^*}{kT}\right] = \frac{D}{d_m^4} \exp\left[-\frac{\pi \gamma_{CL}^2 d_m^4}{(kT)^2 \ln(S)}\right] \tag{6.22}$$

The dimension of B_s is number of embryos per m^2 crystal surface per second. Two final steps are required to come to an expression, which has the dimension of nuclei per unit volume of solution per second.

Firstly, not all cylinders on the surface will create nucleation in the solution. Only a fraction E of the cylindrical embryos is removed and therefore only this fraction causes nucleation in the solution. So E represents the fraction of surface nuclei that is removed from the surface to become a volume nucleus (Mersmann, 1996). The value of E is not known and is a parameter.
Secondly, the surface nucleation rate is proportional with specific surface area. The final formula for surface nucleation is:

$$B_{surf} = Ea_v B_S = \frac{Ea_v D}{d_m^4} \exp\left[-\frac{\pi \gamma_{CL}^2 d_m^4}{(kT)^2 \ln(S)} \right] \tag{6.23}$$

Mersmann substitutes an equation for the interfacial energy into the final equation for the surface nucleation rate.

$$\gamma_{CL} \approx \frac{kT}{3d^2{}_m} \ln\left(\frac{c_c}{c_{sat}} \right) \tag{6.24}$$

As a result the final equation as given by Mersmann(1996) is:

$$B_{Surf} = \frac{Ea_v D}{d_m^4} \exp\left(-\frac{\pi}{9} \frac{\left[\ln\left(c_c / c_{sat} \right) \right]^2}{\ln\left(S \right)} \right) \tag{6.25}$$

The interfacial energy is eliminated from the final equation. The estimate described by Equation 6.24 has been tested for 58 inorganic systems (Mersmann, 1990). The mismatch between the calculated and the experimental determined interfacial energy is on average 21%. From Equation 6.25, it is no longer clear that there is so much uncertainty inside the exponential term and it is therefore advised to use equation 6.23.

6.3.2 Sensitivity analysis

Surface nucleation contains only one parameter and this is the removal efficiency E. The activated behavior of surface nucleation is mainly caused by the exponential term, whereas E appears only in the pre-exponential term. Hence, the influence of this parameter E is very weak. Hence, terms inside the exponential term have a very pronounced influence on the surface nucleation rate. These terms are temperature, interfacial energy and off course, supersaturation.

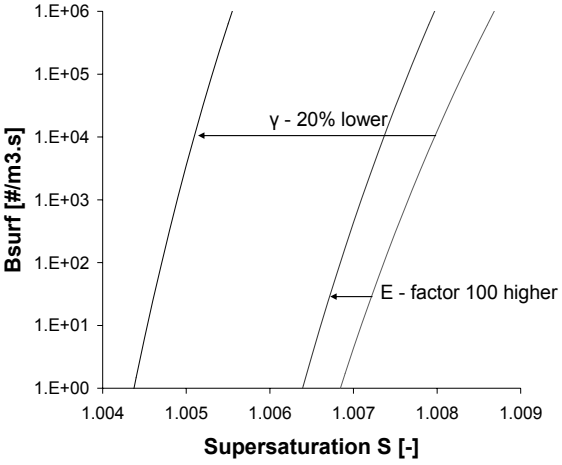

Figure 6.7 Sensitivity of surface nucleation with respect to E and γ_{CL} (T=50°C, a_v=1000 m²/m³, E=0.5 and γ_{CL}=6.76 mJ/m²)

Figure 6.7 compares the influence of the parameter E and interfacial energy. The expected inaccuracy in interfacial energy is 21%. The influence of this uncertainty is much larger than the influence of E. Based on Figure 6.7, one can conclude that E and γ_{CL} have the same influence on the surface nucleation rate and that it is much more effective to use the uncertainty in γ_{CL}. The figure also gives an illustration of the activated nature of the mechanism. Only a small increase in supersaturation is required to increase the nucleation rate by several orders of magnitude. Temperature is also present in the exponential term in the form of kT. But temperature also affects the interfacial energy and solubility. Temperature variations of 5 °C have been used to test the sensitivity with regards to temperature. The influence turned out to be very weak. The same is true for the specific surface area a_v . Surface nucleation is only proportionally related to a_v. Details on the sensitivity analysis are presented in Appendix A6.3.

6.3.3 Is Surface Nucleation Realistic ?

Mersmann(1996) made some approximations (with regards to edge energy, interfacial energy and height of a embryo) to get to an easy-to-use equation. These approximations introduce some quantitative uncertainties, but do not undermine the basic concepts. The chief limitation with the 2D-nucleation theory is the fundamental understanding of the removal of surface nuclei into the bulk. This removal is taken into account by introducing a simple efficiency factor E, while the physical origin of this removal remains unclear. Mersmann(1996) suggests that dendrite detachment mechanism is the most likely removal mechanism, and further suggests that removal is enhanced by collisions and by fluid-shear.
Dendrite detachment is not very likely. The formation of dendrites requires high supersaturation. At the base of a dendrite, the surface area is curved and therefore the base of the dendrite dissolves and subsequently the dendrite is released into the bulk. For 2D-surface nuclei, this is not possible, as the nuclei are assumed to be cylindrical-shaped with a height of around one molecular diameter. One can therefore not distinguish between a base of a dendrite and a top.
Collisions and fluid-shear are unlikely candidates to explain the removal. Fluid-shear forces are not powerful enough to do so, besides the cylinders are much too flat to exert a reasonably force on. Collisions are off course more powerful. However the decrease in metastable limit due to the presence of seeds is also observed in stagnant solutions.

6.4 PRIMARY AND ACTIVATED NUCLEATION MECHANISMS

Experimentally, it has often been observed that the metastable limit of a solution decreases in the presence of seeds. It is likely that some secondary nucleation mechanism exists, which has a strong dependency on supersaturation. The existence of such a mechanism could be a reason for the occurrence of oscillatory behavior in industrial crystallizers.

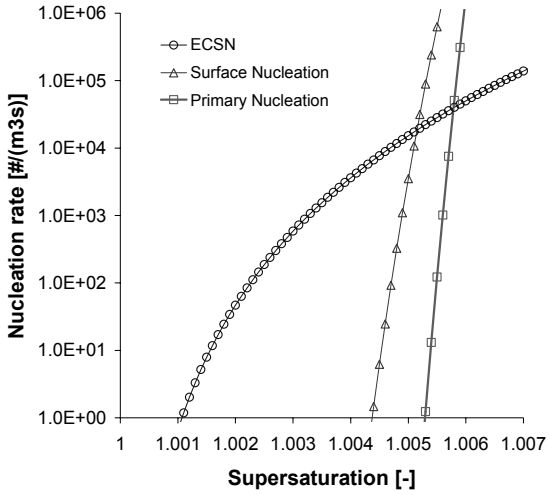

Figure 6.8 Dependency of various nucleation mechanisms on supersaturation

Figure 6.8 compares the dependency on supersaturation of surface nucleation, ECSN and primary nucleation (Kashchiev, 2000). The activation barrier for primary nucleation is slightly higher than for surface nucleation. In general, it is noticed that ECSN has a much weaker activated behavior than surface nucleation, regardless of the parameters used. The parameters in the models are very useful in switching the curves to higher or lower supersaturation, but are less effective in changing the steepness of the curves.

6.5 DYNAMIC SIMULATIONS

The two-population balance model approach, discussed in section 5.5 in Chapter 5 is used here to test whether the activated nucleation mechanisms reproduce the sustained cyclic behavior observed in a 1100L DTB crystallizer. The term B_0 in Equation 5.16 is given by either B_{ECSN} or B_{surf}, depending on the activated nucleation model being used. The system studied was the evaporative crystallization of ammonium-sulphate from water, for the same process conditions as listed in Table 5.1 (see Chapter 5). The first goal is to see whether a combination of attrition with one of these activated nucleation models is able to give rise to oscillatory behavior. Hence, the mechanisms have first been tested with a single compartmental structure. Thereafter, the rigorous crystallizer model is extended into a multi-compartmental model that includes a boiling zone and a fines dissolution system.

6.5.1 One-compartmental model

The results for surface nucleation are presented first and subsequently the results for the ECSN mechanism. For model analysis and to check the sensitivity of the different model parameters, the CSD experimental data, viz. the L_{10}, L_{50} and the L_{90} will be used as a basis. Here, the 1100L DTB crystallizer is treated as a single compartment model without any provision for a fines dissolution zone. This is not a realistic case and this also renders the crystallizer as a uniformly well-mixed vessel without accounting for any possible hot-spots in localized regions. Hence, this single-compartment model is used as an exploratory case-study to check the sensitivity of the model parameter(s) on the process dynamics.

6.5.1.1 Surface Nucleation

The simulation results are in reasonable agreement with experimental data. The first peak of the experimental data is higher then the other peaks. But, as seen from Figure 6.9, the simulations don't exhibit any such behavior. The simulations have been optimized to describe the amplitudes of the dynamic steady-state and therefore, the initial amplitude is a bit off-mark. The amplitudes for L_{10} and L_{50} of the simulations have approximately the same magnitudes as the amplitudes of the experimental

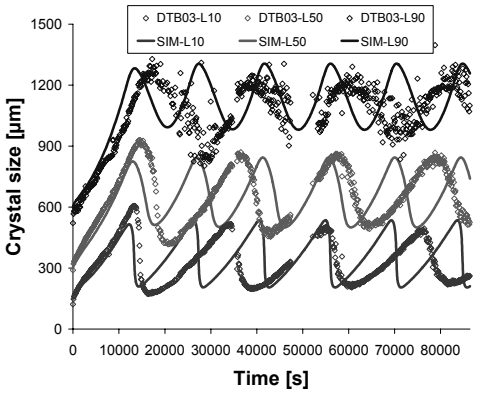

Figure 6.9 Quantiles for experimental and simulated results

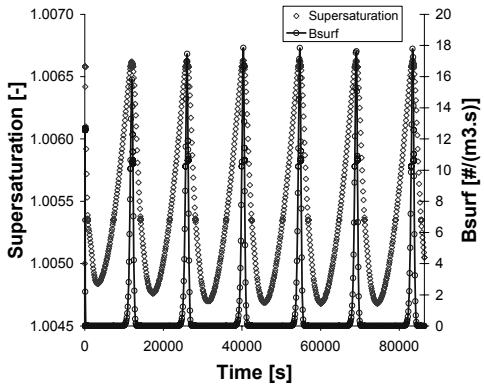

Figure 6.10 Supersaturation (left axis) and surface nucleation rate (right axis)

Γ_s =2.4.10^{-3} Jm/mol, k_r =6.10^{-7} m^4/(mol s) and γ_{CL}=6.76 mJ/m^2

data while it predicts slightly smaller amplitudes for the L_{90}. For all crystal sizes, the period of oscillation is too short compared to the experimental data, for eg. in case of the L_{50}, the experimental data has 4 complete periods, while the simulated L_{50} has 5.5 periods.
Figure 6.10 shows a periodic surface nucleation burst occurring at regular intervals, when the supersaturation has reached a certain critical value. This periodic crop of fresh secondary nuclei is essentially responsible for the sustained cyclic behavior observed in experiments. Later on, a more comprehensive analysis on these oscillations will be presented.

The results concerning the median sizes are quite similar to the results obtained by Menon (2005), in which primary nucleation instead of surface nucleation was used. The values of the kinetic parameters are however different and the predicted supersaturation level in the crystallizer is much higher (Figure 6.10) . However, the height of the surface nucleation peaks corresponds again with the height of the primary nucleation peaks published by Menon.

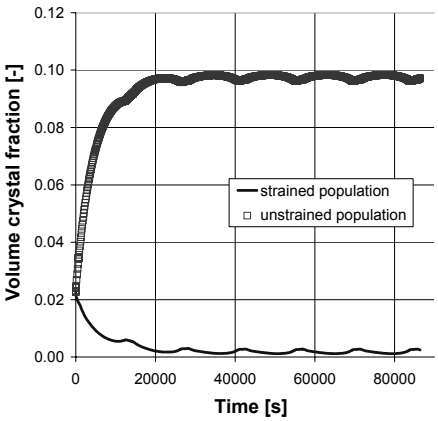

Figure 6.11 Volumetric crystal fraction of strained crystals and unstrained crystals for Γ_s =2.4.10^{-3} J.m/mol, k_r =6.10^{-7} m^4/(mol s) and γ_{CL}=6.76 mJ/m^2.

It is interesting to look at the distribution of the crystals over the two populations(see Figure 6.11). The first population contains the unstrained population. These crystals originate from surface nucleation. The second population contains the strained crystals. Strained crystals are formed by attrition. It is obvious that the unstrained population is much larger than the strained population. The interaction between the two populations due to attrition can be seen back in Figure 6.11. A decrease in the unstrained crystal fraction goes together with an increase in the strained crystal fraction. This is similar to the observation for the two-population balance model, embedding the primary nucleation model within it (Menon, 2005).

Influence of model parameters

The two-population balance model equipped with Gahn & Mersmann kinetics and with surface nucleation contains four parameters. Two parameters result from the kinetic framework (k_r and Γ_s from Equations 3.61 and 3.63 in Chapter 3) and two from the surface nucleation mechanism (uncertainty in γ_{CL} and E). Unfortunately, parameter estimations studies could not be realized. Hence, insights into how each of the parameters influences the dynamic behavior are important.

The basic approach is that the supersaturation level can be set by the kinetic parameters Γ_s and k_r. All crystallization phenomena are in some way coupled to the supersaturation level, especially surface nucleation. Once the supersaturation in the crystallizer has been set, the parameter E and the uncertainty in interfacial energy can be adjusted in such a way that surface nucleation is triggered at the predicted supersaturation level.

Kinetic parameters k_r and Γ_s

The surface related energy increase Γ_s and the integration rate constant k_r are two parameters from the kinetic framework described in Chapter 5. Small changes can be used to fine-tune the median sizes. For example, a small increase in k_r can be used to increase the median sizes (Figure 6.12). An increase in k_r leads to lower supersaturation levels in the crystallizer and at a certain value of k_r, the supersaturation is too low to activate surface nucleation. On the contrary, a decrease in Γ_s leads to a lower supersaturation. Large variations in these parameter values are able to affect the shape of the dynamic behavior, since they influence the supersaturation level. This is illustrated in Figure 6.13, where Γ_s has been decreased until the dynamic steady state disappears. Too large changes in either k_r or Γ_s can switch off the dynamic steady state or lead to unrealistically high nucleation rates.

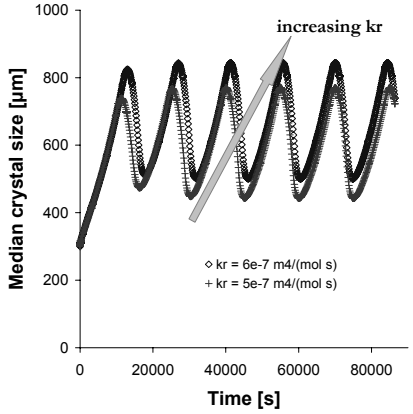

Figure 6.12 Influence of changes in k_r on L_{50}

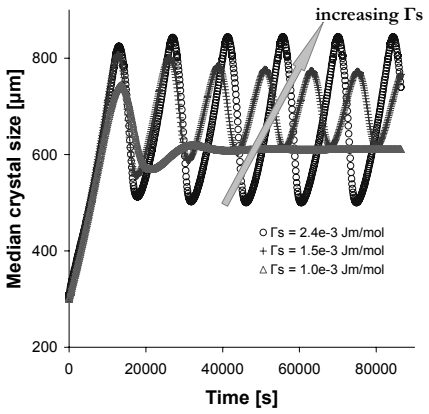

Figure 6.13 Influence of changes in Γ_s on L_{50}

Removal efficiency E and uncertainty in γ_{CL}

The influence of E and γ_{CL} do not directly change the supersaturation level in the crystallizer like the kinetic parameters. Instead, they change the dependency of surface nucleation on supersaturation. Mersmann (1990) has tested Equation 6.24 for 58 systems. The average mismatch between the calculated interfacial energy and the experimentally determined one is 20%. In addition, there is an uncertainty in the relation between the edge free energy and the interfacial energy. This uncertainty can be used as a parameter in the simulations.

Again small changes in γ_{CL} can be used for fine-tuning the quantiles (see Figure 6.14). For example, an increase in interfacial energy from 6.76 mJ/m^2 to 7.12 mJ/m^2, shows an increase in values of the quantiles without affecting the dynamics, whereas still larger changes result in completely different dynamic behavior.

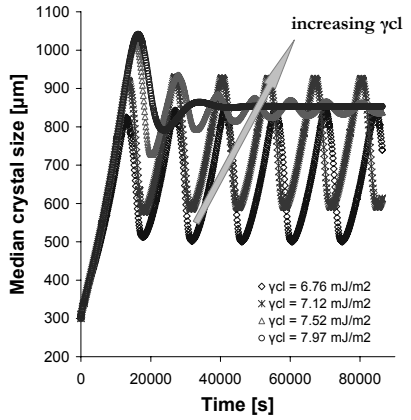

Figure 6.14 Influence of changes in γ_{CL} on L_{50}

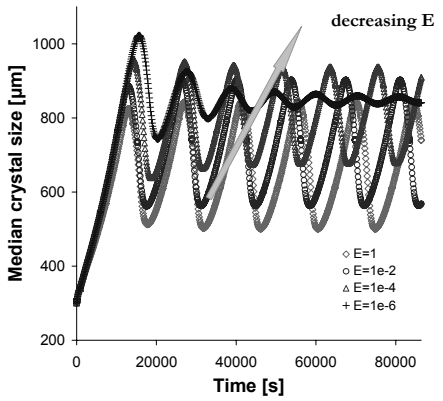

Figure 6.15 Influence of changes in E on L_{50}

The same is true for E, but only in this case, large changes are observed by changing E by a factor exceeding 1.10^5 (see Figure 6.15). And therefore the effect of E is easily compensated by a change in γ_{CL}, as was already analyzed in the sensitivity analysis in sub-section 6.3.2 (see Figure 6.7).
The effect of the individual parameters on the amplitude and period of the oscillations is very difficult to map. Small changes don't lead to significant differences in amplitude and period. For larger changes, each of the parameters is able to change the dynamic response of the system. Therefore, a change in one of the parameters often leads to a change in dynamic behavior and sustained oscillations change into damping oscillations and it is thus, not possible to analyze the effect of a single parameter on amplitude and period.
Generally, it is noticed that an increase in Γ_s and γ_{CL} in combination with a decrease in k_r leads to oscillations with a larger amplitude and a longer period. This process has been repeated in small steps until the interfacial energy has reached the value of 6.76 mJ/m^2, which is the value as calculated by Equation 6.24. A parameter-set of Γ_s = 2.4 .10^{-3} J.m/mol and k_r = 6. 10^{-7} m^4/(mol.s) leads to the best description of the experimental results for γ_{CL}=6.76 mJ/m^2, as was depicted in Figure 6.9, for a single-compartment model.

Insight into the oscillations
In this sub-section, a closer look into the oscillations is presented. The consumption of supersaturation by crystal growth depends on the surface area of the crystals. Also the surface nucleation rate is proportional with the surface area of the crystals. Therefore, the specific surface area is an important variable to monitor. In Figure 6.16, the specific surface area of the two populations are shown.
The specific surface area a_v of the unstrained population is much larger compared to the strained population. This is off course expected from the crystal fractions of both populations. The specific surface area is not only a function of the crystal fraction but also of the crystal size. The specific surface area of the unstrained population shows oscillations with a large amplitude.

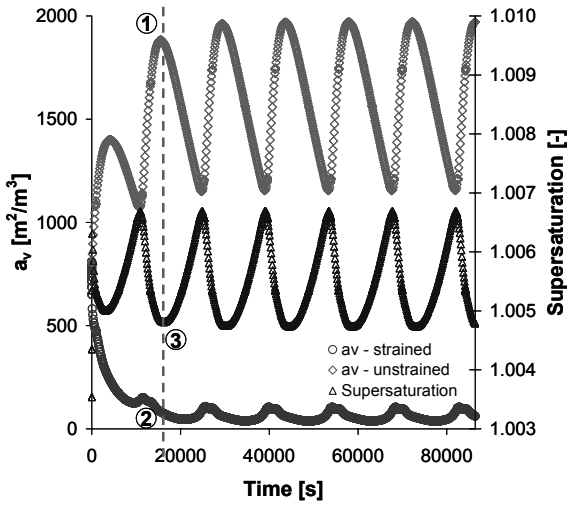

Figure 6.16 Specific surface area of the strained and unstrained populations (left axis) and supersaturation (right axis)

First, let's focus on the unstrained population. The minima in specific surface area coincides with the maxima in supersaturation. At these points, a surface nucleation burst occurs (as shown in Figure 6.10). These surface nuclei are assumed to be strain free and are introduced into the unstrained population. These surface nuclei start to grow and due to the high number of these new nuclei, the specific surface area of this population increases very rapidly. Consumption of supersaturation by crystal growth (which is proportional to the product of the growth rate and the specific surface area) is therefore also rapidly increasing.
As the maximum in surface area (point 1) for the unstrained population is reached, the supersaturation passes through a minimum(point 3). The crystal growth rate is a positive function of supersaturation and is therefore also minimal. At these points, there is equilibrium between consumption of supersaturation by crystal growth and production of supersaturation by evaporation. As the surface area of the unstrained population starts to reduce due to growth, continuous product removal and attrition, then the supersaturation increases again. This increase continues until a burst of surface nuclei is generated again.

A closer look at the strained population shows that just after point 2, the specific surface area of the strained crystals starts increasing which is a result of the increase in secondary nucleation rate by attrition. In the above qualitative analysis, the influence of the strained population is neglected because the strained population is much smaller than the unstrained population. Hence, the dominant secondary nucleation mechanism that influences the process dynamics to a greater extent, is the surface nucleation population.

Number densities
The main reason for oscillations is the periodic burst of surface nuclei and subsequently their outgrowth. To see how such a burst influences the number densities, a closer look at a single oscillation period is presented. The selected oscillation (see Figure 6.10) starts approximately at 30,000 s and ends around 45,000 s.
At the starting point around 30,000 s, the supersaturation is minimal (see Figure 6.16). The line representing the number densities of the unstrained population (see Figure 6.17a) at this moment in time shows a small bump around 250 μm. As time progresses to the second point at 35,000s[1], the bump has moved to larger size classes due to crystal growth, but also the height of the bump has decreased due to product removal. The next point in time (at t=39,000s) has been selected at the moment of a surface nucleation burst, which creates a lot of new unstrained nuclei. It is clearly perceptible that the number densities in the lower size classes have increased enormously, which are introduced into the first population balance via boundary condition 5.16 (Chapter 5). Note that a logarithmic grid is used with respect to the size classes. The absolute width of a size class at the lower end of the distribution is in the order of microns, while at the upper end the width is two orders in

[1] This curve cannot be clearly seen in the figure.

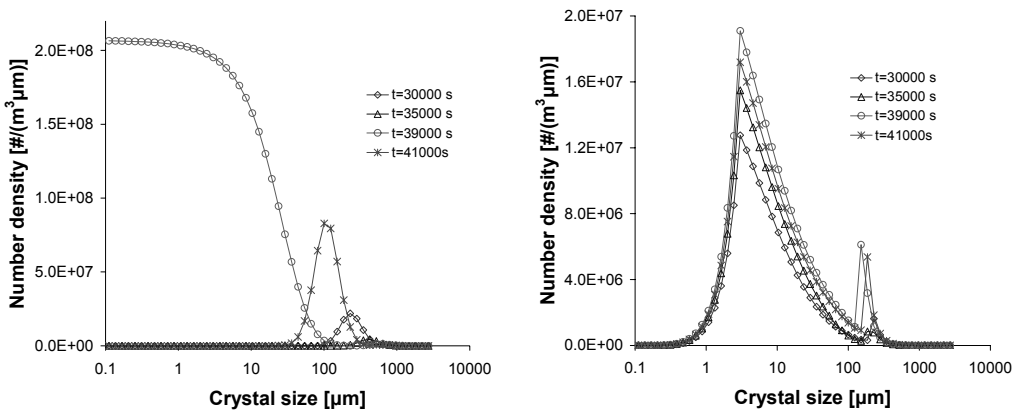

(a) for unstrained population (b) for strained population

Figure 6.17 Change in number densities during an oscillation

magnitudes larger. This implies that at the lower size classes, the time required to grow to a higher size class is relatively small. Therefore at 39,000 s the nucleation burst has been distributed almost evenly over the first 20 size classes. The surface nuclei grow out to larger sizes and the number densities are lowered due to product removal, resulting in a smaller peak around 100 µm at t=41,000 s. The oscillation period ends at 45,000 s and then the number densities are approximately the same as at the starting position, and this trend continues with time.

The number densities of the strained population (see Figure 6.17b) are monitored at the same time intervals as the number densities for the unstrained population. As expected from the crystal fraction, the number densities are much lower when compared with the unstrained population. As seen in Figure 6.17b, the number distribution of the strained population is bimodal. A closer look at the large peak shows an increase in number densities from 30,000 s to 35,000 to 39,000 s. The reason for this is the supersaturation increase in this period (Figure 6.16), which causes an enhanced outgrowth of attrition fragments. Also, the number of newly generated attrition fragments increases as well in this period due to the increasing crystal size. At 39,000 s, the secondary nucleation mechanism is taken over by surface nucleation, hence from here on the number densities start to decrease for the strained population. This makes sense, because the supersaturation decreases and therefore the outgrowth of the strained attrition fragments is also correspondingly lower. The second small peak which is seen around 150 µm is a result of the switch in growth rates from a negative to positive value after a certain size class, for the strained nuclei. This forms a sort of trap for the particles as the growth rate is low at that part of the size class domain, due to which the crystals start piling up thus, resulting in a peak in the number density. But, as soon as they move further in the size class, the growth rate increases and the number density drops as well.

6.5.1.2 Embryo Coagulation Secondary Nucleation

The Embryo Coagulation Secondary Nucleation (ECSN) mechanism is the second activated secondary nucleation mechanism that has been tested in order to explain oscillatory behavior. In this section, three simulation results for the ECSN mechanism are discussed. The parameter settings for each simulation can be found in Table 6.1 :

Table 6.1 Parameters for ECSN simulations

Simulation	k_r $[m^4/(mol\ s)]$	Γ_s $[Jm/mol]$	A_{131} $[J]$	x/r_1 $[-]$	g $[-]$	γ_{CL} $[mJ/m^2]$
ECSN_1	6.10^{-07}	$2.4.10^{-03}$	4.10^{-20}	2	60	6.76
ECSN_2	$6.\ 10^{-07}$	$2.4.10^{-03}$	4.10^{-20}	3	800	1.68
ECSN_3	$6.\ 10^{-07}$	$2.4.10^{-03}$	4.10^{-20}	3	700	1.68

The three ECSN simulations all use the same values for the kinetic parameters k_r and Γ_s. These kinetic parameters set the supersaturation level in the crystallizer around 1.006. The ECSN equations (equation 6.11 and 6.12) contain three parameters which all have a strong influence on the nucleation rate and can be used to trigger activated secondary nucleation at a supersaturation level of around 1.006.

The ECSN model wasn't able to obtain a dynamic steady state at these parameter values. A lot of simulations were done for different parameter combinations and ECSN_1 (Figure 6.18) is a representative result. The nucleation rate is low (Figure 6.19) and reaches a steady-state value after approximately seven residence times. ECSN_1 uses a value of 6.76 mJ/m^2 for the interfacial energy, which is calculated from Equation 6.24. Qian and Botsaris (1997) make the assumption that the interfacial energy for clusters is lower than for crystals. In sub-section 6.2.4, it was shown that this assumption makes the mechanism more activated. Hence, to check this effect, simulations ECSN_2 and ECSN_3 use a lower value for the interfacial energy.

ECSN_2 and ECSN_3 both exhibit more oscillatory behavior compared to ECSN_1. This is because the dependency of the ECSN rate on supersaturation is stronger in case of ESCN_2 and ECSN_3. But, still no dynamic steady state has been obtained from the simulations and the oscillations were found to damp out after a few cycles. In case of surface nucleation, such behavior could easily be transferred to sustained oscillations by increasing the nucleation rate.

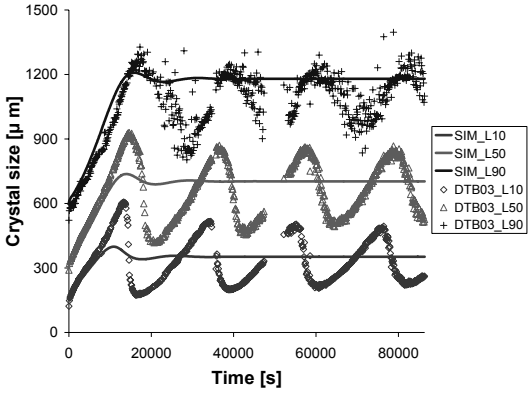

Figure 6.18 Quantiles for experimental and simulated data for simulation ECSN_1

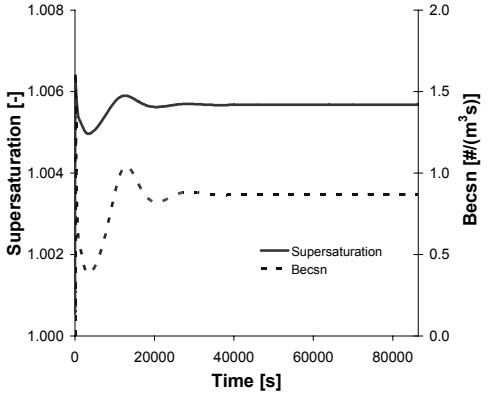

Figure 6.19 Supersaturation (left axis) and ECSN nucleation rate (right axis) for simulation ECSN_1

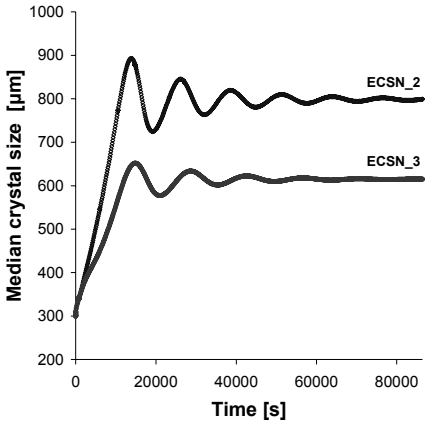

Figure 6.20 Dynamic median crystal size (L_{50}) for simulations ECSN_2 and ECSN_3

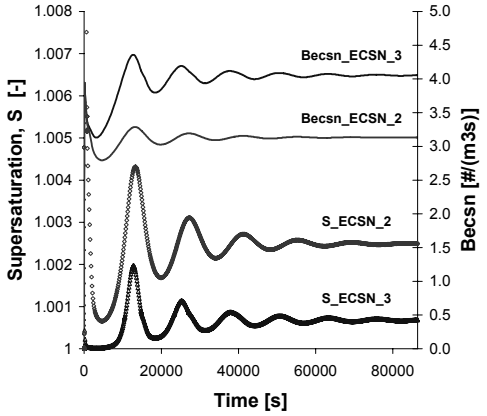

Figure 6.21 Supersaturation (S) on the left axis and ECSN nucleation rate (B_{ECSN}) on the right axis, for simulations : ECSN_2 (g=800) and ECSN_3 (g=700)

The next step was therefore to increase the ECSN rate in order to get a higher burst of nuclei and probably also induce the sustained cyclic behavior. One-way to do this is by using a lower value for *g*. ECSN_3 uses *g=700* instead of *g=800*. From Figure 6.20, it is clear that still no sustained oscillations occurred. ECSN is activated at lower supersaturation for *g=700* and therefore its steady state nucleation rate is higher. Figure 6.21 shows the influence of *g* on the supersaturation level and the ECSN nucleation rates. For *g=700*, the supersaturation is lower compared to *g=800*, but the ECSN rate is higher and consequently, the L_{50} is lower. Figure 6.21 clearly shows that the dependency of embryo coagulation is too weak to cause oscillatory behavior. After a peak in supersaturation has been reached, the ECSN mechanism is not switched off, but instead it goes to a lower nucleation rate. Surface nucleation was able to be switched on and off and therefore, periodic bursts of nuclei were produced. The weaker dependency of ECSN on supersaturation was already pointed out in sub-section 6.4 (Figure 6.8) .

6.5.2 Two-compartmental model

Multi-compartmental modelling has only been executed for surface nucleation, since the ECSN mechanism wasn't able to produce oscillations. The local supersaturation level in the boiling zone is higher than in the bulk. In literature, it is often suggested that oscillatory behavior might be caused by a periodic nucleation burst in the boiling zone. The first step is to add a boiling zone to the crystallizer models. The main objective at this stage is to isolate surface nucleation in the boiling zone and not in the bulk compartment. Two different compartmental modelling structures were constructed to validate the two-population balance model.

Structure 1

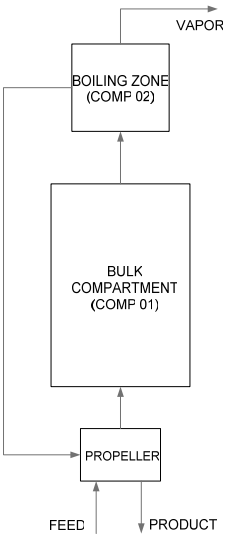

Figure 6.22 Two compartmental model of the 1100 l DTB crystallizer

Figure 6.22 depicts a very simple compartment model of the 1100L DTB crystallizer. In addition to the propeller (mixing compartment), the crystallizer is split into two compartments that include a bulk compartment (Comp 01) and a boiling zone (Comp 02) at the top. The propeller compartment does not count as a concrete compartment, since it has no volume. It is a virtual compartment, in which the Gahn attrition kinetics is calculated. Such a two-compartmental structure introduces one additional unknown, namely the volume of the boiling zone. The first run for the two-compartmental model has been with the optimal parameter set for surface nucleation, obtained from the one-compartmental model. The volume of the boiling zone was set to 5% of the total crystallizer volume.

The surface nucleation rate in the boiling zone is approximately 160 #/m^3.s and in the main body around 10 #/m^3.s (see Figure 6.24). The volume of the main body is however 20 times larger than the boiling zone, and therefore the contribution of the main body to surface nucleation is more than 50%. The supersaturation difference between the two compartments is too small (Figure 6.23). The optimal parameter set obtained from the one-compartmental model combined with a boiling zone of 5% didn't yield an isolated nucleation event in the boiling zone due to this very small segregation achieved in the supersaturation levels in the two compartments. Two methods have been tested in order to locate surface nucleation exclusively into the boiling zone:

- Use uncertainty in interfacial energy to trigger surface nucleation only in the boiling zone
- Reduce the volume of the boiling zone to create larger supersaturation difference between boiling zone and main body

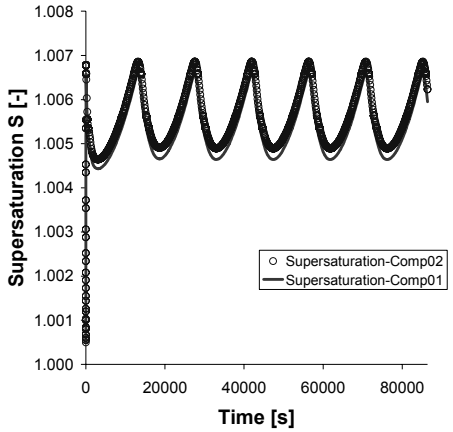

Figure 6.23 Supersaturation in boiling zone (Comp02) and main body (Comp01)

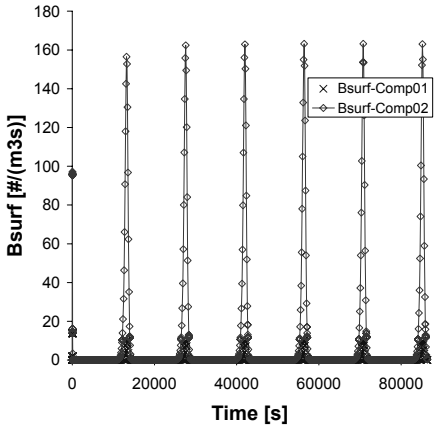

Figure 6.24 Surface nucleation rate in boiling zone (Comp02) and main body (Comp01)

Γ_s =2.4.10^{-3} J.m/mol, k_r =6.10^{-7} m^4/(mol s) and γ_{CL}=6.76 mJ/m^2

The total surface nucleation rate $B_{surf,total}$ in the entire volume of the crystallizer can be defined as:

$$B_{surf,total} = \frac{\sum_{i=1}^{Number\ of\ compartments} (V_i . B_{surf,i})}{\sum_{i=1}^{Number\ of\ compartments} V_i} \tag{6.26}$$

V_i is the volume fraction of compartment i and $B_{surf,i}$ (#/m^3.s) is the surface nucleation rate in compartment i. The contribution of the boiling zone to the surface nucleation rate is then calculated as:

$$Contribution\_bz = \frac{V_2 B_{surf,2}}{\sum V_i . B_{surf,total}} \cdot 100\% \tag{6.27}$$

Uncertainty in surface tension

The easiest way to locate activated nucleation into the boiling zone is by changing its critical supersaturation. For surface nucleation, the uncertainty in interfacial energy has the strongest influence in manipulating the supersaturation level in the crystallizer. For γ_{CL} = 6.76 mJ/m^2, surface nucleation is triggered in both the compartments, as seen in Figure 6.24. The boiling zone has a higher supersaturation and therefore, to locate the surface nucleation exclusively in the boiling zone, it has to be triggered at a higher supersaturation, which in turn implies a higher interfacial energy. The results are presented in Table 6.2. The change in interfacial energy is still within 20% deviation from the value of 6.76 mJ/m^2, which is the expected uncertainty.

Table 6.2 Influence of interfacial energy on location of surface nucleation

Run	γ_{CL} *[m]/m^2]*	B_{surf2}/B_{surf1} *[-]*	$B_{surf,total}$ *[#/(m^{3}s)]*	*Contribution boiling zone [%]*
Sim2C_1	6.76	16.1	17.9	45.8
Sim2C_3	7.12	13.8	8.5	42.2
Sim2C_4	7.52	13.4	4.9	41.5

The results presented in Table 6.2 are calculated from the second peak of the runs. Table 6.2 shows that the method described in this section is not suitable to locate activated nucleation exclusively into the boiling zone as the supersaturation difference is just too small to achieve this.

Influence of boiling zone volume

The extension to two compartments introduced a new parameter, namely the volume of the boiling zone V_2. The volume of the boiling zone has been varied between 1% to 10% to see if this helps in localizing surface nucleation exclusively in the boiling zone.

Table 6.3 Influence of volume of boiling zone on location of surface nucleation

Run	V_2 *[%]*	B_{surf2}/B_{2surf1} *[-]*	$B_{surf,total}$ *[#/(m^{3}s)]*	*Contribution boiling zone [%]*
Sim2C_5	10	14.3	18.6	61.3
Sim2C_1	5.0	16.1	17.9	45.8
Sim2C_2	2.5	16.5	17.6	29.7
Sim2C_6	1.0	16.7	17.7	14.5

The results presented in Table 6.3 again show that the supersaturation difference between the boiling zone and the bulk is too small to locate surface nucleation into the boiling zone. For the default value

of 5%, the nucleation rate in the boiling zone is a factor 16.1 higher, but its volume is a factor 20 smaller. Therefore, the total contribution of surface nucleation located in the boiling zone is only 45.8%. SIM2C_5 shows that surface nucleation is located even better into the boiling zone by using larger boiling zone volumes. This is an unexpected result, since a larger boiling zone decreases the supersaturation difference. Still, the nucleation bursts are not located exclusively into the boiling zone.
Table 6.3 shows that the volume of the boiling zone does not influence the total surface nucleation rate which stays at about 18 nuclei per m^3 per s. Therefore, the volume of the boiling zone has only a marginal influence on the median sizes.

Structure 2

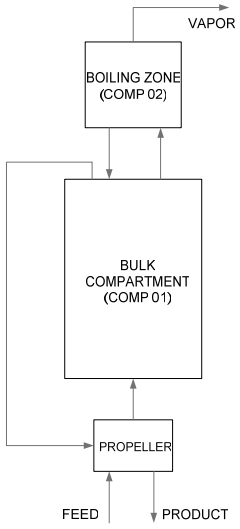

Figure 6.25 Two compartmental model of the 1100 l DTB crystallizer, with separate flow to boiling zone

A second compartmental structure (Figure 6.25) has been constructed wherein the circulation stream is decoupled from the boiling zone. The boiling zone has its own circulation stream. This stream to the boiling zone becomes a new variable, which makes it possible to create larger differences between the bulk and the boiling zone compartment. The flow towards the boiling zone and the boiling zone volume both have to be specified in the rigorous crystallizer model specifications.

Influence of the boiling zone volume
The influence of the boiling zone volume has been tested in a similar way as for the first structure. The flow to the boiling zone is kept constant at 50 l/s.
For all boiling zone volumes, the contribution in surface nucleation was more than 99% (see Table 6.4). The boiling zone volume has no large influence on the crystal sizes. Compare, for example, the first two simulations in Table 6.4. The volume of the boiling zone has been halved from 10% to 5%, as a result of which the surface nucleation rate in the boiling zone doubles. But, the total nucleation rate stays more or less constant and therefore, the influence on the crystal sizes is hardly noticeable.

Table 6.4 Influence of boiling zone volume on nucleation rate

Simulation Run	V_2 *[%]*	$B_{surf,1}$ *[#/(m³s)]*	$B_{surf,2}$ *[#/(m³s)]*	$B_{surf,2}/B_{surf,1}$ *[-]*	$B_{surf,total}$ *[#/(m³s)]*	*Contribution Boiling zone [%]*
Sim2C_O2_4	10	0.0584	222.2	3805	22.28	99.8
Sim2C_O2_1	5.0	0.0542	440.2	8122	22.06	99.8
Sim2C_O2_10	2.5	0.0771	839.1	10879	21.05	99.6
Sim2C_O2_5	1.0	0.1707	1915	11220	19.32	99.1

In Appendix A6.4 , Figure A6.4.1 shows the plots for the median crystal size(L_{50}), for the simulations listed in Table 6.4. The lines for 5% and 10% can hardly be distinguished and hence, it's decided to fix the boiling zone volume at 5.0%.

Influence of flow to the boiling zone
Table 6.5 shows the influence of this new variable, i.e. flow stream to the boiling zone, which has been tested for a fixed boiling zone volume of 5.0%.

Table 6.5 Influence of flow towards the boiling zone on nucleation rate

Simulation Run	$Flow_{BZ}$ *[l/s]*	$B_{surf,1}$ *[#/(m³s)]*	$B_{surf,2}$ *[#/(m³s)]*	$B_{surf,2}/B_{surf,1}$ *[-]*	$B_{surf,total}$ *[#/(m³s)]*	*Contribution Boiling zone [%]*
Sim2C_O2_6	37.5	1.832e-3	477.8	2.608e5	23.89	100
Sim2C_O2_1	50.0	5.421e-2	440.2	8122	22.06	99.8
Sim2C_O2_3	75.0	1.106	365.6	330.6	19.33	94.6
Sim2C_O2_7	100	3.924	289.2	73.70	18.19	79.5

The effect of the flow to the boiling zone is slightly larger than the influence of the volume of the boiling zone. The median crystal sizes shift to smaller sizes for smaller flows (see Appendix A6.4) and the surface nucleation rate is also somewhat higher, however, the amplitude and period of oscillations remain unchanged. At low flow rates to the boiling zone, the description of the start-up behavior of the median crystal sizes is much worse, but this can be improved by changing the initial crystal size distribution, the initial crystal concentration and the initial supersaturation.

Best fit for the two-compartmental model

The best description of the median sizes was achieved for the second compartmental model structure, at the same kinetic parameter set for k_r and Γ_s , as for the 1-compartmental model. In addition, a boiling zone with a volume of 5% of the total crystallizer volume, has been added and the flow to the boiling zone has been set to 75 l/s. Figure 6.26 compares the difference between the single and two-compartmental model.

The amplitudes and periods are almost identical for the 1 and 2-compartmental model. The two-compartmental model starts with a smaller initial crystal size and this introduces a small time-lag. Figure 6.27 shows the nucleation rates and the supersaturation difference between the two compartments.

Figure 6.27 clearly shows that only a small difference in supersaturation is required to exclusively locate surface nucleation into the boiling zone. The nucleation rate in the bulk compartment can be neglected. The nucleation bursts in the boiling zone reach a peak value of approximately 360 #/(m³s) at supersaturation levels of around 1.007. The boiling zone is only 5% of the crystallizer volume. For the single compartment, the peaks were about 18 #/(m³s), which is 5% of 360. Therefore, the description of the median crystal sizes did not change much. The introduction of a second compartment does not lead to a better description of the experimental data, but it does prove that a small boiling zone is able to create nucleation bursts that result in an oscillatory behavior.

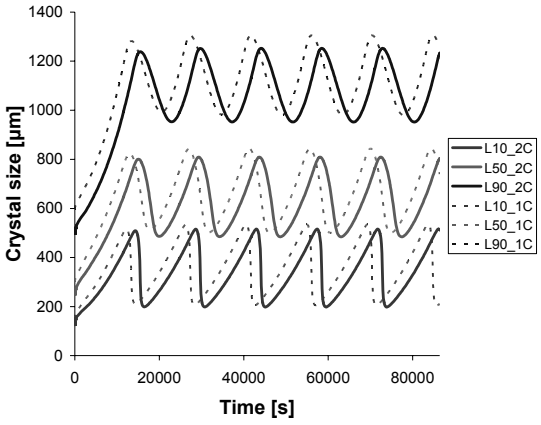

Figure 6.26 Comparison of single (1C) and two-compartmental (2C) models

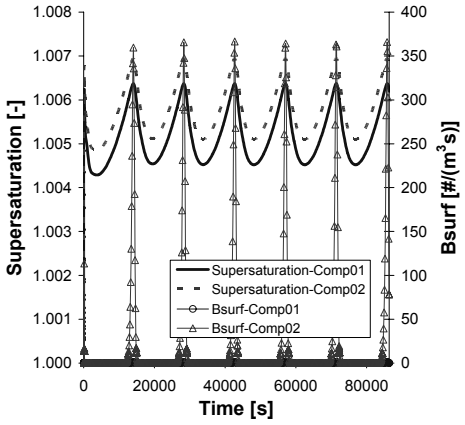

Figure 6.27 Supersaturation and surface nucleation rate for two-compartmental model

Γ_s =2.4.10^{-3} J.m/mol, k_r =6.10^{-7} m^4/(mol s) and γ_{CL}=6.76 mJ/m^2

6.5.3 Three-compartmental model (with fines dissolution)

The second structure of the two-compartmental model is further extended to a three-compartmental model (Figure 6.28), by adding a fines dissolver zone (Comp 03). Addition of the fines dissolver does not introduce any new variables. The flow to the fines dissolver in the experiment was fixed at 2 l/s and the volume of the fines loop is 240L. The heat input of 120 kW/m^3 leads to a 19ºC temperature increase in the fines dissolution loop, which is in line with experimental observations of Neumann (2001).

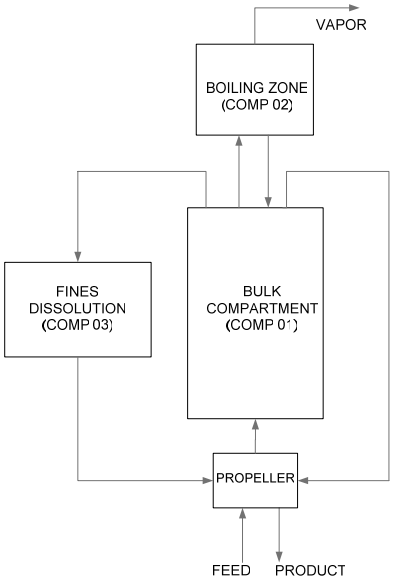

Figure 6.28 Three-compartmental model of the 1100 l DTB crystallizer

Classification in the pilot plant takes place in the annular zone. Fines are removed and destructed; hence the average crystal size increases. In the three-compartmental model, classification is modelled in the stream towards the fines dissolver. The Barnea and Mizrahi model (Barnea, 1973) has been used to simulate the classification behavior. The experimentally determined cut size is 95 μm while the simulations predict a cut size of 94.3 μm. The simulation performed for the three-compartment model (using the optimal parameter set obtained from the two-compartmental model) showed an increase in the supersaturation level in the crystallizer. This makes sense, since fines are continuously being removed and dissolved, which results an increase in supersaturation in the boiling zone from 1.0065 (two-compartment) to 1.0095. The uncertainty in interfacial energy has been used to increase the metastable limit of surface nucleation. Equation 6.24 predicts a value of 6.76 mJ/m^2 for the interfacial energy while the simulation done here uses a value 8.3% higher which is well within the expected uncertainty. The kinetic parameters k_r and Γ_s were set at 6.10^{-7} m^4/mol.s and 3.10^{-3} J.m/mol, respectively.

The description of the median sizes did not improve by adding a fines dissolver (Figure 6.29). The main mechanism behind the oscillations is that the periodic nucleation burst results in a tremendous increase in specific surface area available for growth and subsequently, a decrease in supersaturation. This decrease in supersaturation is partly neutralized by the reduction of surface area due to the removal and destruction of fines. But, at the same time, the dissolution of fines also increases the supersaturation. A combination of these effects is likely to make the oscillations less severe. As seen from Figure 6.29, the periods and the amplitudes of the oscillations decreased when compared to the two-compartmental model (see Figure 6.26). The peaks in supersaturation for the boiling zone compartment reach a value of almost 1.0085 (see Figure 6.30). The oscillatory behavior at even higher supersaturation values has been tested but is regarded as being unrealistic. Metastable limits for clear solutions of ammonium sulphate measured during laboratory

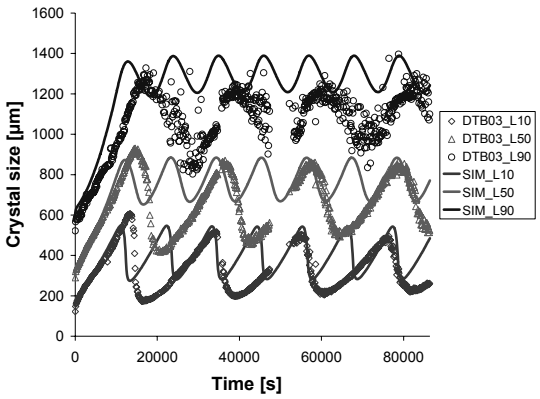

Figure 6.29 Quantiles for experimental and simulated data for three-compartmental model

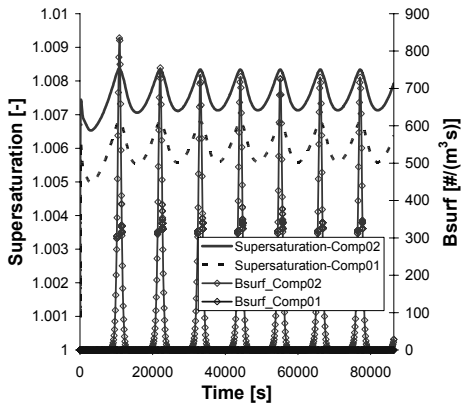

Figure 6.30 Supersaturation and surface nucleation rate for the bulk compartment (Comp01) and boiling zone (Comp02)

Γ_s =3.10^{-3} J.m/mol, k_r =6.10^{-7} m^4/(mol s) and γ_{CL}=6.76 mJ/m^2

experiments on the 1100L DTB crystallizer were found to lie in the vicinity of a supersaturation level of ~1.01 (Menon, 2005). The metastable limit for activated secondary nucleation is lower than for primary nucleation. Hence, an arbitrary value of 1.0085 has been chosen as the upper limit for the metastable limit in the boiling zone of the crystallizer. The height of the nucleation peaks doubled from 360 #/(m^3.s) for the two-compartmental model (see Figure 6.27) to 730 #/(m^3.s) for the three-compartmental model (see Figure 6.30). Higher nucleation bursts are required due to the fact that the fines dissolver reduces the effect of the nucleation bursts.

The periodic nucleation bursts can be found back in the number densities entering the fines dissolver. Experimentally, Neumann(2001) observed sharp periodic peaks in the solid concentrations in the fines loop which coincides with the maxima in median crystal size (Figure 6.31a and Figure 6.31b). The simulated periodic nucleation bursts also coincide with the maxima in median size. This is experimental evidence for the occurrence of periodic nucleation bursts in the 1100L DTB crystallizer. Also, experimentally there is some evidence that a fines dissolver evokes oscillatory behavior, see for example, Eek(1995), Kind and Nieken(1995).

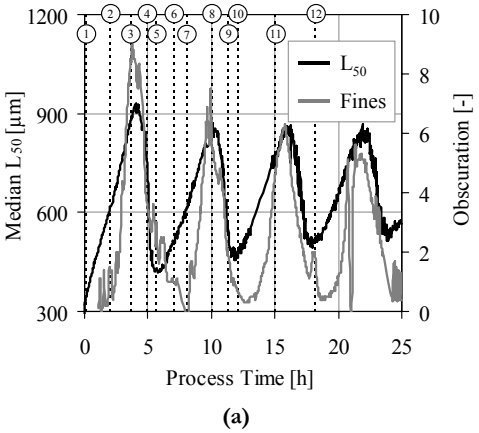

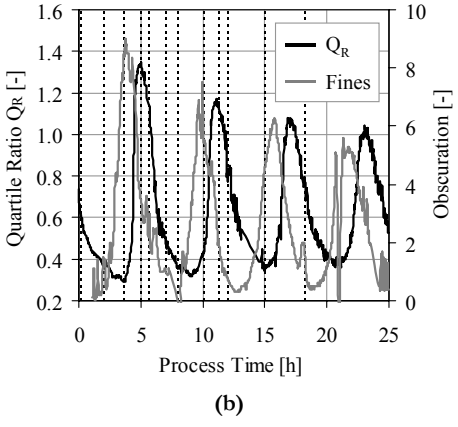

Figure 6.31 Solids concentration in fines flow and (a) median crystal size, (b) quartile ratio (Neumann, 2001)

Oscillations are in general not observed during the operation of laboratory-scale crystallizers. This could be because supersaturation does not exceed the metastable limit for activated nucleation. However, when a fines dissolver is added, the supersaturation level in the crystallizer is expected to increase as the fines do not consume supersaturation by crystal growth, but instead produce supersaturation due to dissolution of fine particles. Due to the increased supersaturation levels, the energy barrier to nucleation is overcome more easily, and hence could induce activated nucleation, which leads to oscillatory behavior. The simulation results from this chapter also predict this result, i.e. if one takes the parameter set of the three compartmental model and uses them in the two-compartmental model, than the oscillatory behavior would disappear. The parameters in the two-compartmental model set the supersaturation level at 1.0065, while the metastable limit is set at 1.0085. Hence, no oscillations occur since the metastable limit is not exceeded. When a fines dissolver is added, the supersaturation in the crystallizer increases to 1.0085 and the metastable limit is exceeded and results in the oscillatory response. So, the experimental results from literature and the simulation results do not contradict each other.

6.6 CONCLUSIONS

It was already shown by Menon(2005) that periodic primary nucleation bursts are able to describe the sustained oscillations in DTB crystallizers. But the probability of multiple primary nucleation events occurring after the first event was not entirely convincing. Multiple primary nucleations are observed in the case of precipitation systems, but if this is a possibility in the case of solution crystallization of ammonium-sulphate from water has still not been confirmed. In this study, two secondary nucleation mechanisms have been analyzed to explain the sustained cyclic behavior in DTB crystallizers. A selection criterion for these mechanisms was a low energy barrier to nucleation and a strong dependency on supersaturation.

The surface nucleation mechanism (Mersmann, 1996) and the embryo coagulation secondary nucleation (ECSN) mechanism (Qian, 1997) were chosen as candidates for implementation in the two-population balance model framework. Both these mechanisms show a strong dependency on supersaturation, but lack a physical explanation for the final removal step of the secondary nuclei. For surface nucleation, it is not clear why surface nuclei are released from the surface while for ECSN, it is not clear how nuclei are removed from the surface layer to the bulk. Hence, future work should look into reviewing these theories and make it physically more sound and complete. Nevertheless, both these mechanisms have been tested within the dynamic crystallizer models.

A two-population balance model approach allows a distinction between strained attrition fragments and unstrained activated nuclei. Surface nucleation in addition to attrition (described by the model of Gahn and Mersmann (1999)) is able to predict the sustained oscillatory behavior, whereas the ECSN model fails to do so due to it's weak dependency on supersaturation.

Compartmental modelling approach using a two-compartmental model has been used to simulate a crystallizer with a boiling zone having a locally higher supersaturation. The surface nucleation bursts could exclusively be located into the boiling zone, which proves that even a small spatial region like the boiling zone can have a large influence on the dynamic behavior of evaporative crystallizers. Extension to a three-compartmental model with a fines dissolver gave less severe oscillations. The periodic nucleation bursts can be found back in the solid concentration of the fines dissolver which partly nullifies the nucleation bursts, resulting in less severe oscillations.

Finding the optimal fit with the experimental results could have been much easier if parameter estimation studies could have been realized. The kinetic framework contains two parameters, viz. the surface integration rate constant k_r and the surface related energy increase Γ_s while additional parameters are introduced by the activated nucleation mechanisms. Furthermore, in addition to the pilot-plant crystal size distribution data, experimental data on supersaturation would be helpful to find reliable values for these parameters.

Another important observation was that the unstrained population is dominating over the strained population. During this study, the optimal results were found at relatively large values for Γ_s due to which the attrition fragments dissolve and this is one of the reasons that the unstrained population is much larger than the strained one. This is in conformity with the observation of Menon (2005). The value of Γ_s seems not to be a critical parameter in the distribution of crystals over the strained and unstrained population. To improve on the distribution between strained and unstrained population, it is suggested to introduce strain in the activated nuclei. The assumption that activated nuclei are unstrained may not be entirely true and this is reinforced by the fact that laboratory experiments have shown that growth rate dispersion is also present in primary nuclei (Valcic (1975), Davey (1979) and Garside and Ristic (1983)). Nuclei, which are supposed to be formed by surface nucleation or embryo coagulation, are therefore likely to be strained to some extent, but the strain content would off course be less than that for attrition fragments generated via crystal-impeller or crystal-wall collisions.

NOTATIONS

A	pre-exponential factor primary nucleation	[#m^{-3}.s^{-1}]
A	surface area	[m^2]
A_{131}	hamaker constant	[J]
a	height of surface nucleus	[m]
a_v	specific surface area	[m^2.m^{-3} solution]
B_s	birth rate	[#.m^{-2}.s^{-1})]
B_{surf}	surface nucleation rate	[#.m^{-3}.s^{-1})]
B_{ECSN}	ECSN nucleation rate	[#.m^{-3}.s^{-1})]
c_c	crystal density	[mol.m^{-3}]
c	concentration	[mol.m^{-3}]
c_{sat}	saturated concentration	[mol.m^{-3}]
c^*	solubility	[kmol.m^{-3}]
d_m	molecular diameter	[m]
d_{imp}	impeller diameter	[m]
D	diffusion coefficient	[m^2.s^{-1}]
E	removal efficiency surface nucleation	[-]
E	impact energy	[J]
g	size of a cluster or embryo	[# molecules]
g^*	critical cluster size	[# molecules]
G	gibbs free energy	[J]
H	hardness	[N.m^{-2}]
k	boltzmann constant	[J.K^{-1}]
k_a	surface shape factor	[-]
k_r	surface integration rate constant	[m^4.mol^{-1}.s^{-1}]
k_v	volume shape factor	[-]
K	constant in ECSN rate	[#.m^{-3}.s^{-1}]
K_r	efficiency	[-]
L	crystal size	[m]
M	molar mass	[kg.mol^{-1}]
n	cluster concentration	[#.m^{-3}]
n	number density	[#.m^{-3}.μm^{-1}]
n^*	critical cluster concentration	[#.m^{-3}]
n'	cluster concentration close to surface	[#.m^{-3}]
N_A	avagadro number	[mol^{-1}]
r	radius of cluster	[m]
r_1	radius of solute molecule	[m]
r_g	radius of cluster of g -mer	[m]
r^*	critical cluster size	[m]
S	supersaturation ratio	[-]
t	time	[s]
t_{ind}	time in which clusters coagulate to nuclei	[s]
T	temperature	[K]
T_c	coagulation half time	[s]
v	molecular volume in cluster	[m^3]

V	compartment volume	[m^3]
V_m	molecular volume	[m^3]
x	distance	[m]

Greek Symbols

ε	mean specific power input	[$W.kg^{-1}$]
ε	energy of interaction between crystal surface and embryo	[J]
η	viscosity of solution	[Pa.s]
γ_{CL}	interfacial energy at crystal-liquid interface	[$J.m^{-2}$]
γ_e	edge energy	[$J.m^{-1}$]
Γ_s	surface related energy increase	[$J.m.mol^{-1}$]
Γ	effective Fracture surface energy	[$J.m^{-2}$]
μ	shear Modulus	[$N.m^{-2}$]
ϱ_l	density of solution	[$kg.m^{-3}$]
ϱ_s	density of crystals	[$kg.m^{-3}$]

Abbreviations

CSD	Crystal Size Distribution
DTB	Draft Tube Baffle
ECSN	Embryo Coagulation Secondary Nucleation

REFERENCES

Barnea, E. and Mizrahi, J. (1973).A generalized approach to fluid dynamics of particulate systems, *Chemical Engineering Journal.*, 5, pp.171-189

Bergstrom, L.(1997). Hamaker constants of inorganic materials, *Adv. in Colloid and Interface Sci.,* 70, pp.125-169

Daudey, P.J. (1987). *Crystallization of Ammonium Sulphate*, PhD Thesis, Delft University of Technology, The Netherlands

Davey, R.J., Ristic, R.I. and Zizic, B. (1979). The role of dislocations in the growth of ammonium dihydrogen phosphate crystals from aqueous solutions, *Journal of Crystal Growth*, 47, pp.1-4

Dirksen, J.A. and Ring, T.A. (1991). Fundamentals of crystallization: Kinetic effects on particle size distributions and morphology, *Chemical Engineering Science*, vol. 46, No. 10, pp.2389-2427

Eek, R.A., Dijkstra, S. and van Rosmalen,G.M. (1995). Dynamic modeling of suspension crystallizers using experimental data, *AIChE Journal*, 41 (3), pp.571-584

Farrell, R.J., Belokovskiy, A., Bennett, D. (1995). Simulated oscillations and control strategy for an ammonium sulfate DTB crystallizer, *AIChE Annual Meeting*, Miami beach, Florida, Nov.12-17, 1995, Paper 12e

Gahn, C. & Mersmann, A. (1999a).Brittle fracture in crystallization processes Part A: Attrition and abrasion of brittle solids, *Chemical Engineering Science*, 54, pp.1273-1282

Gahn, C. & Mersmann, A. (1999b). Brittle fracture in crystallization processes Part B: Growth of fragments and scale-up of suspension crystallizers, *Chemical Engineering Science*, 54, pp.1283-1292

Garside, J. and Ristic, R.I. (1983). Growth rate dispersion among ADP crystals formed by primary nucleation, *Journal of Crystal Growth*, 61, pp.215-220

Kashchiev, D.(2000). *Nucleation: Basic theory with applications,* Butterworth-Heinemann Ltd., Oxford, UK

Kim, K. and Mersmann, A. (2001). Estimation of metastable zone width in different nucleation processes, *Chemical Engineering Science*, 56, pp.2315-2324

Kind, M. and Nieken, U. (1995). On the dynamics simulation of mass crystallization from solution, Chemical Engineering and Processing, 34, pp.323-328

Menon, A.R., Kramer, H.J.M., Grievink, J., Jansens, P.J. (2005). Modelling the Cyclic Behavior in a DTB Crystallizer – a two-population balance model approach, *Journal of Crystal Growth*, 275, pp.1373-1381

Menon, A.R., Kalbasenka, A.N., Kramer, H.J.M., Jansens,P.J. (2005). Characterization of final product quality in unseeded fed-batch crystallization processes of inorganic salts in crystallizers of different scale and type., *Proceedings of the International Symposium on Industrial Crystallization* (ISIC16), 143-148, Dresden, 11-14 September, Germany

Mersmann, A. (1990).Calculation of interfacial tension, *Journal of Crystal Growth*,, 102, pp.841-847

Mersmann, A. (1996). Supersaturation and nucleation, *Trans. Inst. Chem. Eng. A.*, 74, pp.812-820

Neumann, A.M.(2001).*Characterizing industrial crystallizers of different scale and type.* PhD Thesis, Delft University of Technology, Delft, the Netherlands, ISBN 90-6464-882-4

Nyvlt, J. (1970). Metastable zone width of some aqueous solutions, *Journal of Crystal Growth*, 6, pp.151-162

Qian, R. and Botsaris, G.(1996). Laboratory Simulation of Industrial Crystallizer Cycling, *Ind. Eng. Chem. Res.,* 35, pp.1163-1172

Qian, R. and Botsaris, G. (1997). A new mechanism for nuclei formation in suspension crystallizers: the role of interparticle forces, *Chemical Engineering Science*, vol. 52, No. 20, pp.3429-3440

Valcic, A.V. (1975). Influence of dissolution on the growth rates of saccharose crystals, *Journal of Crystal Growth*, 30, pp.129-136

7

Modelling of growth rate dispersion – a two-dimensional population balance model†

A new mechanism postulating the healing of a plastically deformed crystal due to growth rate dispersion (GRD) has been incorporated in a bi-dimensional population balance equation model. Besides the size of the crystals also the strain in the crystal lattice has a pronounced effect on the growth rate of the individual crystals, justifying the need to include strain as an internal particle coordinate when modelling crystallization processes which involve secondary nucleation by attrition. Strain and size can be seen as two independent states of each particle, which change with time due to the release of strain by the plastically deformed crystal. Healing, a phenomenon which describes the mechanism how a plastically deformed crystal releases it's strain, is assumed to be proportional to the strain and to the rate of change of either the length, the area, or the volume of the crystal. The application of a multi-dimensional growth model in a rigorous crystallization modelling tool enables the description of the steep upward curvature resulting from the higher content of fine particles and provides an interesting insight into the observed broadening of the crystal size distribution (CSD) due to GRD.

† Parts of this chapter have been submitted for publication in Journal of Crystal Growth(2006)

7.1 INTRODUCTION

The product quality cannot be solely defined in terms of chemical and phase composition. A crystalline product is also characterized by its size distribution, morphology, polymorphism and the amount of strain as well as the uptake of solvent or impurities in the crystal lattice. The properties of the final product result not only from the chemical and thermodynamic properties of the compound to be crystallized, but also from the fluiddynamics and the crystal-hardware interactions, either directly or through the kinetic processes of nucleation, growth, attrition, and agglomeration. In this contribution, an attempt is made to describe non-ideal growth behavior encountered in the operation of industrial crystallization processes, viz. the broadening of the CSD and the upward curvature of the semi logarithmic plot of the crystal size distribution (CSD), effects that are commonly attributed to a phenomenon called growth rate dispersion.

In crystallization, the growth rate dispersion phenomenon was initially recognized in 1969 by White and Wright (1971). In their study of the batch crystallization of sucrose, they have shown that in the same environment, crystals of the same size could grow at different rates. This phenomenon would lead to the accumulation of small particles as was also observed experimentally. The plot of the logarithm of the population density vs crystal size function deviated significantly from the straight line predicted by the ideal Mixed Suspension Mixed Product Removal (MSMPR) model. The deviations occurred mainly in the small particle size ranges (see Figure 7.1)

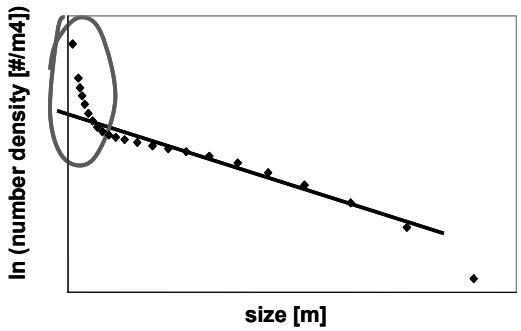

Figure 7.1 Semi-logarithmic plot of population number density vs crystal size

This steep upward curvature is usually attributed to either *size dependent growth* (SDG) (Garside and Jancic (1979), Jones et.al. (1986), Wang and Mersmann(1992), Gahn and Mersmann (1999b)) or *growth rate dispersion* (GRD). For the higher size classes, an additional non-ideality is seen. The curvature in the number density is denoted as *growth retardation*, and is the result of secondary nucleation via attrition (O'Meadhra, 1995).

SDG is defined as a phenomenon whereby crystals of different sizes grow at different rates, under identical conditions of supersaturation, temperature and the overall hydrodynamics. GRD is the phenomenon wherein crystals of the same size and material exhibit a stochastic variation in crystal growth rates, under identical conditions of supersaturation, temperature and hydrodynamics. SDG and GRD are not linked to a specific mechanism; rather they are just a phenomenological classification of non-ideal growth behavior which can be caused by a number of mechanisms:

- Difference in dislocation density when a spiral growth mechanism is dominant.
- The presence of strain within the crystal lattice.
- The curvature of the crystals resulting in the higher internal pressure and as such a higher solubility for smaller particles (Ostwald ripening).
- Size dependent diffusion constant.
- Attrition of crystals.

The nature of the mechanism involved will decide whether this will lead to a GRD or a SDG behavior. For instance, if the dislocation density is only a function of the size of the crystals, this effect will lead to a SDG. However when the dislocation density is a stochastic function, which is not connected to the size of the crystals, it will result in GRD. It should be noted that GRD will in most cases lead to a size dependent growth, due to the fact that the slow growing crystals will accumulate in the small crystal

area, leading to a lower average growth rate for the small crystals, as has already been noticed by Rojkowski (1993).

Modelling crystallization processes using only a SDG mechanism results in deviations between the predicted and experimental dynamic and steady-state results (Neumann, 2001). This has been chiefly attributed to improper modelling of GRD or absence of mechanisms which take into account the phenomenon of GRD. Why such crystals should exhibit a wide distribution in growth rates from zero to some maximum value is not fully understood. What is known is that GRD has a significant influence on the crystal size distribution (CSD) of the crystalline product in industrial crystallizers, especially in the low size range. In practice, it is possible that combinations of these phenomena can occur simultaneously, and subsequently make the analysis of the crystallizing system much more difficult. Usually, the population balance equation which forms the model relating the CSD to the operating variables, needs to be modified to account for the effect of the presence of one or more of these phenomena.

GRD has been observed for many different crystal types and sources of crystal generation (Garside,1983). Direct observations by photographic microscopy, used by a number of investigators (Garside (1979); Garside (1979), Rusli (1980); Berglund and Larson (1983); Garside and Larson (1978)) clearly showed that secondary nuclei had a variety of growth rates. Also the growth of small single crystals produced by primary nucleation processes has been investigated by Valcic (1975), Davey(1979) and Garside and Ristic (1983). All these studies provide strong experimental evidence of the existence of significant variations in the growth rates of nuclei produced in the microscopically visible range, both by primary or contact secondary nucleation processes.
Ó Meadhra(1995) analyzed the growth pattern of fine crystals of ammonium-sulphate from a 1100L DTB crystallizer, using Laue diffraction techniques. A SDG mechanism function was determined for the crystallization of ammonium-sulphate from water, which was done on-line by measuring the growth rate of a suspension of sub-250 μm crystals isolated into a 2L growth cell. The Laue diffraction analyses showed that a SDG/GRD mechanism for ammonium-sulphate is to be expected up to sizes of 300 μm. Ó Meadhra also concluded that the average level of mosaic spread decreases with increasing crystal size and above a size of about 200 μm, very little mosaic spread was observed in the crystals. The experimental observations confirmed the fact that the increased levels of internal strain in nuclei produced by an attrition process leads to a reduced growth rate of crystals.

Many theories can be cited in literature which explain this phenomenon of GRD. The prominent amongst them attribute GRD to the dislocation structure of individual crystals and varying degrees of strain in the crystal lattice (Ristic (1990), Van der Heijden (1992), Zacher and Mersmann (1995), Herden (1997)). Variation in the number of dislocations at the surface of secondary nuclei, induced by the formation process was reported to explain the observed differences in the growth rate (Berglund and Larson (1982), Bhat (1987)). For the sodium nitrate growth rate distributions, integral strain and dislocations have both been cited (Jones, 2000) as determining factors of crystal growth rates.
Gahn and Mersmann (1999a;1999b) presented a SDG model, in which he transforms the equation derived by van der Heijden(1992) to describe the influence of the lattice strain on the equilibrium concentration and thus on the growth rate, into a size dependent function assuming that the lattice strain is a function of the crystal size only. Thus, this model remains a one-dimensional model without really accounting for the lattice strain as an internal coordinate in the population balance equation. Also, this SDG model has it's limitations, such as dissolution of small crystals and unsatisfactory description of the broadening of the CSD in growth experiments (Westhoff, 2002). More recently, Gerstlauer (2001) presented a *relaxation* mechanism model in the form of a two-dimensional population balance model, in which the growth is dependent on the crystal length and the internal lattice strain of the individual crystals.
Sahin and Bulutcu(2002) claim another factor besides dislocations and strain which affects the crystal GRD : surface charge. Heterogeneous charge dispersion on the crystal surface can cause the rate dispersion. Observations indicate that the crystals have a surface charge originating from specific ion

adsorption or desorption even in the case of a large particle size range and this causes the formation of an electrical double layer. The results obtained showed that the formation of dendritic structure is not a function of supersaturation but a function of surface charge. The rate of dissolution of a crystal with a high surface charge is greater than that with a low surface charge.

In this contribution, a healing mechanism as suggested by Westhoff (2002) and Menon (2003), has been incorporated into the population balance equation. This hypothesis proposes the release of the lattice strain during the outgrowth of the strained crystals and is assumed to be proportional to the initial strain and to the rate of change of either the length, the area, or the volume of the crystal lattice. Strain and size can be seen as two independent states of each particle, which change with time due to either the growth or to the release of strain by the plastically deformed crystal. The main attempt here is to show that a multi-dimensional population balance model is necessary to capture growth rate dispersion in it's entirety. For this purpose, dynamic simulation studies on industrial scale crystallizers for the continuous crystallization of ammonium-sulphate from water are presented.
First, GRD will be briefly reviewed before explaining the concept of the two-dimensional population balance model.

7.2 GROWTH RATE DISPERSION THEORIES

There are mainly three schools of thought on the phenomenon of growth rate dispersion, and these are briefly summarized here:

- Screw dislocations
- Lattice strain
- Surface charge/potential

7.2.1 Screw dislocations

Screw dislocations or dislocations with a screw component, that emerge at the crystal surface operate as such. These defects are normally developed in the crystals during their growth process. Around the defect line the step will curve and a spiral hill is formed, because steps are preferred sites for growth units to become integrated in the surface. After a layer is completed, the dislocation is still present (see Figure 7.2). These ideas were developed by Frank (1949), and Burton, Cabrera and Frank formulated this concept in a (BCF) growth model (1951), also referred to as the spiral growth-step propagation model.

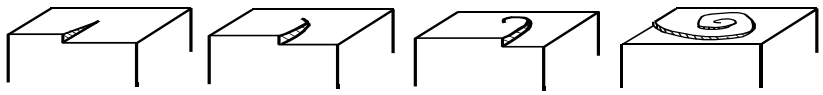

Figure 7.2 Screw dislocations on the crystal surface

Based on the Burton–Cabrera–Frank (BCF) growth theory (Burton, 1951), the most likely cause for the presence of GRD is a variation in dislocation density on the surface of various nuclei resulting in different growth rates. This was put forward by Garside(1983), Davey(1979), Valvic(1975) and Chernov(1990). The BCF theory indicates that the growth rate of a crystal is dependent on the number of screw dislocations present on the surface and the activity (ε) of the dominating group of dislocations on a crystal surface. Experimental work has shown that changes in the location or density of screw

dislocations can cause large changes in the crystal growth rate. Collisions of the crystals with the impeller, walls and each other can result in damage to the dislocations on the surface of crystals and therefore, changes in the crystal growth rate (Berglund and Larson (1982), Bhat (1987)). This is especially true with secondary nuclei that could display very different dislocation densities. For the primary nuclei as well, the imperfect nature of the crystal growth process could lead to changes in the dislocations of the crystal faces.
The screw dislocation theory can be an important contributor to explaining GRD, but this depends strongly on the system under consideration. For the crystallization of ammonium-sulphate from water, which is more secondary nucleation (attrition) dominated, GRD arising due to dislocations on the surface of crystals do not play a large role in industrial crystallization processes.

7.2.2 Lattice strain

The presence of strain in a crystal leads to a strain energy which must be added to the internal energy of the crystal, thus increasing the chemical potential of the solid phase. An increase in the chemical potential difference between the solid and liquid phases will lead to a decrease in the growth rate of the crystal (Bhat(1987), Ristic(1988, 1997), van der Heijden(1992)). The effect of strain on the chemical potential difference will be discussed in more detail in sub-section 7.3.
The presence of strain in the crystal lattice will lead to some degree of mis-orientation between adjacent parts in the lattice structure during the further outgrowth of the crystal. This phenomenon is called *mosaic spread* which can be measured by exposing the crystal to an X-ray beam in order to record a Laue diffraction pattern (Roberts, 1995). This strain is embedded within the crystal lattice of secondary nuclei which are generated via contact nucleation (attrition) due to crystal-impeller or crystal-wall collisions. Whether these strained nuclei survive and grow into the population depends on their stress content and on the prevailing supersaturation. When these crystals grow further, the stress content of the outer shell of the crystals decreases, a phenomenon called *healing*, and beyond a certain size, the average growth rate of the crystals becomes the same as that of their parent crystals.

7.2.3 Surface charge/potential

Sahin and Bulutcu(2002) claim another factor besides dislocations and strain which affects the crystal GRD—this is surface charge. Heterogeneous charge dispersion on the crystal surface can cause the rate dispersion. The effect of the surface charge on crystal growth rate is based on Knapp's approach to solubility. Knapp(1922) corrected the Ostwald–Freundlich equation which gives the effect of particle size on the solubility by using the surface electrical charge concept. He considered the total surface energy of very small solid particles to be a function of their normal surface energy and the surface electrical charge.
Mullin and Garside (1968) state that *"during growth, solute molecules are diffusing towards the crystal surface, whilst during dissolution they are travelling in the opposite direction. It is possible that electrostatic charge attracting solute molecules to the crystal surface would increase the rate of diffusion in the former case but decrease the rate in the latter."*
All these observations indicate that the crystals have a surface charge originating from specific ion adsorption or desorption even in the case of a large particle size range and this causes the formation of the electrical double layer.
Sahin and Bulutcu(2002) measured the growth and dissolution rates of sodiumperborate crystals in a flow-type single-crystal cell. Sodiumperborate grows dendritically at any level of supersaturation and shows growth and dissolution rate dispersion. Both the growth and dissolution rates of sodiumperborate were found to be controlled by surface charge distribution which is represented by applied voltages in an electrostatic separator. It was determined that high surface charge dominates the crystal growth rate when compared with low surface charge under identical conditions. The results obtained showed that the formation of dendritic structure is not a function of supersaturation but a function of surface charge. The rate of dissolution of a crystal with a high surface charge is greater than that with a low surface charge. This experimental evidence suggests that SDG does not occur for crystals growing in the sodiumperborate–water system. Rather, a wide range of GRD occurs in crystals

growing under identical conditions. In addition, each crystal seems to possess some constant inherent growth and dissolution rate. Crystals with a high surface charge grow more slowly than those with a lower surface charge. The other important result obtained in this study is that the surface charge can control the dendritic structure of sodiumperborate crystals.

For crystallization of systems like ammonium-sulphate from water, secondary nucleation via attrition has been widely reported to play a dominant role in determining the final product specifications. The attrition process leads to the formation of new nuclei (secondary) which will have a certain amount of strain energy embedded within their crystal lattice. As the system studied in this thesis is ammonium-sulphate, the analysis of GRD caused by strain effects within the crystal lattice of secondary nuclei will be the focus of study here. This strain energy arises due to the impact of collisions of the crystals with a foreign body like the impeller or the crystallizer vessel wall.

7.3 EFFECT OF STRAIN ON THE DRIVING FORCE

The driving force for crystal growth is provided by the supersaturation (Δc). For an ideal, stress-free crystal, the driving force can be given as :

$$\Delta c = c - c_{sat} \tag{7.1}$$

where c is the bulk concentration c_{bulk} and c_{sat} is the saturation concentration (solubility) of the crystal/fragment.
Once a crystal undergoes contact nucleation by attrition (crystal-impeller collisions), this results in a plastic deformation of the crystal lattice. The newly created surface caused by the formation of an attrition fragment contains certain amount of strain energy within it's lattice which increases the chemical potential of the crystal and consequently its solubility, c^*_{real}, (van der Heijden and van Eerden, 1992), which can be given as:

$$c^*_{real}(L) = c_{sat} \exp(\frac{w_s}{RT}) \tag{7.2}$$

Thus, for a non-ideal, plastically deformed crystal, the driving force for growth can be described as:

$$\Delta c = c - c^*_{real} = c - c_{sat}.\exp(\frac{w_s}{RT}) \tag{7.3}$$

The supersaturation (Δc) is dependent on the lattice strain (w_s). If w_s is high enough, crystals will even dissolve.

Table 7.1 Effect of strain on supersaturation

Case	w_s	c^*_{real}	Δc
1	0	$= c_{sat}$	$= \Delta c_{\max}$
2	> 0	$> c_{sat}$	$< \Delta c_{\max}$
3	$= w_{max}$	$= c_{bulk}$	$= 0$
4	$> w_{max}$	$> c_{bulk}$	< 0

Four different scenarios can be visualized for the crystals. Case 1 applies to an ideal crystal which has no strain within it. Here, the driving force which is the difference in the bulk and saturation concentrations, will be the maximum driving force ($\Delta c_{\max}$) for crystallization as depicted in Figure

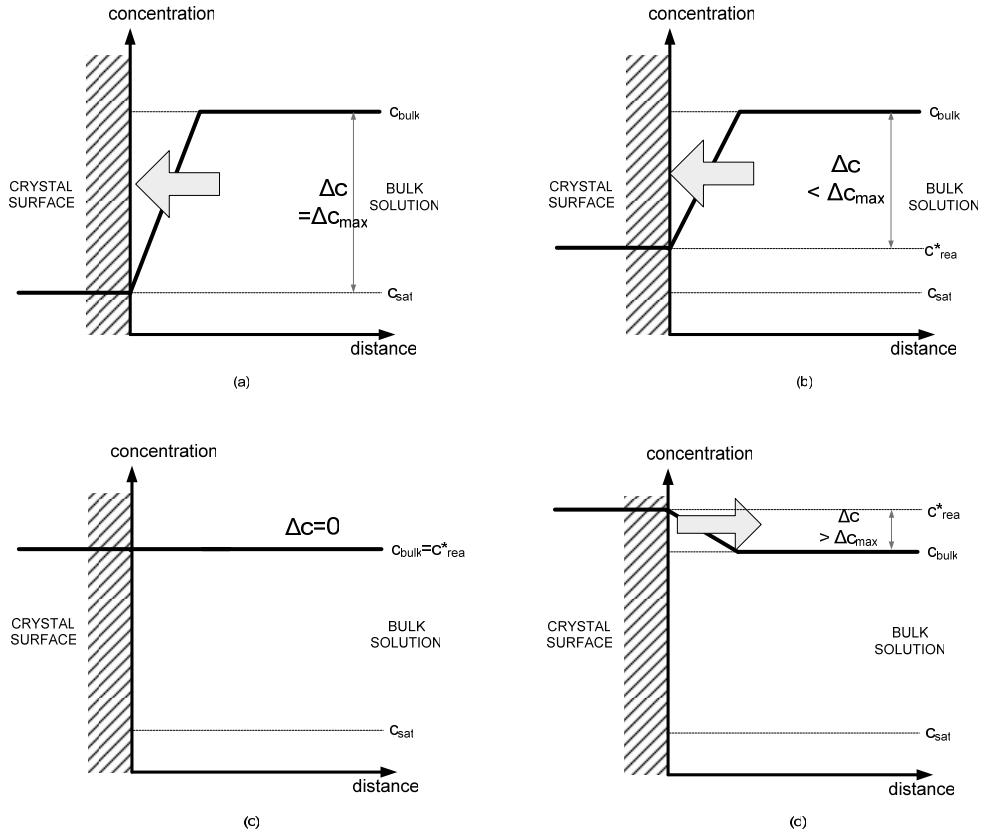

Figure 7.3 Effect of strain on driving force for crystallization

7.3(a). For crystals with a certain energy (Case 2), the solubility increases as given in Equation 7.2, hence the driving force becomes less than $\Delta c_{\max}$, but is still positive. This is shown in Figure 7.3(b). The third case is when the strain is so high that c^*_{real} equals the bulk concentration, c_{bulk}. Here, the crystal neither grows nor dissolves and remains at equilibrium with the bulk solution (Figure 7.3(c)). The final scenario is when the strain exceeds this value, c^*_{real} exceeds c_{bulk}. Here, there is a reversal of the driving force (Figure 7.3(d)), which becomes negative and the crystal undergoes dissolution. Concluding, the lattice strain energy has a strong influence on the chemical potential difference, hence for a crystal to grow, the molar strain energy (w_s) must be lower than w_{max}..

7.4 GROWTH RATE DISPERSION MECHANISMS ACCOUNTING FOR LATTICE STRAIN

In order to capture growth rate dispersion in it's entire complexity, it is imperative that the conventional form of the population balance equation be modified to account for more internal crystal coordinates, than just the crystal size (L). Here, we discuss the possibility of including the internal

molar lattice strain as the additional characteristic coordinate for the crystal lattice. To implement such a multi-dimensional population balance model, it is first necessary to come up with an expression (mechanism) for the evolution of strain (dw_s/dt) upon growth or dissolution of the crystals. Here, two approaches for the relaxation of strain will be briefly discussed before incorporating them into a two-dimensional population balance model framework.

7.4.1 Relaxation mechanism

Gerstlauer(2001) proposed a relaxation mechanism to identify approaches for the release of the internal molar lattice strain (w_s) during crystal growth. Here, the absolute internal lattice strain is interpreted as the overall energy absorbed in a single crystal having a unit of (J). The absolute lattice strain W_s is calculated from the molar lattice strain w_s, by using the volume shape factor k_v according to:

$$W_s = k_v c_s L^3 w_s \tag{7.4}$$

The total differentiation of Equation 7.4 with respect to time yields:

$$\frac{dW_s}{dt} = k_v c_s \left[3L^2 w_s \frac{dL}{dt} + L^3 \frac{dw_s}{dt} \right] = k_v c_s [3L^2 w_s G(w_s, L) + L^3 R_G] \tag{7.5}$$

where : R_G = relaxation rate = $\dfrac{dw_s}{dt}$

Four limiting cases for the change of the absolute lattice strain are identified. The first case represents a constant absolute lattice strain during crystal growth, the other three cases assume a change of the absolute lattice strain proportional to the crystal length ($\sim L$), proportional to the crystal surface area ($\sim L^2$) and proportional to the crystal volume ($\sim L^3$), respectively. An overview of the four different cases is given in Table 7.2.

Table 7.2 Relaxation mechanisms proposed by Gerstlauer (2001)

Case	W_s	dW_s/dt	dw_s/dt
1	constant	0	$-\dfrac{3w_s}{L}G$
2	$\sim L$	$k_v c_s K_2 G$	$\left(\dfrac{K_2}{L^3} - \dfrac{3w_s}{L}\right)G$
3	$\sim L^2$	$2k_v c_s K_3 L G$	$\left(\dfrac{2K_3}{L^2} - \dfrac{3w_s}{L}\right)G$
4	$\sim L^3$	$3k_v c_s K_4 L^2 G$	$\left(\dfrac{3K_4}{L} - \dfrac{3w_s}{L}\right)G$

The above four cases are illustrated for the system ammonium-sulphate water for the strained secondary nuclei that result from crystal-impeller collisions. Gahn and Mersmann (1999a,b) use the Rittinger's law (von Rittinger, 1867) to attribute the strain to the newly born secondary nuclei. Rittinger's hypothesis states that the product between the molar lattice strain and the characteristic crystal size is proportional to the fracture surface energy Γ_s which characterizes the hardness of a crystal and hence, is unique to the particular system under consideration. For a certain initial crystal size for the newly attrited fragment, Rittinger's law gives the following initial molar lattice strain :

$$w_{s,initial} = \frac{\Gamma_s}{L_{initial}} \tag{7.6}$$

This initial point for the trajectory of the individual fragment in the particle state space defined by the particle coordinates L and w_s, is thus determined by Equation 7.6. For the system ammonium sulphate – water, using a fracture surface energy Γ_s of 7.10^{-5} J.m/mol and an initial crystal size of 10μm, the initial molar lattice strain, $w_{s,initial}$ is 7 J/mol. This value of Γ_s is chosen as experiments performed on single crystals (Virone, 2004) have revealed that the smallest crystals born above a strain energy of 10 J/mol were found to completely dissolve and never actually recovered and healed itself to grow again.

Figures 7.4 (a-d) are single crystal simulations under constant supersaturation conditions. All the relaxation mechanisms for the change of W_s (except for the first case of W_s =constant), are determined by the crystal growth rate G and a free parameter. A more detailed comparison of the relaxation mechanisms with other existing theories like constant crystal growth (CCG) is given by Gerstlauer (2001). Figures 7.4 (a-d) depict the trajectories in the two-dimensional particle state-space during crystal growth for the four different cases proposed above.

In cases 1 and 2 (Figure 7.4(a) and Figure 7.4(b)), the strain monotonously decreases with crystal size, at a rate much faster than that given by the model of Gahn and Mersmann (Equation 7.6). In both these instances, it is not possible to approximate the curve as given by Gahn and Mersmann. However, an interesting aspect that is seen in case 3 (Figure 7.4(c)), is that at a certain parameter value of K_3 = $7.3.10^{-5}$ J.m/mol, the relaxation mechanism gives an identical progression as given by the model of Gahn and Mersmann.

Cases 2 to 4, depicted in Figures 7.4 (b-d) respectively, show that the strain does not necessarily decrease with increasing crystal size. For these case, at certain parameter values, there is an increase in strain upon growth, either temporarily or permanently, which is not very likely to occur. This is in contradiction with the theory of van der Heijden (1992) who proposed the concept that the lattice strain always decreases with crystal growth. In cases 1-3, for all parameter values, the lattice strain does decrease to zero at larger sizes, but for case 4, interestingly, it can be seen for the parameter K_4=10 J/mol, the strain actually increases with increase in the crystal size and remains at a certain limiting value, which is the same as the value of the parameter K_4. Thus, the strain content remains at a constant level, which can be higher or lower than the initial strain value, depending on the chosen parameter value. This is not a physically realistic behaviour as the strained crystals are more likely to release the strain and thus, grow in size during the process.

Concluding, the relaxation models as proposed by Gerstlauer (2001), provides an insight into the evolution of strain in the growth behavior of the secondary nuclei, but do not account for certain discrepancies, which are not explained well. A further analysis on the relaxation mechanisms will be presented once they are embedded in a two-dimensional population balance model.

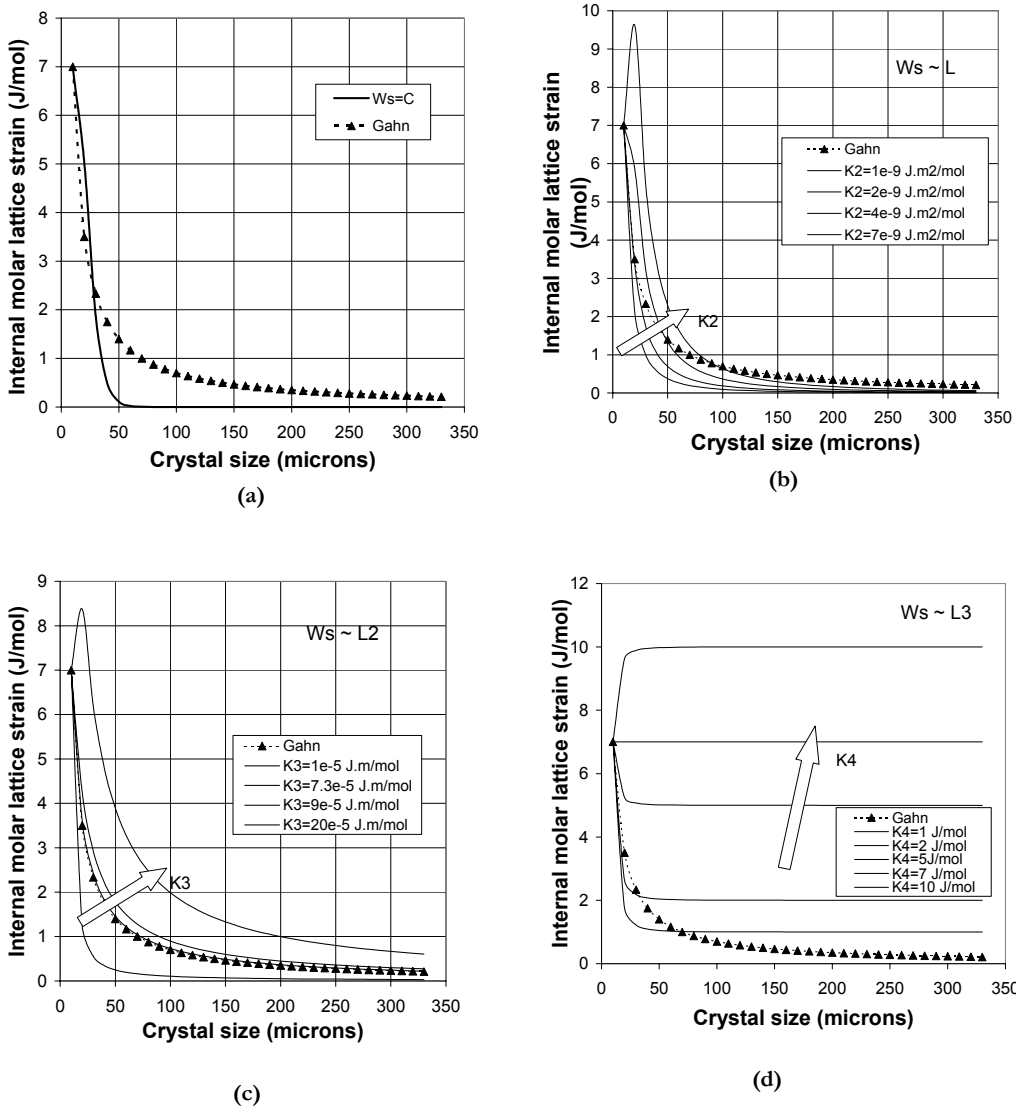

Figure 7.4 Relaxation trajectories during crystal growth for: (a) constant lattice strain, (b) lattice strain proportional to the crystal length (~L), (c) lattice strain proportional to the crystal surface area (~L^2) and (d) lattice strain proportional to the crystal volume (~L^3)

7.4.2 Healing mechanism

An alternative healing mechanism postulating the release of strain with crystal growth has been proposed by Westhoff (2002) and Menon (2003). Healing, a phenomenon which describes the mechanism how a plastically deformed crystal releases it's strain, is assumed to be proportional to the strain and to the rate of change of either the length, the area, or the volume of the crystal.

$$dw_s = -k_H . w_s . d\left(L^n\right), k_H > 0 \tag{7.7}$$

where the exponent n can assume the value of 1, 2 or 3 for the three possible cases when the healing rate H (dw_s/dt) is proportional to the size (L), the surface area (L^2) or the volume (L^3), respectively. A solution to the differential equation (Equation 7.7) is:

$$w_s = w_{s,initial} e^{k_H (L_{initial}^n - L^n)}; k_H > 0 \tag{7.8}$$

Equation 7.7 satisfies the boundary condition ($L_{initial}, w_{s,initial}$) for all k_H, L and n.

As seen from Equation 7.7, the exponent n can take the value of 1, 2 or 3. We consider the healing mechanism to be more closely associated with the crystal surface area (i.e. n =2) and thus, more of a surface related phenomenon. Here, the healing mechanism assumes that the lattice strain is not distributed uniformly over the entire volume of the crystal, but rather that the strain is localized at the outer layers of the crystals i.e. at the locations where the deformation in the breakage process are the highest. Thus, the chemical potential considered here is confined to the crystal surface and hence, is determined by the plastic deformation of the crystal lattice occurring near the surface. During the growth process, dissolved particles from the solution will be structured on the crystal lattice on top of the already existing deformed crystal lattice. This growth process during which the newly growing crystal lattice layers approximate the ideal crystal lattice better than the underlying ones is called *healing of the crystal surface*. But if the supersaturation is not high enough to compensate for the increased strain levels on the crystal surface, then dissolution of that part of the crystal surface occurs, i.e. the main consequence here is that not the entire attrition fragment dissolves at high strain energies but, rather the dissolution is restricted to the *deformed* crystal surface layer. This process leads to a reduction in the strain levels the crystal experiences, thus providing an opportunity to grow again.

The three possible cases for the healing mechanism are shown in Table 7.3. The healing mechanism is illustrated here for the system ammonium-sulphate water.

Table 7.3 Healing mechanisms proposed by Westhoff (2002)

n	dw_s	H
1	$\sim L$	$-k_H w_s G$
2	$\sim L^2$	$-2k_H w_s L G$
3	$\sim L^3$	$-3k_H w_s L^2 G$

For an initial crystal size of 10 μm, the internal molar lattice strain, $w_{s,initial}$ is calculated to be around 7 J/mol. Figures 7.5 (a-c) depict the trajectories in the two-dimensional particle state-space during crystal growth for the three possible scenarios proposed above.

The strain monotonously decreases with crystal size in each case which is very much in line with the hypothesis of van der Heijden (1992). Unlike the model of Gerstlauer (2001) for the case when the relaxation is proportional to the volume ($\sim L^3$), wherein there is a limiting value of the molar lattice strain w_s for an increasing crystal length (see Figure 7.4(d)), the healing mechanism does not exhibit any such behavior (Case 3 - Figure 7.5(c)) . Rather, the strain relaxes much more gradually but ultimately reaches zero, which can be considered as a more likely possibility.

An increase in the healing constant (k_H) implies that the strained crystal can heal itself faster, thus contributing to the release in strain faster, as shown in Figures 7.5(a-c).

At higher values of the exponent n, the release of strain is much slower which implies that there are more strained crystals at higher size classes. This is clearly seen in Figure 7.5(c) where the healing is proportional to the crystal volume and in (Figure 7.5(b)) where the healing is proportional to the crystal surface area.

The healing mechanisms illustrated above give a better picture about the release/evolution of strain under plastically deformed conditions for the secondary nuclei. Next, these models will be implemented

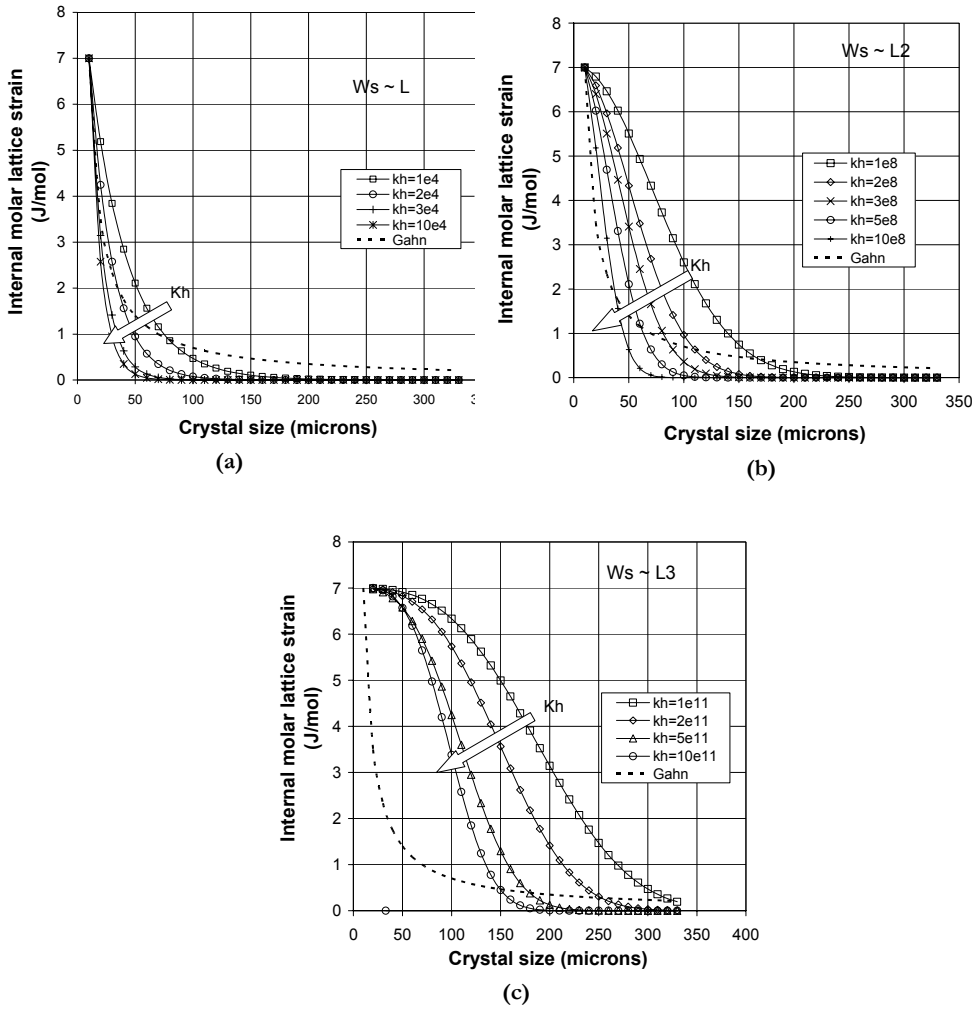

Figure 7.5 Healing trajectories during crystal growth for lattice strain proportional to : (a) the crystal length ($\sim L$), (b) the crystal surface area ($\sim L^2$) and (c) the crystal volume ($\sim L^3$)

in a two-dimensional population balance model framework to see the effects of growth rate dispersion on the evolution of the crystal size distribution and the quantiles.
It is worth mentioning that a proper estimation of the excess free energy of the individual crystals owing to their degree of imperfection or stress together with their healing pattern during outgrowth, put together in an appropriate expression for their growth rate is still missing. Also, a proper validation of these models is difficult as one cannot observe both the growth rate and the strain of the crystals simultaneously. Secondly, with crystallization experiments in solution in industrial-scale crystallizers (of the MSMPR type), it is very difficult and virtually impossible to study the fundamental growth behavior of these strained crystals under uniform and stagnant conditions. Hence, what is needed from a fundamental perspective, is single-crystal observations where in it would be possible to isolate individual crystals and study the growth/dissolution behavior under strained conditions.

In more recent investigations on ammonium sulphate attrition fragments, diverse growth behavior ranging from growth to dissolution, as well as partial dissolution with subsequent outgrowth was

observed (Virone, 2004). This investigation was focused on the observation of primary nuclei and attrition fragments grown in stagnant solutions in a laboratory scale set up, under well-known process conditions. These experiments which were performed in a stagnant solution permits to follow the evolution of single particles in time. The deviation of the growth rates of attrition fragments from that of unstrained primary nuclei provides evidence and information about the strain content in the secondary nuclei. More fundamental understanding is needed for the growth behavior of the attrited fragments, which is being done in parallel by Virone (2006) mainly aimed at single crystal healing experiments to arrive at a better description of the healing pattern of strained crystals.

7.5 2D - POPULATION BALANCE MODEL : SIZE AND STRAIN DEPENDENT

The evolution of the CSD in an industrial crystallization process can be described using population balance equations (PBEs) and the appropriate mass and enthalpy balance equations combined with the equations describing the relevant kinetic phenomena. The concept of population balance equations was introduced to crystallization by Randolph in 1962 (Randolph and Larson, 1988) and it accounts for the number balance of crystals and their change in size. The PBE for a uniformly mixed volume, with the amount and the size of particles expressed in terms of number density(n) and particle length(L) respectively, can be expressed in the conventional form as follows:

$$\overbrace{\frac{\partial(n(L,t)V(t))}{\partial t}}^{\text{number rate of accumulation}} = \overbrace{-V(t)\frac{\partial(n(L,t)\cdot G(L,t))}{\partial L}}^{\text{rate of number gain due to crystal growth and dissolution}} + \overbrace{\sum \phi_{V,in}(t)\,n_{in}(L,t)}^{\text{number rate in}} - \overbrace{\sum \phi_{V,out}(t)\,n_{out}(L,t)}^{\text{number rate out}} + \overbrace{[B(L,t)-D(L,t)]V}^{\text{birth and death of crystals}} \tag{7.9}$$

The terms in this unsteady state equation represent different contributions to the number balance on a differential increment L to $L+dL$ in the crystal size coordinate. The first term on the right hand side represents the net flux of particles by crystal growth, the second and third terms represent the net flux of particles entering or leaving the crystallizer respectively, while the last two terms represent the birth and death/destruction of crystals by processes such as nucleation, agglomeration, breakage or attrition. The secondary nucleation model of Gahn and Mersmann (1999a,b) which provides the basis for a predictive crystallizer model, has been implemented within the simulation framework. Here, the growth rate equation is briefly discussed to bring out the relevance of a multi-dimensional population balance model to describe growth rate dispersion in it's entire complexity.

The growth of crystals is considered to be a two step process, a diffusion step followed by an integration step of the solute to the crystal lattice (Mersmann, 1992). Mersmann gives an expression for the growth rate $G = G(L)$ for surface integrated (integration rate constant k_r) and diffusion limited (mass transfer coefficient $k_d(L)$) crystal growth:

$$\frac{G(L)}{2k_d(L)} = \frac{\Delta c(L)}{c_s} + \frac{k_d(L)}{2k_r c_s} - \sqrt{\left(\frac{k_d(L)}{2k_r c_s}\right)^2 + \frac{k_d(L)}{k_r c_s}\frac{\Delta c(L)}{c_s}} \tag{7.10}$$

The mass transfer rate coefficient which is size dependent, can be calculated using a Sherwood type relation developed by Herndl (1982):

$$k_d(L) = \frac{D_{AB}}{L}\left[2 + 0.8\left(\frac{\bar{\varepsilon}L^4}{\upsilon_L^3}\right)^{1/5}\left(\frac{\upsilon_L}{D_{AB}}\right)^{1/3}\right] \tag{7.11}$$

From Equations (7.2), (7.6), (7.10) and (7.11), it is clearly deducible that the growth rate is size dependent. Due to the Rittinger equation, which relates the lattice strain directly to the length of the crystal, the strain is not an independent variable anymore and the 2D PBE reduces to a 1D PBE, with only the crystal size as the internal coordinate. So, these equations do imply size dependent growth, but not necessarily growth rate dispersion.
Strain and size can be seen as two independent states of each particle, which change with time due to phenomena like *healing* or *relaxation*. Consequently, the population balance will include two terms, describing the change in the distribution of the population due to the rates of change of size and strain, respectively.
If the number density is assumed to be a function of both, characteristic length L and molar strain energy w_s :

$$n = n(t, L, w_s) \tag{7.12}$$

then, the variable H (Healing Rate) can be defined :

$$H(L, w_s) = \frac{dw_s}{dt} \tag{7.13}$$

Introducing H into the population balance equation (PBE) results in the following two-dimensional model:

$$\overbrace{\frac{\partial(n(L,w_s,t)V(t))}^{\text{number rate of accumulation}}}{\partial t} = \overbrace{-V(t)\frac{\partial(n(L,w_s,t)\cdot G(L,w_s,t))}^{\text{rate of number gain due to crystal growth and dissolution}}}{\partial L} - \overbrace{V(t)\frac{\partial(n(L,w_s,t)\cdot H(L,w_s,t))}^{\text{rate of number gain due to healing}}}{\partial w_s} + \overbrace{\sum\phi_{V,in}(t)n_{in}(L,w_s,t)}^{\text{number rate in}} - \overbrace{\sum\phi_{V,out}(t)n_{out}(L,w_s,t)}^{\text{number rate out}} + \overbrace{[B(L,w_s,t) - D(L,t)]V}^{\text{birth and death of crystals}} \tag{7.14}$$

Agglomeration of crystals is not considered here. In the birth and death terms, only the secondary nucleation contribution via attrition appears. Suitable initial and boundary conditions need to be defined for the two-dimensional PBE.

Initial Condition
The initial condition can be used to express a trivial solution such as a clear liquid (no crystals) or a size distribution of seed crystals.

$$n(L,w_s,t=0) = n_L(L,w_{s,initial}) \tag{7.15}$$

Boundary conditions
The classical boundary condition (B.C.) with respect to crystal size for the PBE is:

$$n(L=0,w_s,t) = \frac{B_0(t)}{G(L=0,w_s,t)} \; ; G(L) \geq 0 \; \forall L \tag{7.16}$$

This B.C. is applicable and sufficient when the crystal growth is positive for all crystal sizes. B_o denotes the birth rate of crystals at the lower limit of the size domain.
If the growth rate is negative for all sizes, a B.C. at infinite length is required and sufficient (Bermingham, 2003):

$$n(L=\infty,w_s,t) = 0 \; ; G(L) < 0 \; \forall L \tag{7.17}$$

So, the appropriate B.C. must be applied for the size interval, depending on whether there is positive or negative growth rate.
The third B.C. is for the internal molar lattice strain, i.e. there are no crystals with a lattice strain larger than a maximum defined lattice strain $w_{s,max}$:

$$n(L, w_s = w_{s,max}^+, t) = 0 \forall L \tag{7.18}$$

This B.C. requires that the birth rate of crystals with $w_s > w_{s,max}$ is zero, i.e. $B(L, w_s) = 0$. The maximum lattice strain $w_{s,max}$ depends on the chemical system being used, as discussed earlier.

7.6 DYNAMIC SIMULATIONS ON A 1100L DTB CRYSTALLIZER

The two-dimensional population balance equation was implemented in a rigorous crystallizer model framework. Dynamic and continuous simulation studies are presented here for the evaporative crystallization of ammonium sulphate from water in a 22L DT and 1100L DTB crystallizer. The process and kinetic parameters used for the simulation studies are listed in Table 7.4.
The dynamic flowsheeting program gPROMS[1] was used as the modelling tool for this work .The dynamic form of the PBE is a PDE and thus needs to be reduced to a set of DAEs to be solved numerically. To this end, numerical methods belonging to the family of the Method of Lines are frequently used. A comprehensive overview on various numerical methods proposed for solving PBEs can be found in Kumar and Ramkrishna (1996). Based on the general crystallizer model developed by Bermingham(1998, 2003a,b), the finite volume method is used here for the solution of the PBEs. The finite volume method is known to be robust for highly convective PDEs such as the PBE, even when the sign of the convective term changes (eg. from growth to dissolution).
In the proposed healing mechanism (Equation 7.7), there are several parameters involved like the healing constant (k_H), the exponent (n) and also the strain in the crystal lattice w_s. From recent experiments (Virone, 2004), an idea about the initial strain in the attrition generated secondary nuclei is known, i.e. it is found to be in the range 5-10 J/mol. There are two possibilities to assign the strain content within the newly born secondary nuclei due to attrition. A constant initial value of strain (say 10 J/mol) can be assigned to the initial CSD, i.e. to say that all secondary nuclei are born at the same strain level. The second possibility which is more likely, is to assign a distribution for the initial CSD (Figure 7.6), where the strain is distributed over the CSD depending on the crystal size. As an initial

[1] Process Systems Enterprise Ltd, Bridge Studios, 107a Hammersmith Bridge Rd., London, UK

approximation, Rittinger's law (Equation 7.6) is assumed to provide this distribution. Starting from this initial CSD, where the internal molar lattice strain can range anywhere between 10 J/mol to values close to or equal to zero, the two-dimensional population balance model will be used to illustrate the effects of GRD on the evolution of the CSD as a function of the crystal strain (w_s) and crystal size (L). An estimate for the healing constants can also be derived using Rittinger's law (Equation 7.6).

Table 7.4 Overview of settings for dynamic simulation studies

Process/Simulation parameters	**22L DT**			**1100L DTB**		
Temperature [^{0}C]	50					
Impeller frequency[rpm]	775			370		
Fines removal rate [l/s]	-			2		
Volume specific heat input [kW/m^3]	120					
Feed temperature [^{0}C]	50					
Feed density [kg/m^3}	1248					
Product residence time [s]	4500					
Maximum strain energy [J/mol]	10					
Kinetic parameters						
One-dimensional population balance equation						
SIM_1D	k_r = 1.02. 10^{-5} m^4/mol.s Γ_s = 2.07. 10^{-4} J.m/mol			-		
2D model : Relaxation mechanism(Gerstlauer, 2001) constants						
Mechanism	Constant (SIM22_G1)	~ L (SIM22_G2)	~ L^2 (SIM22_G3)	~ L^3 (SIM22_G4)	Constant (SIMG2)	~ L (SIMG3)	~ L^2 (SIMG1)
Relaxation constant (K_i)	-	K_2 1. 10^{-8} J.m^2/mol	K_3 3. 10^{-4} J.m/mol	K_4 2 J/mol	-	K_2 1. 10^{-8} J.m^2/mol	K_3 3. 10^{-4} J.m/mol
2D model : Healing mechanism constants							
Mechanism (n)	1 (~ L)	2 (L^2)	3 (L^3)	1 (~ L)	2 (L^2)	3 (L^3)	
k_r [m^4/mol.s]	1.02. 10^{-5}			9 .10^{-4}			
k_{H1}	15. 10^2 m^{-1} (SIM22_01)	3. 10^6 m^{-2} (SIM22_02)	15. 10^{10} m^{-3} (SIM22_03)	15. 10^2 m^{-1} (SIMSD3_11)	7. 10^6 m^{-2} (SIMSD3_6) 3. 10^6 m^{-2} (SIMSD3_15) 1. 10^6 m^{-2} (SIMSD3_16)	8. 10^9 m^{-3} (SIMSD3_14)	

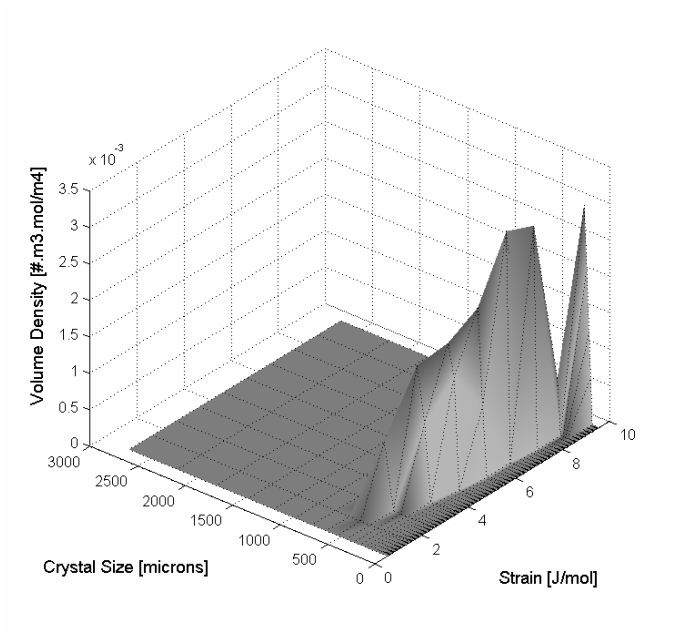

Figure 7.6 Distribution of strain over the initial CSD

7.6.1 CSD broadening

Here, the effects of the healing mechanism on the evolution of the CSD is presented. As discussed earlier in sub-section 7.4.2, there exist three possible scenarios for healing of strained crystals. For the sake of argument, we shall focus on the scenario where the healing is assumed to be a surface-based phenomenon. This is the most plausible situation having a higher physical relevance to the study at hand and hence, SIMSD3_6 (where $n = 2$) is used to illustrate the effect of GRD on the evolution of the CSD.

Figures 7.6(a-g) are all snapshots of the CSD at various time intervals. The birth of the strained attrition fragments occurs within the strain interval of 10 J/mol to some value greater than zero. Figure 7.6(b) shows how the crystals in the highest strain class (10 J/mol) have moved to the lower strain classes as a result of healing. This trend continues until there are almost no strained crystals at 10 J/mol (Figure 7.6(c)), when the next wave of secondary nuclei appear at 10 J/mol (Figure 7.6(d)). Again, depending on the healing rate, some crystals will survive the high strain values and grow to a higher size class. During this growth process, they lose some strain at the crystal surface thus, lowering it's solubility and hence, increasing the driving force for growth. The crystals that cannot withstand the very high strain energy levels will dissolve. The consequence of this transfer of crystals from a higher strain level to a lower one and the progression along the crystal size axis, is a broadening of the CSD at lower values of strain energy as seen in Figure 7.6(c-g).

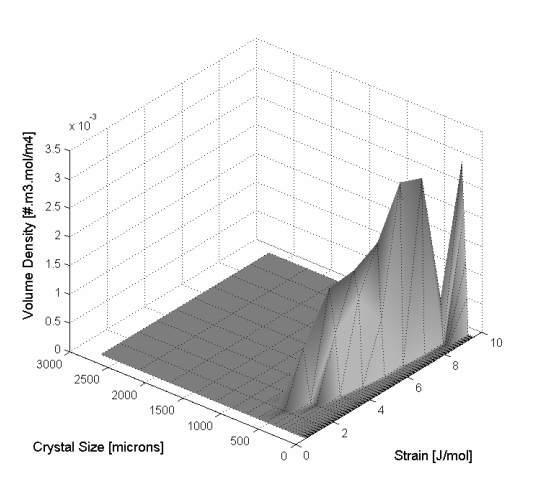

(a) t=0s

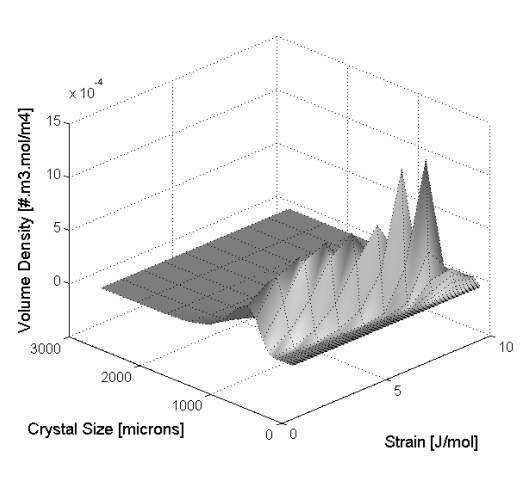

(b) t=480s

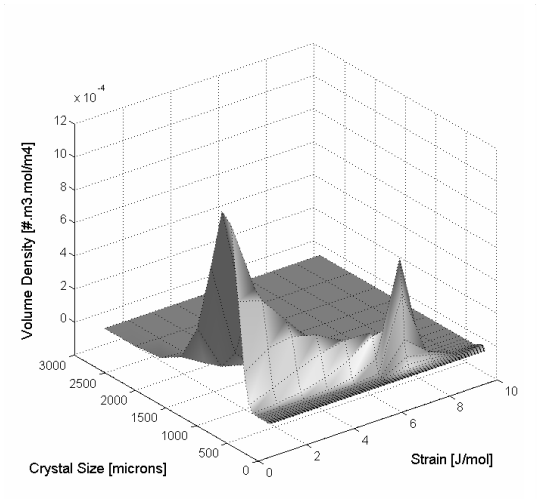

(c) t=1440s

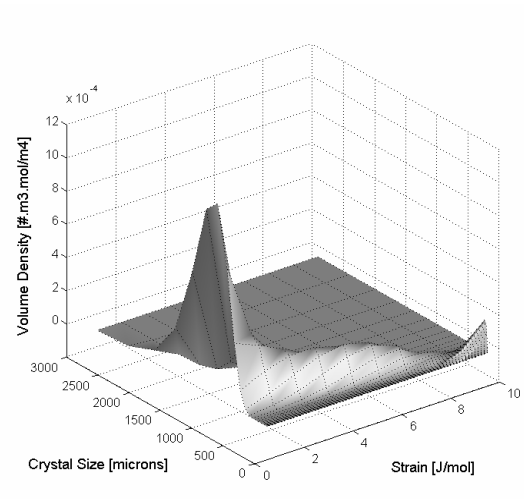

(d) t=2640s

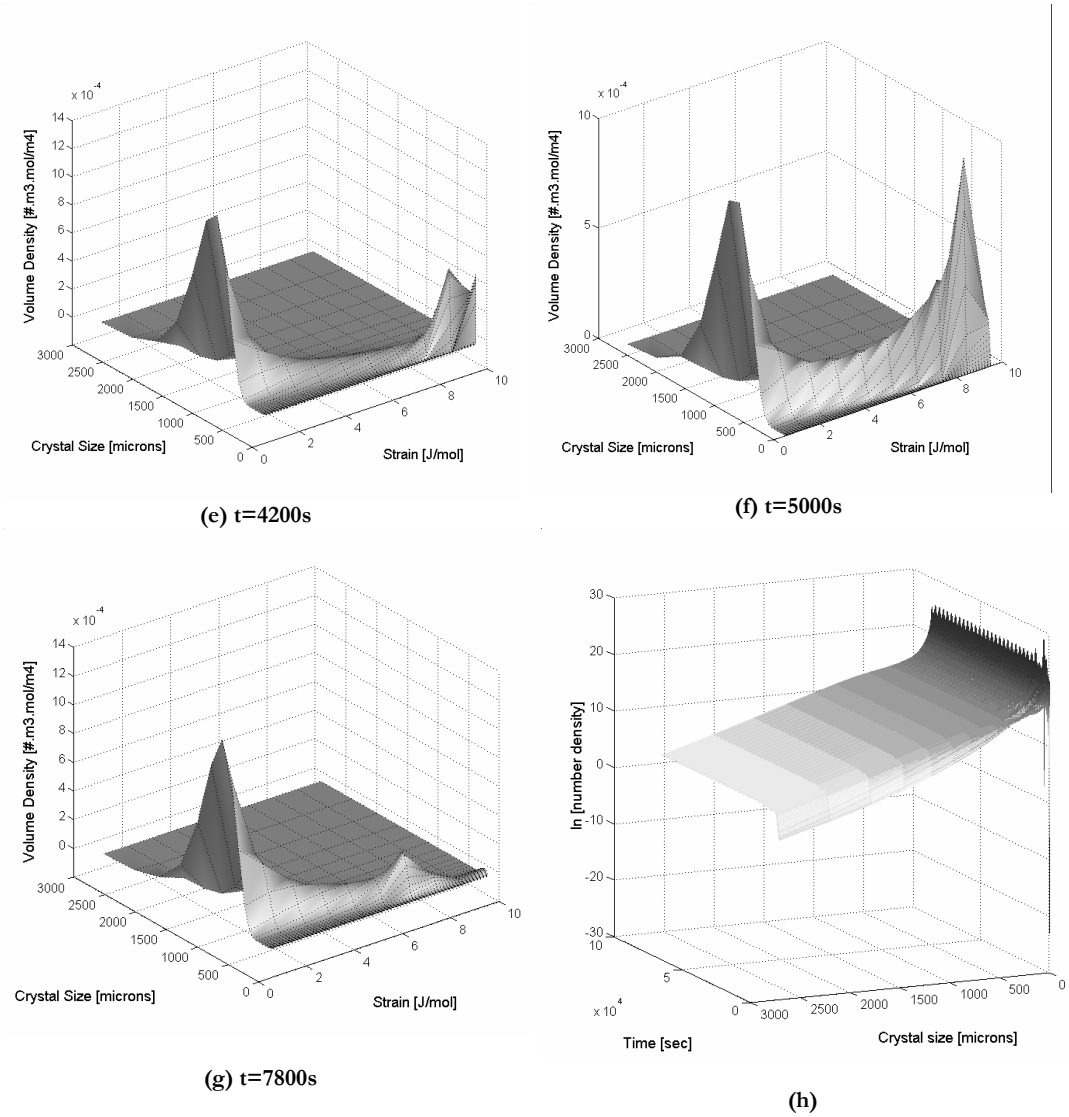

Figure 7.7 3-D snapshots at various time intervals (a-g) : CSD w.r.t. crystal size and strain; (h) Semi-logarithmic plot of population density vs crystal size (depicting the steep upward curvature in the low size-class range at steady state)

Another interesting aspect of GRD that is also captured quite well is the steep upward curvature observed in the lower size class domain. This is depicted in Figure 7.6(h) for the semi-logarithmic plot of population number density vs. crystal size, at steady-state conditions.

7.6.2 Effect of healing constant

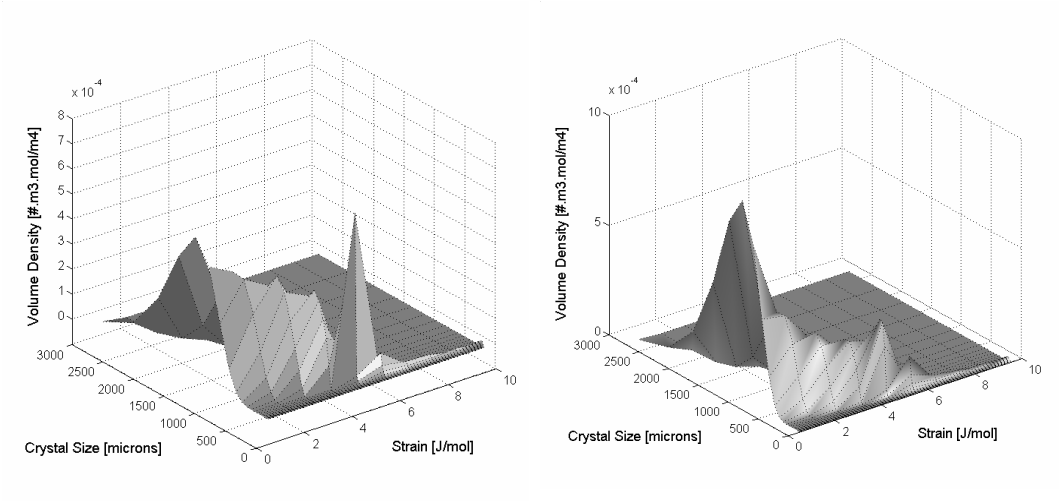

(a) k_H=1. 10^6 m^{-2} **(b)** k_H =3. 10^6 m^{-2}

Figure 7.8 CSD w.r.t. crystal size and lattice strain (at steady-state) for simulations where the strain is proportion to the crystal surface area: (a) SIM SD3_16, and (b) SIM SD3_15

Figures 7.8(a,b) show the influence of the healing constant on the final steady-state CSDs. An increase in the healing constant is bound to increase the healing rate of the strained fragments(see Figures 7.5(a-c)). This implies that even the highly strained crystal in the higher strain classes get an opportunity to heal even more, thus increasing it's chances of survival by getting transferred to lower strain classes. Thus, there is a lower accumulation of finer crystals at higher strain classes(because they escape faster) as shown in Figure 7.8(b) as compared to the case when the healing constant is lower (Figure 7.8(a)) where the volume density function peak at around 5 J/mol is higher than in Figure 7.8(b).
The resulting increase in the number of survived nuclei (at higher healing rates) leads to a lower steady-state median crystal size, as depicted in Figures 7.9(a,b).

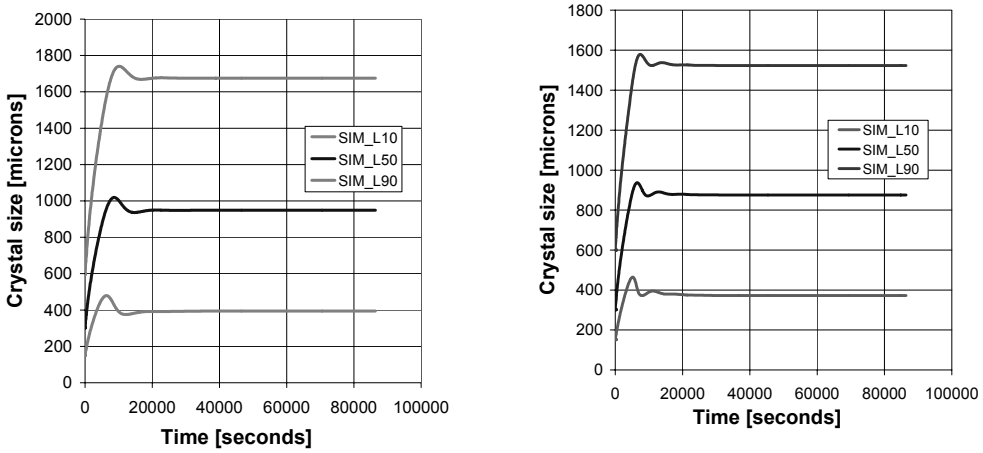

(a) k_H =1. 10^6 m^{-2} **(b)** k_H =3. 10^6 m^{-2}

Figure 7.9 Simulated transients of the quantiles for CSD for simulations where the strain is proportion to the crystal surface area: (a) SIM SD3_16, and (b) SIM SD3_15

7.6.3 Effect of n

Figures 7.10(a-c) give a comparison between the three different scenarios for the healing mechanism, i.e when the healing is proportional to the crystal size (L), crystal surface area (L^2) and the crystal volume (L^3), respectively. Here again, the volume density distribution is plotted as a function of the crystal size (L) and the strain in the crystal lattice (w_s). The figures below are snapshots of the CSD at steady-state.
For the CSD in the case of n=1 (Figure 7.10(a)) no crystals are left in the highest strain class (10 J/mol). From the earlier discussion in Figure 7.5(a-c), it has been shown that the release of the internal lattice strain is much faster than in the cases of n=2 and n=3. Hence, the majority of strained crystals arrive in the lower strain classes, with the highest strained crystals falling under 6 J/mol. As the dependency on L increases, the release of strain with crystal growth is more sluggish resulting in more strained crystals at higher strain classes. Figure 7.10(b) shows that for n=2, the volume density for crystals at 8 J/mol is quite high, while for n=3 (Figure 7.10(c)) there are even crystals in the highest strain class of 10 J/mol. Figure 7.10(b) and Figure 7.10(c) clearly depict the higher volume of strained fragments along the strain axis.
The evolution of the quantiles (L_{10}, L_{50}, L_{90}) as a function of time is given in Figure 7.11(a-c). At steady-state, the growth and secondary nucleation (due to attrition) rates are in equilibrium with each other under the prevailing process conditions. As seen from Figure 7.10(a), there are fewer crystals at higher strained classes for n=1, which imply that there are fewer small fragments that can consume the supersaturation. On the contrary when the healing is proportional to the crystal surface area (n=2) and the crystal volume (n=3), there are more number of attrited small fragments at higher strain classes, which in turn consume the supersaturation more due to even higher specific surface areas. As a consequence, the effective supersaturation and subsequently the crystal growth rate decreases. This is possible only if the strained crystals at higher strain energy levels survive dissolution, which of course depends on the prevailing supersaturation. Consequently, the median size (L_{50}) shifts towards smaller crystal sizes as the dependency of the healing rate on L increases.

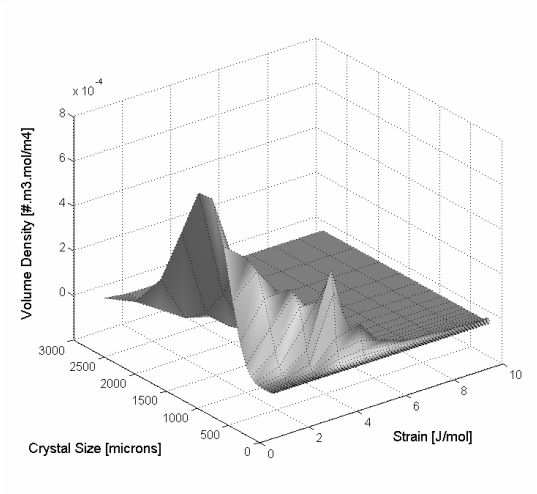

(a) n=1, k_H = 15.10^2 m^{-1}

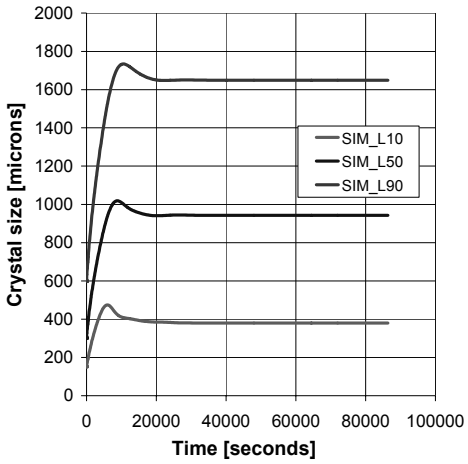

(a) n=1, k_H = 15.10^2 m^{-1}

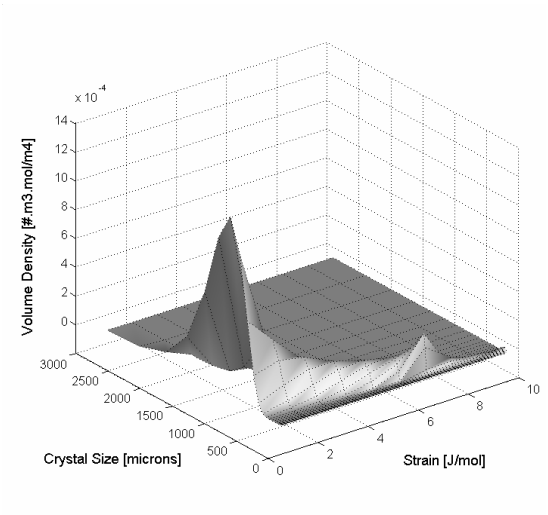

(b) n=2, k_H = 7.10^6 m^{-2}

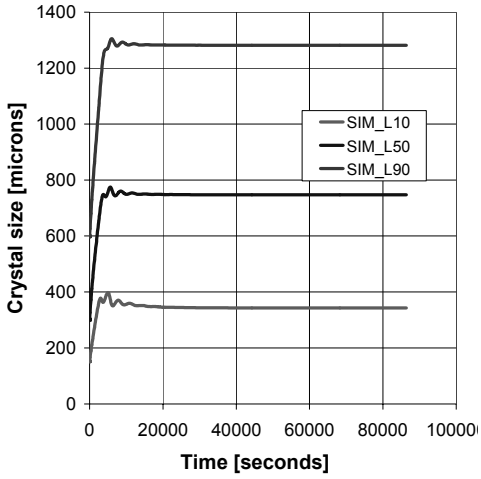

(b) n=2, k_H = 7.10^6 m^{-2}

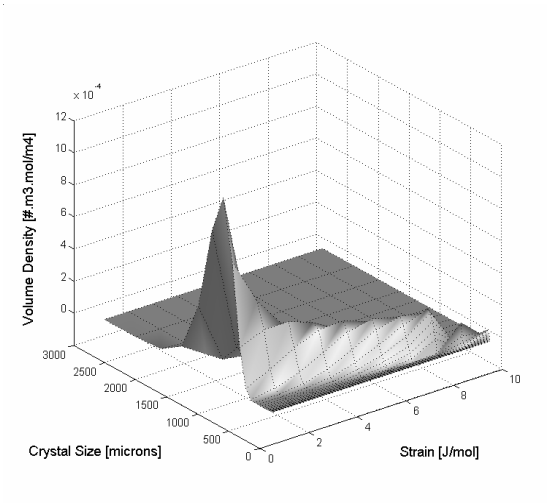

(c) n=3, k_H = 8.10^9 m^{-2}

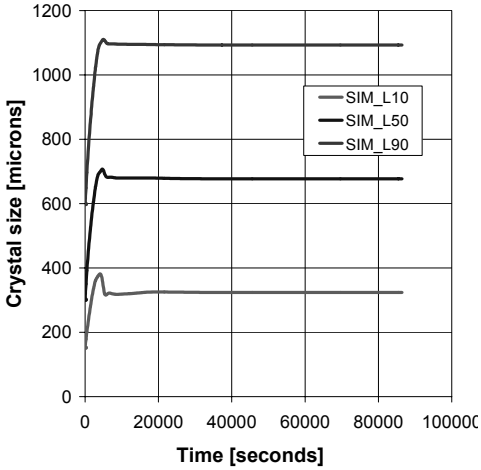

(c) n=3, k_H = 8.10^9 m^{-2}

Figure 7.10 CSD w.r.t. crystal size and lattice strain (at steady-state) for simulations illustrating the effect of *n:* (a) SIM SD3_11, (b) SIM SD3_6 and (c) SIMSD3_14

Figure 7.11 Simulated transients of the quantiles illustrating the effect of *n:* for (a) SIM SD3_11, (b) SIM SD3_6 and (c) SIMSD3_14

7.6.4 Comparison with relaxation mechanism using 2D PB model

In order to test if the relaxation mechanisms suggested by Gerstlauer(2001) are able to describe GRD, they were implemented in the two-dimensional population balance model framework. The simulations

done here were identical to those done, employing the healing mechanisms, i.e. system studied was ammonium sulphate – water for the 1100L DTB crystallizer, with the process conditions as listed in Table 7.4. Here, for illustration purpose, the final steady-state CSDs are shown (Figure 7.12(a-c)) for a few cases discussed by Gerstlauer(2001). The 2D population balance model enables the description of the broadening of the CSD which suggests that the relaxation mechanism is also capable of explaining aspects pertaining to GRD. Similarly, the steep upward curvature in the semi-logarithmic plot of population number density vs. crystal size (see Figure 7.16), can also be reproduced.
Concluding, it can be said that the simulations indeed show a strong dependence of the steady-state volume density function on the different relaxation mechanisms, which justifies the inclusion of a second characteristic particle coordinate like strain in modelling crystallization processes.

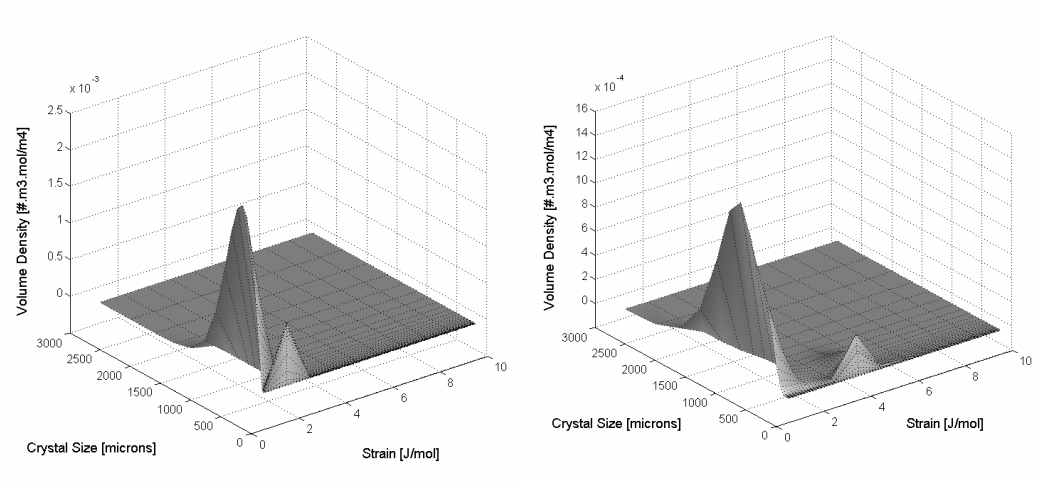

(a) ($W_s \sim C$) **(b) ($W_s \sim L$)**

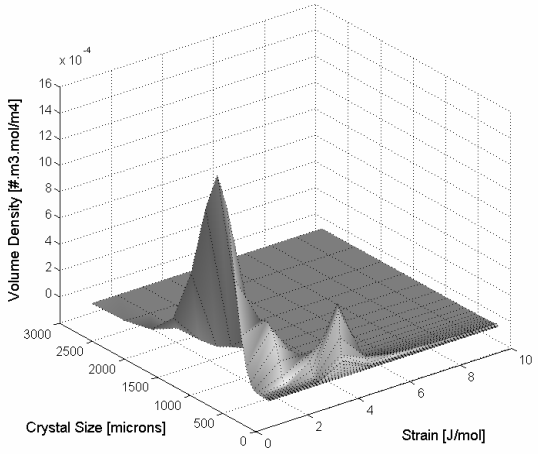

(c) ($W_s \sim L^2$)

Figure 7.12 CSD w.r.t. crystal size and lattice strain (at steady-state) for simulations using relaxation mechanisms of Gerstaluer (2001): (a) SIMG2, (b) SIMG3 and (c) SIMG1

7.6.5 Model validation with pilot-plant data

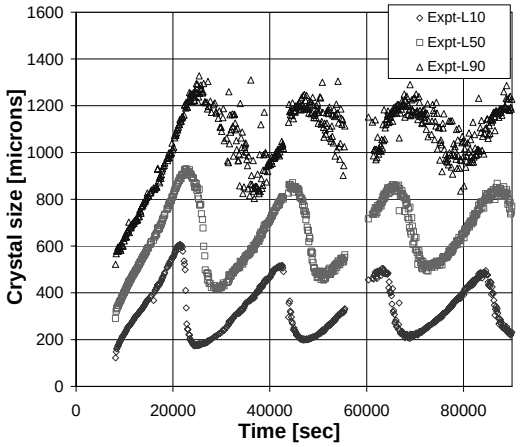

Figure 7.13 Sustained cyclic behavior for the quantiles observed in a continuous experiment in a 1100L DTB crystallizer (Neumann, 2001)

The 2D healing model is now subjected to model validation using experimental data for the 1100L DTB crystallizer. Figure 7.13 shows the actual experimental data from the 1100L DTB crystallizer (Neumann, 2001) for the process conditions listed in Table 7.4. Here, there is a sustained oscillatory behavior observed which is not reproduced by the 2D population balance model (see Figures 7.9 and 7.11).

A DTB crystallizer has an annular zone in it's geometry which allows for the selective removal of fine particles. This results in different growth behavior for the crystals within the crystallizer due to higher levels of supersaturation resulting from the removal of fine particles. In certain regions of the DTB crystallizer (eg. the boiling zone where the supersaturation attains the highest value), periodic nucleation bursts can be triggered during the process, which can explain the sustained cyclic behavior as has been shown by Menon(2005).

However, such a sustained oscillatory behavior is not observed in the case of draft tube crystallizers, which makes them an ideal candidate for the validation of the 2D population balance model. Hence, the experimental data-set obtained from a 22L DT crystallizer (Neumann, 2001) is used instead for model validation purposes.

Figure 7.14 depicts the trends of the median crystal sizes (L_{50}) for a particular continuous experiment (DT25) performed on a 22L DT crystallizer. These simulations were done for the various relaxation and healing mechanisms discussed in this chapter (see Table 7.4 for overview on the simulations).

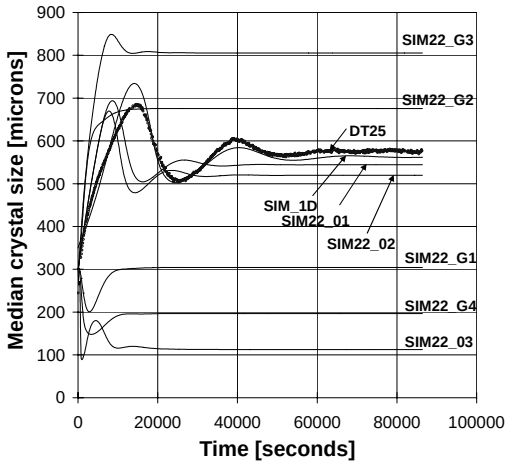

Figure 7.14 Simulated transients of the median crystal size for a 22L DT crystallizer (model validation for experiment DT25), *see Table 7.4 for legend*

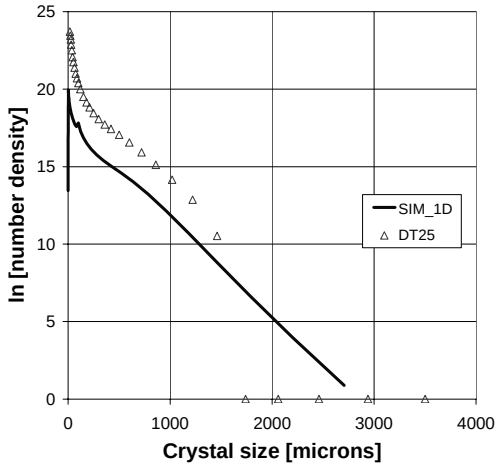

Figure 7.15 Semi-logarithmic plot of population number density vs crystal size (at steady-state) for 1D population balance model, *see Table 7.4 for legend*

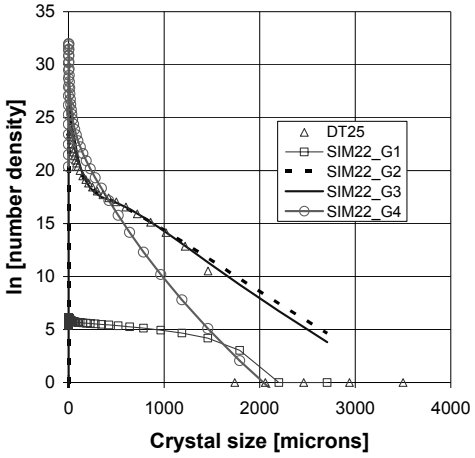

Figure 7.16 Semi-logarithmic plot of population number density vs crystal size(at steady-state) for 2D population balance model using relaxation mechanisms, *see Table 7.4 for legend*

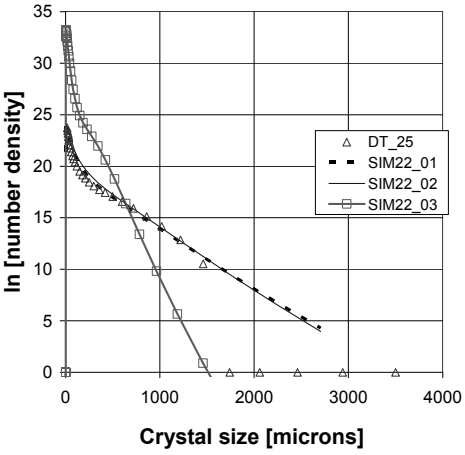

Figure 7.17 Semi-logarithmic plot of population number density vs crystal size (at steady-state) for 2D population balance model using healing mechanisms, *see Table 7.4 for legend*

It must be mentioned that the simulations done for 1D were performed using the parameter set for k_r and Γ_s obtained via parameter estimation runs by Bermingham(2003). Hence, these results match the closest to the experimental data set of DT25.
Parameter estimation studies using the 2D population balance model have been quite challenging in view of the huge computational effort required, using advanced dynamic optimization tools within gPROMS. Therefore, numerous simulations were done at different kinetic parameter combinations. Hence, the results for the growth rate dispersion mechanisms are only indicative of the dynamics of the median crystal sizes.
As seen from Figure 7.14, SIM22_G1 (case 1 of relaxation mechanism where $W_s \sim constant$), SIM22_G4 (case 4 of relaxation mechanism where $W_s \sim L^3$) and SIM22_03 (case 3 of healing mechanism where $w_s \sim L^3$) are far off from the experimental result. The remaining healing and relaxation mechanisms show potential in describing the process dynamics closer to real plant-data. Hence, they look the most promising candidates for future parameter estimation studies. Actually, SIM22_01 (case 1 of healing mechanism where $w_s \sim L$) and SIM22_02 (case 2 of healing mechanism where $w_s \sim L^2$) give the best match with the experimental data.

Next, the 2D models are also validated for the steep upward curvature observed in the lower size classes, in the semi-logarithmic plot of population density vs crystal size. Figures 7.15, 7.16 and 7.17 show the steady-state plots for the different mechanisms.
Figure 7.15 clearly shows a gross mismatch between the experimental data and the 1D population balance model. This is also the case for the relaxation models suggested by Gerstlauer(2001) (see Figure 7.16). None of the relaxation mechanisms are able to predict the trend in the semi-log plot of population number density vs. crystal size. When it comes to the healing mechanisms (see Figure 7.17), SIM22_01 (case 1 of healing mechanism where $w_s \sim L$) and SIM22_02 (case 2 of healing mechanism where $w_s \sim L^2$) again provide a very good fit with experimental data.
This suggests that the hypothesis where healing is proportional to the surface area of the strained crystals holds true. These results are in line with our physical interpretation of GRD that the strain is more localized on the surface layers of the strained crystals. But the simulations also suggest that healing proportional to the crystal length could also play a role. Hence, it is recommended to further

validate/develop the healing models based on further understanding of the growth behavior from lab-scale experiments.

7.6.6 Limitations of the healing model

The simulations and experimental validation on a 22L DT crystallizer needs to be backed up with more fundamental understanding of growth rate dispersion occurring at a molecular scale. This should also enable a better understanding of the mechanism, that is, to say whether healing is proportional to the crystal length or surface area or a combination thereof. This is only possible by investigation into the growth behavior (ranging from growth to dissolution, as well as partial dissolution and subsequent outgrowth). Investigations carried out by Virone (2006) on single crystal healing experiments under stagnant conditions should throw more light into the healing behavior of strained crystals.
Another limitation is with regards to the accuracy of the values used for internal lattice strain within secondary nuclei in suspension crystallizers. Using state-of-the-art measurement technologies available, it is difficult to validate this 2D model as it is virtually impossible to get an idea about the initial distribution for the strain in newly born secondary nuclei, under suspension conditions in solution.

7.7 CONCLUSIONS

A multi-dimensional population balance model with two internal coordinates was implemented for a dynamic and continuous crystallization process, to describe the healing of plastically deformed crystals that stem from secondary nucleation via attrition. Apart from the size (L) of the crystal, the internal molar lattice strain (w_s) of the individual crystals was used as an internal coordinate in the PBE.
The influence of the healing mechanism on the predicted dynamic behavior clearly shows that besides the size of the crystals, the strain in the crystal lattice also has a pronounced effect on the growth rate of the individual crystals, as seen from the CSD plots. This justifies the need to include strain as an important characteristic particle coordinate when modelling crystallization processes which involve secondary nucleation by attrition. The modeling approach also allowed the analysis of different models for the decrease of the strain upon growth or dissolution. Two such models were implemented and studied, the healing model proposed by Westhoff (2002) and Menon(2003) and the relaxation model developed by Gerstlauer (2001).
The simulation results give an interesting insight into the broadening of the crystal size distribution due to GRD. The application of a two-dimensional growth model enables the description of the steep upward curvature that is observed at lower size classes, in the semi-logarithmic plot of population number density vs crystal size.
As seen from the median crystal size (L_{50}) of the CSDs for the simulation of an evaporative crystallization process in a 22L DT crystallizer, certain relaxation and healing mechanisms show potential in describing the process dynamics when compared with plant data. Cases 1 and 2 of the healing mechanism where $w_s \sim L$ and $w_s \sim L^2$ respectively, give the best match with the experimental data. Both these scenarios fit reasonably well with the dynamics for the median crystal size and also the steep upward curvature curve.
These simulation results suggest that the hypothesis where healing is proportional to the surface area of the strained crystals holds true. These results are in line with our physical interpretation of GRD that the strain is more localized on the surface layers of the strained crystals. But the simulations also suggest that healing proportional to the crystal length could also play a role. Hence, it is recommended to further validate/develop the healing models based on further understanding of the growth behavior from lab-scale experiments.
Due to the computational intensity of the simulations, parameter estimation studies could not be realized for a crystallizer on an industrial scale. Further, a lack of precise knowledge on the initial distribution for strain adds to the uncertainties within the 2D model.

From a fundamental perspective, more understanding is needed on the growth behavior of the attrited fragments in order to determine which healing mechanism actually governs GRD. Parallel work is in progress (Virone, 2006), mainly aimed at single crystal healing experiments to arrive at a better description of the healing pattern of strained crystals.

NOTATIONS

B	size and strain dependent birth rate	[#.mol.m^{-4}.s^{-1}.J^{-1}]
B_o	birth rate at lower size limit	[#.mol.m^{-3}.s^{-1}J^{-1}]
c	concentration	[kg.m^{-3}]
c_s	concentration of the solid phase	[kg.m^{-3}]
C	solution concentration	[kg.kg^{-1}]
C^*	saturation concentration	[kg.kg^{-1}]
C_{sat}	saturation concentration	[kg.m^{-3}]
D	size dependent death rate	[#.mol.m^{-4}.s^{-1}J^{-1}]
D_{AB}	binary diffusion coefficient	[m^2.s^{-1}]
E	total surface energy	[J]
G	linear growth rate	[m.s^{-1}]
H	healing rate	[J.mol^{-1}.s^{-1}]
k_d	mass transfer coefficient	[m.s^{-1}]
k_H	healing rate parameter	[m^{-n}]
k_r	integration rate constant	[m^4.mol^{-1}.s^{-1}]
k_v	volumetric shape factor	[-]
L	crystal length	[m]
$L_{initial}$	Initial crystal size	[m]
M	molecular weight	[kg·mole^{-1}]
n	constant/exponent value	[-]
n_L	population number density at a certain size	[#.mol.m^{-4}.J^{-1}]
r	particle radius	[m]
R	universal gas constant	[J.mol^{-1}.K^{-1}]
R_G	relaxation rate	[J.mol^{-1}.s^{-1}]]
t	time	[s]
T	temperature	[K]
$w_{s,initial}$	initial value of elastic strain energy	[J.mol^{-1}]
w_{max}	maximum value of strain	[J.mol^{-1}]
w_s	strain energy/chemical potential difference	[J.mol^{-1}]
W_s	absolute lattice strain	[J]
t	time	[s]
T	temperature	[K]
V	volume	[m^3]

Greek

$\bar{\varepsilon}$	specific power input	[W·kg^{-1}]
γ_{ef}	effective specific surface energy	[J.m^{-2}]
Γ_s	surface related energy increase	[J.m.mol^{-1}]
ν_l	kinematic viscosity of the liquid	[m^2·s^{-1}]
ϕ_V	volumetric flow rate or volumetric flux	[m^3·s^{-1}]
ρ	crystal density	[kg·m^{-3}]

Indices

in	incoming stream
out	outgoing stream

Abbreviations

B.C.	Boundary condition
CSD	Crystal Size Distribution
CSTR	Continuous Stirred Tank Reactor
DT	Draft Tube
DTB	Draft Tube Baffle
GRD	Growth Rate Dispersion
MSMPR	Mixed Suspension Mixed Product Removal
PBE	Population Balance Equation
SDG	Size Dependent Growth

REFERENCES

Berglund, K.A. & Larson, M.A.(1982).Growth of contact nuclei of citric acid monohydrate, *AIChE Symposium series*, 78, 215, 9

Bermingham, S.K. (2003a). *A Design Procedure And Predictive Models For Solution Crystallization Processes- Development And Application*, Ph.D. Thesis, Delft University of Technology, the Netherlands, ISBN 90-407-2395-8

Bermingham, S.K., Verheijen, P.J.T. and Kramer, H.J.M. (2003b). Optimal design of solution crystallization processes with rigorous models, *Trans. IChemE*, 81, part A, pp.893-903

Bermingham, S.K., Kramer, H.J.M. and Rosmalen van, G.M. (1998). Towards on-scale crystallizer design using compartmental models, *Computers and Chemical Engineering*, 22, pp.S355-S362

Bhat, H.L., Sherwood, J.N., Shripathi, T. (1987). The influence of stress, strain and fracture of crystals on the crystal growth process. *Chemical Engineering Science*, 42, pp.609-618

Berglund, K.A., Kaufman, E.L. and Larson, M.A. (1983). Growth of contact nuclei of potassium nitrate, *AIChE Journal*, 29, pp.867-869

Burton, W.K., Cabrera, N., Frank, F.C. (1951). *Phil. Trans. Roy. Soc.* , London, A243, pp.299-358

Chernov, A.A. (1990).In: *Industrial Crystallization '90,* ed. Mersmann, A., Physics of single crystal growth from aqueous solution: ADP, KDP, DKDP, pp.343-348

Davey,R.J., Ristic, R.I. and Zizic, B.(1979). The role of dislocations in the growth of ammonium dihydrogen phosphate crystals from aqueous solutions, *Journal of Crystal Growth*, 47, pp.1-4

Frank, F.C. (1949). Symposium on crystal growth, *Discussions of the Faraday Society*, no.5

Gahn, C. & Mersmann, A.(1999). Brittle fracture in crystallization processes Part A: Attrition and abrasion of brittle solids, *Chemical Engineering Science*, 54, pp.1273-1282

Gahn, C. & Mersmann, A.(1999). Brittle fracture in crystallization processes Part B: Growth of fragments and scale-up of suspension crystallizers, *Chemical Engineering Science*, 54, pp.1283-1292

Garside, J. (1979). Growth of small crystals, In: Jancic, S.J. and de Jong, E.J. (Eds.), *Industrial Crystallization '78*, North-Holland, Amsterdam, pp.143-151

Garside, J., Rusli, I.T., Larson, M.A. (1979). Origin and size distribution of secondary nuclei, *AIChE Journal*, 25, pp.57-64

Garside, J. and Ristić,R.I. (1983). Growth rate dispersion among ADP crystals formed by primary nucleation, *Journal of Crystal Growth*, 61, pp.215-220

Gerstlauer, A., Mitrovic, A., Motz, S. and Gilles, E.D. (2001). A population model for crystallization processes using two independent particle properties, *Chemical Engineering Science,* 56*,* pp. 2553-2565

Garside,J. and Jančić, S.J. (1979). Measurement and scale-up of secondary nucleation kinetics for the potash alum-water system, *AIChE Journal*, 25, pp.948-958

Herden, A., and Lacmann, R.(1997). The crystallization of potassium nitrate II. Growth rate dispersion, *Journal of Crystal Growth*, 179, pp.592-604

Heijden, A.E.D.M and van der Eerden, J.P. (1992). Growth rate dispersion: The role of lattice strain, *Journal of Crystal Growth* , 118, pp.14-26

Herndl,G. (1982) *Stoffübergang in gerührten Suspensionen*, PhD Dissertation, TU München, Germany

Jones, A.G., Budz, J. and Mullin, J.W. (1986). Crystallization Kinetics of Potassium Sulfate in an MSMPR Agitated Vessel, *AIChE Journal* , 32, 12, pp.2002-2009

Jones, C.M., Larson, M.A., Ristic, R.I. and Sherwood, J.N. (2000). The role of dislocations, integral strain, and supersaturation on the growth rates of sodium nitrate, *Journal of Crystal Growth*, 208, pp.520 - 524

Knapp, L.F. (1922). The solubility of small particles and the stability of colloids, *Transactions of the Faraday Society*, 17, pp.457-465

Kumar, S. and Ramkrishna, D. (1996). On the solution of population balance equations by discretization--I. A fixed pivot technique, *Chemical Engineering Science,* Volume 51, Issue 8, pp.1311-1332

Kumar, S. and Ramkrishna, D. (1996). On the solution of population balance equations by discretization--II. A moving pivot technique, *Chemical Engineering Science,* Volume 51, Issue 8, pp.1333-1342

Menon, A.R., Kramer, H.J.M., Grievink,J. and Jansens, P.J. (2004). A multi-dimensional population balance model for growth rate dispersion in industrial crystallizers, *Proceedings of the International Workshop on Industrial Crystallization* (BIWIC11), Gyeongju, 15-17 September, South Korea

Menon, A.R., Kramer, H.J.M., Grievink, J., Jansens, P.J.(2005). Modelling the cyclic behavior in a DTB crystallizer - A two-population balance model approach, *Journal of Crystal Growth*, Vol.275, Issues 1-2, pp. e1373-e1381

Menon, A.R., Kramer, H.J.M., Grievink,J. and Jansens, P.J.(2003). Modelling of growth rate dispersion in industrial crystallizers using a two-dimensional population balance model. *Proceedings of the International Symposium on Process Systems Engineering and Control*, pp.143-148, Bombay, 3-4 January 2003, India

Mersmann, A., Angerhöfer, M., Gutwald, T., Sangl, R. and Wang, S. (1992). General prediction of median crystal sizes, *Separation Technology*, 2, pp.85-97

Neumann, A.M.(2001).*Characterizing industrial crystallizers of different scale and type.* PhD Thesis, Delft University of Technology, Delft, the Netherlands, ISBN 90-6464-882-4

Ó Meadhra, R. (1995). *Modelling of the kinetics of suspension crystallizers – a new model for secondary nucleation.* PhD Thesis, Delft University of Technology, the Netherlands, ISBN 90-407-1190-9

Ó Meadhra, R.S., Kramer, H.J.M. and van Rosmalen, G.M. (1995). Size dependent growth behaviour related to the mosaic spread in ammonium sulfate, *Journal of Crystal Growth*, 152, pp.314-320

Randolph, A.D. & Larson, M.A. (1988). *Theory of particulate processes, Second edition*, Academic Press, San Diego, USA

Ristić,R.I., Sherwood, J.N., Shripathi, T. (1990). Strain variation in the growth sectors of potash alum single crystals and it's relationship to growth rate dispersion, *Journal of Crystal Growth*, 102, pp.245-248

Ristic, R.I., Sherwood, J.N. and Wojciechowski, K. (1988). Assessment of the strain in small sodium chlorate crystals and its relation to growth rate dispersion, *Journal of Crystal Growth*, 91, pp. 163-168

Ristic, R.I., Sherwood, J.N. and Shripathi, T.(1997). The influence of tensile strain on the growth of crystals of potash alum and sodium nitrate, *Journal of Crystal Growth*, 179, pp. 194-204

Roberts, K.J. (1995). In: *Science and Technology of Crystal Growth*, eds. J.P. van der Eerden and O.S.L.Bruinsma, Kluwer Academic Publishers, Dordrecht, The Netherlands

Rojkowski, Z.H. (1993). Crystal growth rate models and similarity of population balances for size dependent growth rate and for constant growth rate dispersion, *Chemical Engineering Science*, 48 (8), pp.1475-1485

Rusli, I.T., Larson, M.A. and Garside, J. (1980). Initial growth of secondary nuclei produced by contact nucleation. Design, control and analysis of crystallization processes. *AIChE symposium series*,76 (193), pp.52-58

Sahin, Ö and Bulutcu, A.N.(2002). Effect of surface charge distribution on the crystal growth of sodiumperborate tetrahydrate, *Journal of Crystal Growth*, 241, pp.471-480

Valcic, A.V. (1975). Influence of dissolution on the growth rates of saccharose crystals, *Journal of Crystal Growth*, 30, pp.129-136

Virone,C., ter Horst, J.H., Kramer, H.J.M. and Jansens, P.J.(2004). The strain content of ammonium sulphate attrition fragments. *Proceedings of the International Workshop on Industrial Crystallization* (BIWIC11), Gyeongju, 15-17 September, South Korea

Virone, C. (2006), PhD thesis, Delft University of Technology (to be published)

von Rittinger, R.(1867). *Lehrbuch der Aufbereitungskunde*, Berlin: Ernst and Korn Verlag

Wang, S. and Mersmann, A. (1992). The initial size dependent growth rate dispersion of attrition fragments and secondary nuclei, *Chemical Engineering Science* , 47 (6), pp.1365-1371

Westhoff, G.M.(2002). *Design and analysis of suspension crystallizers: Aspects of crystallization kinetics and product quality*, PhD Thesis, Delft University of Technology, the Netherlands, ISBN 90-6464-138-2

Westhoff, G.M., Van de Rijt, J., Kramer, H.J.M., Jansens, P.J.(2002). Modelling growth rate dispersion in industrial crystallizers. *Proceedings of the 15th International Symposium on Industrial Crystallization*, Vol.2, pp.143-148, Sorrento, 15-18 September, Italy

White, E.T. and Wright, P.G. (1971). Magnitude of size dispersion effects in crystallization, *CEP Symp. Ser.*, 67 (No.110), pp.81-87

Zacher, U. and Mersmann, A.(1995). The influence of internal crystal perfection on growth rate dispersion in a continuous suspension crystallizer, *Journal of Crystal Growth*, 147, pp.172-180

8

Conclusions & Perspectives

This dissertation focuses mainly on modelling and design strategies for industrial crystallization processes in solution. Chapter 1 introduced the state-of-the-art in crystallizer design and modelling of industrial crystallization processes. Based on this, the objectives of this research as well as research hypotheses were formulated with focus on integrating this state-of-the-art knowledge into better design procedures and modelling tools. Here, the key contributions to the field of crystallization will be summarized and evaluated. Furthermore, an outlook is presented with regards to unattended research issues and areas that still need to be explored/covered.

The main thrust for the subject matter in this research was motivated from practical problems encountered in the design, operation and control of industrial scale crystallization processes. Crystallization is applied in continuous operation on a large scale for bulk production of inorganic and organic materials while on a small scale, crystallization is often applied as a batch process to obtain high purity on fine chemicals or pharmaceuticals. Hence, both continuous and batch processes have been the subject of study in this thesis.

Here, the main findings of the research are summarized and evaluated with respect to the underlying research questions. In addition, suggestions for future work are put forward as an outlook to the general improvements needed in the modelling and design of industrial crystallization processes. These can also serve as prospects for a continuation of crystallization process research at Delft University of Technology.
For the design of industrial crystallization processes, an expert design platform is needed that conceptually guides the designer at arriving at the *optimum* configuration and operational conditions, for the crystallization process and the crystallization equipment(s). This platform basically entails a systematic design procedure and a process modelling framework with state-of-the-art fundamental rate models, to support process synthesis and analysis. From the research presented in this thesis, there are mainly three concrete results that come forward as deliverables to the objectives and research questions that were formulated in Chapter 1 of this thesis :

- A taxonomical treatment of a novel task-based design ontology for the synthesis and design of crystallization processes and crystallizer equipment(s).
- Crystallization models (developed within UNIAK-III) validated against fed-batch crystallization experimental data.
- Next-generation models which account for the phenomenon of growth rate dispersion and explain the sustained cyclic behaviour observed in certain crystallization processes.

Design
At the beginning of this PhD research, the state-of-the-art in terms of systematic design procedures for industrial crystallization processes, resulted from the thesis of Bermingham(2003a). The strength of the design approach developed by Bermingham(2000), extended by Westhoff(2002) with instrumentation and control design levels, is in the careful structuring of the decision making process and in covering the full range of conceptual design. This work provided a solid frame to refine two levels in the systematic procedure. Pursuing this idea resulted in two main additions to the systematic hierarchical design procedure proposed by Bermingham(2000).
First of all, at the process block diagram level (3), the existing concept of a superstructure was made applicable to the generation of superstructures for crystallization process flowsheet(s). This approach can potentially provide significant savings in terms of investment costs and lower levels of energy consumption.
Secondly and the more significant contribution, is the development of a novel task-based design approach, with the focus mainly on the synthesis of crystallization equipment. Here, the line of thinking is that the equipment under design must facilitate the physical tasks rather than allowing the physical performance to be the result of pre-conceived equipment shapes. An ontological treatment of the physical task and state concept has been realized in this thesis, which enables the generation of superstructures, made up of a network of tasks, which can ultimately yield the optimum equipment configuration. Here, the crystallization mechanisms and essential function(s) to realize the desired product specification(s) were identified as physical tasks. Each task is endowed with its own attributes which help in characterizing its nature. Each task is further built up using appropriate phase building blocks, which is an essential step in realizing the changes of state. An optimum combination of tasks can be set up in a network. There were ten synthesis sub-levels identified, with a discrimination between the spatial and temporal domains. These synthesis steps range from identifying the relevant

tasks needed for crystallization to their connection in a network to the formation of design compartments and finally the operational unit identification which realizes the final crystallizer configuration(s).
The newly developed ontology, comprising a description of the structural and the behavioral models, is a pre-requisite for the development of a computer supported synthesis procedure. Such a computerized procedure will facilitate the generation and screening of many alternative design options. The further development of this task-based procedure involves its implementation in a modelling framework, and doing some pilot applications. It needs to be critically tested with respect to its effectiveness for generating innovative designs.
Such a task-based and synthesis-oriented approach is seen as a promising way forward in order to arrive at not only out-of-the-box designs, but also improved and optimized designs for existing configurations. Of course, this task-based approach is not limited to grass-roots design and will also aid in retrofit decisions. In this context, the task-based synthesis-driven approach is expected to lead to the development of new knowledge for design and operation of *innovative* production systems for crystallization (supply chains, products, processes, equipment, components) with excellent sustainability features, aiming specifically at market-responsive operation of intensified industrial scale units. As such it will contribute to process intensification.

Hence, the first step forward from a process engineering research perspective is to derive a modular structure for the task-based design, to be implemented in a computer environment. It is advised that the crystallization models should be kept as simple as possible as the computational effort is bound to increase, especially when it comes to the solution of superstructures as an optimization problem. But, with tremendous increase in computational power by the year, this self-imposed restriction on model complexity is not seen as a very serious limitation for the distant future as it can be gradually relaxed.
Secondly, novel intensified structures for crystallization units must have good operability features. This is not to be taken for granted, since counter examples have been found. So, what is needed is a better understanding of the interactions between design and control issues at various levels in the design hierarchy. This may also evolve into two possible approaches in the design of industrial crystallization equipment, viz. one focussing on grass-roots design and retrofit from a task-based design approach, while the other focuses more on the de-bottlenecking of existing structures in which the options offered by control might become more relevant.
Thirdly, in order to test the effectiveness of the task-based design approach, it is recommended that a design, made by this approach, is actually built on a lab-scale and assessed on its promised performance.
Finally, another important aspect is the application of this task-based design approach on an industrial case study, either at a grass-root level or as a retrofit case and to assess the outcome in comparison with existing, conventional designs. Such testing will provide an answer to a key assumption made for crystallization design: creative thrust is gained by taking a physical task-driven approach to process synthesis.

Batch crystallization
The main experimental effort in this research was contributed towards gaining a better understanding of batch crystallization technology with a two-fold objective: one to study the effect of different actuators on the product quality and second to use the plant data for model validation and parameter estimation purposes. The study on fed-batch crystallization experiments on crystallizers of different scale and type revealed a significant influence of the actuators (propeller frequency and the fines removal rate) on the product quality and the dynamic behavior of the CSD. The data generated from these unseeded experiments has been very useful in the validation of the rigorous crystallization models. Parameter estimation studies have shown a very high correlation between the two kinetic parameters k_r and Γ_n present in the crystallization model framework. But, with still scope for further improvement, future research on this subject should look into the incorporation of additional

crystallization mechanisms to arrive at a model framework with limited parameters, applicable to a wide range of crystallization processes and crystallizers of different type and scale.
Experiments on the 1100L DTB crystallizer revealed that the initial conditions (which are difficult to capture experimentally) have a huge impact on the evolution of the process dynamics, for batch crystallization processes. The simulations also show evidence of this fact. This implies that seeding can be a very effective actuator in realizing the desired product specification(s). Hence, the next effort, needed more from a process control and analysis perspective, is to perform seeded crystallization experiments, to draw out strategies for the efficient and optimal operation of the plant, and a better control of the process and the product specifications as such.
Future research also needs to focus on detailed spatially distributed measurements within the crystallization vessel as well as the annular zone with respect to flow patterns and temperature profiles. Solely such measurements will give a final certainty on the reasons for any observed unpredictability's in the dynamic behaviour.
Of course, extending the systems studied to other than inorganic systems will be a huge plus for model validation, to test the applicability and potential of such rigorous models to arrive at a more general modelling framework.

Modelling
The accuracy and predictive capability of the rigorous crystallizer models depends on the intended use of the model. When the model is used solely for control purposes (eg. stabilizing feedback controller design where topics of model reduction and model linearization assume importance), then accurate estimate of the kinetics are less necessary. On the other hand, for process design and optimization of plant operation purposes, often detailed models with very good accuracy are needed. In this thesis, the predictive crystallizer models developed by Bermingham(1998, 2003b) were improved further by using novel extensions of the particle state and the associated population balance equations, viz:

- **the two-population balance model approach to describe the sustained oscillatory behavior in a 1100L DTB crystallizer**

  A novel approach was introduced here to improve the description of the dynamic behaviour of industrial crystallizers using a two population balance model, which enabled a discrimination between different sources of nuclei. To this extent, the heterogeneous primary nucleation model (Kashchiev, 2000) and a couple of secondary nucleation models (Mersmann (1996) and Qian Botsaris(1997)) were the subject of this study. Simulations were performed with varying combinations of the parameters k_r and Γ_s (Gahn's growth model) and the degree of heterogeneity, ψ. This approach has shown that just including the secondary nucleation (attrition) model of Gahn and Mersmann (1999a,b) is not enough to explain the dynamics of the process. The single compartment models showed that the value of ψ needed to trigger a primary nucleation event is too low and unrealistic ($\psi < 0.1$). The multi-compartment models improved on the value of ψ (0.135 – 0.14) making it a more realistic value, to trigger primary nucleation for the system ammonium sulphate. Here it is possible to create higher supersaturation levels in certain localized region(s) of the crystallizer, say the boiling zone. Hence, the energy barrier to nucleation in these compartment(s) can be significantly reduced to effect a primary nucleation event. One of the main observations from the one-compartment and multi-compartment simulations, which was counter-intuitive, was the distribution of the crystals over the primary and secondary populations, wherein the primary class was found to be the more dominant population of the two. This could be an artifact of the simulation or from another perspective, this could as well be a matter of fact that primary nucleation plays a more dominant role in determining the process dynamics. Validation of the models with experimental data, for the continuous evaporative crystallization of ammonium-sulphate from water, in 1100L DTB and 75L DT crystallizers have shown that the inclusion of multiple nucleation events definitely increases the descriptive capability of the model, thus justifying the need for

two interacting nucleation mechanisms. The simulation results give a very good description of the start-up phase of the crystallizer operation, the dynamics of the process as well as the final steady-state values.

- **a two-dimensional population balance model to account for the phenomenon of growth rate dispersion resulting from the lattice strain embedded within secondary nuclei**

  In order to check the influence of strain on the growth behavior of secondary nuclei, a multi-dimensional population balance model using two internal coordinates, was implemented for a dynamic and continuous crystallization process. Apart from the size (L) of the crystal, the internal molar lattice strain (w_s) of the individual crystals was used as an internal coordinate in the population balance equation. Healing of the strained crystals was assumed to be more closely associated with the crystal surface area and thus, more of a surface related phenomenon, that is to say the lattice strain is not distributed uniformly over the entire volume of the crystal, but rather the strain is localized at the outer layers of the crystal where the deformation in the breakage process are the highest. Using this hypothesis, the simulation results give an interesting insight into the broadening of the crystal size distribution due to GRD. The application of the 2D growth model also enables the description of the steep upward curvature that is observed at lower size classes, in the semi-logarithmic plot of population number density vs crystal size. Model validation by means of plant data for an evaporative crystallization process in a 22L DT crystallizer shows that healing of the strained fragments is proportional to either the crystal length or the surface area of the crystals, which partially supports the hypothesis that healing is a surface-based phenomenon.

For a better applicability of these next generation models towards a wide range of crystallization processes and for a better understanding of the fundamentals of rate processes and how these affect process operation and process dynamics, there still lie areas that can be improved. Some recommendations to further improve upon these models are listed here:

- *Activated nucleation mechanisms*: The activated nucleation models proposed by Mersmann(1996) and Qian & Botsaris(1997) lack a fundamental physical explanation for certain inconsistencies in the model development, especially as to why surface nuclei are released from the surface while for ECSN, it is not clear how nuclei are removed from the surface layer to the bulk. Hence, it is recommended to revisit these models to make it more holistic and fundamentally correct.

- The assumption that primary nuclei or secondary nuclei generated via activated nucleation are strain-free is not necessarily true and this is reinforced by the fact that laboratory experiments have shown that growth rate dispersion is also present in primary nuclei. This assumption has an impact on the distribution of the different sources of nuclei in the separate crystal populations. To improve on the distribution between strained and unstrained population, it is suggested to introduce strain for nuclei in the primary population.

- *Growth Rate Dispersion*: One of the important conclusions from the 2D population balance model, is that Cases 1 and 2 of the healing mechansim where $w_s \sim L$ and $w_s \sim L^2$ respectively, give the best match with the experimental data. Both these scenarios fit reasonably well with the dynamics for the median crystal size and also the steep upward curvature curve. So from a fundamental perspective, more understanding is needed on the growth behavior of the attrited fragments in order to determine which healing mechanism actually governs GRD. Experimental investigation is a must to test the applicability of these models for scale-up purposes as well. As a start, the work of Virone(2006) can be used to improve the healing mechanism and confirm which of the crystal characteristic dependencies is contributing to

GRD. It could also be a combination of characteristics or the mechanism may even lie somewhere in between. Also, there is evidence of GRD for primary nuclei for the system ammonium-sulphate water, as investigated by Virone(2006). This enforces the fact that strain in secondary nuclei due to crystal – foreign body collisions cannot be counted as the only factor causing GRD. For primary nuclei, imperfections in the crystal lattice, mainly stemming from screw dislocations could also play an important role, thus inducing a strain content of a different kind. Hence, to take all these phenomena into account, a more comprehensive GRD model, embedding both the healing of secondary nuclei via strain release and the screw dislocation theory for primary nuclei may need to be incorporated into the 2D population balance model.

- Parameter estimation studies have not yet been realized for the two-population balance and two-dimensional population balance models, due to numerical difficulties, mainly resulting from an ill-scaled problem. This is seen as a major liability at this point, as this inevitably leads to more time and effort in model validation.

- As pointed out by Bermingham(2003), further improvements in the process dynamic behavior can be expected by including certain material properties (eg. critical work for indentation, W_C, and the Vicker's hardness, H) in parameter estimation studies. Even better would be to arrive at a better estimate or better models to determine these parameters from experimental investigations.

In addition to the above mentioned recommendations for future work, there is still an enormous expanse that needs to be bridged, in order to arrive at a more holistic process modelling framework. This especially lies in the field of fluiddynamics and particle technology. In the crystallizer models used/developed in this thesis, simple fluiddynamic models were employed and also the particle characteristics were limited (eg. crystal size and crystal lattice strain).
Non-uniformity in the process conditions and particle properties will greatly increase with increase in the crystallizer scale of operation, which is where fluiddynamic considerations come into play. Fluiddynamics is an area that makes the modelling issue a compromise between two extremes, i.e. whether to opt for sophisticated modelling architectures (say, involving Computation Fluid Dynamics (CFD) calculations) focussing on the minutest details and where a high spatial resolution is required or to go for a compartmental modelling approach that is simulation-timewise more practical for design purposes. Currently, CFD has been used to generate information like the circulation flow rate or the energy dissipation rate gradients within the crystallizer, which can in turn be used as useful input data in the compartmental models.
Most of the domain knowledge in the field of particle technology is strongly empirical in nature but, this trend is slowly changing as emerging disciplines like molecular modelling are increasingly being used to fill this void. This implies that introducing more product-related design specifications like lattice structure, morphology, crystal-habit, etc. in addition to the existing specifications like crystal size and lattice strain, will greatly enhance the design capability of the modelling tools to meet end-consumer demands and specifications.
With more sophisticated modelling tools becoming available in the areas of fluiddynamics and molecular modelling, and the increase in computational speed and robustness alongwith the possibility for parallel computing using supercomputers, there is tremendous scope for coupling of such tools with the process modelling framework say, built within a dynamic flowsheeting program like gPROMS.

REFERENCES

Bermingham, S.K., Neumann, A.M., Kramer, H.J.M., Verheijen, P.J.T., van Rosmalen, G.M. and Grievink, J. (2000). A design procedure and predictive models for solution crystallization processes. *AIChE Symp. Series 323*, **96**, pp. 250-264

Bermingham, S.K. (2003a). *A Design Procedure And Predictive Models For Solution Crystallization Processes- Development And Application*, Ph.D. Thesis, Delft University of Technology, the Netherlands, ISBN 90-407-2395-8

Bermingham, S.K., Verheijen, P.J.T. and Kramer, H.J.M. (2003b). Optimal design of solution crystallization processes with rigorous models, *Trans. IChemE*, 81, part A, pp.893-903

Bermingham, S.K., Kramer, H.J.M. and Rosmalen van, G.M. (1998). Towards on-scale crystallizer design using compartmental models, *Computers and Chemical Engineering*, 22, pp.S355-S362

Gahn, C. & Mersmann, A. (1999a). Brittle fracture in crystallization processes Part A: Attrition and abrasion of brittle solids, *Chemical Engineering Science*, 54, pp.1273-1282

Gahn, C. & Mersmann, A. (1999b). Brittle fracture in crystallization processes Part B: Growth of fragments and scale-up of suspension crystallizers, *Chemical Engineering Science*, 54, pp.1283-1292

Kaschiev, D. (2000). *Nucleation: Basic Theory with Applications*, Butterworth-Heinemann Ltd. Oxford, U.K.

Mersmann, A.,(1996). Supersaturation and nucleation, *Trans. Inst. Chem. Eng.*, 74, pp. 812-820

Qian, R. and Botsaris,G. (1997). A new mechanism for nuclei formation in suspension crystallizers: the role of interparticle forces, *Chemical Engineering Science*, vol. 52, No. 20, pp.3429-3440

Virone, C.V. (2006), PhD Thesis, Delft University of Technology, The Netherlands

Westhoff, G.M.(2002). *Design and analysis of suspension crystallizers: Aspects of crystallization kinetics and product quality*, PhD Thesis, Delft University of Technology, the Netherlands, ISBN 90-6464-138-2

A1.1 CRYSTALLIZATION RESEARCH AT DELFT UNIVERSITY OF TECHNOLOGY

Delft University of Technology is amongst the few research institutes globally, that is pursuing research in the field of industrial crystallization from a multi-disciplinary point of view. Over the last two decades (UNIAK: 1985-2000, CrysCODE: 2000 -), a lot of research and development has gone into the understanding of industrial crystallization processes from various perspectives, resulting in 10 PhD theses dissertations, at Delft University of Technology. This list, along with the ongoing research in the various disciplines, is summarized in Figure A1.1.

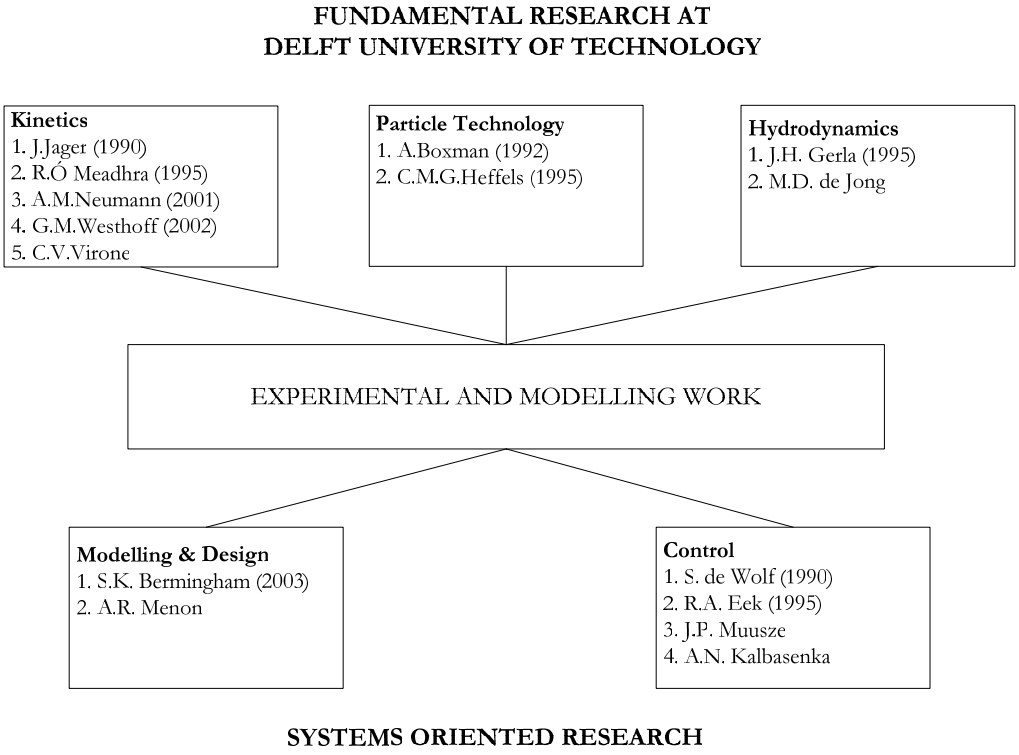

Figure A1.1 Multi-disciplinary crystallization research program at Delft University of Technology – An overview

A2.1 THE CONTROL SYSTEMS DESIGN LAYER

The overall decomposition of the control systems design layer follows from Seborg (2003). At this level, cost correlations for control can be developed (for eg. the number of set points in the process vs. the cost required for satisfying a given number of set points) to see whether they satisfy the economic constraints.

2.1.1 Determination of Control Objectives

The control objectives come from the initial levels of process design layer. At this level they are revisited specifically in relation to control systems design. They can be classified as follows.
Safety, equipment and environment related

- Limitations due to operating conditions for temperature, pressure, flow etc.
- Alarms, emergency shutdowns procedure
- Release of hazardous material in case of eventualities
- Failure of process / control equipment
- Human mistakes and its consequences

Smooth operation related

- Minimum and maximum level of inventories
- Disturbance source and its possible effects on process operation

Product related

- Mean, CSD, constraint violations for variables
- Production rate
- Impurity content

Monitoring and diagnosis related

- Fouling in the heat exchangers, corrosion etc.

2.1.2 Top-Down analysis

The top-down analysis approach identifies both the scope and complexity of a plantwide control design and its control structure. In case of highly integrated system, where control system design cannot be developed independently, this analysis will help to decompose the system into subsystems.

Design of Instrumentations (sensor measurements) in plant-wide context
Here the process variables that can be measured are determined; their number and measurement location/s within the equipment is decided. This level is separated from the actuator level because typically the actuators in a process are fixed; their presence in the process is almost always necessary and it affects the process. Surplus measurements can be taken if necessary with the process remaining unaffected.

Determine Manipulated variables (MV), controlled variable (CV), constraints and disturbances
Preliminary Degree of Freedom (DOF) analysis can be done here. The manipulated variables (MV), controlled variables (CV), constraints and disturbances are determined.

Input/Output Controllability Analysis of the Process
Here the multivariable process used by Skogestad (1996) can be used. It should be noted that this step takes into account model reduction part implicitly.

Evaluate possibilities for decomposition of control problem
For this, Seborg (2003) proposes a method in which pressure and temperature are assumed to be decoupled from the plant hold-ups, concentration and liquid flows. If this is valid, then the

approximate model formed can be used to find input-output pairing using Relative Gain Array (RGA). The possibilities are based on the insight into the problem.

Establish the overall control structure in conceptual form
The method of measuring and controlling the production rate of product/s and its quality is decided. For each recycle loop, its throughput/ composition controlling strategy is identified. The method of handling major disturbances and constraints is defined.

2.1.3 Bottom – up approach

After the plant has been decomposed into subsystems, it is controlled using conventional techniques.

Basic Control
Here basic inventory control (level and/or pressure) is done. Level is manipulated with either product flow or feed flow. Pressure can be manipulated with heat input in case of evaporative crystallization. Specifications of how the control system will deal with unsafe or abnormal operations and constraints will be given.

Design of Soft Sensors/Observers
This level will be required when there are no direct measurable states from the process. Statistical process monitoring can be used at this stage for supervision. For example in distillation, when quality measurements are not available, it is estimated using temperature measurements. Here they can be estimated using Kalman filter, neural network, inferential correlations, receding horizon control (which contains only the state estimation part out of the whole optimization of control moves,) or fuzzy logic. Some kind of model reduction techniques may be required here as well because of the large number of state variables involved in the model. Typically in a plant, the number of state variables is in the order of 100-1000 whereas the number of inputs is of the order of 10-100. So the observer identification problem is much larger than the control problem. This level can also be seen as a noise reduction level. Here both the input and output variables can be measured/inferred by simple equations but the state variables may not be measured and thus may need the help of model(s) to evaluate. So it can be estimated with the help of Kalman filter. These state variables will be checked against the set point of the controller to be designed in the next level.

Extensions to Basic Control and Design of Nominal Controller(s)
Extensions to the basic control like cascade, feedforward, feedforward with feedback etc. can sometimes improve the performance. If no improvement is seen after implementation of extensions, the design procedure is stopped and not propagated to next level. If improvements are seen, the extensions to basic control can be cast in form of Internal Model Control (IMC), as described in next section. Instead of developing a new control system design each time a new crystallization system is designed, a map of possible control configuration of crystallization can be made, which can be referred during control design (similar to standard quality control schemes for distillation columns).

Design of Operational Processes
Here the operational processes like operator training, start-up, shut-down, automated and non-automated processes, servicing etc. are defined. It is evaluated whether the start-up process (order of start-up etc.) can be described by controller. (for e.g. heat-integrated columns may need a small heat exchanger for start-up.) There must be some control degrees of freedom left for designing it. Keeping excess manipulated variable at the design of manipulated variables stage is an option but it is generally not employed.

Advanced Process Control (APC)
This includes Model Predictive Control (MPC), Internal Model Control (IMC), Dynamic Nyquist Array (DNA), Inverse Nyquist Array (INA) just to name a few. The IMC form is one of the most robust forms (with its limitations) but is very laborious to apply. When MPC is to be applied, since it is based on a linearized model, care should be taken in case of non-linear control schemes like ratio control. The problem here is that MPC will take action every min, whereas a flow, controlled by a ratio control will act after every second. So the control scheme is not necessarily improved by application of APC.

2.1.4 Validation and Simulation

Here the whole model along with applied control system is simulated and the results are checked against the required constraints and specifications. Various scenarios for possible cases (for example, failure of a pump) are generated and the ability of the strategy to cope with these scenarios is checked. Finally the model is tested on the real plant data.

A2.2 THE SUPPLY- CHAIN (OPERATIONS) LAYER

This layer closely follows the approach given by Tousain(2002). It should be noted that the term indicates (for the time being) only the operations part of a supply chain layer in a business.

2.2.1 The market subsystem

This is divided into purchase department and marketing & sales department. In case of a pull market, a price for the product is determined by sales people and market decides the demand. Since predicting market behavior is very difficult and there are many aspects like contracts, partnerships etc. that cannot be easily captured in mathematical relationships, a transaction-base market description has been proposed which considers the effect of interactions. They are categorized as orders (long term/short term commitments) and opportunities (estimation of future sales).

2.2.2 The storage subsystem

This is divided into raw material storage and end product storage. Since larger stocks are undesirable, production must be on demand, with minimal storage to tackle emergencies like shortage of supply or delivery on demand.

2.2.3 The production scheduler/planner

Currently in industry, fixed production requirements are set which the scheduler has to meet. When purchase and sales people start to interact with the production, the inventories can be kept to a minimum. The plant can be described in terms of operating tasks with accompanying precedence rules. The time interval, within which the task execution is considered, is either fixed or left as a degree of freedom. The scheduling problem thus set can be solved using either mathematical programming or using heuristics.

2.2.4 Real Time Process Optimization

The set points generated for the control layer will be applied through Real Time Process Optimization (RTPO) only after the design process has been finished. Such a rigorous approach may not be required in practice for relatively simpler processes. In such a case, just the set points generated in the design layer will be sufficient.

A2.3 NEED FOR SPLIT IN SPATIAL AND TEMPORAL DOMAINS

Here, a case is presented as to why a split in the spatial and temporal dimensions (synthesis levels 4.7 – 4.10) can be useful.

For that, it's worthwhile pointing out the difference between a batch and plug-flow reactor (PFR). In a batch reactor, the composition changes take place temporally whereas it happens spatially in the case of a PFR. Hence, the space equivalent of a single batch reactor can be considered to be a PFR with no side streams. A PFR can be approximated by using a number of mixed-flow reactors (CSTRs) in series. As was explained in synthesis levels 4.3, 4.4 and 4.6, tasks can be combined together in task zones which can further be combined into design compartments. Any given task or design compartment can be considered as a PFR, i.e. a series of well-mixed tasks/design compartments will yield a plug-flow unit. A comprehensive representation in the form of a superstructure is given by Kokossis and Floudas (1990). Modelling a plug flow unit[1] that takes into account an axial and radial distribution involves solution of PDEs as opposed to ODEs for the dynamic conservation equations and introducing additional partial derivates in the population balance equation.

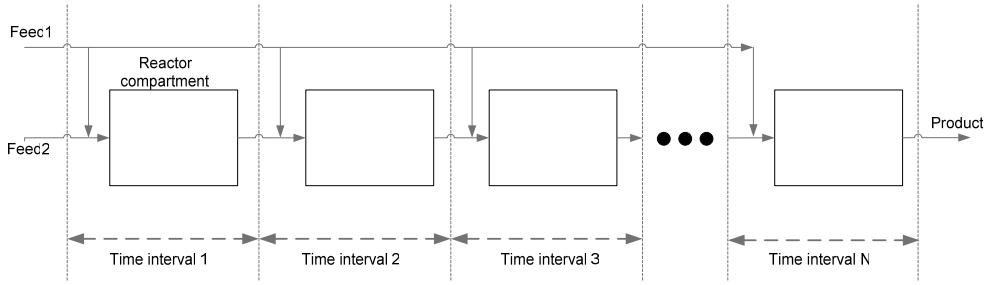

Figure A2.3.1 A temporal superstructure of a batch reactor (Smith, 2004)

In a similar way, a temporal superstructure can be generated (Zhang & Smith, 2004) to represent a batch reactor by a series of reactor compartments with mixed-flow features connecting to each other sequentially in the time domain (Figure A2.3.1).

Structural changes of the superstructure can generate different operating modes (batch or semi-batch). This superstructure model also embeds the operating variables such as batch cycle time, temperature, feed addition rate, amount of reactants and pressure. The length of each time interval equals the whole reaction time divided by the number of time intervals. The greater the number of the time intervals, the closer the model approaches the batch reactor modelled. For perfect mixing, one perfectly mixed compartment is employed in each time interval for modelling.

The advantages of a split in space and time, when applied to superstructure network for crystallizers are:

1. In the task representation, the time dimension can be eliminated from the superstructure at one time instant which means the conceptual thinking is better understood. This freedom of separation between temporal and spatial domain is not achieved otherwise.
2. Several tasks can be added / deleted at different times in a network which is not the case with the compartmental modelling approach (Bermingham, 2003).
3. The approach is independent of the complexities of the equations involved in describing the process which makes it suitable to be applied to task based approach since the 'behavior' attribute of a task can be described in various degrees of details.

[1] The key advantage in using a cascade of CSTRs is that only algebraic equations are sufficient for the mathematical description of a PFR unit.

4. Ready made algorithms (Upadhye and Grens (1975)) are available in the literature over the number and types of streams to be torn etc. The only disadvantage that is understood at this time is that the algorithm requires a closed system in terms of streams.

Thus, a task can be in both temporal domain and spatial domain or it can be in only the spatial domain at a time instant (for example, during different phases in crystallizer operation, different tasks can be switched on and off). In any case, the user has to specify in which domain the task is to be performed. The synthesis levels (Level 4.7 to 4.10) for the temporal domain are briefly introduced here.

2.3.1 Level 4.7 - Connection of tasks identified (temporal connection)

A task can occur many times in temporal domain till it satisfies the design targets/specifications. The guidelines are the same as those defined earlier for "Connection of tasks (spatial connection)".

2.3.2 Level 4.8 - Integration of tasks within a design compartment (temporal integration)

In addition to the heuristics for "Integration of tasks in a design compartment (spatial integration)", the temporal integration of tasks can be done only in real time at which the tasks occur (i.e. one cannot connect tasks which occur in a compartment in the past or future!).

2.3.3 Level 4.9 - Operational unit identification (temporal domain)

Additional operational units can occur in temporal domain. For example, after a batch is over, the product needs to be put in a different vessel so that the crystallizer is emptied, cleaned and can be ready for the next batch. Unless there is a different vessel the crystallizer can not be used.

2.3.4 Level 4.10 - Connection of different design compartments into process units (temporal connection)

A design compartment can occur many times in temporal domain till it satisfies the design targets/specifications. The guidelines are the same as those defined earlier for "Connection of design compartments (spatial connection)".
Levels 4.7 to 4.10 are supported by an example for illustration purpose (see Figure A2.3.2). The configuration generated from Figure 2.20(d) in sub-section 2.4.4.3, is used as a base case. Here, a temporal superstructure has been built to represent a fed-batch crystallizer by a series of crystallizer compartments with mixed-flow features connected to each other in the time dimension. In this network, the batch cycle time has been divided over equal time intervals for ideal mixing.
A mixed-flow crystallizer compartment within a time interval acts as the recipient of input from compartments in the preceding time interval and generates output to the succeeding compartment(s) in the next time interval. The streams connecting different time intervals for material input and output connect the compartments in the same way as in the mixing compartment network, but cross time intervals. This is realized by tearing streams within a compartment network and re-connected to the corresponding compartments in the network of the previous and next time intervals. For a more detailed overview on how this is done, please refer Smith (2004). In this particular example, the feed supply is done in a fed-batch mode. The recycle streams in Figure 2.20(d) originate from the *growth* and *mixing* tasks. Hence, these streams are torn and sent to the corresponding tasks in the next time interval. The vapor is continuously removed from each time interval whereas, the product is finally withdrawn at the end of batch, at the final time interval.

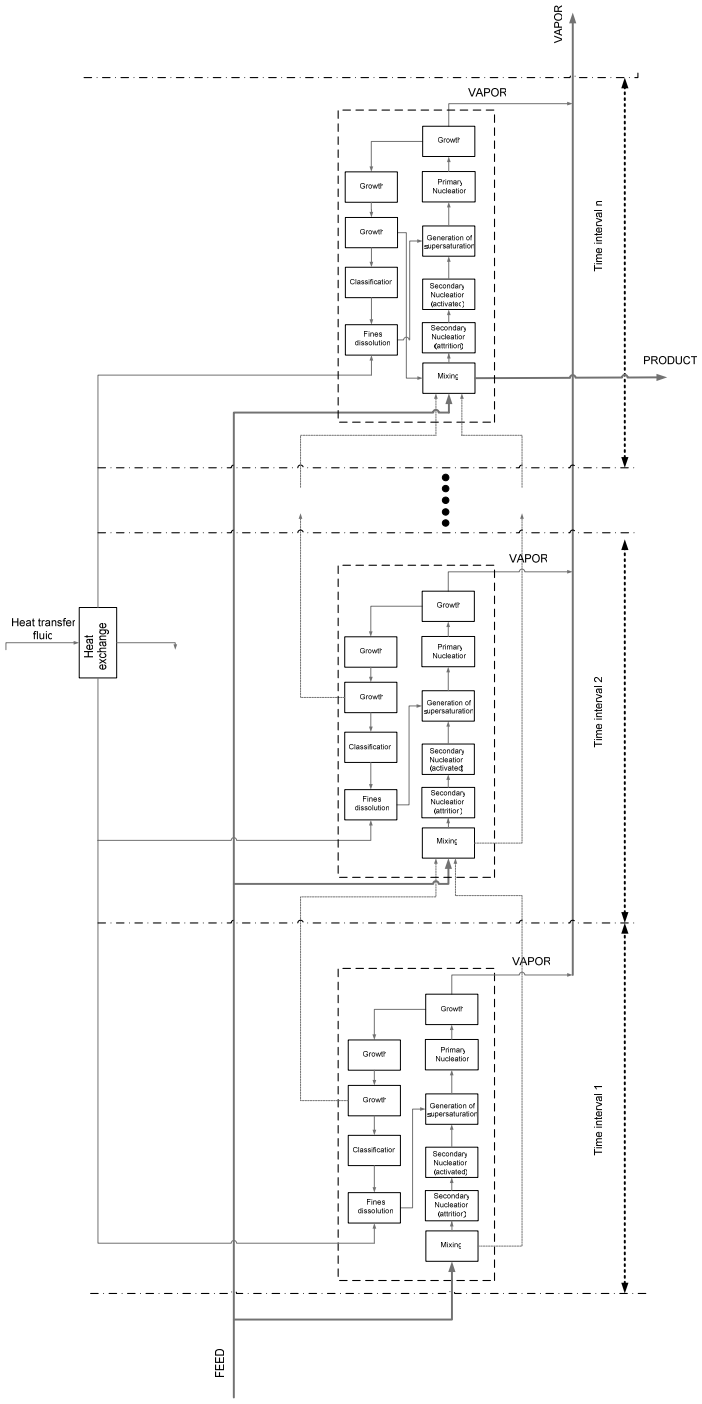

Figure A2.3.2 Temporal superstructure of a crystallizer in a fed-batch process

A3.1 MATERIAL PROPERTIES FOR $(NH_4)_2SO_4$

This appendix on material properties is reproduced here after Neumann (2001).

A3.1.1 Solubility

Solubility (Daudey, 1987 and Jager, 1990):

$$c_0 = 0.4117 + 9.121 \cdot 10^{-4} \cdot T \qquad [kg\ solute/\ kg\ solution] \tag{A3.1}$$
$$-6^o C \le T \le 90^o C$$

Solubility (Westhoff, 2001):

$$c_0 = 0.7008 + 26.8 \cdot 10^{-4} \cdot T + 2 \cdot\ 10^{-6} \cdot T^2 \qquad [kg\ solute/\ kg\ H_2O] \tag{A3.2}$$
$$35^o C \le T \le 55^o C$$

A3.1.2 Density

Solid phase ($(NH_4)_2SO_4$) – (Jager, 1990):

$$\rho_c = 1777.5 - 0.19697 \cdot T \qquad [kg\ /\ m^3\ ] \tag{A3.3}$$
$$0^o C \le T \le 80^o C \quad ; \quad 0 \le c_w \le 50 wt\%$$

Saturated crystal free solution ($(NH_4)_2SO_4$)-H_20) – (Jager, 1990):

$$\rho_l = A_0 + A_1 \cdot c_w + A_2 \cdot c_w{}^2 + A_3 \cdot c_w{}^3 + A_4 \cdot T + A_5 \cdot T^2 + A_6 \cdot T^3 \qquad [kg\ /\ m^3\ ] \tag{A3.4}$$
$$0^o C \le T \le 100^o C \quad ; \quad 0 \le c_w \le 50 wt\%$$
with

$$A_0 = 1008.51 \qquad A_1 = 6.00874 \qquad A_2 = -7.77478 \cdot 10^{-3}$$
$$A_3 = 3.10023.10^{-5} \qquad A_4 = -0.222764 \qquad A_5 = -2.76467 \cdot 10^{-3}$$
$$A_6 = 6.25116.10^{-6} \qquad 0^o C \le T \le 100^o C \qquad 0 \le c_w \le 50 wt\%$$

Vapor (H_20):

$$\rho_v = 2500 - 0.19697 \cdot T \qquad [kg\ /\ m^3\ ] \tag{A3.5}$$
$$0^o C \le T \le 80^o C \quad ; \quad 0 \le c_w \le 50 wt\%$$

A3.1.3 Viscosity

Saturated crystal free solution ($(NH_4)_2SO_4$)-H_20) – (Jager, 1990):

$$\eta_l = 10^{B_0+B_1\cdot c_w+B_2\cdot c_w^{\,2}+B_3\cdot c_w^{\,3}+B_4\cdot T+B_5\cdot T^2+B_6\cdot T^3} \qquad [mPa.sec] \tag{A3.6}$$

$0^oC \le T \le 80^oC \quad ; \quad 0.02 \le c_w \le 0.42$

with

$$B_0 = 0.219497 \qquad B_1 = 5.71007.\ 10^{-3} \qquad B_2 = 1.22202\cdot 10^{-4}$$
$$B_3 = -1.92549.10^{-7} \qquad B_4 = -1.25024.10^{-2} \qquad B_5 = 7.81444\cdot 10^{-5}$$
$$B_6 = -2.66152.10^{-7}$$

A3.1.4 Diffusivity

The volume diffusivity - Stokes-Einstein equation (Mersmann, 1995)

$$D_{AB} = \frac{k\cdot T}{2\cdot\pi\cdot\eta_l\cdot d_m} \approx \frac{k\cdot T\cdot(c_s\cdot N_A)^{1/3}}{2\cdot\pi\cdot\eta_l} \qquad [m^2/s] \tag{A3.7}$$

with

$$c_s = \frac{\rho_s}{\tilde{M}} \qquad [mol\ solute/m^3\ solution]$$

According to Mersmann, the experimental diffusivity data published in the literature can be described by Stokes-Einstein's equation with a mean accuracy of ±50% and maximum deviation of ±100%.

Effective volume diffusivity (Westphal and Rosenberger, 1978)

$$D_{AB_{eff}} = D_{AB}\cdot\frac{1-c_w\cdot\dfrac{\partial\rho_l}{\partial c_c}}{1-c_w} \approx D_{AB}\cdot\frac{1}{1-c_w} \qquad [m^2/s] \tag{A3.8}$$

with

$$c_w = \frac{c_c}{\rho_l} \qquad [kg\ solute/kg\ solution]$$

Due to the advective flux towards a growing crystal the mass transfer is larger than predicted if a stagnant liquid is assumed. To correct for this effect an effective diffusion coefficient must be used (Daudey, 1987).

A3.1.5 Specific Heat Capacity

Solid phase ($(NH_4)_2SO_4$) – (Jager, 1990):

$$c_{ps} = 1.3760 + 2.13\cdot 10^{-2}\cdot T \qquad [kJ/kg.^0C] \tag{A3.9}$$
$$25^oC \le T \le 323^oC$$

Saturated crystal free solution ($(NH_4)_2SO_4$-H_20) – (Jager, 1990):

$$c_{pl} = 4.259 - 3.0321 \cdot c_w - 1.7668 \cdot 10^{-3} \cdot T + 4.2874 \cdot 10^{-6} \cdot T^2 \qquad [kJ/kg.^0C] \qquad \text{(A3.10)}$$

$$25^oC \le T \le 323^oC$$

A3.1.6 Additional Material Properties

No.	Material properties of $(NH_4)_2SO_4$	Value	Unit
1	Vickers hardness, H_v	$355 \cdot 10^6$	[N.m^{-2}]
2	Shear modulus, μ	$8.90 \cdot 10^9$	[N.m^{-2}]
3	Young's modulus, E	$23.4 \cdot 10^9$	[N.m^{-2}]
4	Critical work to form visible cracks , W_c	$41.10 \cdot 10^{-10}$	[J]
5	Average atomic distance, l_o	$2 \cdot 10^{-10}$	[m]
6	Effective fracture surface energy, Γ / K_r	3.2	[J.m^{-2}]
7	Attrition constant, C	$11.73 \cdot 10^{-6}$	[m^3.J$^{-4/3}$]
8	Minimum impact energy, $E_{p.min}$	$2.624 \cdot 10^{-10}$	[J]
9	Minimum attrition fragment size, L_{min}	2.411	[μm]
10	Molar mass, $\tilde{M}$	0.1321	[kg.mol^{-1}]
11	Diffusivity, D_{AB} [1]	$1.66 \cdot 10^{-9}$	[m^2.s^{-1}]
12	Effective diffusivity, $D_{AB_{eff}}$ [1]	$8.06 \cdot 10^{-9}$	[m^2.s^{-1}]

[1]taken from Daudey (1987), the material peroperties (nos. 1-5) are taken from Gahn (1997b)

A4.1 PROPELLER SPECIFICATIONS FOR THE CRYSTALLIZERS

A4.1.1 Propeller specification - 75-litre DT crystallizer (Westhoff, 2002)

The stainless steel stirrer is a 4-blade marine impeller and has a diameter of 0.186 m. The propeller shaft diameter is equal to 0.036 m. The edge of the impeller is $4 \cdot 10^{-3}$ m. The angle of the blades is 25°. The following equation describes the shape of the upper part of one of the blades.

$$h = p_1 \cdot \sin(p_2 \cdot r + p_3) + p_4 \cdot \sin(p_5 \cdot r + p_6) + p_7 \cdot (r - p_8)^2 + p_9 \qquad \text{(A4.1)}$$

where

h - blade height [m]

r - distance from axes [m]

p_1 to p_9 - function paramters [-]

Table A4.1 Function parameters of the stirrer blade

Function parameter	Value	Function parameter	Value
p_1	$-2.548 \cdot 10^{-4}$	p_6	-1.68
p_2	-222.48	p_7	-648
p_3	14.85	p_8	0.028
p_4	78.21	p_9	78.23
p_5	4.064		

A4.1.2 Propeller specifications - 1100L DTB (Neumann, 2001)

The 1100L DTB crystallizer is fitted with a 3-blade marine type propeller for which the propeller specifications are listed in Table A4.2. The face of the blade (h) which is a function of the blade radius (r), is given by the same expression as given in Equation (A4.1) . The propeller shaft diameter is equal to 0.072 m. The edge of the impeller is $6 \cdot 10^{-3}$ m and the propeller diameter is 0.485m. The angle of the blades is 21°. The following equation describes the shape of the upper part of one of the blades.

Table A4.2 Function parameters of the stirrer blade

Function parameter	Value	Function parameter	Value
p_1	100	p_6	7.4
p_2	-2.47	p_7	$-6.2 \cdot 10^{-6}$
p_3	1.84	p_8	22.21
p_4	-34.76	p_9	65.71
p_5	4.19		

A5.1 PARAMETERS FOR AMMONIUM SULPHATE

These calculations have been performed for ammonium sulphate-water system at 50°C. The values of various parameters have been listed in Table A5.1. A constant value of ψ (heterogeneity factor) of 0.045 is used, unless otherwise stated. This value was chosen so as to get the best possible fit with experimental data during the simulation runs, which are described in Chapter 5 of this thesis.

Table A5.1 Values of various quantities used for calculation of different dependences in nucleation and growth of $(NH_4)_2SO_4$ crystals in aqueous solutions at T = 323 K.

Quantity	Notation	Value	Unit
Molecular weight	M	0.132	$kg.mol^{-1}$
Universal gas constant	R	8.314	$J.mol^{-1}.K^{-1}$
Temperature	T	323	K
Concentration	C	572.3	$kg.m^{-3}$
Saturation concentration	C_{sat}	571.36	$kg.m^{-3}$
Boltzmann constant	k_B	$1.38.10^{-23}$	$J.K^{-1}$
Crystal density	ϱ_s	1767	$kg.m^{-3}$
Avogadro's number	N_{av}	$6.02.10^{23}$	mol^{-1}
Molecular volume	v_o	$1.24.10^{-28}$	m^3
Heterogeneity factor	ψ	0.045	-
Sticking coefficient	ξ	0.8	-
Diffusivity	D	$2.5.10^{-9}$	$m^2.s^{-1}$
Concentration of nucleation sites	C_0	1.10^{20}	$\#.m^{-3}$
Diameter of a molecule	d_0	1.10^{-9}	m
Jump frequency	w_0	1.10^{13}	s^{-1}

A5.2 3D PLOTS FOR CSD

A 3-D representation of Figure 5.10 for SIM9P is depicted in Figures A5.2.1(a,b) and Figures A5.2.2(a,b) in terms of the number and volume density distributions within the two classes of crystals.

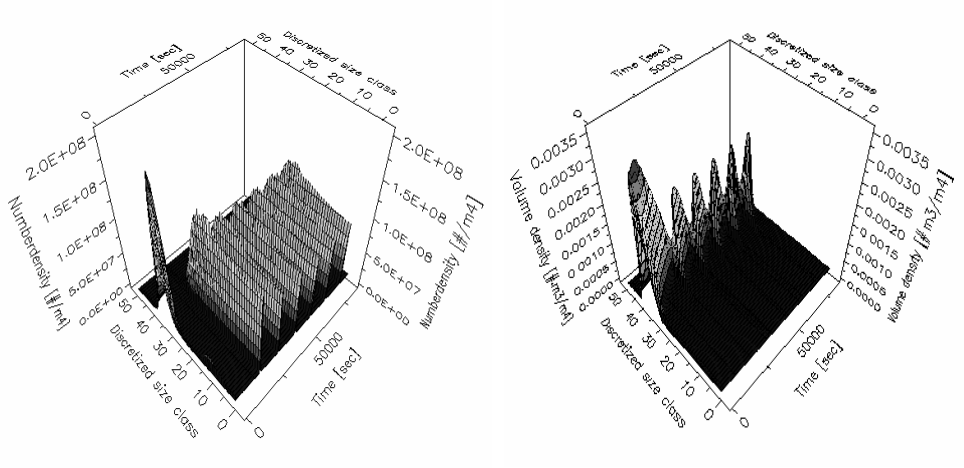

(a) number density distribution **(b) volume density distribution**

Figure A5.2.1 Crystal size distribution for primary population of crystals (SIM9P)

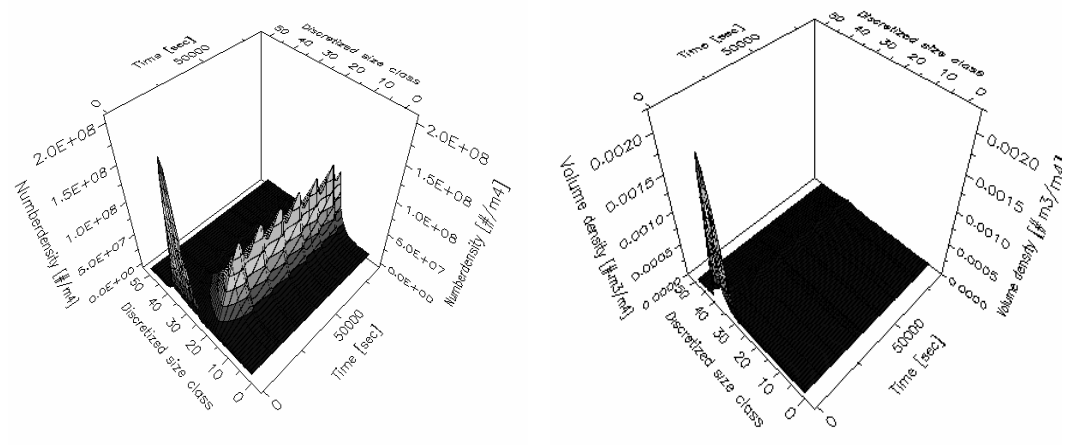

(a) number density distribution **(b) volume density distribution**

Figure A5.2.2 Crystal size distribution for secondary population of crystals (SIM9P)

A6.1 PROPERTIES OF AMMONIUM SULPHATE

The following relations have been used to calculate the properties of ammonium sulphate:

Solubility [kmol/m^3] (Daudey, 1987):

$$c^* = (0.41179 + 9.121 \cdot 10^{-4} T) \cdot \frac{\varrho_l}{M} \tag{A6.1.1}$$

Interfacial energy [J/m^2] (Mersmann, 1990):

$$\gamma_{CL} \approx \frac{kT}{3d_m^2} \ln\left(\frac{c_c}{c_{sat}}\right) \tag{A6.1.2}$$

Molecular diameter [m]:

$$d_m \approx (c_c N_{av})^{-1/3} \tag{A6.1.3}$$

Minimum size of attrition fragment [m]:

$$L_{\min} = \frac{32}{3} \frac{\mu}{H^2} \frac{\Gamma}{K_r} \tag{A6.1.4}$$

Table A6.1.1 Material properties

Property	*Value and dimension*
D	2.5·10^{-9} m^2/s
c_c	13.39 kmol/m^3
M	132.1 kg/kmol
ϱ_l	1248.9 kg/m^3
η	1.45·10^{-3} kg/(m.s)
H	355e6 N/m^2
μ	8.90·10^9 N/m^2
Γ/Kr	3.2 J/m^2
k_a	4
k_v	0.43

Table A6.1.2 Calculated properties at T=50°C

Property	*Value and dimension*
c_{sat}	4.324 kmol/m^3
γ_{CL}	6.76 mJ/m^2
d_m	0.499 nm
L_{min}	2.411 µm

A6.2 SENSITIVITY ANALYSIS ON ECSN

The sensitivity for the ECSN mechanism has been performed at two values for the interfacial energy. The high value is 6.76 mJ/m^2. This is the value predicted by Equation 6.24 and is an estimate for the interfacial energy of crystals.

Qian and Botsaris claim that sub-critical clusters have a much lower interfacial energy than crystals. Therefore the sensitivity analysis has also been performed at a value of 1.68 mJ/m^2.

A6.2.1 Sensitivity analysis at high interfacial energy

In addition to the properties described in Appendix A6.1, the following values have been used for the sensitivity analysis on the ECSN mechanism.

Table A6.2.1 Values used for sensitivity analysis

Property/condition	Symbol	Value
Hamaker constant	A_{131}	$4 \cdot 10^{-20}$ J
Coagulation distance	x/r_1	1
Coagulation size	g	50 [monomers]
Interfacial energy	γ_{CL}	6.76 mJ/m^2

Hamaker constant A_{131}
The symbol for the Hamaker constant (A_{131}) contains three numbers. The first one represents the material of the parent crystal (1 stands for ammonium sulfate), the second number represents the medium (3 stands for water) and the third number represents the material of the embryos (so again 1 of ammonium sulfate). There are several techniques to calculate Hamaker constants, but they are all complicated and require accurate dielectric data. No values for the Hamaker constant of ammonium sulfate have been found in literature. Therefore the Hamaker constant is used as parameter.

Bergstrom(1997) has calculated Hamaker constants for 31 different inorganic materials in water. Ammonium sulfate is not concluded in this study, but at least a range for the value of the Hamaker constant can be obtained. The values of the Hamaker constant for these 31 inorganic species range from $0.31 \cdot 10^{-20}$ J to $15.5 \cdot 10^{-20}$ J. The upper limit of $15.5 \cdot 10^{-20}$ J is for diamond. For salts the Hamaker constant does not exceed $8 \cdot 10^{-20}$ J.

Therefore the Hamaker constant is expected to be in the following range:

$$0.31 \cdot 10^{-20}\, J < A_{131} < 8.0 \cdot 10^{-20}\, J$$

Figure A6.2.1 shows how the Hamaker constant affects the embryo concentration in the surface layer.

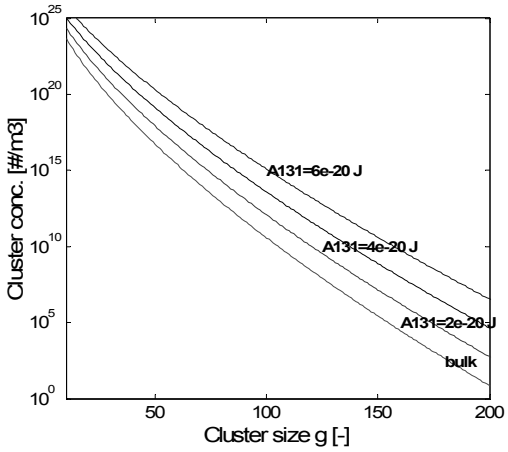

Figure A6.2.1 Influence of Hamaker constant on cluster concentration in surface layer.

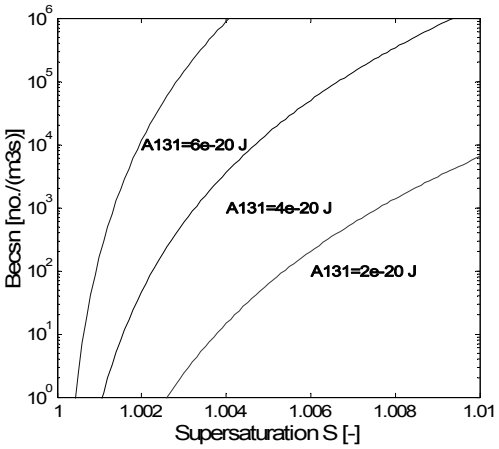

Figure A6.2.2 Influence of Hamaker constant on ECSN nucleation rate.

The Hamaker constant is a measure for the attractive forces between clusters and crystals. The concentration of clusters in the surface layer is therefore higher for larger Hamaker constants. As a result , ECSN nucleation is activated at lower supersaturation levels for higher Hamaker constants. Note that in theory the Hamaker constant is a material property and not a parameter.

Coagulation distance x/r_1

The distance from the surface at which coagulation takes place is unknown. It has been made dimensionless by the radius of a solute molecule. Distances closer to the surface than half the radius of a single molecule seem unlikely. Therefore 0.5 has been taken as lower limit and at a dimensionless distance of around 8 the increased concentration of clusters in the surface layer is no longer noticeable. At this distance, the concentration in the surface layer comes very close to the bulk concentration.

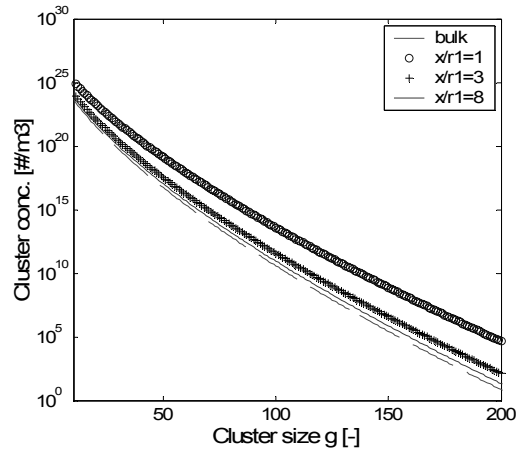

Figure A6.2.3 Cluster concentration versus cluster size for various distances from the surface. The bulk concentration corresponds to the ratio of $x/r_1=\infty$.

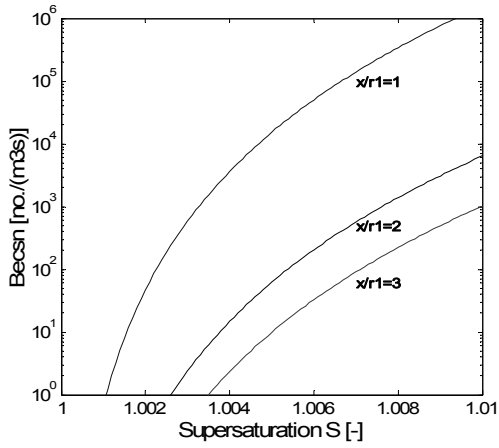

Figure A6.2.4 ECSN nucleation rate versus supersaturation for various coagulation distances.

The cluster concentration is a function of the distance to the surface of a crystal. The attractive forces decrease with increasing distance and therefore the concentration also decreases with distance. Figure A6.2.3 shows a higher cluster concentration closer to the surface. Hence, nucleation is triggered at lower supersaturation for distances closer to the surface (see figure A6.2.4).

A6.2.2 Sensitivity analysis for low interfacial energy

The sensitivity analysis has been repeated for a lower interfacial energy. The value used is 1.68 mJ/m^2 instead of 6.76 mJ/m^2. In addition to the properties described in Appendix A6.1, the following values have been used for the sensitivity analysis on the ECSN mechanism.

Table A6.2.2 Values used for sensitivity analysis

Property/condition	Symbol	Value
Hamaker constant	A_{131}	$4{\cdot}10^{-20}$ J
Coagulation distance	x/r_1	3
Coagulation size	g	500 [monomers]
Interfacial energy	γ_{CL}	1.68 mJ/m^2

The parameters have the same influence as at high interfacial energy. The difference is that larger clusters are easier formed for lower interfacial energy.

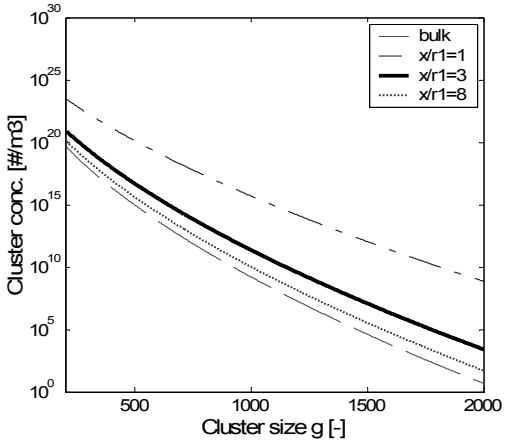

Figure A6.2.5 Influence of Hamaker constant on cluster concentration in surface layer. The pink line is the cluster concentration in the bulk.

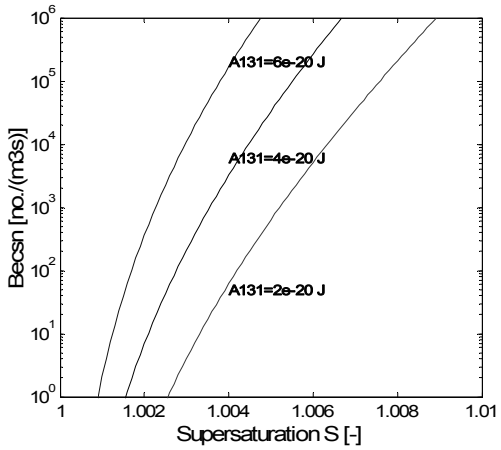

Figure A6.2.6 Influence of Hamaker constant on ECSN nucleation rate.

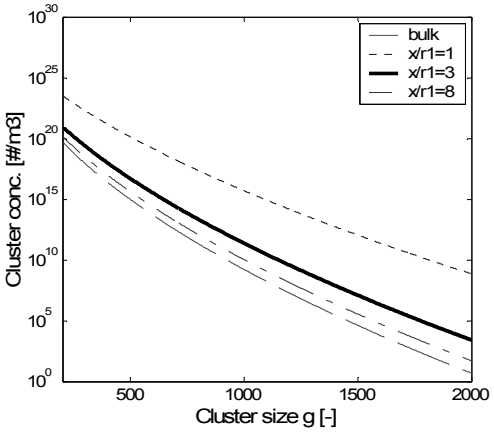

Figure A6.2.7 Cluster concentration versus cluster size for various distances from the surface. The bulk concentration corresponds to the ratio of $x/r_1=\infty$.

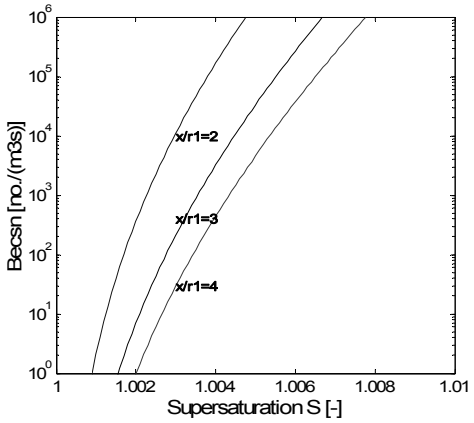

Figure A6.2.8 ECSN nucleation rate versus supersaturation for various coagulation distances.

A6.3 SENSITIVITY ANALYSIS ON SURFACE NUCLEATION

The final surface nucleation rate is described by equation:

$$B_{surf} = Ea_v B_S = \frac{Ea_v D_0}{d_m^4} \exp\left[-\frac{\pi \gamma_{CL}^2 d_m^4}{(k_B T)^2 \ln(S)} \right] \tag{A6.3.1}$$

The sensitivities of T, a_v, E and γ_{CL} have been tested with regards to the nucleation rate at the following conditions:

Table A6.3.1 Values used for sensitivity analysis

Property/condition	*Symbol*	*Value*
Temperature	T	50°C
Specific surface area	a_v	1000 m^2/m^3
Removal efficiency	E	0.5

The material properties of ammonium sulphate can be found in Appendix A6.1.

Removal efficiency
The removal efficiency E has a value in the range 0 to 1.

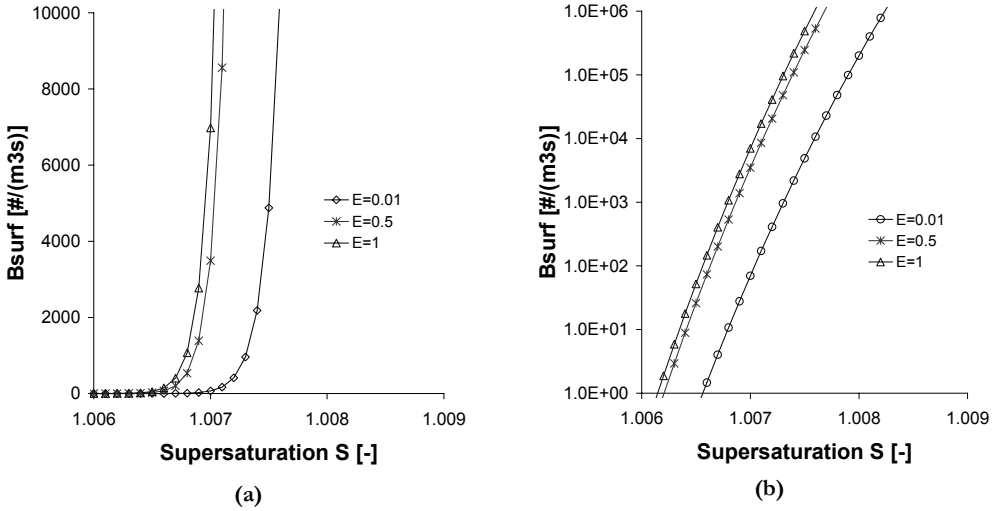

Figure A6.3.1 Influence of removal efficiency E on surface nucleation rate. Figure (a) with normal y-axis, Figure (b) with logarithmic y-axis.

Figure A6.3.1a clearly shows the activated behavior of surface nucleation. E has a weak influence on the surface nucleation, since activated behavior is caused by the exponential term in Equation A6.3.1. Even a change in magnitude of 100 has only a moderate influence.

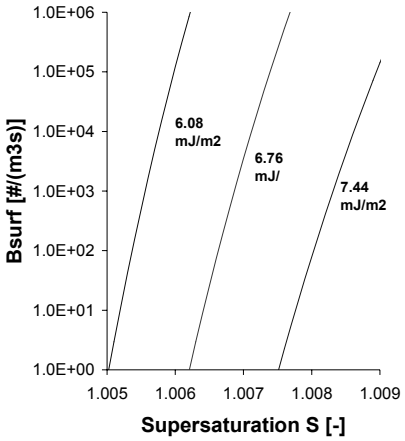

Figure A6.3.2 Influence of interfacial energy on surface nucleation rate

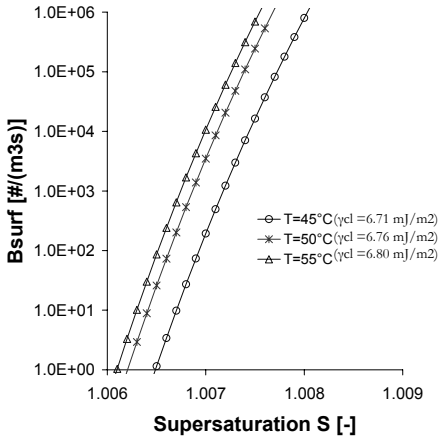

Figure A6.3.3 Influence of temperature on surface nucleation rate

Interfacial energy

Equation 6.24 gives a value of 6.76 mJ/m^2 for the interfacial tension. Figure A6.3.2 plots the interfacial tension for a 10% higher and a 10% lower value. The expected uncertainty in interfacial energy is 21.0 %. From figure A6.3.2, it is clear that the surface nucleation rate is strongly influenced by the interfacial energy and its uncertainty. The rate is increased for lower values of the interfacial energy. An effect that is similar to primary nucleation.

Temperature

The temperature in the crystallizer is 50°C. The sensitivity analysis has been made for deviations of 5°C. The temperature might have a large influence, since temperature has an influence on the interfacial energy. Both temperature and interfacial energy are present in the exponential term in Equation 6.23. The influence of temperature on interfacial energy is very limited as seen in Figure A6.3.3. Small changes in temperature have a moderate influence since temperature is present inside the exponential term. Increasing the temperature decreases the critical supersaturation.

Specific surface area

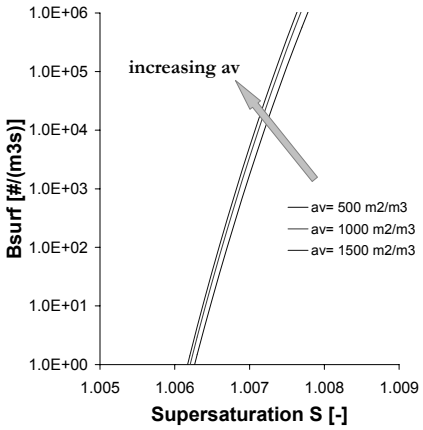

Figure A6.3.4 Influence of specific surface area on surface nucleation rate

The specific surface area of the crystals inside a crystallizer is a function of the CSD and is therefore a variable. The specific surface area is expressed in m^2 of crystal surface per m^3 solution. A typical value in an industrial crystallizer is around 1000 m^2/m^3. The specific surface area is varied between 500 and 1500 m^2/m^3. The specific surface area is only present in the pre-exponential term and therefore the influence is weak, as seen in Figure A6.3.4.

A6.4 INFLUENCE OF BOILING ZONE VOLUME AND FLOW TO BOILING ZONE FOR SECOND TWO-COMPARTMENTAL STRUCTURE

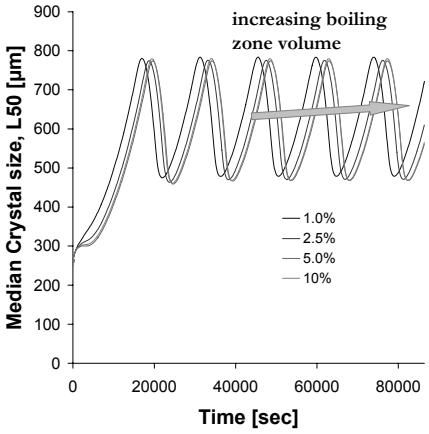

Figure A6.4.1 Influence of boiling zone volume on dynamic behavior of L_{50}

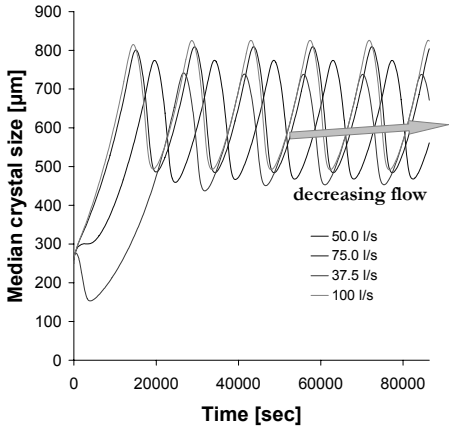

Figure A6.4.2 Influence of flow to the boiling zone on dynamic behavior of L_{50}

Samenvatting

EEN TAAKGERICHTE ONTWERPPROCEDURE EN MODELLEERAANPAK VOOR INDUSTRIËLE KRISTALLISATIEPROCESSEN.

Abhilash R. Menon
ISBN-10: 90-9021029-6 / ISBN-13: 978-90-9021029-2
December 2006

De procesindustrie moet reageren op de behoeftes en verwachtingen van de maatschappij, zoals een grotere duurzaamheid van materiaalcyclussen, competitieve kapitaalopbrengst en hogere verwachtingen van consumenten met betrekking tot productfunctionaliteit en prestaties. Om deze doelstelling te ondersteunen zijn effectieve en inventieve ontwerpmethodieken nodig vanuit het perspectief van de levensduur van product en proces. Hoewel kristallisatie één van de oudste operaties in de chemische industrie is, geeft het ontwerp en de operatie van kristallisatieprocessen nog steeds veel problemen. Vele fabrieken produceren kristallen die niet aan de gedefinieerde kwaliteitsspecificaties voldoen. De huidige behoefte van de markt is om kristallisatie- en downstreamprocessen op een optimale en kosteneffectieve manier te opereren, in sterk fluctuerende marktomstandigheden. Ondanks het belang van kristallisatie, is er een relatief tekort aan systematische ontwerpprocedures en voorspellende modellen om de eerder genoemde problemen aan te pakken en om kristallisatoren te ontwerpen voor flexibele productspecificaties in multifunctionele fabrieken.

Dit proefschrift streeft ernaar om deze kwesties van drie kanten te bekijken:

1. Formulering van een synthesegeoriënteerde aanpak voor het conceptueel ontwerp van (innovatieve) configuraties voor kristallisatieapparatuur.
2. Validatie van bestaande kinetische kristallisatiemodellen, gedeeltelijk ontwikkeld binnen de Technische Universiteit Delft, met fed-batch experimentele data.
3. Verbetering van de ontwerpmodellen om specifieke fenomenen te verklaren die in de praktijk zijn waargenomen in bepaalde continue kristallisatieprocessen.

In Hoofdstuk 1 is kristallisatie als een operatie in de chemische procesindustrie geïntroduceerd met betrekking tot de toepassing, voordelen en problemen uit de praktijk. Een motivatie is gegeven voor de keuze van ontwerp en modellering als onderzoeksonderwerpen om kristallisatietechnologie te verbeteren. Daarna is een kort overzicht gepresenteerd in de vorm van de stand van de technologie op het gebied van modellering en ontwerp van industriële kristallisatieprocessen. In essentie is dit de voorbereiding voor het vaststellen van de doelstellingen en het onderzoekskader van dit proefschrift, welke in het kort kunnen worden samengevat als een nieuwe bijdrage voor het modelleren van populatiebalansen en een synthesegeoriënteerde aanpak voor industriële kristallisatieprocessen. Het

kader van dit onderzoek is beperkt door de eigenschappen van het chemische systeem, kristallisatiemethode, operatiewijze en type kristallisator.

Een nieuwe taakgerichte procedure voor het conceptueel ontwerp van een proceseenheid voor kristallisatie uit oplossing wordt voorgesteld in Hoofdstuk 2. Het doel is om kosten van grondstoffen en kapitaal te reduceren en mogelijkerwijs procesintensificatie te bereiken. Het ontwerp van processen met vaste stoffen en in het bijzonder kristallisatieprocessen zijn in het verleden onderwerp van onderzoek geweest. Rossiter en Douglas (1986) en Ng (2001) bediscussiëren systematische procedures voor het ontwerpen van geïntegreerde kristallisatiesystemen waarbij de interactie tussen kristallisatie en downstreamprocessen in beschouwing wordt genomen. De interactie tussen product- en procesontwerp in beschouwing nemend, stelde Bermingham (2000, 2003a) een systematische en hiërarchische ontwerpprocedure voor om de kwaliteit van zowel het ontwerp van kristallisatieprocessen als het ontwerpproces te verbeteren. Deze m*ulti-level* ontwerpprocedure dekt de hele reeks van productontwerp tot het achter elkaar zetten van meerdere kristallisatoren. Op ieder niveau stelt het men in staat om systematisch en simultaan om te gaan met een groot aantal initiële ontwerpspecificaties, ontwerpvariabelen, operationele variabelen en beschikbare kennis, die betrokken zijn bij een bepaald gedeelte van het ontwerpproces.
De taakgerichte ontwerpaanpak zoals voorgesteld in dit proefschrift, is ingebed binnen de uitgebreide systematische en hiërarchische ontwerpprocedure zoals voorgesteld door Bermingham (2000), richtend op een nieuwe, optimale configuratie voor kristallisatie-eenheden. Het fysische taakconcept maakt een meer synthesegeoriënteerde aanpak mogelijk, als een functioneel alternatief ten opzichte van de traditionele manier van denken in geometrische structuren voor apparatuur in procesanalyse. De syntheseaanpak kan worden omschreven als het representeren van het kristallisatieproces als een set van basisfuncties (taken) waarvan elke basisfunctie de fysische status van materie van een initiële status naar een zekere uiteindelijke gewenste status transformeert door middel van een fysische gebeurtenis. Deze taken zijn verbonden in een netwerk om de omzetting van de voeding naar het product te bewerkstelligen binnen kwaliteitsspecificaties. De hoofdmoot van dit hoofdstuk is het ontwikkelen van een ontologie voor de taakgerichte aanpak. In deze aanpak worden alternatieve manieren om de taken te structureren toegestaan, wat zal leiden tot de ontwikkeling van superstructuren, waarvan optimale kristallisatieprocessen en kristallisatieconfiguraties kunnen worden geïdentificeerd. Aangezien het procesnetwerk, gegenereerd door middel van taakgericht ontwerpen, gebaseerd is op fysische gebeurtenissen, kan het ook gebruikt worden in een modelleeromgeving van het proces met compartimentstructuren voor synthese, analyse en optimalisatiestudies. Zulke studies zijn de laatste stap in de toepassing van het taakgerichte concept.

Hoofdstuk 3 levert een overzicht van de dominante mechanismen die een rol spelen in kristallisatieprocessen uit oplossing. Een introductie in de thermodynamische aspecten van kristallisatie is ook gepresenteerd. In het tweede gedeelte van dit hoofdstuk wordt het modelleerkader dat ontwikkeld is door Bermingham (1998, 2003a,b) kort besproken. Dit modelleerkader, dat de vergelijkingen van de populatiebalans samen met de massa- en energiebalansen bevat, is in de dynamische modelleeromgeving gPROMS gebouwd. Dit procesmodel kan worden toegepast voor ontwerp en optimalisatiedoeleinden en kan worden gebruikt om het verband tussen de geometrie van de kristallisator en condities aan de ene kant en productiecapaciteit en kristalkwaliteit aan de andere kant te voorspellen.

Fed-batch experimenten uitgevoerd voor *unseeded* verdampingskristallisatie van ammoniumsulfaat uit water in een 75L Draft Tube en 1100L Draft Tube Baffle kristallisator zijn het onderwerp van discussie in Hoofdstuk 4. De warmtetoevoer, menging en de snelheid van de verwijdering van fijn materiaal waren geselecteerd als primaire actuatoren voor het proces. Gedurende de experimenten werden de actuatoren op een constant niveau gehouden of stapsgewijs gevarieerd en het effect op de uiteindelijke productkwaliteit van de batch was bestudeerd. De studie onthult een significante invloed van de actuatoren, in het bijzonder de roerdersnelheid en de snelheid van het verwijderen van fijn materiaal, op de initiële start en dynamisch gedrag van het proces. De warmtetoevoer bleek minder belangrijk te zijn

voor het beïnvloeden van de procesdynamica in *fed-batch* processen. Studies waarbij dynamisch parameters worden geschat laten zien dat de kinetische parameter voor oppervlakte-integratie (k_r) en de oppervlaktegerelateerde energietoename (Γ) sterk gecorreleerd zijn. De verkregen parameters geven een redelijke fit met de experimentele data als deze gebruikt worden om de beschrijvende en voorspellende kwaliteit van de rigoureuze kristallisatiemodellen te testen, voor verschillende procescondities.

Een nieuwe aanpak wordt in Hoofdstuk 5 geïntroduceerd om de beschrijving van het dynamische gedrag van industriële kristallisatoren te verbeteren waarbij een model met twee populatiebalansen wordt gebruikt om onderscheid te maken tussen primaire en secundaire kiemen. Een heterogeen primair nucleatiemodel (Kashchiev, 2000) is toegepast in een rigoureus kader voor kristallisatiemodellen om het voortdurende oscillerende gedrag mee te nemen dat is waargenomen in industriële *Draft Tube Baffle* (DTB) kristallisatoren voor de kristallisatie van goed oplosbare componenten. Het onderscheid tussen primaire en secundaire kiemen in het modelleerkader is gerealiseerd door twee verschillende groeisnelheden in de disperse fase te gebruiken. De totale kristallisatiepopulatie is opgesplitst in twee verschillende en interactieve populaties, één vertegenwoordigt de primaire populatie (zonder spanning) van kristallen en de andere de secundaire populatie (met spanning). Een dergelijk model met twee populatiebalansen vertoont het voortdurende cyclische gedrag voor een 1100L DTB kristallisator, voor een ammoniumsulfaat water systeem. Inclusief de mate van ongelijksoortigheid (ψ) en de twee parameters; snelheid van oppervlakte-integratie (k_r) en conditie van deformatie (Γ) van het groeimodel, heeft het primaire nucleatiemodel drie onbekende parameters welke geschat zijn met gemeten data van experimenten met pilot-plant kristallisatoren. Het effect van de *heterogeneity factor* (ψ) op de dynamica van het proces, wekt de indruk dat de parameter ψ erg gevoelig is en daarom een erg kritieke rol speelt in het voorspellen van de start en dynamica van het proces.
De modellen met één compartiment laten zien dat de waarde van ψ die benodigd is om een primaire nucleatiegebeurtenis te veroorzaken te laag en onrealistisch is ($\psi < 0.1$). De modellen met meerdere compartimenten verbeterden de waarde van ψ (0.135 – 0.14) resulterend in een realistischer waarde om primaire nucleatie voor een ammoniumsulfaat water system te veroorzaken. In dit geval is het mogelijk om een hoge oververzadiging te creëren in bepaalde lokale gebieden van de kristallisator, te weten de kookzone. Als gevolg daarvan kan de energiebarrière voor nucleatie in deze compartimenten significant verminderd worden om een primaire nucleatiegebeurtenis te beïnvloeden.
Eén van de belangrijkste waarnemingen van de simulaties met één en meerdere compartimenten was de verdeling van de kristallen over de primaire en secundaire populatie, waarvan de primaire klasse de meest dominante bleek van de twee. Dit was tegen de verwachting in. Dit zou een artefact kunnen zijn van de simulatie of, vanuit een ander perspectief, zou dit er ook op kunnen duiden dat primaire nucleatie een dominantere rol speelt in het bepalen van de procesdynamica.
Validatie van het model met experimentele data voor de continue verdampingskristallisatie van ammoniumsulfaat uit water, in 1100L DTB en 75L DT kristallisatoren, laat zien dat het opnemen van een primaire nucleatiegebeurtenis zeker de beschrijvende capaciteiten van het model versterkt, en dus de noodzaak van twee interactieve nucleatiemechanismen rechtvaardigt. De resultaten van de simulaties geven een erg goede beschrijving van de beginfase van een kristallisatieproces, de dynamica van het proces alsmede de uiteindelijke *steady-state* waarde.

Twee secundaire nucleatiemechanismen met een afhankelijkheid van oververzadiging, te weten het *embryo coagulation secondary nucleation* (ECSN) mechanisme voorgesteld door Qian en Botsaris (Qian, 1997) en het mechanisme met oppervlaktenucleatie voorgesteld door Mersmann (1996), zijn geanalyseerd in Hoofdstuk 6 om het voortdurende cyclische gedrag in DTB kristallisatoren uit te leggen. Een strategie met twee populatiebalansen was gehanteerd om onderscheid te maken tussen twee concurrerende nucleatiemechanismen. De modellen uitgerust met het ECSN mechanisme waren niet in staat om het oscillerende gedrag te beschrijven omdat de afhankelijkheid van het ECSN model met de oververzadiging te zwak bleek te zijn. Oppervlaktenucleatie leverde veel betere resultaten en een modelleeraanpak met twee compartimenten is gebruikt om een 1100L DTB kristallisator met een kookzone te simuleren die lokaal een hogere oververzadiging heeft. De uitbarstingen van

oppervlaktenucleatie konden alleen gevonden worden in de kookzone en de resultaten van de simulaties geven een erg goede beschrijving van de beginfase van een kristallisatieproces, de dynamica van het proces alsmede de uiteindelijke *steady-state* waarden. Dit bewijst dat zelfs een kleine ruimte als een kookzone een grote invloed kan hebben op het dynamische gedrag van verdampingskristallisatoren. Uitbreiding naar een model met drie compartimenten met oplossing van fijn materiaal gaf minder heftige oscillaties.

Om het fenomeen van *growth rate dispersion* (GRD) te verklaren, is een nieuw mechanisme, dat het herstellen van een misvormd kristal door GRD verondersteld, opgenomen in een tweedimensionale populatiebalans. Dit is het onderwerp van Hoofdstuk 7. Naast de grootte van de kristallen heeft ook de spanning in het kristalrooster een uitgesproken effect op de groeisnelheid van de individuele kristallen, wat de noodzaak om spanning op te nemen als een intern deeltjescoördinaat rechtvaardigt als kristallisatieprocessen met secundaire nucleatie door attritie worden gemodelleerd. Spanning en grootte kunnen als twee onafhankelijke toestanden van elk deeltje gezien worden, welke veranderen met de tijd door het loslaten van spanning door het misvormde kristal. *Healing*, een fenomeen wat het mechanisme beschrijft hoe een misvormd kristal zijn spanning verliest, is aangenomen rechtevenredig te zijn met de spanning en de snelheid van verandering van of de lengte, het oppervlak of het volume van het kristal. In dit proefschrift wordt aangenomen dat het mechanisme van *healing* nauw verbonden is met het kristaloppervlak en dus meer een oppervlakte gerelateerd fenomeen is, in andere woorden, de kristalroosterspanning is niet evenwichtig verdeeld over het volledige volume van het kristal, maar de spanning is gelokaliseerd aan de buitenste randen van het kristal waar de vervorming tijdens het breekproces het hoogst is. Het belangrijkste gevolg is dat niet het hele attritiefragment oplost bij hoge spanningen, maar de oplossing blijft beperkt tot het misvormde kristaloppervlak. Dit proces leidt tot een verlaging in het spanningsniveau van de kristalstructuur en zo krijgt het kristal dus de gelegenheid om weer te groeien, wat fysisch als een meer realistisch scenario wordt beschouwd. De toepassing van een dergelijk multi-dimensioneel groeimodel in een rigoureuze modelleeromgeving bewerkstelligt de beschrijving van de steile opwaartse curve afkomstig van het hogere gehalte fijne deeltjes en levert dus een interessant inzicht in de waargenomen verbreding van de kristalgrootteverdeling door GRD. Validatie van het model door middel van data van de *pilot-plant* voor verdampingskristallisatie in een 22L DT kristallisator laat zien dat *healing* van de gespannen fragmenten proportioneel is met het oppervlak van de kristallen, wat de hypothesis in dit proefschrift onderbouwt.

De belangrijkste resultaten van het onderzoek zijn samengevat en geëvalueerd in Hoofdstuk 8 met betrekking tot de onderliggende onderzoeksvragen. Het onderzoek naar ontwerp kan in twee richtingen worden uitgesplitst. Ten eerste is de ontologie een geschikt platform om een door de computer ondersteunde synthese tool te ontwikkelen voor kristallisatie-eenheden. Voor dit doeleinde is een structuurmodel nodig om superstructuren te genereren in combinatie met een techniek om de beste opties te selecteren. Ten tweede moet de praktische levensvatbaarheid van de taakgerichte aanpak en de resultaten bewezen worden door middel van experimentele programma's waarin kleinschalige nieuwe ontwerpen worden gebouwd een getest.
Op het modelleergebied kunnen sommige van de huidige vereenvoudigde aannames losgelaten worden en getest worden op praktisch belang. Dit kan een meer fundamentele kijk naar de rol van spanning in kristallen afkomstig van primaire en geactiveerde nucleatie en de groei van attritiefragmenten bevatten. Bovendien kan de interactie tussen hydrodynamica en deeltjeskinetiek verfijnd worden. Het is wenselijk om een geschikt compromis te vinden tussen de eenvoudige beschrijving met compartimenten en de extreem gedetailleerde CFD modellen.
Ten slotte, met de vooruitgangen in moleculair modelleren in gedachte, kan het aantal van producteigenschappen die in beschouwing worden genomen tijdens het modelleren en simuleren van productvorming uitgebreid worden, naast kristalgrootte en roosterspanning, met de roosterstructuur en morfologie.

REFERENTIES

Bermingham, S.K., Neumann, A.M., Kramer, H.J.M., Verheijen, P.J.T., van Rosmalen, G.M. and Grievink, J. (2000). A design procedure and predictive models for solution crystallization processes. *AIChE Symp. Series 323*, **96**, pp. 250-264

Bermingham, S.K. (2003a). *A Design Procedure And Predictive Models For Solution Crystallization Processes- Development And Application*, Ph.D. Thesis, Delft University of Technology, the Netherlands, ISBN 90-407-2395-8

Bermingham, S.K., Verheijen, P.J.T. and Kramer, H.J.M. (2003b). Optimal design of solution crystallization processes with rigorous models, *Trans. IChemE*, 81, part A, pp.893-903

Bermingham, S.K., Kramer, H.J.M. and Rosmalen van, G.M. (1998). Towards on-scale crystallizer design using compartmental models, *Computers and Chemical Engineering*, 22, pp.S355-S362

Kaschiev, D. (2000). *Nucleation: Basic Theory with Applications*, Butterworth-Heinemann Ltd. Oxford, U.K.

Mersmann, A.,(1996). Supersaturation and nucleation, *Trans. Inst. Chem. Eng.*, 74, pp. 812-820

Qian, R. and Botsaris,G. (1997). A new mechanism for nuclei formation in suspension crystallizers: the role of interparticle forces, *Chemical Engineering Science*, vol. 52, No. 20, pp.3429-3440

Rossiter, A.P. and Douglas, J.M. (1986). Design and optimization of solids processes. I: A hierarchical decision procedure for process synthesis of solids systems. *Chem. Eng. Res. Des.*, 64, pp.175-183

Wibowo, C., Chang, W., Ng, K.M. (2001).Design of Integrated Crystallization Systems, Vol. 47, No.11, *AIChE Journal,* pp.2474-2492

Acknowledgements

A very challenging and dynamic four years of research has culminated in this dissertation. Five years ago, I took a daring decision to delve into the mysteries of crystallization – an area, which in all honesty, was entirely new to me and that too in a very multi-disciplinary research program. In fact, this was precisely one of the reasons I chose to do my PhD within this program. And I must say that I am more than happy and satisfied with that decision, for I feel that this research period took me beyond the realms of crystallization – it also sharpened the many facets of my professional and personal development. This would have not been possible if it were not for the many wonderful people who touched my life during these years. And here is my opportunity to thank you all who have directly or indirectly contributed to this piece of work and thus, helped me in the *crystallization* of this research and thesis.

First of all, my deepest gratitude goes towards my promoters: Johan Grievink and Peter Jansens. Thank you very much for accepting me as a 'hybrid' PhD student interfacing the departments of Process Systems Engineering (PSE) and Separations Technology (API). This opportunity gave me the much desired possibilities to work on conceptual design, modelling and experimental work on large-scale equipments, in a very complex discipline as crystallization. Johan – my philosopher and guide – I must admit that you scared me a bit on my first meeting with you (where you used the term *superstructure* of which I and almost everybody at API was totally ignorant of) ….. little did I know then that this term would resonate within the API corridors by the time I would compile my work on task-based design. Thank you very much for fostering and stimulating my interests in conceptual design and to think about simplifying complex issues in process design and engineering. Your words of inspiration and encouragement throughout my years in Europe have meant a lot to me in my professional and personal life. And just like all of your students who have promoted before, I cannot but once again commend your wonderful hospitality in serving tea (with loose tea leaves !) and surely they provided the necessary thrust to carry on our brainstorming sessions. Peter, thank you for the flexibility and freedom you provided me in this research program which allowed me to approach the outstanding research issues from different perspectives. Also this opportunity to work in a multi-disciplinary project definitely honed my project management skills. Herman - my crystallization guru and 'day/night' supervisor : I had a great time with you over these years in Delft. Thank you for your guidance and effort in solving the complex modelling issues. The many Monday morning sessions on population balances and gPROMS and the Friday afternoon debates on cricket and beer is something which I will really miss for sure. You must be relieved that you don't have to tolerate my 'Binglish' anymore ! And yes, I hope to join you for ice-skating in the future as well.

Now to API…where I spent most of my time, as the experimental facilities were located here. It's here that I met some of the most amazing and wonderful people. Let me begin with the CrysCODians which was a potpourri of multi-cultural identities: Cristiana, I was glad to have you as my 'roomie' for these four years. It was nice working with you and also to learn how crystals (mis-)behave on the micro-scale. Plus you always amazed me with your quick-witted one-liners. It was nice having you as a pal. *Grazie* for the wonderful times ! Alex, it was also a pleasure working with you on the 'big monster', although I learnt later that you tamed it ! Good luck with wrapping up your thesis.

Another important group of the CrysCODians were the students who played a core role – be it running the crystallizers or digging into the mysteries of crystallization. Wouter, Bas, Fabio, Vani, Ashish, Peter, thank you all. Wouter, you were of great help in the re-commissioning of the crystallizers and you certainly had a knack of getting things on track !...and after a couple of month's hard work, it's always nice to hang out over a Bruce Springsteen concert ! Ashish, you came to grips with the concept of task-based design very quickly and I'm glad that your work has found its way into my thesis. You actually set the ball rolling ! Fabio, it was fun to have you in our group…and yeah, your Italian lessons will help me – I hope ! Peter, you got yourself so dynamically involved in unravelling the dynamics of the DTB, but eventually you took a dynamic turn to run away from crystallization ! Hope you are having fun in your research at Dortmund.

Running experiments on these industrial-scale equipments would have been a nightmare without the earnest efforts of my friends from the mechanical and electrical workshop. Jan, Jan, Theo, Stefan, Martijn, Gerard, Andre, Paul – bedankt allemaal voor de gezellige tijd and sfeer !!
Now, I want to thank a few gorgeous ladies – Brenda, Helma, AnneMarie, Petra, Angela, Leslie – the nucleus of API. Without you, I wouldn't have had my appointments set, my housing problems sorted out and other important administrative tasks neatly done. So also, Caroline from PSE, who very meticulously synchronized my meetings with Johan. Thank you all very much.
A very important club who made sure that the computer systems and network servers were in good shape : Gerben – the Linux guru – thanks a lot for your timely assistance with problems with the UNIAK server. So also the helpdesk (82001) – thanks for all the backup of important data and emails – guess they must be wondering why their phone rings a bit less nowadays. Aris, Toine and Roy, thank you for handling all the administrative and financial dealings meticulously.

As for the spirit of API, we had an interesting mix of folks from different parts of the globe (21 countries in fact at one point of time !). All you guys : Albert, Andreanne, Christof, Chris, Daniella, Dima, Elif, Ferize, Frans, Haruo, Joop, Joachim, Jelan, Kazu, Maaike, Marcel, Mark, Martijn, Marcos, Marjan, Paulo, Pieter, Richard, Raymond, Robert, Steve, Sjangfeng, Takuya, Vanessa, Yohana and all the staff members – thank you for providing such a fantastic work environment. My life outside India wouldn't have been as exciting, adventurous and happening if it weren't for the many 'gezellige borrels', ice-skating, squashing, eventful times at the *Wijnhaven* and *Beestenmarkt* and the many other social activities that were always running through API. In fact, you all were the reason that made Delft my second home over these years.
Frans, you were a good friend in times of need and thanks for tolerating me for 2 ½ months in your home ! Takuya-san, *ookini* for your pleasant company when you were in Delft and also for the wonderful moments with you and Madoka in Osaka. My best wishes for the completion of your PhD. Richard – *bedankt* for writing one chapter of this thesis – your meticulous translation of 'de samenvatting' definitely deserved the Hoogarden(s) ! and Jelan, *bedankt* to you too for the translation of 'de stellingen'.

I'd also like to thank our industrial partners who financially supported the CrysCODE research program – Ajinomoto, Akzo Nobel, BP, DSM, Purac Biochem and Solvay. The bi-annual sponsors' meetings were a great opportunity to interact with you and also provided a platform to understand crystallization problems from an industrial perspective.

A big *dhanyavaad* to all the Indian folks in Delft and in the Netherlands who provided a home away from home. Be it getting together for the DIYA/NIA parties or for the Diwali, Ganeshotsav get-togethers, I had a ball-of-a-time with you guys – Nilesh, Pramod, Saikat , Bharghav, Raji , Sachin, Vijay and all the TUDIndians. Thanks also to my squash-mates, Patrick and Camillo, for making sure I got my weekly break from research. And to all my friends back home in Bombay : Solds, Santo, Shoaib…..thanks for keeping in touch all these years and being good buddies !

And now, my paranymphs : Gregory and Leo. Greg, what a coincidence that badminton made us good friends ! Your sojourn in API was one of the most colourful and happening phases of my API life. *Dhanyavaad* for being a very good friend even after you left API. Leo, as fate would have it, I had to meet you in Germany and although, it was a very short tryst, we shared some memorable moments (especially the ones in Zülpicher). *Aish karo* !

I would like to share a few words with my family : Mummy and Papa, both of you have played a huge role in bringing me up to where I am today. You always enforced upon me the beautiful truth that *knowledge is power*. It would be strange if I have to thank you, but without your sacrifices and the opportunities that you provided me during my life's journey, I wouldn't have been able to achieve so much. I consider myself fortunate for the freedom that you provided in taking some of life's toughest decisions. Even if you were never physically near me through these years in Europe, your thoughts and blessings have always been a beacon for me. Achamma, your blessings and good wishes too have taken me well throughout these years. And Jeetu, I might have not told you, but you provided the much needed 'heads-up' whenever you asked me : " So, what is the new idea that you have come up with in your PhD ?". I'd like to thank the entire *Menon family* in India for their continued support and good wishes and blessings throughout these years.

And finally but the most important for me - the unseen divine force above - YOU who provided me with the right ideas and the right support needed at the right time and also the stamina, determination and focus to remain bent on completing my research. Without YOU, this journey would have been an unlived dream….

Thank you all.

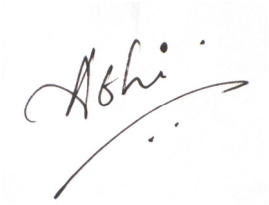

Rotterdam, November 2006

List of Selected Publications

Publications in Journals

- **Menon, A.R.**, Pande, A.A., Kramer, H.J.M., Jansens, P.J., Grievink, J. (2006). A task-based synthesis approach towards the design of industrial crystallization process units. *Submitted to Industrial & Engineering Chemistry Research.*
- **Menon, A.R.**, Kramer, H.J.M., Grievink, J., Jansens, P.J.(2006). Scale-up, dynamic modelling and parameter estimation studies for evaporative batch crystallization of $(NH_4)_2SO_4$ in a 1100L DTB and 75L DT crystallizer. *Submitted to A.I.Ch.E Journal*
- **Menon, A.R.**, vanBeijeren, P., Kramer, H.J.M., Grievink, J., Jansens, P.J.(2006). Incorporating a fluid-shear nucleation model to explain the CSD transients observed for the continuous crystallization of $(NH_4)_2SO_4$ in DTB crystallizers *Submitted to Chemical Engineering Science.*
- **Menon, A.R.**, Kramer, H.J.M., Grievink, J., Jansens, P.J.(2006). A compartmental modeling approach using a two-population balance model, to explain the sustained oscillatory behavior for continuous crystallization of $(NH_4)_2SO_4$ in industrial crystallizers *Submitted to A.I.Ch.E Journal.*
- **Menon, A.R.**, Kramer, H.J.M., Grievink, J., Jansens, P.J.(2006). Using lattice strain to model growth rate dispersion for the crystallization of $(NH_4)_2SO_4$ – a two-dimensional population balance model *Submitted to Journal of Crystal Growth.*
- **Menon, A.R.**, Kramer, H.J.M., Grievink, J., Jansens, P.J.(2005). Modelling the cyclic behavior in a DTB crystallizer - A two-population balance model approach, *Journal of Crystal Growth*, vol.275, Issues 1-2, pp. e1373-e1381

Publications in Conference Proceedings

- **Menon, A.R.**, Pande, A.A., Kramer, H.J.M., Grievink, J.(2005). A novel task-based superstructure for industrial crystallization processes, *Proceedings of the 16th International Symposium on Industrial Crystallization* (ISIC16), Dresden, 11-14 September, Germany
- **Menon, A.R.**, vanBeijeren, P., Kramer, H.J.M., Grievink, J., Jansens, P.J.(2005). Simulating the sustained oscillations in a DTB crystallizer using two interacting secondary nucleation models. *Proceedings of the 16th International Symposium on Industrial Crystallization* (ISIC16), Dresden, 11-14 September, Germany
- **Menon, A.R.**, Kramer, H.J.M., Grievink, J., Jansens, P.J.(2005). Next generation tool for master-model based integrated crystallizer control and design. *Proceedings of the 16th International Symposium on Industrial Crystallization* (ISIC16), Dresden, 11-14 September, Germany
- **Menon, A.R.**, Kalbasenka, A.N., Kramer, H.J.M., Jansens, P.J.(2005). Characterization of final product quality in unseeded fed-batch crystallization processes of inorganic salts in crystallizers of different scale and type. *Proceedings of the 16th International Symposium on Industrial Crystallization* (ISIC16), Dresden, 11-14 September, Germany
- **Menon, A.R.**, Kramer, H.J.M., Grievink, J., Jansens, P.J.(2005). Exploring multiple nucleation mechanisms to capture the dynamics in industrial crystallizers. *Proceedings of the 7th World Congress of Chemical Engineering* (WCCE7),Glasgow, July 2005, United Kingdom
- H.J.M.Kramer, A.A.Pande, **A.R.Menon**, S.K.Bermingham, J.Grievink (2004).Design and modelling strategies for industrial crystallization processes. *Proceedings of the 2nd International Symposium on Industrial Crystallization Inspiring Powder Technology*, (ISICIPT),Tokyo, pp.26-31, November, Japan
- **Menon, A.R.**, Kramer, H.J.M., Grievink, J., Jansens, P.J.(2004). A multi-dimensional population balance model for growth rate dispersion in industrial crystallizers. *Proceedings of the 11th International Workshop on Industrial Crystallization* (BIWIC11),Gyeongju, pp.9-16, 15-17 September, South Korea In: Kwang-Joo Kim (Ed.), BIWIC 2004, Gyeongju, South-Korea: Korea Research Institute of Chem, Tech., Yuseong, Taejeon.

- C.Virone, **A.R.Menon**, J.H. terHorst, H.J.M.Kramer, J.Grievink, P.J.Jansens (2004). Analysis and modelling of growth rate dispersion in industrial crystallisers. *Proceedings of the Swiss Symposium on Crystallization and Precipitation* (SSCP2004), ETH-Zurich, 9-10 March, Zurich, Switzerland
- **Menon, A.R.**, Kramer, H.J.M., Grievink, J., Jansens, P.J.(2003). Modelling of growth rate dispersion in industrial crystallizers using a two-dimensional population balance model. *Proceedings of the International Symposium on Process Systems Engineering and Control*, pp.143-148, Bombay, 3-4 January, India
- Bermingham, S.K., **Menon, A.R.** (2003). Procedure for compartment design, Ref. nr: SincPRO-TUD-LPE-TRP-0008, European Project report (SINC-PRO), Delft, The Netherlands
- Bermingham, S.K., **Menon, A.R.** (2002). Rigorous Crystallizer Models – State Of The Art, Ref. nr: SincPRO-TUD-LPE-TRP-0003, European Project report (SINC-PRO), Delft, The Netherlands

Oral Presentations

- Exploring multiple nucleation mechanisms to capture the dynamics in industrial crystallizers, 7th World Congress of Chemical Engineering (WCCE7), July 2005, Glasgow, United Kingdom
- Continuous crystallization of ammonium sulphate in industrial scale crystallizers, International workshop for the EU project SINC-PRO: Modelling, Optimization and Model Predictive Control of Industrial Crystallization Processes, April 2005, Delft, The Netherlands
- To balance using a 2Dimensional or 2Population model for crystallization processes, 4th Netherlands Process Technology Symposium (NPS4), October 2004, Veldhoven, The Netherlands
- A multi-dimensional population balance model for growth rate dispersion in industrial crystallizers, 11th International Workshop on Industrial Crystallization (BIWIC11), 15-17 September 2004, Gyeongju, South Korea
- CrysCODE® - Next generation supermodels for task-oriented design of crystallization processes, Sept.2004, Sumitomo Chemicals, Osaka, Japan
- CrysCODE® - State-of-the-art in rigorous crystallizer modelling and simulation, Workshop on industrial crystallization organized by the 'Working party on industrial crystallization in Japan', Sept.2004, Hiroshima University, Hiroshima, Japan
- Modelling of growth rate dispersion in industrial crystallizers using a two-dimensional population balance model, International Symposium on Process Systems Engineering and Control, January 2003, Bombay, India
- Modelling of crystallization kinetics in industrial crystallizers, 2nd Netherlands Process Technology Symposium (NPS2), October 2002, Zeist, The Netherlands

About the Author

Abhilash Menon was born on June 30, 1977 in Palghat (Kerala), India. After finishing his high school studies (1993) from St.Anne's High School in Malad - Bombay, he joined Sathaye College, Bombay to pursue his higher secondary school in science. On completion of this study in 1995, he began an undergraduate study in Chemical Engineering at the University of Bombay, Dept. of Chemical Technology (UDCT). As part of his study, he also spent a couple of months at Rashtriya Chemical Fertilizers, Bombay as a trainee.

In 1999, he graduated from UDCT as a Bachelor in Chemical Engineering and moved to the University of Twente, the Netherlands to pursue a two-year post-graduate program (TwAIO) in the field of process development and design. As part of this program, he did a one-year internship at Shell Global Solutions, Amsterdam. The subject of his Masters' thesis was on the design and operability study on swirl-tubes.

Then he joined Delft University of Technology to pursue a PhD program in the field of Industrial Crystallization. He worked at the interface of the process systems engineering group and the separation technology group, where he conducted the major part of the research presented in this thesis. The research results have been published(submitted) in various international journals and presented at various refereed conferences in the field of industrial crystallization, crystal growth, chemical engineering and process systems engineering.

Colophon

This dissertation was typeset on a Pentium M workstation using Microsoft Office Word. Figures were generated with Microsoft Office Excel, Matlab and gRMS (graphics tool within gPROMS). Drawings were produced with Microsoft Office Visio. The MS-Office Word document was converted into portable digital file (.pdf) using Adobe Distiller with a resolution of 2400 dpi.
The front and back cover of this thesis illustrates building blocks embedded within a spider web, which is a philosophical representation of tasks embedded within an intricate network as presented in the task-based design procedure.
This dissertation was printed by PrintPartners Ipskamp (http://www.ppi.nl) in Enschede-The Netherlands with a production volume of 300 copies.